eman ta zabal zazu

Universidad del País Vasco · Euskal Herriko Unibertsitatea

Free and extracellular vesicle-associated microRNAs from endometrial fluid as non-invasive diagnostic biomarkers of implantative endometrium

Jone Ibáñez Pérez
Doctoral thesis
2022

0.2 µm

eman ta zabal zazu

Universidad del País Vasco
Euskal Herriko Unibertsitatea

CICbioGUNE
MEMBER OF BASQUE RESEARCH & TECHNOLOGY ALLIANCE

Faculty of Medicine and Odontology -Department of Medical-Surgical Specialties

Center for Cooperative Research in Bioscience (CIC bioGUNE) - Exosomes Lab

Free and extracellular vesicle-associated microRNAs from endometrial fluid as non-invasive diagnostic biomarkers of implantative endometrium

Jone Ibáñez Pérez

Doctoral Thesis

Thesis directors:

Dr. Roberto Matorras Weinig
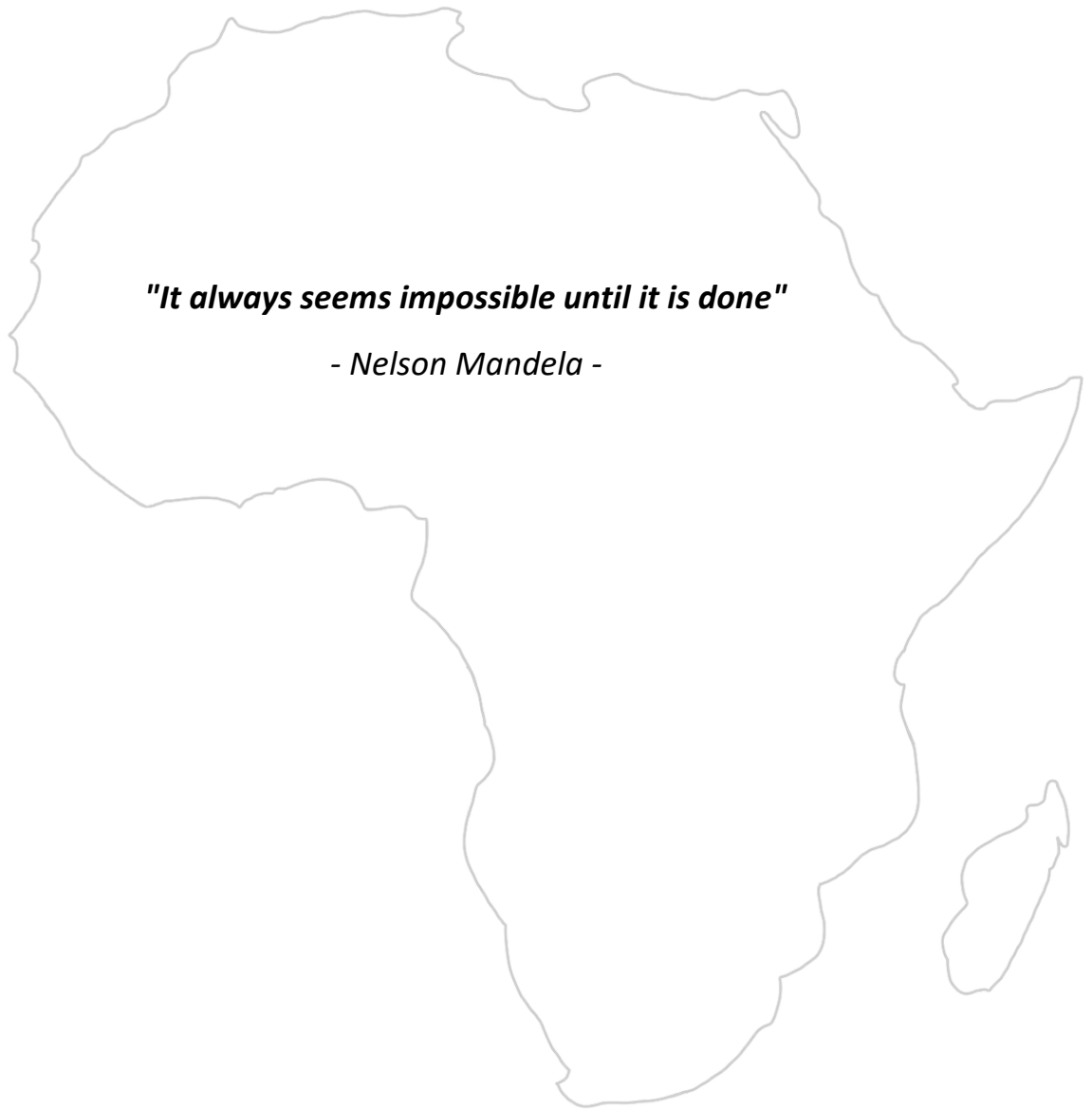
Dr. Juan Manuel Falcón Pérez

Bilbao, 2022

Nire gurasoei,

Arkaitzi,

"It always seems impossible until it is done"

- Nelson Mandela -

TABLE OF CONTENTS

AGRADECIMIENTOS

Quiero aprovechar esta oportunidad para dar las gracias a todas las personas que me han acompañado en esta aventura y me han ayudado a realizar esta tesis.

A Roberto, por haberme apoyado desde el primer momento y por haber confiado en mí. Gracias por darme la libertad de compaginar la tesis con la carrera de medicina, por ser paciente cuando no daba abasto con la vida y por animarme en la recta final cuando más lo necesitaba.

A Juanma, por haber creído en este proyecto y haberte unido a esta aventura. Gracias por confiar en mí, dejarme organizarme a mi manera y gracias por tus frases motivadoras "a mayor difference between a person who succeeds in science and one who fails is the ability to handle rejection". Seguimos.

A todo el equipo de la Unidad de Reproducción Humana del hospital de Cruces. A Bea y Belén, por hacer del laboratorio de andrología un hogar en el hospital. Por todo lo que me habéis enseñado y los consejos que me habéis dado. A María y a Lucia por apoyarme y animarme, por esos cafés antiestrés y los ratos de escaleras. A María, Aintzane, Miren, y Bego por su ayuda en la recogida de muestras. A las pacientes que han participado en el estudio. Al resto del equipo.

A todos los miembros del Laboratorio de Exosomas y la Plataforma de Metabolómica. A Félix y a Espe, por enseñarme las técnicas y protocolos necesarios para llevar a cabo esta tesis. A mis compañeras y compañeros de laboratorio por todos los buenos momentos vividos, las comidas al aire libre, los cafés en tiempos de COVID: María, Guille, Clara, Oiana, Elisabeth, Rocío, Jon, Marc y Endika por ser los mejores compañeros de laboratorio que podría tener.

A la Kuadrilla lasai enbor, una gran familia de investigadores repartidos por el mundo, por todos los momentos vividos y los viajes compartidos.

A mis compañeras de biotek: Leire, Ainize y Marina. Por habernos animado unas a otras en nuestras respectivas tesis/trabajos y por haber seguido manteniendo el contacto pese a los años.

A mis compañeras y compañeros de medicina y en especial a: Garazi, Nagore, Mirene, June, Lucia, Leire, Anne, Josu, Andoni. Por animarme y motivarme en los momentos más duros.

A todas las personas que me han ayudado a sacar esta tesis a delante.

Nire lagunei, beti nigan konfiantza izateagatik eta hasieratik abentura honetan lagundu izanagatik. Bajoi momentuetan animatzeagatik, egindako bidaiengatik eta festengatik, ez dakizue zein garrantzitsuak izan diren momentu horiek niretzako. Eskerrak bihotz bihotzez: Estitxu, Aitor, Bosco, Jugatx, Oihane, Janire, Miriam, Mikel, Jokin, Jani, Mikel, Irati, Ainhoa, Alex, Garkako gainerako kideei, Pelotaseko kideei, Autoca team-eri…

Nire familia guztiari. Maite eta Jabiri, hainbeste zaintzeagatik, eta, bereziki, Ama, Aita, Julen, Mitxel eta Martari, hasieratik animatzeagatik eta momentu oro maitatua sentiarazteagatik, ez dira urte errazak izan eta asko lagundu nauzue, eskerrik asko bihotzez.

Eta azkenik, zuri, Arkaitz, hasieratik nire alboan egoteagatik eta momentu gogorrenetan animatzeagatik. Eskerrik asko ni zaintzeagatik eta beti irribarre bat ateratzen saiatzeagatik. Asko eskertzen dizut nirekin izandako pazientzia.

PUBLICATIONS

The work of this thesis contributed to the following publication:

- **Ibañez-Perez J**, Díaz-Nuñez M, Clos-García M, Lainz L, Iglesias M, Díez-Zapirain M, Rabanal A, *et al*. microRNA-based signatures obtained from endometrial fluid identify implantative endometrium. Hum Reprod. 2022;37(10):2375-91.

The work of this thesis contributed to the following patent:

- European patent application n° EP21383049.0 for "firma de miRNA para la identificación del endometrio receptivo", on behalf of Asociación centro de investigación cooperativa en biociencias-cic bioGUNE, Universidad del país vasco/Euskal herriko unibertsitatea, Administración general de la comunidad autónoma de Euskadi y Reprodalia, S.L.

ABBREVIATIONS AND ACRONYMS

3' UTR   Three prime untranslated region

AI   Artificial intelligence

AMH   Anti-Müllerian hormone

ApoBDs   Apoptotic bodies

ARTs   Assisted reproduction techniques

ASEBIR Association for the Study of Reproductive Biology

AUC   Area Under the Curve

bp   Base pair

C3   Third component of the complement system

C4   Fourth component of the complement system

CB   Coomassie blue

CPM   Counts per million

Cryo-EM   Cryo-electron microscopy

DCT-M   Direct RNA extraction with mirVana PARIS kit.

DCT-N   Direct RNA extraction with Norgen kit

ddH2O   Double-distilled water (ddH2O)

DET   Double embryo transfer

DPBS   Dulbecco's Phosphate Buffered Saline

dsDNA   Double-stranded DNA

dsRNA Double-stranded RNA

DTT   Dithiothreitol

E2   Estradiol

EF   Endometrial fluid

ESCRT   Endosomal sorting complexes required for transport

ET   Embryo transfer

EVs   Extracellular vesicles

FBS   Fetal bovine serum

FET   Frozen embryo transfer

FGF   Fibroblast growth factor

FSH   Follicle-stimulating hormone

GnRH	Gonadotropin-releasing hormone
GO	Gene Ontology
HPO	Hypothalamic–pituitary–ovarian axis
ICSI	Intrauterine sperm injection
IL	Interleukin
ILVs	Intraluminal vesicles
ISEV	International Society for Extracellular Vesicles
IUI	Intrauterine insemination
IVF	In vitro fertilization
kDa	Kilodalton
KEGG	Kyoto encyclopedia of genes and genomes
LEVs	Large EVs
LH	Luteinizing hormone
LIF	Leukemia inhibitory factor
MAPK	Mitogen-activated protein kinase
mEVs	Medium EVs
miR	Mature microRNA
mir	Predicted stem-loop portion of the primary transcript
miRNAs	microRNAs
MMPs	Matrix metalloproteinases
mRNA	Messenger RNA
MUC1	Membrane-tethered mucin 1
MVB	Multivesicular body
NTA	Nanoparticle Tracking Analysis
OHSS	Ovarian hyperstimulation syndrome
OPN	Osteopontin
P4	Progesterone
PAI-1	Plasminogen activator inhibitor type 1
PBP	Polymer-based precipitation
PBP-M	Enrichment of EVs based on a PBP method and RNA extraction with mirVana PARIS kit
PBP-N	Enrichment of EVs based on a PBP method and RNA extraction with Norgen kit
PGS	Preimplantation genetic screening

pre-miRNAs   precursor-miRNAs

pri-miRNAs   primary-miRNAs

PRT-K   Proteinase K + RNase

qPCR   Real time Quantitative polymerase chain reaction

RISC   RNA-inducing silencing complex

RNA-seq   RNA sequencing

ROC curve   Receiver Operating Characteristic curve

SEC   Size exclusion chromatography

SET   Single embryo transfer

sEVs   Small EVs

SLPI   Secretory Leukocyte Protease Inhibitor

ssRNA   Single-stranded RNA

TF   Tissue factor

TGF-β   Transforming growth factor beta

TIMPs   Tissue inhibitors of metalloproteinases

TMM   Trimmed Mean of M-values

TX-100   Triton X-100 + RNase (TX-100)

TX+PRT   TX-100 + Proteinase K + RNase

UC   Ultracentrifugation

UC-M   Enrichment of EVs by ultracentrifugation and RNA extraction with mirVana PARIS kit.

UIU   Intrauterine sperm injection

uNK   Uterine natural killer cells

US   Ultrasound

VEGF   Vascular endothelial growth factor family

VEGFR2   Vascular endothelial growth factor receptor type 2 family

WB   Western blot analysis

WHO   The World Health Organization

WOI   Window of implantation

x

SUMMARY

Increasing embryo implantation rates has become one of the greatest challenges of assisted reproduction techniques. Implantation is a complex process that requires synchrony between the development of the embryo and the endometrium, but also adequate communication between the two of them. Free or extracellular vesicles (EVs)-associated microRNAs (miRNAs) from endometrial fluid (EF) have been described as mediators of the embryo–endometrium crosstalk. Therefore, the analysis of miRNA from this fluid could become a non-invasive technique for recognizing implantative endometrium. In this prospective study, we firstly optimized different protocols for EV and miRNA analyses using the EF of a setup cohort (n = 72). Then, we examined differentially expressed miRNAs in the EF of women with successful embryo implantation (discovery cohort n = 15/ validation cohort n = 30) in comparison with those for whom the implantation had failed (discovery cohort n = 15/ validation cohort n = 30). Successful embryo implantation was considered when pregnancy was confirmed by vaginal ultrasound showing a gestational sac four weeks after embryo transfer. The EF of the setup cohort was obtained before starting fertility treatment during the natural cycle, 16–21 days after the beginning of menstruation. For the discovery and validation cohorts, the EF was collected from women undergoing frozen embryo transfer (FET) on day 5, and the samples were collected immediately before embryo transfer (ET). In this study, we compared five different methods; two based on direct RNA extraction and the other three with an EV enrichment step prior to RNA extraction. Small RNA sequencing was performed to determine the most efficient method and find a predictive model differentiating between implantative and non-implantative endometrium. The models were confirmed using quantitative PCR (qPCR) in two sets of samples (discovery and validation cohorts) with different implantation outcomes. The protocols using EV enrichment detected more miRNAs than the methods based on direct RNA extraction. The two most efficient protocols (using polymer-based precipitation: PBP-M and PBP-N) were used to obtain two predictive models (based on three miRNAs) allowing us to distinguish between an implantative and non-implantative endometrium. The first, Model 1 (PBP-M) (discovery: AUC = 0.93; p-value = 0.003; validation: AUC = 0.69; p-value = 0.019) used hsa-miR-200b-3p, hsa-miR-24-3p and hsa-miR-148b-3p. Model 2 (PBP-N) (discovery: AUC = 0.92; p-value = 0.0002; validation: AUC = 0.78; p-value = 0.0002) used hsa-miR-200b-3p, hsa-miR-24-3p and hsa-miR-99b-5p. Functional analysis of these miRNAs showed a strong association with key implantation processes such as in-utero embryonic development or transforming growth factor-beta signaling. In this study, we describe new, non-invasive protocols to analyze miRNAs from small volumes of EF. These protocols could be implemented in clinical practice to assess the status of the endometrium before attempting ET. Such evaluation could help to avoid the loss of embryos transferred to a non-implantative endometrium.

RESUMEN

La infertilidad es una enfermedad compleja que hoy en día afecta a aproximadamente a una de cada siete parejas, lo que ha hecho que se recurra cada vez más a las técnicas de reproducción asistida (TRA). Las TRA a pesar de que han mejorado sustancialmente en los últimos años, tienen una baja tasa de éxito.

Uno de los pasos más ineficiente en las TRA está en el momento de la implantación. Para que la implantación sea exitosa es necesario que un embrión sea introducido en el útero justo en el momento en el que el endometrio está receptivo, es decir, durante la ventana de implantación (VI). En este periodo, las glándulas endometriales crean un microambiente uterino en el que se produce el dialogo molecular entre el embrión y el endometrio. Habitualmente, para determinar el momento óptimo de realizar la transferencia embrionaria (TE) se realiza una ecografía, sin embargo, menos del 60% de los embriones que se transfieren llegan a implantar, y un porcentaje aún menor llega a término. Estos porcentajes son muy bajos si se tiene en cuenta que las mujeres son sometidas a un tratamiento hormonal y además a un proceso quirúrgico, por todo ello, se están desarrollando métodos adicionales a la ecografía para determinar el momento óptimo para realizar la transferencia, entre ellos se encuentra la biopsia endometrial y el fluido endometrial.

Actualmente, la biopsia endometrial se utiliza para establecer si el endometrio está listo para realizar la transferencia embrionaria, se trata de una metodología invasiva, y no permite realizar la transferencia en el mismo ciclo en el que se toma la muestra, ya que tiene efectos perjudiciales para la implantación. Si los resultados de la biopsia muestran que el endometrio estaba receptivo, los resultados se extrapolan al siguiente ciclo. Sin embargo, esta suposición no es realista, ya que el ciclo endometrial es un proceso dinámico en el que intervienen muchos factores que afectan a la receptividad del endometrio.

El análisis del fluido endometrial (FE), que se obtiene de manera no invasiva, es una alternativa prometedora. Se ha demostrado que la aspiración del FE inmediatamente antes de la TE no afecta a la implantación. Además, el análisis rápido de la composición del FE podría permitir realizar la TE en el mismo ciclo en el que se ha recogido la muestra. Además, el FE puede obtenerse varias veces durante el ciclo y su análisis podría revelar si el endometrio está listo para la implantación o si es necesaria una intervención terapéutica para un procedimiento exitoso.

El FE es un fluido biológico complejo que puede modular la homeostasis y la receptividad del endometrio, además, es necesario para iniciar el proceso de implantación y desempeña un papel importante en la comunicación embrión-endometrio. Recientemente se ha demostrado que entre las moléculas del FE que se encargan de la comunicación endometrio-embrión, se encuentran los microRNAs (miARN) y las vesículas extracelulares (VEs).

Los miARN son pequeñas secuencias de ARN no codificantes (18-22 nucleótidos) que son importantes reguladores de los genes a nivel postranscripcional. Son esenciales durante el desarrollo embrionario temprano ya que regulan la proliferación y la diferenciación. Algunos de estos miRNAs se han asociado a las VEs, presentes en el FE. Las VEs son mediadoras de la comunicación intercelular, transmitiendo información de una célula a una multitud de otras células y localizaciones. Además, diferentes estudios han demostrado que el contenido de miRNAs de las VEs derivadas del endometrio puede ser captado por los embriones modificando sus fenotipos transcriptómicos y adhesivos.

La implantación es un proceso complejo que requiere una sincronía entre el desarrollo del endometrio y el del embrión, así como una adecuada comunicación embrión-endometrio. En esta comunicación los miRNAs juegan un papel fundamental como reguladores de genes a nivel post-transcripcional, especialmente durante el desarrollo embrionario temprano ya que regulan la proliferación y diferenciación celular. Las VEs contienen miRNAs y pueden tener una gran importancia en esta comunicación como vehículos de liberación de miRNAs, ya que se ha demostrado que las VEs derivadas del endometrio son captadas por los embriones.

Por lo tanto, nuestra hipótesis es que el análisis de miRNAs libres o asociados a VEs a partir de FE obtenido de mujeres sometidas a TE proporcionaría una firma de biomarcadores útiles para diferenciar entre un endometrio implantativo y un endometrio no implantativo.

El objetivo principal es definir un método no invasivo que sea sencillo, sensible, reproducible y que además permita la rápida identificación de un endometrio implantativo mediante el análisis de miRNAs libres y asociados a VEs procedentes del FE. Para lograr el objetivo principal, se han propuesto diferentes objetivos específicos. (i) Optimizar la preparación de la muestra de FE y caracterizar las VEs y miRNAs en las muestras de FE. (ii) Establecer una metodología robusta para analizar miRNAs libres y asociados a VEs del FE en entornos clínicos. (iii) Aplicar la metodología seleccionada en un conjunto de muestras ("discovery cohort") con diferentes resultados de implantación para diseñar un modelo predictivo del endometrio implantativo. (iv) Validar los modelos predictivos en una nueva cohorte independiente ("validation cohort") de mujeres con diferentes resultados de implantación. (v) Investigar la asociación de los miRNAs validados con las VE y su función biológica en el proceso de implantación.

Para optimizar la recogida y preparación de la muestra hemos realizado un experimento con un agente mucolítico llamado ditiotreitol. Luego, hemos caracterizado el contenido de VEs y miRNAs de las muestras de FE mediante cromatografía de exclusión de tamaño y ensayo de RNasa. El contenido proteico de las muestras ha sido caracterizado mediante Western blot análisis y tinción con azul de Coomassie. Para establecer una metodología robusta para analizar miRNAs libres y asociados a VEs de FE en entornos clínicos, hemos comparado cinco métodos diferentes para extraer ARN de FE. Dos de ellos basados en la extracción directa del ARN (DCN) y los otros tres con un paso de enriquecimiento de VEs antes de la extracción del ARN (dos de ellos basados en un método de precipitación basado en polímeros (PBP) y el otro basado en la ultracentrifugación (UC)). (i) DCT-N: extracción directa de ARN con el kit Norgen. (ii) DCT-M: extracción directa de ARN con mirVana PARIS kit. (iii) UC-M: enriquecimiento de VEs mediante UC y extracción de ARN con mirVana PARIS kit. (iv) PBP-M: enriquecimiento de VEs basados en PBP y extracción de ARN con mirVana PARIS kit. (v) PBP-N: enriquecimiento de VEs basados en PBP y extracción de ARN con Norgen kit.

Para diseñar un modelo predictivo del endometrio implantativo se aplicaron las dos técnicas más eficientes en muestras procedentes de la "discovery cohort" ("endometrio implantativo" n = 15/ y "endometrio no implantativo" n = 15) y el ARN se analizó mediante secuenciación de ARN pequeños y PCR cuantitativa (qPCR). Los modelos predictivos se validaron mediante qPCR en una nueva cohorte de pacientes llamada "validation cohort" ("endometrio implantativo" n = 30/ y "endometrio no implantativo" n = 30). La asociación de los miRNAs validados con las VE y su función biológica en el proceso de implantación, se estudió mediante el análisis de sus genes diana predichos.

Para optimizar la preparación de la muestra, tratamos las muestras de FE con un agente mucolítico y lo que vimos fue que en las muestras tratadas obtuvimos más cantidad de VEs y con diferentes tamaños en comparación con la muestra no tratada, donde la población de VEs obtenida era más homogénea. Sin embargo, la amplificación de miRNAs por qPCR mostró una menor detección en las muestras tratadas. Por lo que se decidió no tratar las muestras con el agente mucolítico porque no mejoraba la detección de miRNAs.

A continuación, comparamos 5 metodologías diferentes y la determinación de la eficiencia mediante qPCR mostró que los métodos con un paso previo de enriquecimiento de VEs con el kit comercial PBP (PBP-M y PBP-N) se comportaron mejor en comparación con el resto, siendo PBP-N el más eficiente. Así pues, para profundizar en el ARN extraído con PBP-M y PBP-N realizamos la secuenciación de ARN pequeños (small RNA-seq). Detectamos 251 miRNAs únicos con PBP-M y 151 miRNAs con PBP-N. A continuación, dada la importancia de seleccionar una metodología robusta, realizamos un experimento de reproducibilidad técnica. Para ello, dos operadores repitieron el experimento con las mismas muestras. El coeficiente de variaciones mostró una mayor variabilidad para PBP-M. En general, PBP-M y PBP-N obtuvieron los mejores resultados de este procedimiento de optimización. El método PBP-M resultó ser más eficiente en la small RNA-seq, sin embargo, PBP-N resultó ser más eficiente en términos de análisis de qPCR. Así que decidimos aplicar estas dos metodologías en un conjunto de muestras individuales.

Para diseñar un modelo predictivo del endometrio implantativo aplicamos las metodologías PBP-M y PBP-N en las muestras de la "discovery cohort". El análisis del contenido proteico de las muestras mostró una gran variabilidad en la cantidad total de proteínas, aunque se correlacionaron positivamente el número total de miRNAs en las muestras, que se analizó mediante secuenciación de miRNAs pequeños. Los datos de la secuenciación mostraron 231 miRNAs únicos para PBP-M y 341 miRNAs únicos para PBP-N. Se aplicó un análisis de abundancia diferencial para descubrir miRNAs asociados con el resultado de la implantación. El análisis estadístico aplicado en los datos de PBP-M detectó 13 miRNAs adecuados para una mayor validación y con PBP-N detectamos 5. Para validar los resultados por qPCR tuvimos que seleccionar un control endógeno para normalizar las muestras. Buscamos un control endógeno que se expresara por igual en ambos grupos, que tuviera una correlación positiva con la cantidad de proteína y que fuera detectado en abundancia por small RNA-seq y qPCR. Utilizamos el algoritmo Normfinder y finalmente seleccionamos los miRNA hsa-miR-200c-3p y hsa-miR-92a-5p como controles endógenos para normalizar las muestras. Realizamos un estudio de regresión utilizando la corrección bootstraping con los miRNAs diferencialmente expresados. Los resultados mostraron tanto para PBP-M como para PBP-N un modelo significativamente predictivo basado en tres miRNAs que fue robusto frente a los datos. Obtuvimos dos modelos predictivos basados en tres miRNAs que permiten diferenciar entre un endometrio implantativo y uno no implantativo. (i) Modelo 1 (PBP-M): área bajo la curva (AUC) = 0.93; *p*-valor = 0.003; miRNAs: hsa-miR-200b-3p, hsa-miR-24-3p y hsa-miR-148b-3p. (ii) Modelo 2 (PBP-N): AUC=0.92; *p*-valor = 0.0002; miRNAs: hsa-miR-200b-3p, hsa-miR-24-3p y hsa-miR-99b-5p.

Validamos el rendimiento de los dos modelos (PBP-M y PBP-N) en una cohorte independiente. Este segundo grupo de mujeres estaba formado por 60 mujeres, 30 de las cuales tuvieron una implantación exitosa y 30 que no la tuvieron. En este caso también observamos variabilidad en el contenido de proteínas entre las muestras, y como en el caso anterior, la cantidad de ARN se correlacionaba positivamente con la cantidad de proteínas. Así que utilizamos los mismos controles endógenos para normalizar los datos antes del análisis.

En el caso de PBP-M, el modelo predictivo fue significativo con un AUC=0.69 y valor-p=0.019. El análisis de la curva característica operativa del receptor (ROC) identificó el hsa-miR-148b-3p como la variable más probable para diferenciar el endometrio implantativo del no implantativo, demostrando una expresión diferencial significativa entre los grupos. En el caso de PBP-N, el modelo predictivo también es significativo, con un área bajo la curva de AUC=0.78 y valor-p=0.0002. El análisis ROC identificó el hsa-miR-99b-5p como la variable más probable para diferenciar el endometrio implantativo del no implantativo, demostrando una expresión diferencial significativa entre los grupos.

El análisis funcional de estos miRNAs mostró una fuerte asociación con procesos clave en la implantación: proteínas de la unión de adherencia, señalización del TGF-beta, biosíntesis y metabolismo de los ácidos grasos, desarrollo embrionario en el útero, procesos del sistema inmunitario, y procesos de transporte mediado por endosomas y vesículas.

En resumen, este estudio introduce nuevos protocolos para analizar miRNAs a partir de pequeños volúmenes de FE que podrían implementarse en la práctica clínica para la evaluación del estado del endometrio utilizando herramientas no invasivas basadas en miRNAs. Nuestros resultados sugieren que valores de hsa-miR-99b-5p superiores a 2.81 dCt indicarían un endometrio no implantativo con una sensibilidad de 0.6 y una especificidad de 0.93. Por tanto, los profesionales de los centros de reproducción asistida podrían beneficiarse del uso de este miRNA con el método de detección PBP-N como predictor del estado del endometrio para mejorar las tasas de implantación de las mujeres sometidas a técnicas de reproducción asistida. Al determinar el estado del endometrio, sería posible cambiar la estrategia de la TE cuando los resultados muestren un patrón implantativo desfavorable y así mejorar las tasas de implantación y evitar la pérdida de embriones cuando se transfieran a un endometrio que no está listo para que ocurra la implantación.

INDEX OF FIGURES

INDEX OF TABLES

INTRODUCTION

I. <u>INTRODUCTION</u>

The introduction has been divided into seven blocks, infertility, assisted reproduction, female reproductive system, embryo implantation, evaluation of endometrial receptivity, extracellular vesicles and miRNAs, in which key concepts from each of the topics will be discussed.

1. <u>Infertility</u>

The World Health Organization (WHO) has defined infertility as "a disease of the reproductive system defined by the failure to achieve a clinical pregnancy after 12 months or more of regular unprotected sexual intercourse" (1,2). This definition involves two different infertility types; (i) primary infertility is when a pregnancy has never been achieved by a person and (ii) secondary infertility is when at least one prior pregnancy has been achieved (3). In the last decades, infertility has become an ongoing global challenge (4). The prevalence of infertility has been estimated to be approximately between 8 and 12% among couples of reproductive age worldwide (5–7). The main factors that could impair the spontaneous fertility of couples are the increase in the age of the female partner, decline in semen quality and infertility due to disease **(Table 1)**, which can affect both genders or be specific to one (8). All of these could lead to reproductive problems and infertility, which have increased during the last years, generating a rise in the demand for healthcare services (9).

Table 1. *Summary of diseases related to infertility causes.* From Vander and Wyns (8).

Disease-related infertility		
Both genders	**Female**	**Male**
- Hypogonadotropic hypogonadism - Hyperprolactinemia - Disorders of ciliary function - Infection - Systemic diseases - Lifestyle-related factors	- Premature ovarian insufficiency - Polycystic ovarian syndrome - Endometriosis - Uterine fibroids - Endometrial polyps - Tubal conditions - Uterine malformations - Ovarian dysfunction	- Testicular deficiency - Post-testicular impairment

2. Assisted Reproduction Techniques

Assisted reproduction techniques (ARTs) incorporate a wide range of technologies that are used to enhance the probability of achieving a pregnancy (10). In most cases, the diagnostic process or individual characteristics (women without a male partner, patients without ovarian function, poor semen quality, etc., (**Figure 1**)) allow physicians to determine which of the available techniques would be the most appropriate as the first line of treatment and offer the most appropriate relationship between benefits, complexity, costs, and risks (11).
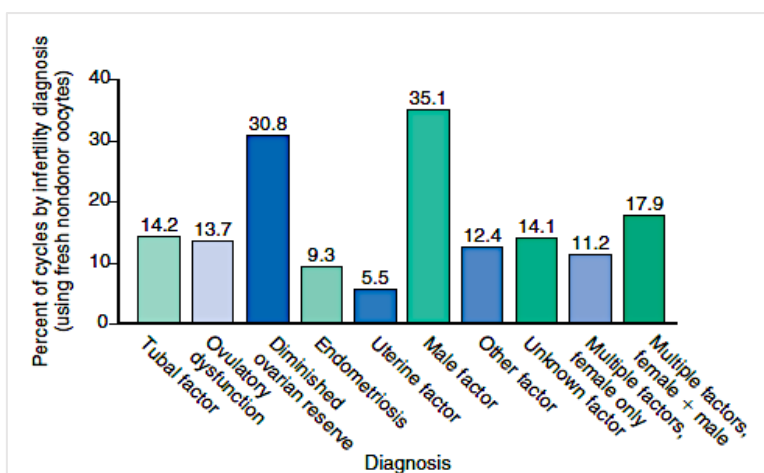
Figure 1. Infertility diagnosis for assisted reproduction technology cycles.

Percentages sum greater than 100% because more than one diagnosis can be reported for a given cycle. From Kaser *et al.,* 2018 (10).

Among the different techniques, there are intrauterine insemination, *in vitro* fecundation and intracytoplasmic sperm injection. The characteristics and utilities of each technique will be mentioned in the following sections.

2.1. Intrauterine insemination

Intrauterine insemination (IUI) is a cost-effective first-line therapy for selected patients (permeable fallopian tubes, appropriate seminogram, etc.,) (12). IUI is defined as the deposit of previously prepared sperm inside the upper uterine cavity, without sexual intercourse, to achieve a pregnancy (**Figure 2**) (11).
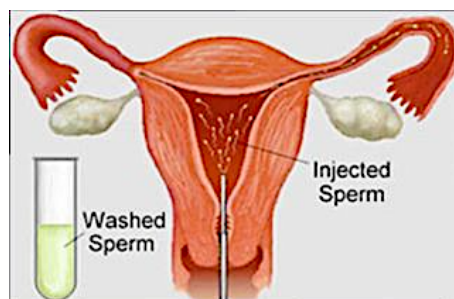
Figure 2. Intrauterine insemination (IUI).

Previously prepared sperm is injected into the uterus. From: https://www.nufertility.com/blog/intrauterine-insemination-iui/

It can be divided into two types according to the origin of the sperm: (i) homologous or partner's sperm; and (ii) donor or heterologous (13,14). The preparation of the sample improves semen quality, which increases the possibility of pregnancy (13,14). The pros and cons of the technique are summarized in **Table 2**.

Table 2. Pros and cons of the IUI technique.

Pros	Cons
• First-line procedure • Simple and easy • Relatively economical • Less invasive • Reduced psychological burden • Good couple compliancy • Low risk for serious complications • Minimal infrastructure required	• Permeable fallopian tubes are necessary • Good semen quality is necessary • Limited indications • Low success rates • High-order multiple pregnancy

2.2. *In vitro* fecundation and intracytoplasmic sperm injection

In vitro fecundation (IVF) and intracytoplasmic sperm injection (ICSI) are mainly used in cases where IUI cannot be used; e.g., bad sperm quality, non-permeable fallopian tube or when IUI has been used but was unsuccessful (15).

Table 3. Pros and cons of IVF/ICSI cycles.

Pros	Cons
• Permeable fallopian tubes are not necessary • Can be performed with low sperm count • Genetic screening can be performed on pre-implanted embryos • Abnormal embryos can be discarded	• More expensive • More infrastructure required • High-order multiple pregnancy • Fertilization failure • Implantation failure

Both IVF and ICSI followed the same protocol, the only difference between them is how the egg is fertilized (**Figure 3**). The first step is ovarian stimulation, the goal being to obtain more than one oocyte by pharmacologically manipulating the physiological ovarian cycle. Then, when the follicle diameter is between 17-19 mm, the egg pick-up is programmed and oocytes are collected by ultrasound-guided aspiration (16). During an IVF cycle, oocytes and semen are recovered and placed together on a laboratory plate to facilitate spontaneous fertilization. On the other hand, ICSI involves intervening more actively and consists of injecting a single sperm into the cytoplasm of the oocyte with the help of a micropipette to fertilize it (16). After fertilization, the embryos are cultured (3-5 days) before performing the embryo transfer (ET) (16).
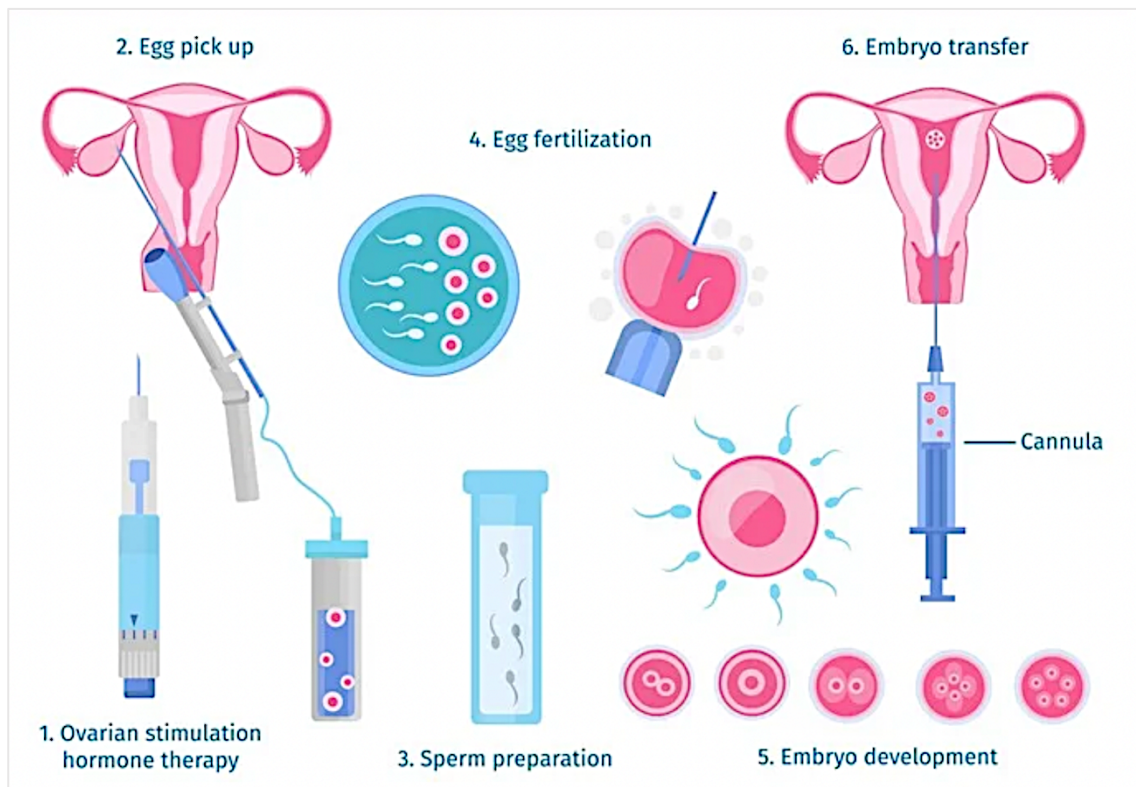
Figure 3. *FIV/ICSI procedure.* Figure from: https://www.news-medical.net/health/Stages-of-IVF.aspx

2.2.1. Embryo transfer procedures

There are two ET procedures, fresh and frozen ET. With fresh ET, the embryo is transferred 3-5 days after egg retrieval; in this situation, estrogen from the ovarian follicles helps prepare the endometrium for implantation. With frozen embryo transfer (FET), the embryo can be transferred months or years later; in this situation, estrogen supplementation is usually required to prepare the uterine endometrium (17). In general, the selection of fresh or frozen ET should be considered on an individual basis. It is appropriate to implement frozen ET in patients at risk of OHSS, hyper-responders, those undergoing preimplantation genetic screening (PGS) at the blastocyst stage or for embryos from previous IVF/ICSI cycles (18). Participants in this study were women that had a day-5 FET from previous IVF/ICSI cycles, a practice which is performed increasingly more often (19).

2.2.2. Improvements in ARTs

During the last decades, several new IVF/ICSI practice regimens have been applied to improve ART results (20). Among these improvements there are:

1) Blastocyst-stage in place of cleavage-stage ET (21).
2) Replacement of fresh ET by embryo cryopreservation ("freezing") and subsequent thawed ET = FET (22).
3) Preimplantation genetic screening (PGS) (23).
4) Single embryo transfer (SET) in place of double embryo transfer (DET) (24).
5) Time-lapse embryo culture monitoring.

However, fertility treatment success rates remain very low (5–7). Of all steps in IVF/ICSI, ET is still one of the most inefficient in ARTs and less than 60% of the embryos transferred to the uterus implant (25,26). For that reason, increasing embryo implantation rates has become one of the greatest challenges in ARTs. Successful implantation requires synchrony between the development of the endometrium and the embryo but, also, adequate embryo-endometrial crosstalk (27,28).

Therefore, in the following sections, we will focus on describing the endometrium, the embryo and factors involved in the endometrium-embryo crosstalk.

3. **Female reproductive system**

The internal organs of the female reproductive system include the vagina, uterus, fallopian tubes, and ovaries (**Figure 4**). The uterus is a hollow muscular organ situated in the female pelvis, between the bladder and the rectum. It consists of three layers (29,30):

i) The endometrium, the inner mucous layer, crucial for the embryo implantation process.

ii) The myometrium, the smooth muscle layer.

iii) The perimetrium or peritoneal cover is the outer serous layer that corresponds to the visceral peritoneum.

There are many uterine factors linked to infertility such as congenital uterine anomalies, endometrial polyps, fibroids, adenomyosis, endometriosis… (31).

The female reproductive system is regulated by the hypothalamus-hypophysis-ovary axis and is responsible for carrying a pregnancy to term (32–34).
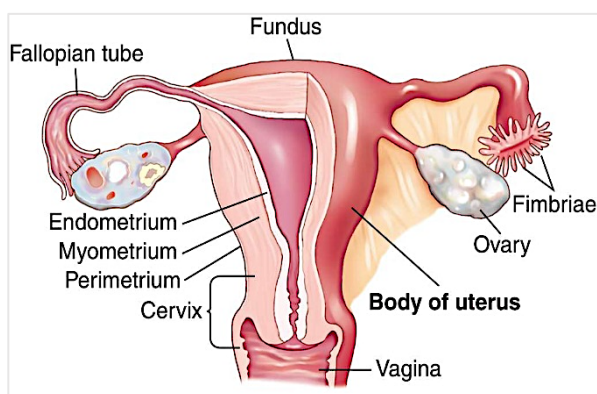
Figure 4. Internal female reproductive system.

From https://medical-dictionary.thefreedictionary.com
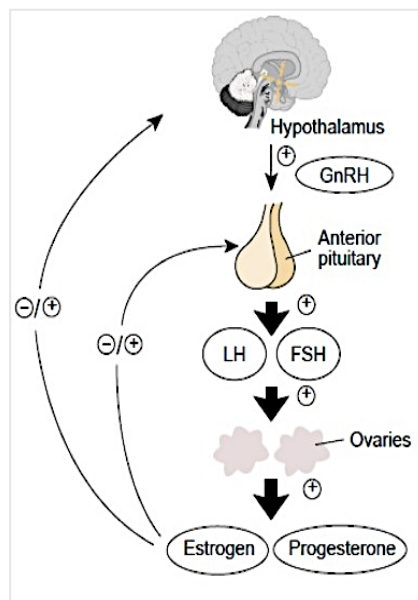
Figure 5. Schematic representation of the hypothalamic–pituitary–ovary (HPO) axis. From Kong *et al.,* 2014 (35).

3.1. Hypothalamic–pituitary–ovarian axis

The hypothalamic–pituitary–ovarian axis (HPO axis) controls the histological and physiological changes that occur during the menstrual cycle (**Figure 5**). This axis consists of three groups of hormones: (i) Gonadotropin-releasing hormone (GnRH) released by the hypothalamus, (ii) follicle-stimulating hormone (FSH) and luteinizing hormone (LH), both of which are gonadotropin hormones secreted by the anterior pituitary in response to GnRH, (iii) estrogens and progestogens are sex hormones released by the ovary in response to FSH and LH and rule the endometrial cycle. Estradiol (E2) is the most important estrogen, while progesterone (P4) is the most important progestogen. On the one hand, E2 promotes the proliferation and growth of endometrial cells, as well as being responsible for the development of a woman's secondary sexual characteristics. On the other hand, the main function of P4 is to prepare the endometrium for implantation and, in case of pregnancy, prepare the breasts for lactation (35–37).

Due to the pulsatile release of the GnRH hormone, it is possible to have a cyclic menstrual cycle with an approximate duration of 28 days, although the physiological interval varies between 21 and 35 days. During this period, two sub-cycles occur simultaneously, both hormonally regulated: the ovarian and endometrial cycles. The ovarian cycle is divided into two phases, the follicular phase (day 1-14) and luteal phase (day 15-28) and ovulation occurs on day 14. On the other hand, the endometrial cycle that has three phases, menstruation (day 1-5), proliferative phase (days 6-14) and secretory phase (days 15-28) (**Figure 6**) (33,37,38).

3.2. Phases of the menstrual cycle

The menstrual cycle begins with menstruation, where E2 and P4 levels are low but gonadotropin levels have begun to increase, (FSH levels > LH levels). FSH is responsible for the recruitment of the ovarian follicles during the luteal phase of the previous cycle, during this time about 8-14 follicles will begin their maturation and E2 is synthesized by follicular cells (33,37).

Then, LH levels increase while FSH decreases and only one follicle will continue to mature; called the primordial follicle or "de Graaf" follicle. This follicle synthesizes a huge amount of E2 that, on the one hand, stimulates endometrial development and proliferation and, on the other hand, stimulates synthesis and prevents the release of gonadotropins (negative feedback), but the pituitary content increases. During the proliferative phase of the endometrium, the functional layer grows, glands and blood vessels lengthen and rounden. At the end of the follicular phase, E2 levels reach maximum values and 24-48 h later, an LH peak appears (LH >>> FSH) (33,37).

According to the siphon hypothesis, this LH peak occurs because E2 increases the gonadotropin synthesis and the pituitary reaches its maximum capacity, resulting in a sudden release of its content. The fact that more LH is released than FSH may be due to the pulsatility of GnRH release (33,37).

Ovulation occurs 36 hours after the LH peak. Under the effects of LH, follicular cells secrete proteolytic enzymes that promote the liberation of the oocyte. After that, the ovulatory follicle fills with blood, becomes a hemorrhagic body and starts the luteinization process where the follicular cells become lutein cells. The proliferation phase of the endometrium ends 2-3 days after ovulation and, during this time, the endometrium reaches its maximum proliferation, which can be visualized by ultrasound as trilaminar endometrium (33,37).

During the luteal phase, the ovulatory follicle changes into a corpus luteum, a highly secretory organ, and mainly secrets P4 but also E2. Gonadotropic hormones LH and FSH both decrease due to the negative feedback of P4 and E2, and their levels remain low until the corpus luteum degenerates into the corpus albicans. Meanwhile, the endometrium becomes secretory, endometrial glands become more tortuous, secretory substances are released into the uterine cavity, stromal tissue starts the decidualization process and angiogenesis increases. Halfway through the luteal phase, the endometrium has reached its maximum development and is ready for embryo implantation (33,37).

The endometrium only is receptive for embryo implantation during a short time period known as "the window of implantation" (WOI) from days 20-24. If implantation does not occur, the corpus luteum degenerates by the end of the luteal phase. With the involution of the corpus luteum, E2 and P4 levels decrease accompanied by an increase in gonadotropins, mainly FSH. Low levels of ovarian steroids determine the thinning of the endometrial mucosa and the onset of menstrual flow (33,37).

In ARTs, determining the optimal moment to perform ET is crucial; thus it is very important to know the regulation, function and composition of the endometrium.
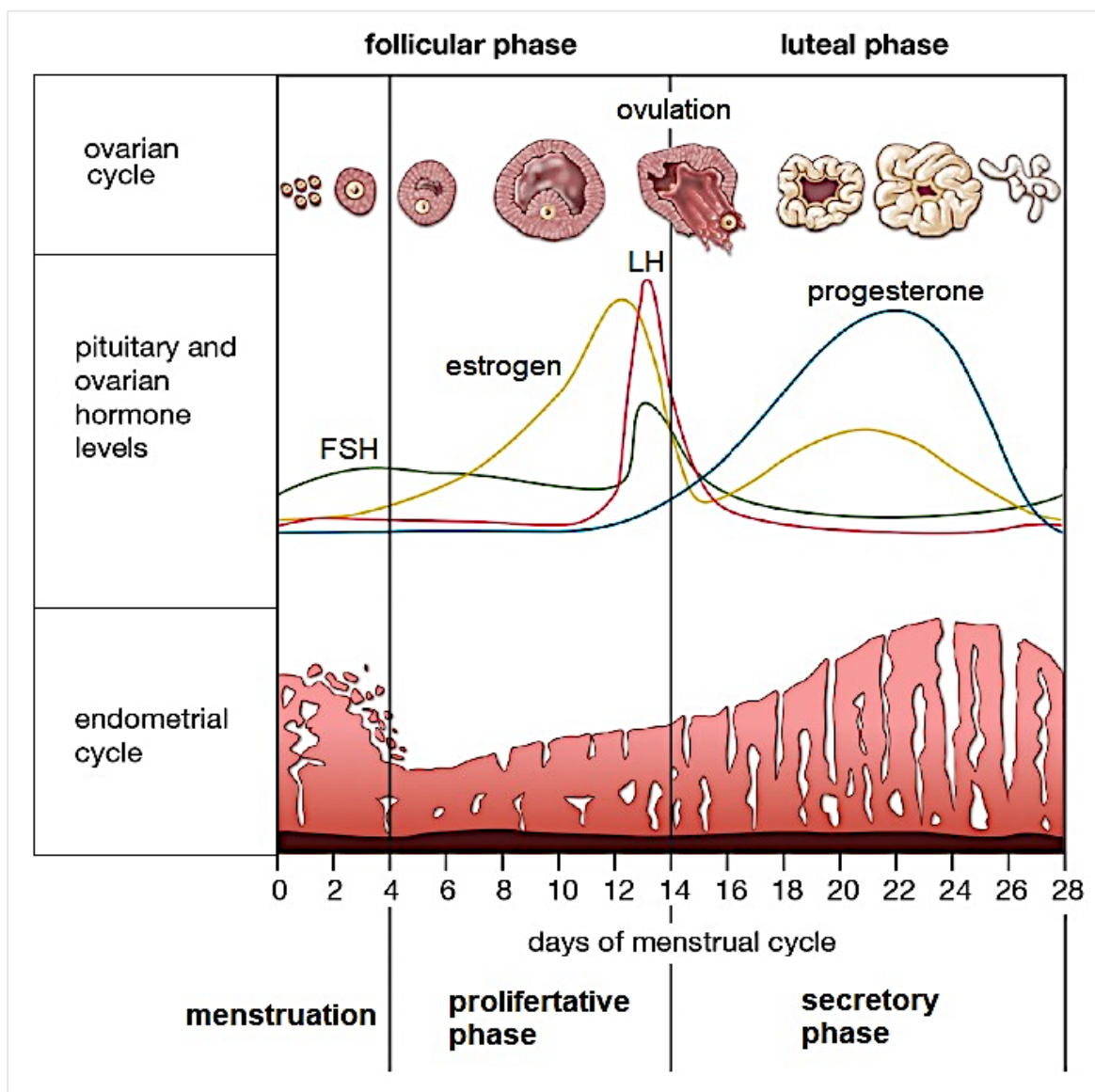
Figure 6. *Ovarian, endometrial and hormonal changes during the menstrual cycle.*

From Clayton, 2019 (38).

3.3. The endometrium

The primary function of the endometrium is to provide an immune-privileged site for embryo implantation as it tolerates the development of the pregnancy (39) and provide a nurturing environment for the fetus during pregnancy (40). It also performs essential functions during the sexual cycle of women as an endocrine, paracrine and autocrine organ (36,37). All this is possible because the endometrium is a very versatile tissue.

Endometrial tissue is composed of epithelium, stroma and vascular components and can be differentiated into two regions: the functional and basal layers (36). The functional layer corresponds to the layer that is replaced cyclically in the menstrual cycle. It is in contact with the uterine cavity and covers 2/3 of the endometrium during the secretory phase, although its thickness changes throughout the menstrual cycle (**Figure 7**). The basal layer is the inner layer that is in contact with the myometrium. It has more cellular stroma than the functional layer and is the area where the endometrial regeneration occurs. This layer does not detach during menstruation because it is necessary to regenerate the functional layer (41,42).

The endometrial epithelium consists of a luminal epithelium and a glandular epithelium (**Figure 7**). The luminal epithelium is a single layer of columnar epithelium with ciliated and secretory cells, being the first maternal surface to have contact with the blastocyst, regulating its adhesion. The glandular epithelium creates simple tubular glands towards the stroma. These epithelial cells synthesize and secrete different substances into the uterine cavity, such as soluble factors and extracellular vesicles, which are necessary for maintenance of the pre-implantative embryo and promote implantation (36,43).
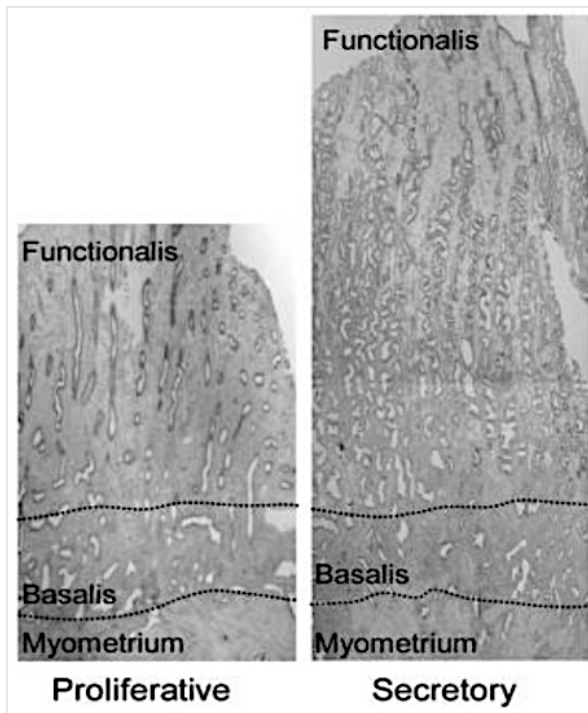
Figure 7. *Layers of the endometrium.*

Differences in the thickness of the functional layer during the proliferative and secretory phases of the endometrium. From Nguyen *et al.,* 2012 (41).

On the other hand, the stroma is a connective tissue composed of different cell types and extracellular matrix. Fibroblasts are the main cellular components and are involved in the remodeling of the extracellular matrix throughout the menstrual cycle, mainly during the secretory phase throughout the decidualization process (36). During decidualization, fibroblasts undergo morphological changes, from elongated to round-shaped cells, in addition to functional changes where they begin to secrete different molecules that promote the decidualization process. In consequence, there is an influx of specialized immune cells such as uterine natural killer cells (uNK), macrophages and lymphocytes (44,45), along with vascular maturation that involves angiogenesis and increases the permeabilization of the blood vessels (36,44).

In the end, all these changes are intended to prepare the endometrium for embryo implantation. It is a very complex process involving the endometrium, the embryo and the uterine microenvironment; therefore, all these points will be explained in the following section.

4. __Embryo implantation__

Embryo implantation is a complex process that consists of three main steps: apposition, attachment, and invasion of the embryo (46–48).

Under physiological conditions, the blastocyst enters the uterus from the fallopian tubes five days after fecundation and it is **apposed** to the internal cell mass toward the endometrial wall. Then, the blastocyst begins to **attach** to the receptive endometrial surface. Finally, it crosses the endometrial epithelium and **invades** the endometrial stroma and is surrounded by stromal cells (**Figure 8**) (46–48).

However, in IVF/ICSI cycles, the blastocyst is created in the laboratory and then placed into the uterus. Therefore, for embryo implantation to be successful, there must be synchronous development between the embryo and the endometrium. It has been described that successful implantation requires: (i) a receptive endometrium, (ii) a developmentally competent embryo/blastocyst and (iii) adequate embryo maternal crosstalk (40,49–56). Each is described below.
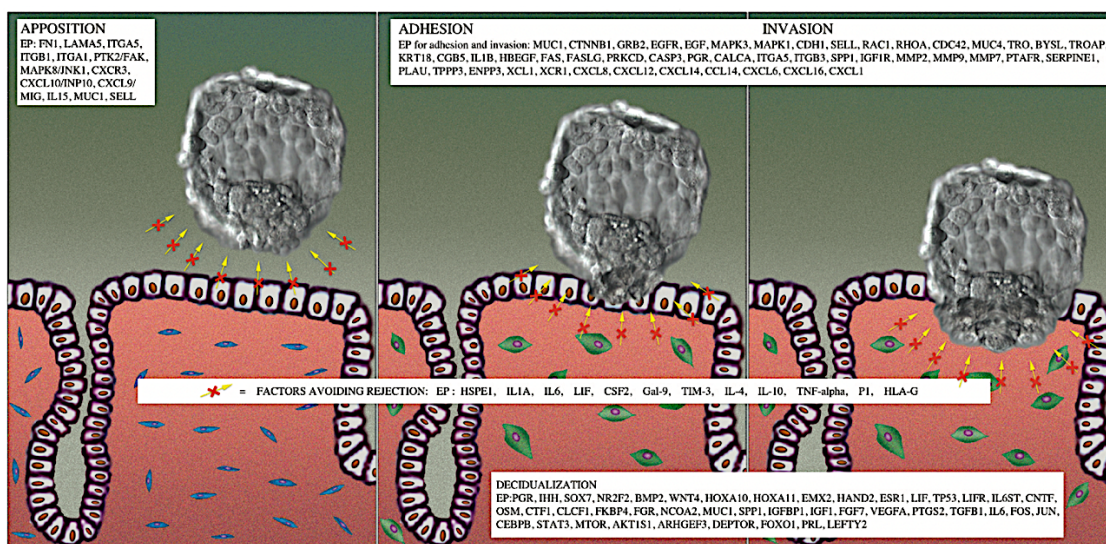
Figure 8. *Overview of the implantation steps.* The figure shows the implantation steps and some key molecules during apposition, attachment, and invasion. From Matorras *el al.* (57).

4.1. Receptive endometrium

As described before, the endometrium undergoes progressive changes in response to ovarian steroid hormones. Adequate proliferation and differentiation during the proliferative phase must be followed by secretory changes and stromal decidualization in the secretory phase. All these events make the endometrium receptive; it is a physiological status in which the endometrium acquires an adhesive phenotype that permits embryo implantation (58,59).

The acquisition of this phenotype allows embryo implantation but only for a short period of time during the mid-secretory phase of the menstrual cycle (40). This timing is also known as the WOI and, in humans, usually occurs between days 20-24 of the menstrual cycle, approximately 5-9 days after ovulation (60).

However, there are many factors that can lead to an impaired synchronization between the embryo and endometrium that will lead to implantation failure. Causes of impaired endometrial receptivity include structural abnormalities, endometritis and abnormal decidualization secondary to progesterone resistance (61). There are several architectural, cellular, biochemical and molecular events in the endometrium that are coordinated within the WOI and constitute crucial elements for the establishment of endometrial receptivity (40,62)

4.1.1. Changes in the endometrium

The following are some changes that occur during the acquisition of receptivity.

4.1.1.1.   Luminal epithelium

In the presence of P4, the luminal epithelium undergoes morphological remodeling leading to apical surface specialization where apical pinopodes appear. Their formation seems to be dependent on P4, while E2 causes them to regress.

The fact that human blastocysts only implant in luminal areas with pinopodes has been supported by *in vitro* studies (**Figure 9**) (40,63). There are also other changes related to cell adhesiveness, where luminal cells express adhesion molecules that permit the adherence of the blastocyst, such as integrins, CD44, trophinin, L-selectin receptors and mucins (56,64).

- Integrins α1β1, α4β4 and αvβ3 have been described to co-localize with pinopodes during the WOI (40,65).

- CD44 is a receptor that plays a role in cell-cell interactions, cell adhesion and migration, helping them sense and respond to changes in the tissue microenvironment (40,66,67).

- Trophinin has been suggested as a homologous pairing partner between trophoblast and endometrium during implantation (40,68).

- Mucins are the major constituents of mucus and generally act as anti-adhesion molecules. MUC1 is a large, bulky and rigid molecule that extends beyond integrins, acting as a physical barrier to embryo implantation, so it has been investigated as part of the molecular repertoire of endometrial receptivity. It was observed that MUC1 levels increase with the presence of P4 during the WOI. However, it was demonstrated that the embryo induces a specific cleavage of MUC1 in the cone of the endometrial epithelium to which it adheres. It is a dynamic process in which P4 induces an increase in MUC1, meanwhile, in the adhesion phase, the blastocyst is responsible for breaking it (69).
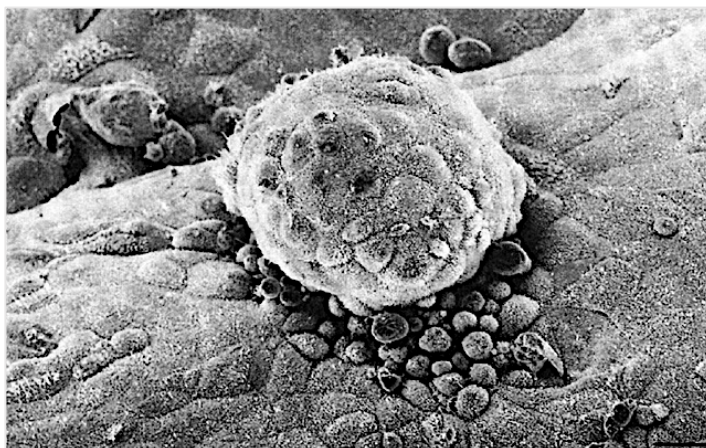
Figure 9. *In vitro culture of a human embryo on cultured endometrial epithelium.*

The figure shows that embryos seem to prefer areas with pinopode expression to implant. From Bentin-Ley, 2000 (63).

4.1.1.2. Glandular epithelium

Glandular epithelial cells increase in size, become more tortuous and remarkably increase their secretory activity during the WOI in the secretory phase. Most of the secreted substances are implicated in the regulation of embryo implantation and support blastocyst attachment, invasion and development. Some of these substances are glycodelin, osteopontin, antimicrobial peptides, complement system… (40,70–72).

- Glycodelin: the most secreted glycogen during the secretory phase, both for endometrial glands and decidua. It is also known as endometrial α2 globulin or progesterone-associated endometrial protein, among others. Its levels in uterine flushings are directly related to the histological date of the endometrium. It is almost undetectable during the follicular and early luteal phase, but six days after ovulation, its concentration rapidly increases. In addition, glycodelin levels have been described to be decreased in the endometrium of women with infertility (73,74).

- Osteopontin (OPN): a glycosylated phosphoprotein secreted mostly during the WOI and binds luminal cell surface receptors like CD44 and αvβ3. This interaction suggests that OPN serves as a bridge between the receptors on the surface of endometrium and embryonal cells (40,75,76).

- Antimicrobial peptides: the glandular epithelium secrets defensins and secretory leukocyte protease inhibitor (SLPI) that play an important role against infections. The levels of defensins and SLPI fluctuate during the cycle, being highest in the secretory phase (40,77,78).

- Complement system: The third (C3) and fourth (C4) components of the complement system have been described in the endometrium. Its control is essential for fetomaternal tolerance against the implantative embryo; therefore, there are also secreted molecules that regulate the complement system, such as CD55 and CD46. Integrin αvβ3, CD44 and OPN also prevent complement activation and their secretion is cyclic and seems to be upregulated during the WOI (40,79–81).

4.1.1.3. Endometrial stroma

During the secretory phase, under the effects of P4, cells from the endometrial stroma enlarge and express a wide repertoire of proteins, cytokines, and growth factors that promote autocrine and paracrine changes (40). The main functions of these factors are to:

- Promote hemostasis: To prevent local hemorrhage caused by trophoblast invasion during implantation. These are some of the factors involved in hemostasis: Tissue factor (TF), plasminogen activator inhibitor type 1 (PAI-1) or Serpin E1 (40,82).

- Immune tolerance: P4 during the WOI acts as an anti-inflammatory immunomodulator making the uterus an immune-privileged organ. There is leucocyte recruitment, principally uNK, which comprises 15% to 25% of the cells in the endometrial stroma. They modulate trophoblast invasion through a noncytotoxic mechanism secreting cytokines and other factors. Some of the factors involved in leukocyte recruitment in the stroma are IL-1, IL-11, IL-15, LIF, TGF-β (40,83–86).

- Extracellular matrix remodeling control: Matrix metalloproteinases (MMPs) are matrix-degrading proteinases responsible for the degradation of the functional layer during menstruation. High levels of P4 in the presence of E2 in the secretory phase indirectly suppress the expression of many MMPs. This action is explained by the changes that occur in stromal cell secretions during the WOI. Some cytokines and factors act as direct inhibitors of MMPs but, also, activate tissue inhibitors of metalloproteinases (TIMPs), for this reason, almost all MMP activity is inhibited during WOI (40,87–90).

4.1.1.4. Blood vessels

Blood vessels suffer vascular remodeling and angiogenesis during the menstrual cycle. Spiral arterioles are characteristic vessels that only appear in the secretory phase; their main function is to create a subepithelial capillary plexus. Different signaling molecules, such as vascular endothelial growth factor family (VEGF), fibroblast growth factors (FGFs), angiopoietins, angiogenin or ephrins control endometrial angiogenesis and vessel remodeling (91–94). The angiogenic process is tightly regulated by activating and inhibiting factors that are secreted throughout the menstrual cycle and their effects vary depending on the receptors to which they attach (40).

- VEGF family: these are the most important angiogenic factors. During the secretory phase, VEGF is secreted by neutrophils and uNKs and can also be detected on the surface of epithelial cells. Its function has been associated with the development of the subepithelial capillary network. However, when P4 levels decrease during the premenstrual phase, the action of VEGF on its receptor 2 (VEGFR2) upregulates the expression of some MMPs (95,96).

4.1.1.5. Uterine microenvironment

The endometrial epithelium releases soluble molecules and EVs into the uterine cavity during the endometrial cycle. In the last few years, EVs have gained importance as key molecules in the implantation process and several groups have studied the changes in EV secretions and composition during the cycle. The group of Ng *et al.*, have demonstrated that the staining intensity for protein CD63 (exosome marker) increased across the cycle, which suggested an increase in EV production, to reach a maximum in the mid-secretory phase, the time of endometrial receptivity for implantation (97). Furthermore, EVs can be taken up by blastocyst cells and enhance their adhesive capacity (98). Disturbance of endometrial EV release, content or uptake could contribute to implantation failure, as occurs in several women presenting with infertility (97).

4.1.2. Preparation and evaluation of the endometrium for implantation in ARTs

During IVF/ICSI cycles, women undergo hormone replacement treatments to prepare the endometrium. In this case, medical professionals administer E2 and P4 to simulate the endometrial cycle and prepare the endometrium for implantation (15,16). Usually, evaluation of the endometrium includes ultrasonographic measurement of endometrial thickness (59,61) and ET is scheduled when the endometrium is trilaminar and between 8-14 mm thick. However, the major problem is that, in this "optimal condition", less than 60% of the embryos transferred to the uterus implant (26,99).

Therefore, it is necessary to develop new mechanisms for endometrial receptivity assessment. On the one hand, there is endometrial biopsy, an invasive method that does not allow ET to be performed in the same cycle in which the sample is collected (100,101). On the other hand, there is the analysis of endometrial fluid, which is a non-invasive method and allows ET in the same cycle in which the sample was collected (61). These alternative mechanisms for assessing endometrial receptivity will be explained in more detail in section 5.

4.2. Developmentally competent embryo/blastocyst

Usually, several embryos are produced from a single IVF/ICSI cycle, and it is crucial to select the most viable ones to perform the ET and try to ensure a live child (16). After 2-5 days in culture, the selected embryo is transferred to the uterus and the remaining embryos are vitrified for the future frozen embryo transfer (FET) cycle (18).

Improvements in embryo vitrification techniques have resulted in no significant differences in reproductive outcomes between fresh and FET cycles (18,22). In addition, freeze-all protocols are recommended in some specific cases, such as hyper-responders, because these women are at a high risk of developing ovarian hyperstimulation syndrome (OHSS) (16,102,103). Therefore, more and more FET cycles are being performed (99).

4.2.1. Embryo quality assessment

Traditionally, the assessment of embryo quality is focused on embryo morphology and morphokinetics and is carried out while they develop in culture media (104). Microscopic visualization is performed from the very beginning at certain time points and morphological features and developmental dynamics are annotated (105).

Although there are other evaluation criteria, such as metabolic consumption (106–110), chromosomic analysis (111) or new technologies like "time-lapse monitoring" (112), they are not available in all ART laboratories and morphological assessment continues to be the most widespread assessment system.

In the end, embryos are given a grade based on the results obtained, which is used to predict their potential to achieve the blastocyst stage, implantation rate and pregnancy rate (113,114).

There are different nomenclatures for grade assignment of the embryo quality evaluation; however, they tend to follow the evaluation criteria established in the Istanbul consensus workshop on embryo assessment (113). In Spain, following those recommendations, the Association for the Study of Reproductive Biology (ASEBIR) proposed a scale classification for each embryonic stage (114). Embryos and blastocysts are categorized from A to D according to their implantation outcome **(Figure 10)**:

- Category A: embryo of optimum quality with maximum implantation capacity.
- Category B: embryo of good quality with high implantation capacity.
- Category C: regular embryo with a medium probability of implantation.
- Category D: embryo of poor quality with a low probability of implantation. In this category, there are embryos with various abnormalities that make their probability of implantation practically null.

Figure 10. *ASEBIR classification for blastocysts.* Blastocyst quality assessment according to its inner cell mass and trophoectoderm quality. Image from ASEBIR (114).

4.2.1.1. Time-lapse technology

The Time-lapse video system is an emerging, non-invasive technology that permits the analysis of the most valuable kinetic parameters of embryo division to improve the selection of a single embryo for transfer (104,112,115,116). These video time-lapse systems consist of incubators with built-in cameras (inverted digital microscope) that take images of embryo development at intervals of 5-20 minutes. From the images obtained, it is possible to generate a video of each embryo's development (117,118).

The main advantages that this technology brings to IVF/ICSI laboratories are: (i) better culture conditions and the possibility of evaluating embryos without removing them from the incubator; (ii) objective and precise qualitative and quantitative information; (iii) less exposure to light compared with the amount of light to which embryos are subjected when analyzed in a conventional inverted microscope. It is possible to make a more exhaustive embryo selection based on the kinetics of embryo divisions since the same video can be evaluated by different embryologists obtaining a more objective result (119,120).

The use of artificial intelligence (AI) in combination with morphokinetic data obtained from time-lapse images to perform embryo selection is being studied. It is not yet implemented in standard clinical practice; however, recent studies show that it is a fast and reliable technology to classify embryos and blastocysts. Routine use of AI in assisted reproduction clinics is just a matter of time, although it is currently under development (121,122).

4.3. Adequate embryo-endometrium crosstalk

Adequate embryo-endometrium communication is crucial for successful embryo implantation (123,124) and it begins when the embryo enters the uterus and contacts with the uterine microenvironment (124). Uterine fluid contains nutrients, proteins, lipids and other molecules mainly secreted by the endometrium, which play an important role as a first line of cell-to-cell communication (123–125).

4.3.1. Extracellular vesicles as signaling vehicles

Among the molecules in the uterine cavity, a new intercellular communication tool mediated by extracellular vesicles (EVs) has emerged (97). EVs are an important mode of cell-to-cell communication as they can transfer their contents to other cells altering the recipient cell's behavior (126,127). The presence of EVs in the uterine microenvironment has been described as a new paradigm for embryo-endometrial crosstalk (97,128,129).

Recent studies have demonstrated that EVs released by human endometrial cell lines were taken up by mouse embryos *in vitro* and were able to modify their transcriptomic and adhesive phenotype (130). In the same way, experiments performed with dye-labeled embryo-derived EVs showed that these EVs were uptaken by human primary endometrial epithelial and stroma cells (131).

The relationship between the menstrual cycle and EV secretion from the endometrium has been described to be hormone specific as the protein cargo of endometrium-derived EVs was found to be hormone specific (98,132). These findings were first described in a human endometrial cell line and then validated in a human primary endometrial cell line (98). Functional experiments were performed with the isolated EVs, where it was found that endometrial cell-derived EVs were internalized by human trophoblast cells and were able to increase the receptor cell's adhesiveness (98).

The group of Ng *et al*., (97) were pioneers in identifying EVs from endometrial fluid. They also isolated, via differential ultracentrifugation, EVs from the associated mucus and the endometrial epithelial cell line (ECC1). In addition, they performed miRNA analysis of ECC1 and its EVs and found that the miRNA pattern differed between the two samples.

Concretely, 13 of 227 miRNAs were enriched in EVs (hsa-miR-200c, hsa-miR-17 and hsa-miR-106a), while five of these were only present in cells. They analyzed the potential targets of the EV-associated miRNAs and found that the biological pathways involved were mostly associated with embryo implantation processes. Furthermore, in a meta-signature analysis study, they found that some proteins from their endometrial receptivity-associated gene list had been experimentally detected in human EVs, supporting the presence of EVs in the uterine cavity and highlighting their role in embryo implantation (133).

Following the study of EV-associated miRNAs, another study showed that 6 of 27 maternal miRNAs were differentially expressed in the human endometrial epithelium during the WOI, of these, hsa-miR-30d was the most upregulated. Moreover, they demonstrated that the EV-associated hsa-miR-30 was internalized by mouse embryos

via the trophectoderm. As a result, there was overexpression of some adhesion molecules involved in embryo implantation (130,134).

In an *in vitro* human implantation study, human trophectoderm spheroids were treated with human endometrium-derived EVs. Then, the proteomics profile of treated and non-treated trophectoderm spheroids was compared and 176 proteins were uniquely identified in the EV-treated group. Most of the proteins were related to cell adhesion molecule binding, cell-cell adhesion mediator activity, and cell adherens junctions (135).

In summary, the results obtained from these studies demonstrated the capacity of human endometrium-derived EVs to regulate important steps of the implantation process and highlighted the importance of cell-to-cell communication during implantation.

The classification, biogenesis, composition and functions of EVs will be explained in section 6 and of miRNAs in section 7.

5. <u>Evaluation of the endometrial status</u>

Traditionally, evaluation of the endometrium includes ultrasonographic measurement of endometrial thickness (61), however, when the endometrium is measured in this way, only 35% of embryos transferred to the uterus implant (26,99). Therefore, over the last 80 years, endometrial receptivity has been the focus of numerous research projects to improve implantation rates in ARTs (136,137).

It is fundamental to establish the correct timing of the endometrium before performing the embryo transfer (136,137). However, little progress has been made in translating this knowledge into clinically meaningful predictive tests or treatments.

For this reason, we still need to identify new biomarkers that could help identify the optimal moment for ET. Along this line, two main methods have been developed: (i) endometrial biopsy and (ii) endometrial fluid.

5.1. Biomarkers based on endometrial biopsy: Invasive biomarkers

Endometrial receptivity has been the focus of study for many years and among the first to analyze endometrial receptivity was the group of Noyes *et al*. (138). In 1953, they established the Noyes criteria based primarily on the study of endometrial biopsies during the menstrual cycle to characterize each of the phases. In this way, they categorized the proliferative phase into early, mild and late. In addition, they described the histological changes that occurred during the secretory phase. With the development of the "-omics" (transcriptomics, proteomics, lipidomics...), as well as obtaining histological data, it has been possible to obtain molecular data for each phase of the cycle (136,139). These high-throughput techniques have allowed the examination of changes in gene expression during the menstrual cycle (140–142), the gene expression profile of the WOI (143), transcriptomic modifications during the cycle (101,133,144) and proteomic (145–147) and lipidomic (148,149) content of the endometrial samples obtained at different time points.

This progress has permitted the development of biomarkers for the determination of the state of the endometrium and whether it is receptive or not. However, a biopsy is required to obtain an endometrial sample and same-cycle embryo transfer is not possible because it is detrimental for proper implantation of the embryo (150).

5.2. Biomarkers based on endometrial fluid: Non-invasive biomarkers

The endometrial fluid (EF) is a complex biological fluid, which is a source of many molecules that are secreted by the luminal epithelium, glands, stromal cells, and other substances transudated from blood due to its direct contact with the endometrial cavity (151,152). EF collection can be carried out in two forms, either aspiration or lavage (flushing) collection; both are less invasive than tissue sampling. Only a small volume of fluid (5-50 µl retrieved by aspiration) is present within the uterine cavity and aspirates will often contain blood indicating damage to the tissue and compromising the integrity of the sample (151). Uterine lavage is collected by gently infusing and retrieving 2–3 ml of saline in the uterine cavity so that it washes over the entire endometrial surface (151,152). Importantly, aspiration and lavage are not interchangeable for the purpose of molecular analysis, presumably because soluble molecules are released from the endometrial glycocalyx during lavage (152). Aspiration may be the better technique if sampling is to be performed in the same cycle as the ET (150–152). In addition, it has been demonstrated that endometrial fluid aspiration immediately prior to ET does not affect embryo implantation (150,153).

Endometrial secretions can modulate endometrial homeostasis and receptivity, as well as maintain the preimplantation embryo and initiate the implantation process (124). Therefore, EF is widely used for the study of different gynecological diseases. For example, proteomic analysis of the EF has been useful to diagnose endometrial cancer and assist in predicting the optimal surgical treatment (154), or to discover candidate biomarkers of endometriosis (155), among others.

In addition, the use of biomarkers obtained in a non-invasive manner is gaining strength in the study of endometrial receptivity. Several studies have analyzed uterine secretions during the endometrial cycle, emphasizing the search for biomarkers during the WOI. Some found differentially expressed proteins between the different phases of the endometrium (156–159). Another study revealed that VEGF levels were reduced in the EF during the secretory phase in women with unexplained infertility compared with fertile women (158). Transcriptomic analysis of the EF also described different patterns of transcripts among the menstrual cycle (130). Along this line, lipidomic analysis of the EF has been described as an emerging tool to predict endometrial receptivity (160). However, in most cases, to define the endometrium as "receptive" they have used histological, biochemical, or genetic methods. Nevertheless, the only manner to confirm that an endometrium is receptive is by taking the sample in the same cycle in which the pregnancy has occurred. Because of this, a new concept has emerged for studying the endometrium from a reproductive point of view: **implantative endometrium** (161–163).

5.2.1. Biomarkers of implantative endometrium

The implantative endometrium is described as the endometrium in which implantation occurred in the same cycle as EF aspiration, while non-implantative endometrium is that in which implantation does not occur (162).

The main objective, in the search for biomarkers in ARTs at time of implantation, is not to damage the uterine cavity and to perform the embryo transfer in the same cycle. It has been demonstrated that aspiration of the EF immediately before ET does not negatively affect implantation rates (150,162). Consequently, analysis of the EF aspirated immediately before embryo transfer has been described to be useful to differentiate between an implantative and a non-implantative endometrium. Along this line, few studies have analyzed the EF at the time of embryo implantation (**Table 4**).

Table 4. *Summary of the studies comparing the EF from implantative vs. non-implantative endometrium.*

Authors	Type	Samples	Sample collection	Embryo transfer (ET)	Analysis	Results
Boomsma *et al.*, 2009 (164)	Research article	Implantative (n=68) Non-implantative (n=142)	Just before ET	Day 4 fresh EF	Cytokines	The ratio of TNF-a and IL-1b may serve as an indicator of endometrial receptivity.
Parks *et al.*, 2013 (165)	Abstract	Infertile patients (n=24)	24 h before ET	Frozen blastocyst transfer	Transcriptomics and cytokines	Increased expression of six cytokines (of them IL-6, VEGF, and IL-8) and 17 miRNAs in positive implantation.
Parks *et al.*, 2014 (166)	Abstract	Infertile patients (n=30)	24 h before ET	Frozen blastocyst transfer	Transcriptomics	29 miRNAs were associated with positive implantation. three miRNAs were absent in non-implantative endometrium (miR-891a, miR-522, miR-198). Reduced expression with positive implantation for the MUC protein family.
Azkargorta *et al.*, 2018 (161)	Research article	Implantative (n=50) Non-implantative (n=60)	Just before ET	Day 3 fresh ET	Proteomics	294 proteins were deregulated in non-implantative endometrium.
Matorras *et al.*, 2018 (162)	Research article	Implantative (n=33) Non-implantative (n=33)	Just before ET	Day 3 fresh ET	Proteomics	23 proteins differentially expressed in implantative endometrium: four up-regulated and 19 down-regulated.
Braga *et al.*, 2019 (167)	Research article	Implantative (n=24) Non-implantative (n=17)	Just before ET	Fresh blastocyst transfer	Lipidomics	13 ratios hyper-represented in the non-implantation group. Two hyper-represented in the implantation group.
Matorras *et al.* 2019 (163)	Research article	Implantative (n=15) Non-implantative (n=14)	Just before ET	Day 3 fresh ET	Lipidomics	The comparative analysis revealed eight altered metabolites: seven glycerophospholipids and an omega-6 polyunsaturated fatty acid.
Li *et al.*, 2020 (168)	Research article	Implantative (n=19) Non-implantative (n=19)	Just before ET	Day 5 fresh ET	Transcriptomics	No small non-coding RNAs was found to be differentially expressed between groups.
Ibañez-Perez *et al.*, 2022 (169)	Research article	Implantative (n=45) Non-implantative (n=45)	Just before ET	Day 5 frozen ET	Transcriptomics	Two models with three miRNAs differentiated implantative *versus* non-implantative endometrium.

6. <u>Extracellular vesicles</u>

In the last years, the study of extracellular vesicles (EVs) as a model of cell-to-cell communication has increased, which has led to a change in the understanding of human pathologies and has opened a huge range of possibilities in clinical practice (170–173).

The first EVs were described at the beginning of the 80s as part of the reticulocyte maturation system, as an independent mechanism of lysosomes for the removal and recycling of proteins (174,175). This idea lasted for approximately ten years until it was described that B-lymphocytes secreted vesicles with antigen-presenting function (176). Since then, numerous studies have shown the existence of different EVs secreted by all types of cells, both eukaryote and prokaryote (177).

In addition, it was described that these vesicles could be isolated from biological fluids such as urine, plasma, peritoneal liquid, semen, breast milk, saliva, serum and EF (178–183). Due to their ubiquity, EVs are considered a rich source of non-invasive biomarkers for diagnosis and prognosis of various human diseases (127,184–187).

6.1. Classification of extracellular vesicles

The International Society for Extracellular Vesicles (ISEV) endorses "extracellular vesicles" as the generic term for particles naturally released from the cell that are delimited by a lipid bilayer, cannot replicate, and do not contain a functional nucleus (188). The term EVs encompasses a series of vesicles of different biological origin, such as apoptotic bodies, microvesicles/ectosomes or exosomes.

However, in practice, absolute purification or complete isolation of a unique vesicle type is an unrealistic goal. For this reason, the ISEV suggested the use of the term EVs to avoid using the terms microvesicles or exosomes inaccurately (189).

6.2. Biogenesis and secretion of extracellular vesicles

Although there are many possibilities when describing EVs according to their characteristics, based on current knowledge, EVs can be broadly divided into three main groups according to biogenesis and secretion properties: apoptotic bodies, microvesicles and exosomes (172,190).

6.2.1. Apoptotic bodies

Apoptotic bodies (ApoBDs) are the products of apoptotic cell disassembly that are released from dying cells during programmed cell death (191). Their size is variable (1-5 μm) and includes large, medium, and small apoptotic vesicles. It was recently described that apoptotic cell-derived EVs could be a key mechanism of immune modulation by dying cells (192). As apoptosis occurs in healthy cells undergoing normal turnover but also during immunological process such as inflammation or infections, their role in immune modulation has been highlighted (**Figure 11**) (191,192).

6.2.2. Microvesicles/Ectosomes

Microvesicles range in size from 50 nm to 1,000 nm in diameter but can be larger (up to 10 μm). They are generated by the outward budding and fission of the plasma membrane and subsequent release of vesicles into the extracellular space (172,193,194). Although microvesicles have been studied mainly for their role in blood coagulation (195,196), they were reported more recently to have a role in cell–cell communication in various cell types, including cancer cells (197), where they are generally called oncosomes (**Figure 11**) (190).

6.2.3. Exosomes

The term exosomes was adopted to refer to membrane vesicles, 30-100 nm in diameter, formed from the endosomal system, thus, not originated in a random way (198). The cellular endocytic system consists of a set of highly dynamic membrane compartments that manage the recycling and degradation of membrane receptors and their membrane ligands (198,199). During this process, early endosomes mature to a late endosome by acidification; at this point, intraluminal vesicles (ILVs) are formed by the invagination of the membrane into the lumen of the endosomes (**Figure 11**) (200).
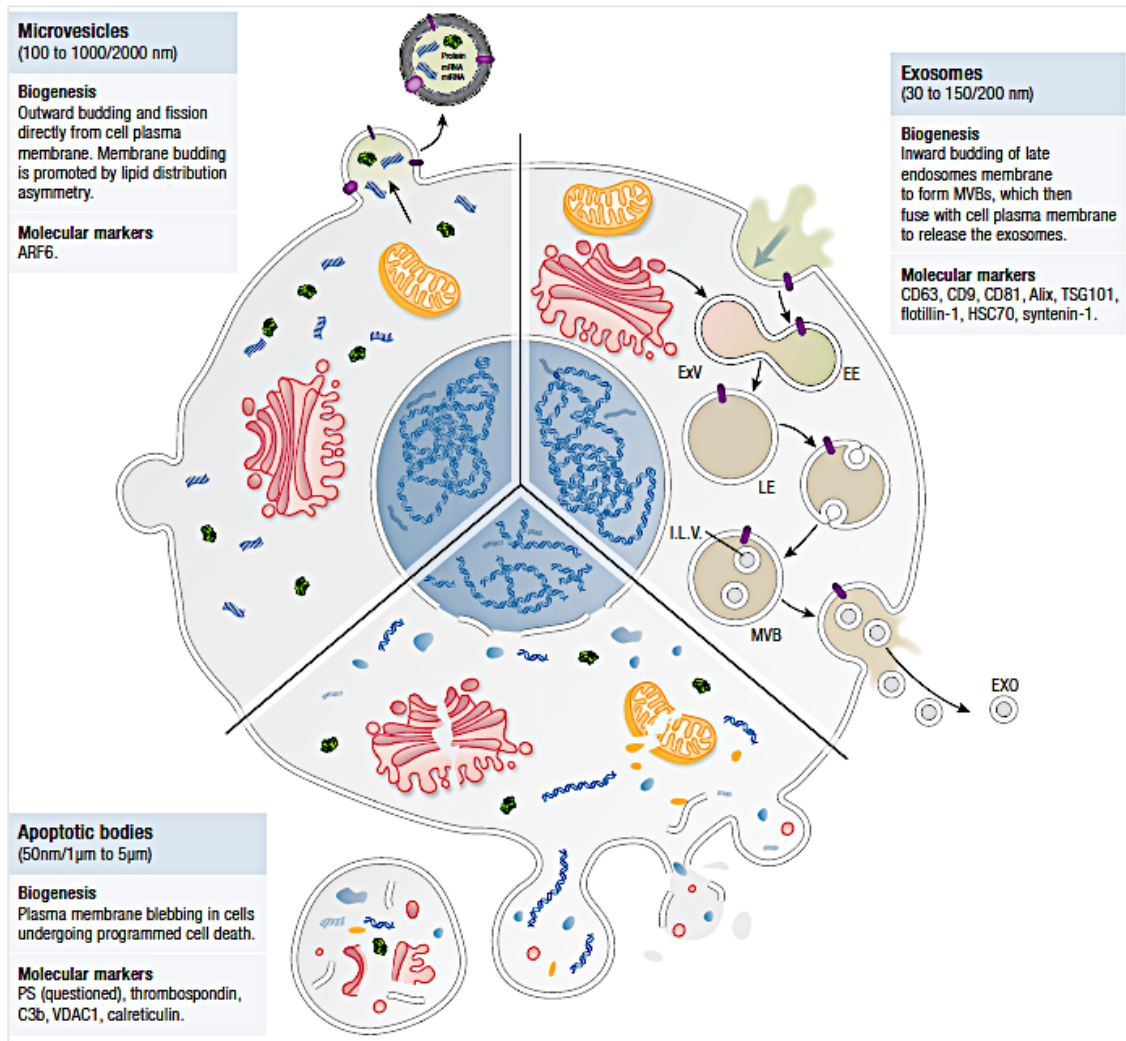
Figure 11. *Different EVs secreted from cells.* From Simon *et al.,* 2018 (200).

During this budding process, cytoplasmic components (miRNAs, mRNAs, DNA, proteins and lipids) are packed inside the ILVs. The late endosome that contains ILVs is called the multivesicular body (MVB), which can transport its content to lysosomes for degradation (degradative MVBs) or, alternatively, to the plasma membrane (exocytic MVBs) (201). When MVBs fuse with the plasma membrane, their content is released into the extracellular space (202). Once the ILVs are outside, they are called exosomes (201,202). Two main pathways have been described as responsible for ILV formation at the endosomal limiting membrane, one ESCRT-dependent and the other ESCRT-independent (190).

6.2.3.1. ESCRT-dependent mechanism

The endosomal sorting complex required for transport (ESCRT) controls vesicle formation, allowing the formation of ILVs (190). The ESCRT machinery is comprised of several protein complexes classified into four subgroups (0, I, II, and III) that have a role in protein cargo selection, clustering and membrane fission (203–205). It has been described that to cluster the ILV formation machinery, it is essential to have specialized tetraspanins-enriched microdomains (CD63, CD9) in the endosomal membrane (206–208). This mechanism is dependent on mono-ubiquitination and clathrin. The ESCRT 0 complex recognizes and binds ubiquitylated proteins, while ESCRT I, II, III induce bud formation and scission, sequentially. ESCRT complex subtypes are associated with multiple proteins such as VPSA, VTA1 or ALIX to control from membrane invagination to final excision of the ILVs (203–208).

6.2.3.2. ESCRT-independent mechanism

The ESCRT-independent mechanism for exosome formation has been related to the presence of certain lipid-microdomains (190). One of these lipid-based mechanisms is lysobisphosphatidic acid, which is enriched in ILVs and has the capacity to drive membrane budding into acidic liposomes just by the pH gradient across the membrane (209–212). A different lipid-based mechanism implicates the sphingolipid ceramide, which at high concentrations appears to help MVB contents escape lysosomal digestion in favor of release as exosomes. Cholesterol is another lipid implicated in MVB/ILV biogenesis. Also, the exosome's surface is enriched in lipid raft microdomains, especially sphingolipids, that may be involved in the initiation of vesicle formation, as lipid rafts are weak points prone to outward bending (209–212).

Taken all together, exosome size is influenced by their cargo and mechanism of formation, suggesting a competitive relationship between ESCRT-dependent and independent mechanisms of ILV formation within single MVBs (213). Lipid-driven mechanism are shared between both mechanisms. The fact that different mechanisms of exosome formation exist could be a possible explanation for the presence of heterogeneous population of MVBs and ILVs and, therefore, exosomes (170).

6.3. Composition of EVs

EVs are phospholipid bilayer enclosed vesicles that contain proteins, lipids and ribonucleic acids. Some of the contents are related to EV biogenesis and, therefore, are common among EV populations, while others are specific to the originating cell (184,202). The EV composition and content can be altered or modified according to cell physiopathology and, therefore, their potential use in therapy and diagnosis has stimulated great interest, as well as the characterization of their molecular composition (184,202). In addition, there are several public databases where information on the EV content can be found: Exocarta (www.exocarta.org) (214), Vesiclepedia (www.microvesicles.org) (215), EVpedia (http://evpedia.info) (177), EVtack (http://evtrack.org) (216).

6.3.1. Protein composition

EVs are enriched in tetraspanins (CD63, CD81, CD9), adhesion molecules (integrins), along with cytoskeleton molecules related to cellular traffic (actin, tubulin), membrane traffic-related proteins (annexin, GTPases (RAB), lipid-raft associated proteins (FLOTILIN-1) and other proteins such as HLA complex proteins, heat shock proteins (HSP70), among others (**Figure 12**) (217). EVs also bear a protein cargo specific to the cell that secretes them. However, due to their origin, exosomes do not have any proteins related to the nucleus (histones, nucleosomes), endoplasmic reticulum, Golgi apparatus, or mitochondria (218,219). Their composition highlights that their formation is not a random packaging, but a specific process that differs in composition and characteristics among different cells and different physiological status (98,218–220).

6.3.2. Lipid components

EVs are enriched in cholesterol, sphingomyelin, glycosphingolipids and phosphatidylserine, while they have a lower proportion of phosphatidylcholine and phosphatidylethanolamine. However, different cellular origins may cause differences in the lipid composition of EVs (221–223) (**Figure 12**).

6.3.3. Ribonucleic acids

The discovery of RNA in EVs and their ability to transfer this material to adjacent cells opened an infinite number of possibilities in diagnosis, regulation and therapy. Like proteins, the microRNA content of EVs began to be seen as a representation of cell status (224). This thought was reinforced by the demonstration that most extracellular miRNAs in serum and saliva were enriched in the EV fractions. On the contrary, the presence of DNA in vesicles is contradictory, the general conception is that DNA associated with vesicles is adhered and not contained within them (**Figure 12**)(217,225).
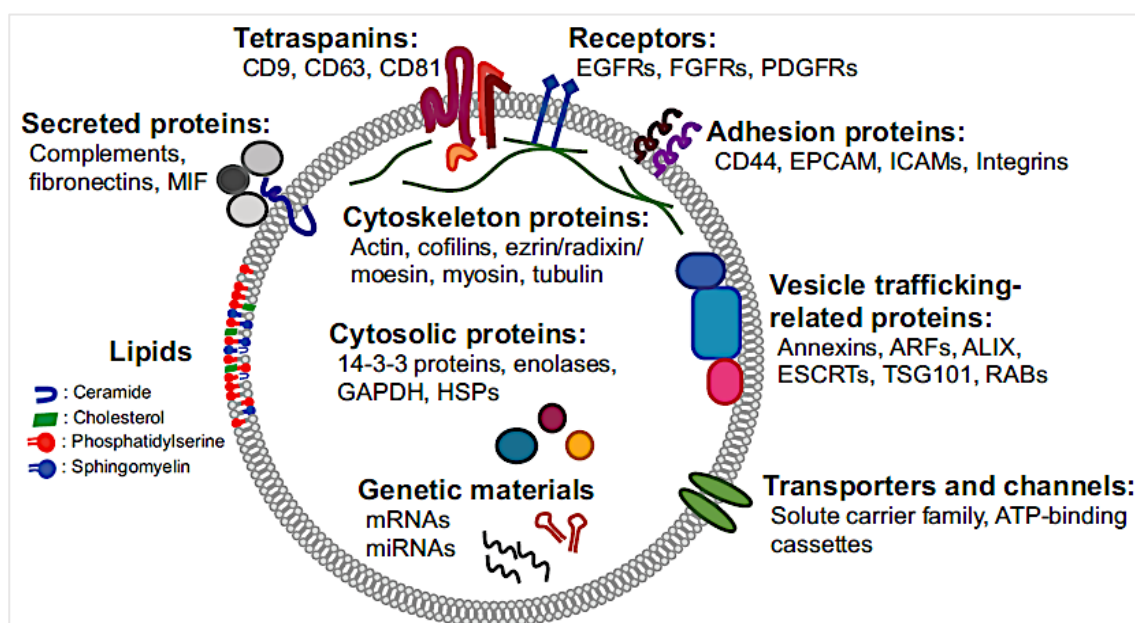
Figure 12. *EVs composition.* From Choi *et al.,* 2015 (217).

6.4. Functions of EVs

EVs are widely known to be mediators of intercellular communications. They act as a medium for the transmission of information to a multitude of cells and locations. As EVs act in autocrine, paracrine, and endocrine manners, this information can modify the behavior of the receptor cells (226). Thus, EVs play important roles in both physiological and pathological processes. Under physiological conditions, EVs are related to different cellular processes, such as proliferation, differentiation, toxicity, control of cellular activity or modulating the immune response, among others (202,227–229).

On the other hand, EVs derived from pathological cells can produce a pro-malignant environment, as is the case of most cancer cells (227,228). EVs derived from cancer cells have been reported to be involved in all stages of cancer development (tumorigenic transformation, angiogenesis, modulation of the immune response…) (202,227–229). However, the mechanisms by which these vesicles can control the different responses are not clearly known.

6.4.1. Internalization of EVs

Once EVs have been secreted, they interact with the recipient cells. Although the interaction mechanisms are still under debate, three major methods have been described: receptor-mediated signaling, direct fusion and internalization/endocytosis (217). In the case of receptor-mediated signaling, the EVs exhibit ligands, such as integrins, which interact with the receptors located on the surface of the target cell, inducing the activation or inhibition of molecular signal transduction pathways (230). On the other hand, in both direct fusion and internalization, the vesicular content is delivered into the cell. In the former, there is a direct interaction between the plasma and vesicular membranes, with a consequent fusion of these. In the second, a receptor-mediated endocytosis will occur (**Figure 13**) (217,230,231).
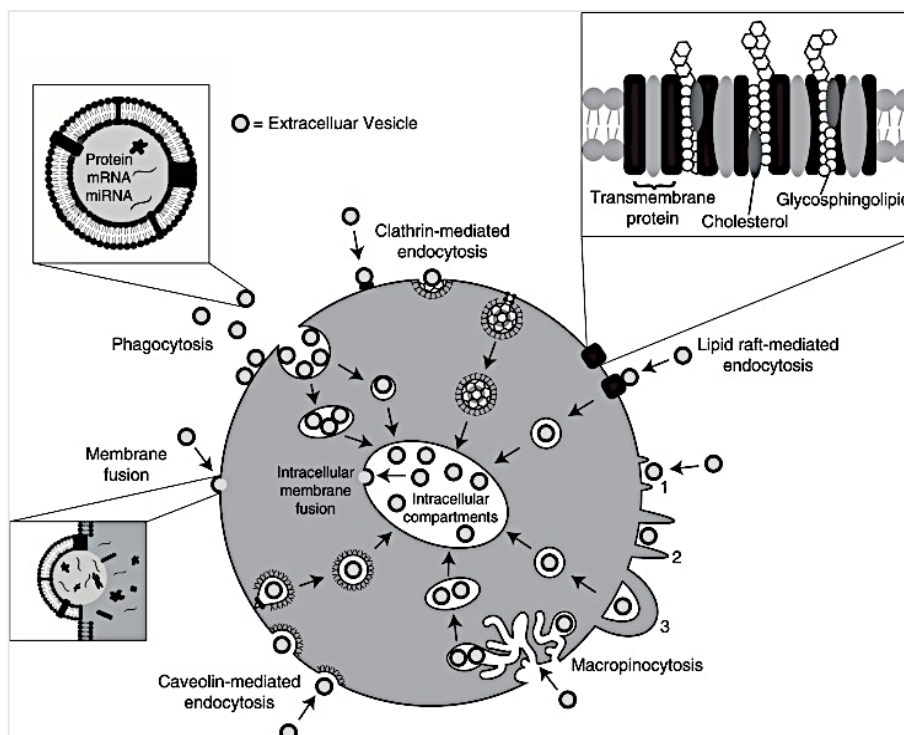
Figure 13. Routes and mechanisms of extracellular vesicle uptake. Release of EVs from donor cell and internalization in the receptor cell. From Mulcahy *et al.,* 2014 (230).

6.5. EVs from biological fluids as a stable biomarker resource

EVs offer many advantages that make them interesting to use as biomarkers. Firstly, EVs are formed by a phospholipid bilayer, composed mainly of saturated lipids. This composition makes the vesicles more resistant and provides greater protection to the internal molecular contents (232). Secondly, the presence of some proteins in the EV membrane may allow the specific identification of the vesicle type (CD63+, CD81+, CD9+), allowing the vesicles to be isolated (using affinity or immunoprecipitation columns, among others) and to selectively study their content (232). Thirdly, the analysis of their content can reveal the cellular state of organs that are difficult to study *in vivo* (233)*.* Therefore, EVs and their content can be used as biomarkers with a great specificity that will allow the identification and classification of different pathologies (232,233).

6.6. Isolation methods

One of the great challenges when it comes to studying EVs as biomarkers is their purification. This can be performed by physical methods (such as gradient ultracentrifugation at speeds of over 100,000 x g) or using surface markers (anti-tetraspanin antibodies such as CD63) (**Table 5**) (200). These techniques involve a great investment in terms of equipment, reagents and time, which clinically can lead to increases in bioassay prices. Likewise, several biotechnology companies have designed rapid EV purification kits, which allow these vesicles to be purified quickly, specific to the type of source. In summary, the trend nowadays is to establish a methodology for analyzing EVs from biological fluids in clinical settings, where the sample is limited and no sophisticated equipment is available (200). Along this line, a few studies have described how to isolate EVs from endometrial aspirates or uterine flushing (234,235). However, one of the studies is based on an ultracentrifugation protocol, which makes its incorporation into clinical practice difficult as not all centers have ultracentrifuges (234). While, in another study, the methodology setup was for analyzing EVs from uterine flushing (235).

Table 5. Classification and summary of the different current methods for EV isolation. From Simon *et al.,* 2018 (200).

Method	Technique	Isolation principle	General Workflow	Advantage	Limitation
Centrifugation	Serial differential ultracentrifugation	Sedimentation velocity	Serial or differential centrifugation: 1) 300xg, 10 min to remove cells 2) 2000xg, 10 min to remove cell debris, apoBDs 3) 10,000/20,000xg 30 min to isolate MVs. 4) 100,000/200,000xg, 70 min to isolate EVs.	- Broad application - Standardization - Ease of use - Reproducibility - Yield	- Sedimentation dependent on density, tube length, sample viscosity, concentration and vesicle aggregation
	Density gradient	Buoyant density	Generally introduced to further purify distinct types of EVs. Various reagents, including sucrose or iodixanol. Crude EV populations loaded either on top (float down) or bottom (float up) of gradient. Ultracentrifugation performed under reestablished conditions	- Purification: increases EV population purity from: protein aggregates, RNA–protein complexes, separation of EV subpopulations within the same type - Soft isolation approach - Clinically applicable medium (iodixanol) - EV homogeneity	- Yield - Reproducibility - Trained user
Size exclusion	Filtration	Size/shape	Generally interspersed within centrifugation steps: prior to centrifugation, supernatants are challenged through syringe filters	- Easy to use - Further stringency of the populations based on their canonical sized - Reproducible	- Yield loss within filtering membrane - Risk of vesicle deformation
	Ultrafiltration	Size	Centrifugal filtration units of prefixed molecular size range that selectively retain vesicles Previous studies shown to isolate distinct subtypes of EVs using this strategy	- Easy to use - Quick technique - Reproducible	- Yield loss within filtering membrane - Risk of vesicle deformation
	Chromatography	Size/charge	Purification of EVs based on surface charge or size	- High resolving power; improved purification of EVs from proteins and lipid particles - Limits EV and protein aggregation based on buffer used - Less sensitive to the viscosity of the media - Respectful with EV functionalities and biological properties - Shorter isolation times	- Usually coupled to centrifugation to remove cell debris and recover EV containing fractions - Often issues with volume or buffer associated with elution

Table 5. *Continued.*

Method	Technique	Isolation principle	General Workflow	Advantage	Limitation
Immunoaffinity		Presence of specific EV surface molecules	Microbeads coupled to antibodies are incubated with EVs for specific surface marker recognition (i.e., A33, EpCAM, CD63). Afterward, beads are washed and recovered by precipitation or magnetism.	- Separation based on specific molecules further than by size - Selectivity - Resolution - Speed of isolation	- Sometimes coupled to centrifugation and/or filtration to initially remove larger cellular debris fractions - Select surface markers of EVs are not always known or available - Cost - Yield
Polymeric precipitation		Weight increase at low centrifugal force	Incubation of polymerization kit reagents with EV solution and recovery by low-speed centrifugation	- High speed - Simple procedure	- Possibility of coprecipitating impurities - Unable to separate EV fractions - Ideal only for small (60 to 180 nm) EV populations
Microfluidics	Different possible principles:	(1) Presence of specific molecules	(1) EVs are passed through a microfluidic system and EV specific markers are recognized by antibodies on a device surface	- Reduced sample volume needed	- Habitually couple to centrifugation to remove undesired EV populations
		2) Physical properties such as size	(2) Still not applicable for EVs	- Smaller processing times and costs, maintaining high sensitivity	- Unable to differentiate EV populations
		(3) Microfluidic filtration	3) Combination of microfluidic and polymer filter that allow the passage of EVs under a certain size	- Possibility to process, quantify and image the samples within the system itself	- Still under development fractions

7. <u>MicroRNAs</u>

Since 1993, when the first small non-coding RNA was identified, knowledge about microRNAs has grown exponentially(236). MicroRNAs (miRNAs) are a type of non-coding RNA that regulate approximately 50% of human genes. MiRNAs comprise a large family of 18-22 nucleotide long RNAs that have emerged as key regulators of genes at the post-transcriptional level (236,237).

7.1. MicroRNA biogenesis

Most miRNA genes are usually transcribed by RNA polymerase II from different locations into long primary transcripts called primary-miRNAs (pri-miRNAs) (300-5000 bp) (237). The main characteristics of these pri-miRNAs are: (i) central double-stranded RNA (dsRNA) region of 30-40 nucleotides; (ii) a terminal loop affording a hairpin structure; and (iii) two single-stranded RNA (ssRNA) regions at each opposite end of the central region (238–240). In the nucleus, the pri-miRNA is processed by a ribonuclease protein complex including DROSHA, which targets and cleaves the flanking ends of the hairpin, and DCGR8 that stabilizes the complex on the pri-miRNA. The newly formed molecules are known as precursor-miRNAs (pre-miRNAs) (70-100 nucleotides-long) and maintain both the dsRNA structure and terminal loop. Following excision, the pre-miRNA stem loop is transported out of the nucleus via the transport protein exportin-5 using an active transport mechanism with RAN GTPase (240–242).

Once in the cytoplasm, the pre-miRNA is targeted by another ribonuclease, DICER, which cleaves the molecule by removing the loop portion of the hairpin leaving a duplex miRNA (≈22 nucleotides-long) (240–242). To form a mature single chain miRNA, the miRNA duplex must be separated. The thermodynamic stability of the two ends of the duplex may determine which strand is selected as mature miRNA (guide strand) and which one is degraded (passenger strand) (243–245).

The mature strand is incorporated into a multiprotein complex known as RISC (RNA-inducing silencing complex), composed of the *EIF2C1* (AGO1), *EIF2C2* (AGO2), *SND1, GEMIN3, GEMIN4* and *CCR-NOT* complex genes (243–245). The RISC complex transports the mature miRNA to its target messenger RNAs (mRNAs). The miRNA binds to mRNA complementary bases at the 3´ UTR region (246,247).

MiRNAs can be separated into two broad categories depending on their position in the genome: canonical and noncanonical (244). Canonical miRNAs are those found in intergenic regions and are cleaved by Drosha/DCGR1 to form the precursor miRNA (pre-miRNA). Noncanonical miRNAs are pre-miRNAs that are cleaved from intron sequences using splicing instead of Drosha (**Figure 14**) (244,248,249).
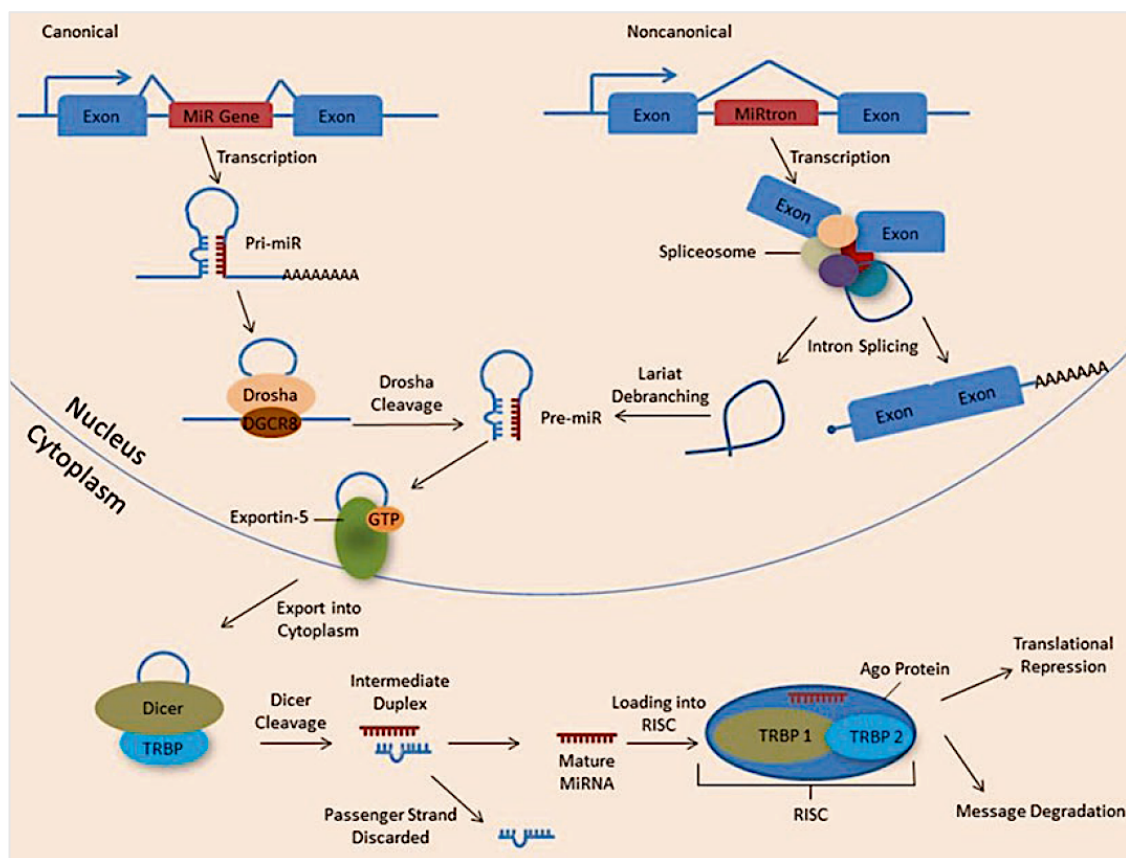
Figure 14. *Schematic view of miRNA biogenesis.* From King and Borchert, 2017 (244).

7.2. miRNA function

miRNAs present a characteristic target recognition sequence of approximately seven base pairs known as the seed region (239,244). The miRNA acts by specific binding of the seed sequence to a complementary target sequence by means of the RISC complex. By sharing the seed region, members of the same miRNA family are potential regulators of the same set of mRNAs and can be grouped into families called miRNA clusters (250,251). The RISC complex consists of several different proteins, is between 200 and 500 kDa and exhibits ribonuclease activity. Messenger RNAs are incorporated into the RISC complex when targeted by miRNAs. AGO proteins in RISC cleave mRNAs that are highly complementary to the incorporated miRNA, whereas mRNAs that are mostly imperfectly bound to the miRNA are silenced by translation inhibition (252,253). The best described protein subunits of RISC are the RNases Dicer, AGO 1 and 2. AGO 1 and 2 serve as the central components of RISC and are responsible for translational repression and cleavage/degradation (250–253). MicroRNAs regulate genes involved in numerous biological processes such as cell development, differentiation and proliferation, as well as hematopoiesis, angiogenesis and apoptosis (239,244,250–253).

However, because the sequence complementary to the seed of an miRNA is short, odds are it can probably be found in more than one place in the human genome. Therefore, an miRNA can degrade or repress the translation of many target mRNAs that contain sequences complementary to its seed region (251–253). On the other hand, there is also the possibility of a gene being regulated by multiple miRNAs. MiRNA-mediated regulation can be affected either by alterations in miRNA levels (due to changes in processing genes and/or pre-miRNAs) or changes in the target binding sequence. Many databases (Mirwalk or Targetscan, among others) propose possible *in silico* miRNA targets, but few interactions are experimentally validated (239,244,250–253).

7.3. Nomenclature

miRNAs are named using a sequence of four identifiers (254). The first three letters signify the organism, for example: hsa refers to human, while mmu refers to mouse. The second part of the name is designated to differentiate between the mature miRNA sequence (miR) from the miRNA gene and the predicted stem-loop portion of the primary transcript (mir). The third identifier is a number, which is sequential, at the time of naming it will receive the next number after the last described miRNA.Finally, the last part is used to determine the strand from which the mature miRNA is going to be produced, 5p refers to 5' arm and 3p to 3' arm (254–256) (**Figure 15**).
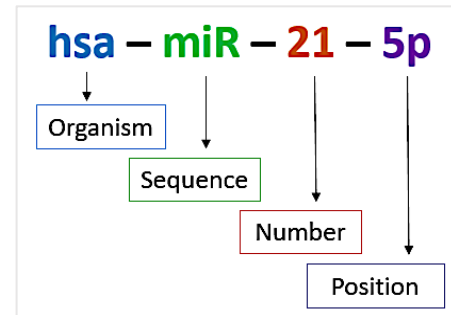
Figure 15. *Nomenclature of miRNAs.*

7.4. Utility of miRNAs as Biomarkers

The utility of extracellular miRNAs as potential biomarkers is being widely studied as they have been shown to be stable (protected from ribonucleases) in different biological fluids, in addition, they are reproducible and exhibit a high tissue specificity between individuals (257,258). Different alterations in miRNA expression have already been described to be strongly related to the appearance and development of diseases such as cancer or neuroblastoma (257,259–261).

The mechanisms by which miRNAs are protected against endogenous ribonuclease activity has been hypothesized to be due to miRNAs being packaged inside EVs, especially exosomes (262,263). The miRNA profile of EVs differs from that of the parent cell, indicating active loading or sorting of miRNAs into these vesicles. Some studies have suggested a role of AGO2 and other RNA-binding proteins in the regulation of miRNA loading into EVs (262,263). Therefore, the isolation of EVs from biological fluids and the analysis of their miRNA cargo has been gaining strength as a novel biomarker discovery procedure (264).

HYPOTHESIS

II. HYPOTHESIS

Implantation is a complex process that requires synchrony between the development of the endometrium and of the embryo, as well as adequate embryo-endometrium communication. Extracellular vesicles are of paramount importance in this crosstalk as it has been demonstrated that endometrium-derived EVs are taken up by preimplantation embryos and can modify their transcriptomic and adhesive phenotype. Among the molecules associated with EVs, miRNAs play fundamental roles as gene regulators at the post-transcriptional level, especially during early embryonic development since they regulate cell proliferation and differentiation.

Therefore, we hypothesize that the analysis of free or EV-associated miRNAs from endometrial fluid obtained from women undergoing FET on day 5 would provide a biomarker signature useful to differentiate between an implantative and non-implantative endometrium.

OBJECTIVES

III.   OBJECTIVES

1. Main objective

1.1. To define, by means of non-invasive methodology, an miRNA signature that recognizes an implantative endometrium.

The main objective of this work is to define, by means of non-invasive methodology, an miRNA signature that allows us to recognize an implantative endometrium. By determining the state of the endometrium, it would be possible to change the ET strategy when the results show an unfavorable implantative pattern, improving the implantation rates and preventing the loss of embryos when they are transferred to a non-implantative endometrium.

2. Specific objectives

To achieve the main goal, the following specific objectives have been proposed:

2.1. To optimize EF sample preparation and characterize the EVs and miRNAs in EF samples.
-   To optimize sample collection and preparation by performing an experiment with a mucolytic agent called dithiothreitol.
-   To characterize the EV and miRNA content of EF samples by size exclusion chromatography and RNase assay.
-   To optimize the polymer-based precipitation method to use it with EF.

2.2. To establish a robust methodology for analyzing free and EV-associated miRNAs from EF in clinical settings.
-   To compare five different methods to extract RNA from EF. Two of them will be based on direct RNA extraction and the other three will have an EV enrichment step before RNA extraction.

2.3. To apply the selected methodology in a sample set (Discovery cohort) with different implantation outcomes to design a predictive model of implantative endometrium.

- To apply the selected method in samples from a discovery cohort. We will collect the EF samples from women undergoing FET on day 5, just before the ET. We will perform the experiment with 30 samples, 15 from women in whom the implantation was successful and 15 in whom it was not.

- To characterize the EF samples by Western blot analysis (WB) and Coomassie blue staining (CB).

- To analyze the extracted RNA with small RNA-seq and we will perform differential abundance analysis to discover miRNAs associated with implantation outcome.

- To confirm the results by qPCR in the same samples and we will design a predictive model of implantative endometrium.

2.4. To validate the predictive models in a new independent cohort (Validation cohort) of women with different implantation outcomes.

- To validate the models by qPCR in the validation cohort (implantative endometrium (n=30) and non-implantative endometrium (n=30)).

- To characterize EF samples by WB, spectrophotometry and CB.

2.5. To investigate the association of the validated miRNAs with EVs and their biological function in the implantation process.

- To investigate the association of the validated miRNAs with EVs by size exclusion chromatography and RNase assay.

- To determine their biological function by analyzing their predicted target genes.

MATERIALS AND METHODS

IV.   MATERIALS AND METHODS

1. Endometrial fluid samples

1.1.   Ethical approval

Ethical approval for the study was obtained from the Cruces University Hospital Ethics Committee and Institutional Review Board (CEIC 11/45) and all participants gave written consent regarding their participation.

1.2.   Study population

The population under study consisted of a cohort of 162 women who attended the Human Reproduction Unit of Cruces University Hospital (Basque Country, Spain) from January 2018 to February 2021.

1.2.1. Inclusion criteria

The inclusion criteria in the setup study were:

  i)   Age between 18 and 37 years.

  ii)   Cycle duration between 27 and 29 days.

  iii)   Absence of ovulatory disorders, myomas, endometriosis, polyps, uterine scars or hydrosalpinges.

  iv)   Normal uterine and ovarian ultrasound.

  v)   Anti-Müllerian hormone > 0.4 ng/ml

  vi)   Absence of history of gynecological infections, immune disorders or gynecological surgery.

The inclusion criteria for the discovery and validation cohorts also included:

  vii)   FET on day 5 of good quality embryos (types A and B of ASEBIR) classification (114).

  viii)   Transfer of 1-2 embryos resulting from own oocytes.

1.2.2. Participants

For the setup and optimization of the techniques, samples were collected from women who came to the examination room before starting any fertility treatment. Samples were obtained during a natural cycle, 16-21 days after the beginning of menstruation. For the application of the selected method, EF was obtained from a group of women undergoing FET on day 5 and the sample was collected immediately before ET.

Of all the women included in the study, 72 participated in the setup, 30 in the discovery of the predicted models and 60 in the validation of the models (**Figure 16**). Of these, 45 achieved pregnancy and were included in the implantative endometrium group, 45 did not achieve pregnancy and were included in the non-implantative endometrium group. Pregnancy was defined as visualization by vaginal ultrasound (US) of a gestational sac four weeks after ET. Cases with a positive β-hCG test where a gestational sac was not seen upon vaginal ultrasound (biochemical miscarriages) were not included in the study. The main characteristics of the study population of women undergoing ART is summarized in **Table 6**.
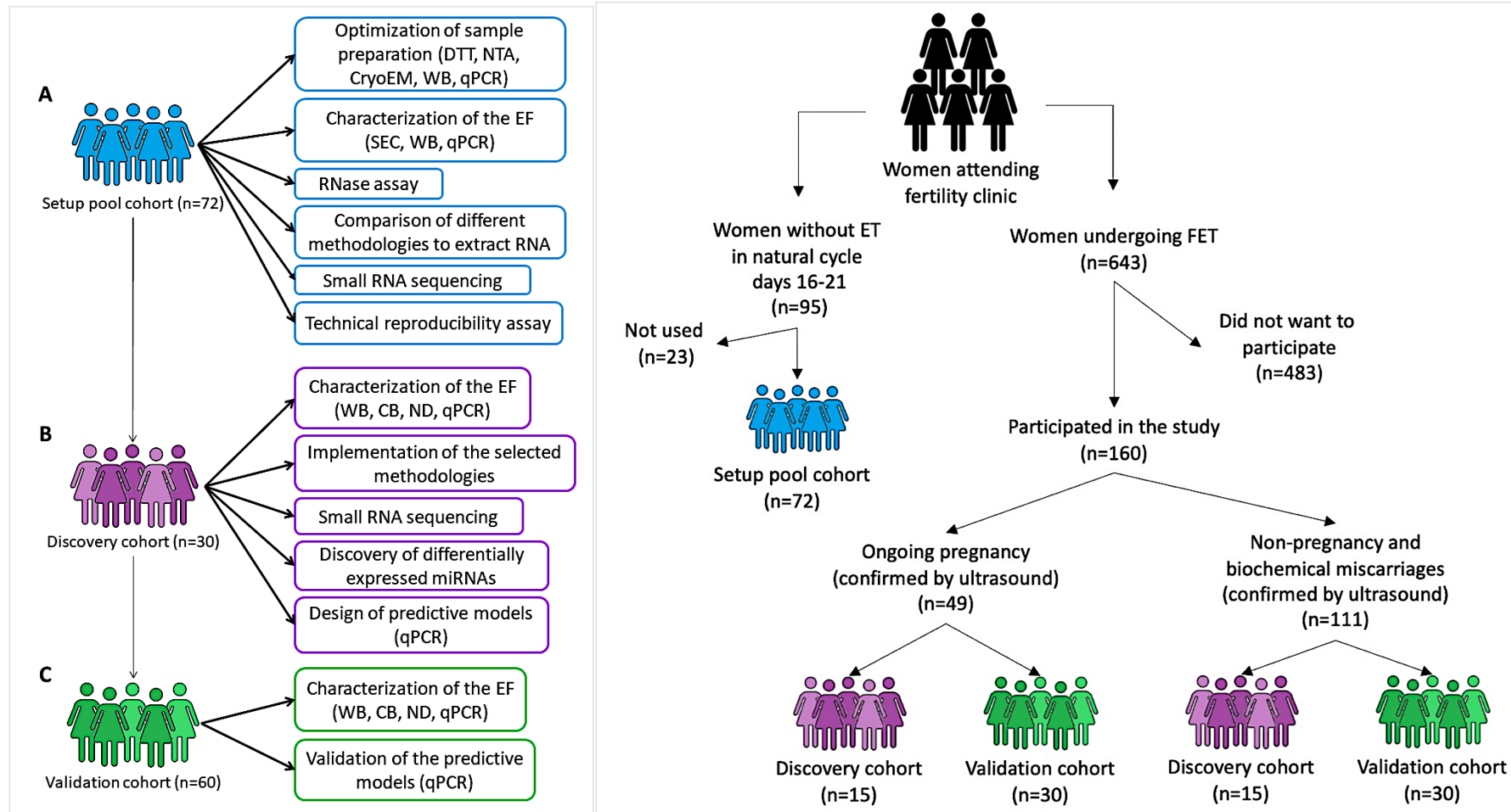
Figure 16. *Workflow summarizing the experimental design.*

(A) Setup pool cohort: endometrial fluid (EF) of volunteer women was collected during the secretory phase of natural cycles, 16-21 days after the beginning of menstruation. EF supernatants had a volume of between 400-1300 µL and an EF pool was made to perform the different experiments. **(B) Discovery cohort:** EF was collected immediately before FET from 30 women. Fifteen achieved pregnancy and were included in the implantative endometrium group and the other 15 did not achieve pregnancy and were included in the non-implantation endometrium group. **(C) Validation cohort:** samples were obtained immediately before the FET from 60 women. 30 achieved pregnancy and were included in the implantative endometrium group and the other 30 did not achieve pregnancy and were included in the non-implantation endometrium group. **CB:** Coomassie blue; **Cryo-EM:** cryo-electron microscopy; **DTT:** dithiothreitol; **ND:** nanodrop, **NTA:** nanoparticle tracking analysis, **qPCR:** real-time quantitative PCR, **SEC:** size-exclusion chromatography, **WB:** western blot. **ET:** Embryo transfer. **FET:** Frozen embryo transfer.

59

Table 6. *Main characteristics of the study population of women undergoing ART.*

	Discovery cohort		Validation cohort	
	Implantative endometrium (n=15)	Non-implantative endometrium (n=15)	Implantative endometrium (n=30)	Non-implantative endometrium (n=30)
Woman's age at transfer (years)	36.7 ± 2.6	36.3 ± 1.8	36.6 ± 2.3	36 ± 3.4
Woman's age at cryopreservation (years)	35.5 ± 2.4	35.1 ±1.7	35.8 ± 2.5	35.1 ± 3.4
BMI (kg/m^2)	26.2 ± 4.4	25.3 ± 1.9	24 ±5.2	23.9 ± 4.7
Smokers (%)	26.7	25	25	14.3
Primary infertility (%)	78.6	73.3	53.6	64.3
Previous insemination failure (%)	40	41.6	17.3	25
Male factor (%)	37.5	26.7	14.8	39.3
Tubal factor (%)	6.7	0	28.6	17.9
Estradiol on the day of hCG (pg / ml)	3580.1 ±1820.2	4101.4 ± 1154.6	3807.9 ± 2560.3	3937.1 ±1445.5
Oocytes obtained	13.5 ±5.2	15.6 ± 7.5	14.1 ±6.9	13.3 ± 6.7
Metaphase II oocytes	11.73 ±5.1	13.2 ±5.7	12.3 ± 5.9	11.2 ± 6.1
Fertilized oocytes	7.2 ± 2.4	7.9 ±3.8	8 ± 4.8	7.5 ± 4.5
Frozen embryos	3 ± 1.7	3.9 ± 3.9	4 ± 3	3.6 ± 2.5
Embryos transferred	1.3 ± 0.5	1.3 ± 0.5	1.4 ± 0.5	1.1 ± 0.4
Twins (%)	6.7	NA	0	NA

Statistical significance was assessed using the unpaired Student's t-test. There were no significant differences between the clinical characteristics of the women in the discovery and validation cohorts (implantative versus non-implantative) or discovery versus validation cohort. Data are expressed as mean ± SD unless specified otherwise. NA: not applicable. The endometrium was considered implantative when pregnancy was confirmed by vaginal ultrasound showing a gestational sac four weeks after embryo transfer.

1.3. Sample collection, preparation and storage

EF was aspirated with a catheter used for ET (Frydman, Instrumentos Médicos Estériles SA, Spain) connected to a 10 mL syringe, under abdominal ultrasound guidance. Sample extraction was performed by gentle manual application of negative pressure with the syringe. To prevent contamination with cervical mucus, aspiration was interrupted at the internal cervical os. Special care was taken in the collection procedure to avoid touching the uterine fundus or injuring the cervix, and to minimize sample contamination with blood and endometrial tissue. In cases with excessive vaginal secretions, the vagina was cleaned with saline solution before aspiration. Aspirate volumes ranged from 5 µL to 50 µL.

After aspiration, the 10 mL syringe was replaced with a 2 mL syringe containing 1.5 mL saline solution and the aspirates were mixed and expelled in a cryogenic tube (5-50 µL of EF + 1500 µL 1X Dulbecco's PBS (DPBS) (Gibco, Thermo Fisher Scientific, # 14190250, MA, USA). The mixed samples were centrifuged to remove contaminants at 2,000 x g for 5 min and supernatants were then frozen at −80 °C until processed. The dilution of the supernatants was 1:30, with a volume comprising between 400 µL and 1300 µL (**Figure 17**).
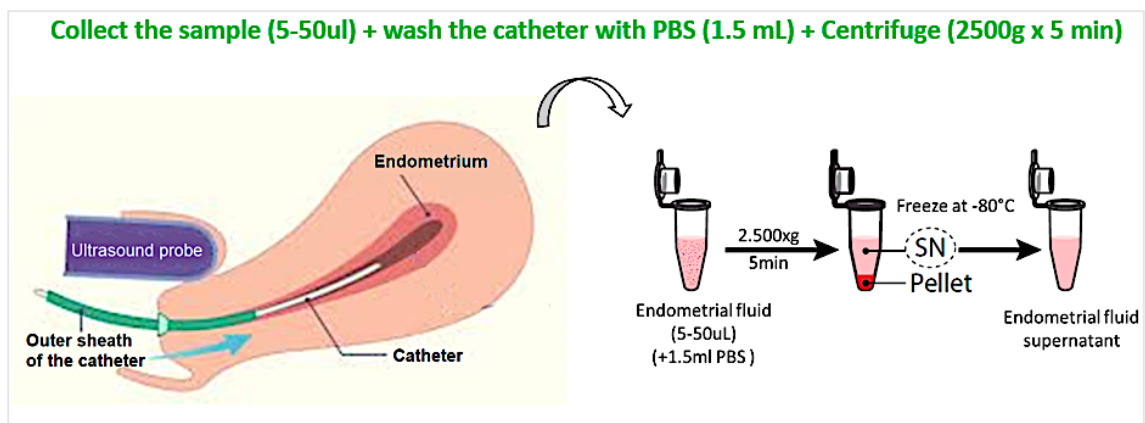
Figure 17. Workflow of sample collection and storage.

1.4. Endometrial preparation before embryo transfer

The management of endometrial preparation was always carried out using the same protocol. A vaginal ultrasound was performed on day 1 or day 2, to confirm ovarian quiescence (absence of follicles > 10 mm). An artificial cycle was started on day 2, administering 6 mg of estradiol daily (Progynova, Bayer, Barcelona, Spain). Endometrial development was monitored by serial vaginal ultrasounds and when endometrial thickness reached 7 mm, the transfer day was scheduled. Vaginal progesterone at a dose of 400 mg/12 h (Utrogestan, SEID, Barcelona, Spain) was started the next morning and ET was performed on the fifth day of progesterone administration. If pregnancy was achieved, the doses of estradiol and progesterone were maintained until the 12th week of gestation.

1.5. Embryo vitrification/thawing

Embryo vitrification was performed on day 4 or day 5 on a Cryotop® device (Kitazato BioPharma Co., Shizuoka, Japan). Embryos were cryopreserved and warmed with the Kitazato vitrification/warming kit (Kitazato BioPharma Co.), according to manufacturer's instructions. Frozen day 4 embryos were thawed and cultured 24 hours prior to ET and day 5 blastocysts 2 hours prior to ET.

2. <u>EV enrichment methods</u>

2.1. Size-Exclusion Chromatography (SEC)

A Poly-prep Chromatography Column (BioRad #731-1550, Hercules, USA) was filled with 2.5 mL of Sepharose CL-2B Cross-Linked resin (Sigma #CL2B300-100ML) and left packing overnight at 4°C. Then, the column was washed twice with 2.5 mL of 1 x DPBS. Three aliquots of 400 μL from a pool made up of samples from the setup cohort were used. Each aliquot was applied to the column and once it had entered, 4 mL of 1 x DPBS were added.

The SEC separated the sample into 12 fractions (F1-F12), the EVs being eluted mainly in F3, but also from F4 to F5 as described by Prieto-Fernández *et al.,* (265). Fractions F1 to F10 had a final volume of 200 μL and F11 and F12 had a final volume of 1 mL. One aliquot was used for RNA extraction with the mirVana™ PARIS™ Kit and the RNA obtained in F3 and F4 was further analyzed by small RNA-seq. The other two aliquots were characterized by WB.

2.2. Polymer-based precipitation method (PBP)

Since there was no published protocol for applying the Invitrogen Total Exosome Isolation Reagent in EF, we compared Total Exosome Isolation Reagent from the cell culture media (Invitrogen by Thermo Fisher Scientific, #4478359) and Total Exosome Isolation Reagent from other body fluids (Invitrogen by Thermo Fisher Scientific, #4484453). Although both worked well with EF, we used #4478359, which has a better cost-effectiveness ratio.

We optimized the following protocol.

1) Centrifuge the EF supernatants at 3000 g for 30 min at 4°C.

2) Transfer the supernatants to a fresh tube and add 1 volume of the Total Exosome Isolation Reagent (1:1).

3) Mix by vortexing until there is a homogeneous solution and incubate the sample for 30 min at room temperature.

4) After incubation, centrifuge the samples at 10,000 g for 1 hour at 4°C.

5) Aspirate the supernatant by pipetting and discard.

6) The EVs are contained in the pellet, which may not be visible, at the bottom of the tube.

7) Add 100 μL of 1 x DPBS to resuspend the pellet. The resuspension volume could be modified according to the requirements of each case.

2.3. Ultracentrifugation (UC)

Ultracentrifugation (UC) was carried out in a single step (100,000 xg for 75 min at 4°C) using a Beckman-Coulter TLA 120.2 rotor. EV pellets were resuspended in 100 µL of 1 x DPBS.

3. <u>RNA extraction methods</u>

We used two RNA isolation methods and followed the manufacturer's instructions for the mirVana PARIS^{TM} Kit (Thermo Fisher Scientific, # AM1556) (DCT-M) and the Norgen Plasma/Serum RNA Purification kit (DCT-N). Two different Norgen kits were used as needed; the midi kit (Norgen Biotek Corp., # 56100, Ontario, Canada) or the mini kit (Norgen Biotek Corp., # 55000). The RNA was eluted in nuclease-free water (Ambion, # AM9930 by Thermo Fisher Scientific).

4. <u>cDNA synthesis and TaqMan miRNA assay</u>

Following the manufacturer's recommendations, cDNA was synthesized from 2 µL of RNA using the TaqMan Advanced miRNA cDNA Synthesis kit (Applied Biosystems, # A28007, by Thermo Fisher Scientific).

The TaqMan reactions carried out were TaqMan Fast Advanced Master Mix (Thermo Fisher Scientific, # 4444557) and TaqMan Advance miRNA assays (Thermo Fisher Scientific, #A 25576).

The qPCR was performed in a Viia7 or QS6 systems and data were analyzed via QuantStudio Real-Time PCR System software version 1.3 (Applied Biosystems, by Thermo Fisher Scientific).

The expression profiles of seven EV-associated-miRNAs were analyzed as reference miRNAs:

1. hsa-let-7-5p (478579_mir, Thermo Fisher Scientific)
2. hsa-miR-17-5p (478447_mir, Thermo Fisher Scientific)
3. hsa-miR-200c-3p (478351_mir, Thermo Fisher Scientific)
4. hsa-miR-30c-5p (478008_mir, Thermo Fisher Scientific)
5. hsa-miR-30d-5p (478606_mir, Thermo Fisher Scientific)
6. hsa-miR-451a (478107_mir, Thermo Fisher Scientific)
7. hsa-miR-92a-3p (477827_mir, Thermo Fisher Scientific)

These miRNAs were previously described to be secreted by endometrial epithelial cell lines (97), as present in EF aspirates (130,234) and as secreted in endometrial EVs in relation to early embryo implantation (130,134).

Two other miRNAs were selected from the small RNA-seq analysis carried out with the setup pool cohort. These miRNAs were among the most (hsa-miR-21-5p) and least (hsa-miR-155-5p) abundant miRNAs in the pool.

8. hsa-miR-21-5p (477975_mir, Thermo Fisher Scientific)
9. hsa-miR-155-5p (483064_mir, Thermo Fisher Scientific)

In addition, two exogenous miRNAs were used as internal controls. To check differences in RNA extraction efficiency, 4 µL of cel-miR-39 (478293_mir, Thermo Fisher Scientific) from a 0.1 nM stock were added to the sample before each RNA extraction procedure. To test differences during the cDNA synthesis process, 0.2 µL of ath-miR-159a (478411_mir, Thermo Fisher Scientific) from a 0.001 nM stock were added at the beginning of each cDNA synthesis reaction. This miRNA was used to calculate the relative quantity of the miRNAs analyzed.

5. <u>Dithiothreitol treatment assay</u>

Two aliquots from the setup pool cohort were used to perform the experiment. One aliquot was treated with 1.4 % dithiothreitol (DTT) solution in a 1:1 ratio (Miller *et al.*, 2012; Wang *et al.*, 2017). The other was used as a control and 1 x DPBS 1:1 was added. The samples were mixed by vortexing and incubated at room temperature for 15 min. Then, 1 x DPBS was added until the EF samples were diluted 1:8 and, afterward centrifuged at 3000 g for 15 min at 4°C. The supernatants were recovered and 400 µL aliquots were made.

After that, the EV enrichment was carried out with 400 µL with the PBP method and the pellet was resuspended in 100 µL of 1 x DPBS, of which 15 µL were reserved for WB, 5 µL for Cryo-electron microscopy, 5 µL for Nanoparticle Tracking Analysis and the rest was used for RNA analysis with Norgen (#55000). The RNA isolated was eluted in 100 µL of nuclease-free water, of which 2 µL were used for subsequent cDNA synthesis and the rest was stored at -80°C.

6. <u>RNase protection assay</u>

The samples used in this step belonged to the setup pool cohort and each aliquot had a final volume of 400 µL. All samples were first EV-enriched using the PBP method (described above) and EVs were resuspended in 200 µl of DPBS.

Aliquots were treated following different procedures (**Figure 18**):

1) Untreated sample as a control.
2) RNase A (Sigma Aldrich # 10109142001, MA, USA) (RNase)
3) Proteinase K (Sigma Aldrich #03115879001) + RNase (PRT-K)
4) Triton X-100 (Sigma Aldrich #T8787) + RNase (TX-100)
5) TX-100 + Proteinase K + RNase (TX+PRT).

Samples were treated with TX-100 at a final concentration of 0.1%. Proteinase K (0.05 mg/mL concentration) was added and incubated for 10 min at 37°C. The reaction was then stopped by adding 5 mM of phenylmethylsulfonyl fluoride (PMSF) (Sigma Aldrich #10837091001) and heating the samples at 90°C for 5 min. Samples were finally treated with 0.1 mg/mL RNase A (RNase) for 20 min at 37°C. Control samples were kept at 4°C until RNA extraction.

Before RNA extraction, β-mercaptoethanol was used to inhibit RNases as described in Norgen (#55000). The RNA was eluted in 50 µL of nuclease-free water. Two µL were used for subsequent cDNA synthesis and the rest was stored at -80 °C. All analyses were performed in triplicate with two technical duplicates, ending up with six TaqMan qPCR replicates.

RNase degrades free circulating miRNAs, but not miRNAs that are protected by proteins or those inside EVs. Treatment with TX-100 permeabilizes EV membranes and Protein K treatment degrades protein-miRNA complexes, thus allowing miRNA degradation by RNAse. Via this assay, it would be possible to determine the association of miRNAs with different components of the EF.
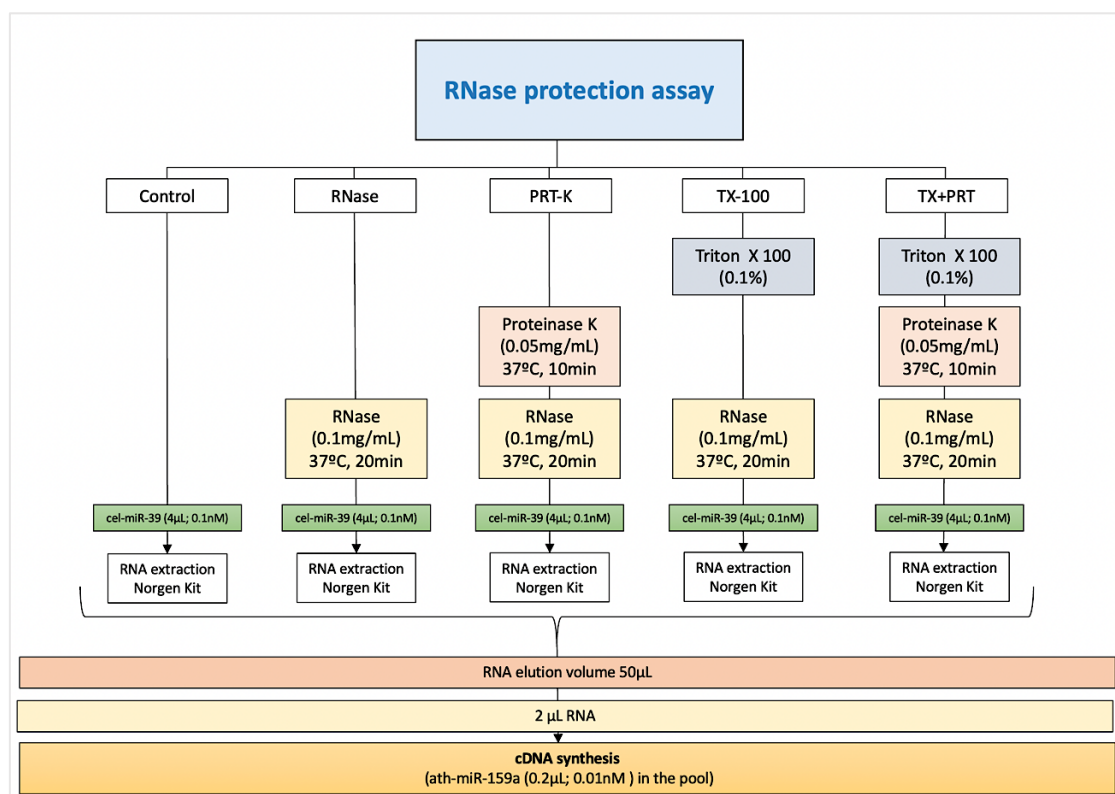
Figure 18. *Workflow of the RNase protection assay.*

7. <u>Analysis and quantification of the EF protein content</u>

7.1. Western blot analysis (WB)

Fifteen µL of sample were mixed with 5 µL of NuPAGE LDS Sample Buffer 4X (Invitrogen, # NP0007, Thermo Fisher Scientific). The fractions obtained via SEC were concentrated using acetone 99.5% (Panreac Applichem, # 161007, Darmstadt, Germany) and resuspended in 20 µL of 1 x LDS sample buffer. Samples were heated for 5 min at 37°C, 10 min at 65°C, and 15 min at 95°C, followed by a centrifugation step for 10 min at 13,000 x g. Each protein preparation was loaded and separated under non-reducing conditions in 4-12% Bis-Tris precast gels (Invitrogen, # NP0336BOX, by Thermo Fisher Scientific) with MOPS SDS Running Buffer 1X (Invitrogen, # NP0001, by Thermo Fisher Scientific).

Precision Plus Protein Dual Color Standard (BioRad, # 161-0374) was used as a protein molecular weight marker. Proteins were transferred to an Immobilon-P Transfer membrane (Merck Millipore, # IPVH00010, MA, USA) using NuPAGE Transfer Buffer 1X (Invitrogen, # NP0006-1 by Thermo Fisher Scientific) for 1 h at 100V. Blocking was performed with 5% Blotting-Grade Blocker (BioRad, # 170-6404) and 0.2% Tween-20 (Sigma-Aldrich, # P2287, MA, USA) diluted in 1X DPBS for 1 h. Primary antibodies were incubated overnight and afterward the membranes were washed three times for 10 min with 1X DPBS. Incubation with the secondary horse-radish peroxidase (HRP) conjugated antibody (1:6000) was performed at room temperature for 30 min.

Chemiluminescence detection of bands was performed using Pierce ECL Plus Western Blotting Substrate (Thermo Fisher Scientific, # 32132), and detection was carried out with high-performance films (GE Healthcare, # 28906844, IL, USA), using the AGFA Curix-60 automatic processor (Agfa, Cologne, Germany).

The intensity, of the bands was quantified by densitometry using ImageJ software v. 1.52a (ImageJ software, MD, USA).

The primary antibodies used in this study were:

- Mouse anti-CD63 (1:500; clone H5C6 from Developmental Studies Hybridoma Bank, IA, USA).
- Mouse anti- CD9 (1:500; clone 209306, R&D Systems, Minneapolis, MN, USA).
- Mouse anti-CD81 (1:500, Clone JS-81, 555675, BD, NJ, USA).
- Mouse anti-CD133 (1:500 clone W6B3C1, Miltenyi Biotec, North Rhine-Westphalia, Germany).
- Mouse anti-RAB8 (1:1000; Clone 4, 610844, BD, NJ, USA).
- Mouse anti-FLOTILLIN-1 (1:500; Clone 18 610820, BD, NJ, USA).
- Mouse anti-CD81 (1:500; Clone JS-81, 555675 BD).
- Mouse anti-HSP90 (1:500; 610418, BD, NJ, USA).
- Rabbit anti-LIMP II (1:500; ab16522, Abcam, Cambridge, UK).

7.2. Coomassie blue (CB) staining

SimplyBlue™ SafeStain from Invitrogen (Cat. # LC6060, Thermo Fisher Scientific) was used following manufacturer's recommendations. The intensity of the bands was quantified by densitometry using Image J software (v. 1.52a).

7.3. Spectrophotometer

Spectrophotometric measurements were performed using a NanoDrop™ One Microvolume UV-Vis Spectrophotometer (Thermo Fisher Scientific) in the 230-576 nm wavelength range. The concentration of RNA and protein was calculated by measuring the absorbance of 1 µL of sample.

8. EV visualization and measurement

8.1. Nanoparticle Tracking Analysis (NTA)

The size distribution of the EV preparations was analyzed by measuring the rate of Brownian motion using a NanoSight LM10 system (NanoSight, Amesbury, UK), which is equipped with fast video-capture and particle-tracking software. NTA acquisition settings were kept constant for all samples, and each video was analyzed to provide the mean and mode of vesicle size, and an estimated concentration (266).

8.2. Cryo-Electron Microscopy (Cryo-EM)

EV preparations were directly adsorbed onto glow-discharged holey carbon grids (Quantifoil, Großlobichau, Germany). The grids were blotted at 95% humidity and rapidly plunged into liquid ethane with the aid of Vitrobot (Maastricht Instruments BV, Maastricht, The Netherlands). Vitrified samples were imaged at liquid nitrogen temperature using a JEM-2200FS/ CR transmission cryo-EM (JEOL, Tokyo, Japan) equipped with a field emission gun and operated at an acceleration voltage of 200 kV.

9. Real-Time quantitative PCR (qPCR) assay

The relative expression levels of the miRNAs analyzed in the experiments carried out with the setup pool cohort were normalized to ath-miR-159 expression and calculated using the $2^{-\Delta Ct\ (Ct\ miRNA\ -\ Ct\ ath-miR-159a)}$ method. The relative expression levels of the discovered and validated miRNAs were normalized to internal controls and differences among the groups were calculated using the $2^{-\Delta Ct\ (Ct\ miRNA\ -\ Ct\ mean\ internal\ controls)}$ method. Subsequently, fold changes were calculated using the $2^{-\Delta\Delta Ct}$ method (267).

Endogenous controls were selected from the reference miRNAs using NormFinder software (268).

To perform regression studies with the discovery cohort and validate the models in the validation cohort, we only considered those samples in which we were able to detect the internal controls with fewer than 30 Ct cycles by qPCR analysis.

10. <u>Small RNA-sequencing</u>

RNA quantity and quality were evaluated using Agilent RNA 6000 Pico Chips (Agilent Technologies, Cat. # 5067-1513, CA, USA). Sequencing libraries were prepared following the protocol included with the kit "NEXTflex™ small RNA-Seq Kit v3," (©Bioo Scientific Corp. Cat. # 5132-06, protocol V19.01, Austin, TX, USA). Briefly, total RNA from each sample was incubated for 2 minutes at 70°C, then 3' 4N adenylated adapter (adapter dilution 1/4) and ligase enzyme were added and ligation was conducted by incubation of this mix overnight at 20°C. After excess 3' adapter removal, 5´-adapter was added alongside ligase enzyme and the mix was incubated at 20°C for 1 hour.

The ligation product was used for reverse transcription with M-MuLV Reverse Transcriptase in a thermocycler for 30 min at 42°C and 10 min 90°C. Next, cDNA enrichment was performed using PCR cycling: 2 min at 95°C; 20-27 cycles of 20 sec at 95 °C, 30 sec at 60 °C and 15 sec at 72°C; a final elongation of 2 min at 72°C and pause at 4°C. PCR products were resolved on 8% Novex TBE polyacrylamide gels (Cat. # EC6215BOX, Thermo Fisher Scientific) and one band between 150 bp and 400 bp was excised from the gel.

SmallRNAs were extracted from polyacrylamide gel using an adapted protocol, in which DNA from gel slices was dissolved in ddH2O overnight at room temperature. Afterward, libraries were visualized on an Agilent 2100 Bioanalyzer using the Agilent High Sensitivity DNA kit (Agilent Technologies, Cat. # 5067-4626) and quantified using the Qubit dsDNA HS DNA Kit (Thermo Fisher Scientific, Cat. # Q32854).

For sequencing, 10 nM of cDNA from each library was used. Sequencing was carried out in pools of isomolar libraries and all were sequenced in a HiSeq2500 (Illumina Inc) to achieve at least 10 million 50-nt single-reads per sample.

10.1. Alignment

FASTQs were trimmed for adapters following recommendations of the NEXTflex™ small RNA-Seq Kit manufacturers. We used the Bowtie program (269) to align reads against the human genome (GRCh38), with mismatch 0 to avoid false positives. We selected mirbase v22 to quantify mature miRNAs employing Partek Flow application, software version 7.0. The FASTQ data are available in the GEO database (access number GSE178917).

10.2. Small RNA-seq data analysis

We performed differential abundance analyses to discover miRNAs associated with implantation outcome. To avoid molecules with sparse presence, following Trimmed Mean of M-values (TMM) normalization we retained miRNAs with (i) counts per million (CPM)>1, (ii) non-zero counts in at least 15 individuals, and (iii) at most 10 zero counts in each of the two subgroups, namely women in whom implantation was successful (n=15) and women in whom it was not successful (n=15).

In this case, we filtered using CPM values rather than counts because they accounted for differences in sequencing depth between samples. The CPM gives an idea of how many counts would we get for an miRNA if the sample had a library size of 1M, and generally, a good threshold can be chosen for a CPM value that corresponds to a count of 10.

Differential expression was then assessed in edgeR (270) using the SARTools R package (271). The Benjamini-Hochberg procedure was used to calculate the false discovery rate for each comparison and obtain adjusted p-values.

10.3. Regression study

A subset of miRNAs was used to generate two linear regression models with k-fold cross-validations, one per miRNA extraction protocol assessed. Samples were randomly divided into training and testing datasets (80-20%).

Three miRNAs were used per modelling process, and hsa-miR-24-3p, hsa-miR-200b-3p and hsa-miR-148b-3p were selected for PBP-M and hsa-miR-24-3p, hsa-miR-200b-3p and hsa-miR-99b-5p for PBP-N. The resulting reproducibility was further tested by bootstrap correction, with 500 replications. All analyses were performed with R v4.0.0 software (R Development Core Team; http://cran.r-project.org) with *ROCR* (272) and *caTools* packages.

11. <u>Correlation analysis</u>

The Corrplot package (273) in R 3.6.2 program was used to analyze correlation among proteins (2019-12-12, R Foundation for Statistical Computing, Vienna, Austria).

12. <u>Statistical analysis</u>

GraphPad Prism v.8.0 (GraphPad Software, San Diego, CA, USA) was used for analysis. The statistical significance of the experiments carried out with the setup pool cohort was determined by paired t-test analysis, while an unpaired t-test with Welch's correction was used in experiments carried out in the discovery and validation cohorts. Statistical differences were considered significant at p-value less than 0.05 (two-sided). Sample size and p-values are all cited in the figures and figure captions.

13. <u>miRNA functional analysis</u>

The target genes of the validated miRNAs were obtained from the TarBase v7.0 database. The biological processes in which these miRNAs are involved were analyzed via the Kyoto Encyclopedia of Genes and Genomes (KEGG) and Gene Ontology (GO) in terms of biological process categories with DianamiRPath v3.0 (274). To select enriched KEGG pathways and GO processes, the analysis was performed with Fisher's exact test and false discovery rate correction was applied. We selected only those pathways and processes with p-values <0.05. The results for KEGG were merged by ''pathway union'' and the results for GO by ''category union''.

RESULTS

V. RESULTS

We have organized the results section according to the specific objectives. We, therefore, have five sections of results and in each, we detail the experiments carried out and the results obtained.

1. To optimize EF sample preparation and characterize EVs and miRNAs in EF samples

Before starting the comparison of the methodologies, we had to optimize sample collection and preparation and we also characterized the EV and miRNA content of EF samples. In addition, we optimized the PBP method as there were no protocols described for its use with EF.

1.1. Set up of the polymer-based precipitation method

We wanted to use the commercial kit "Invitrogen Total Exosome Isolation Reagent" in EF but there was no protocol for its use with EF. Therefore, we optimized the protocol based on the manufacturer's recommendations for "other type of fluid" and the expertise of our group with cerebrospinal fluid (265), and we ended up with the protocol described in Materials and methods section 2.2.

To decide the amount of reagent that we wanted to add, we compared the three options given by the Invitrogen Total Exosome Isolation Reagent kit: 1 volume (1:1), 0.5 volume (1:2) and 0.2 volume (1:5). In all cases, we began the experiment with 400 µL of EF and added the corresponding reagent volume in each case (400 µL, 200 µL and 80 µL). We then extracted RNA with the mirVana PARIS kit and analyzed the seven reference miRNAs via qPCR. These reference miRNAs were selected because they had previously been described to be involved in embryo-endometrium crosstalk as described in section 4 of materials and methods.

We only were able to detect all miRNAs when using 1 volume of reagent. In the case of 0.5, we were able to detect three miRNAs: hsa-miR-17-5p, hsa-miR-451a and hsa-miR-92a-3p. In the case of 0.2, we only detected two miRNAs: hsa-miR-451a and hsa-miR-92a-3p (**Figure 19**). Considering the results, we decided to perform the subsequent experiments using 1 volume (1:1) of reagent.
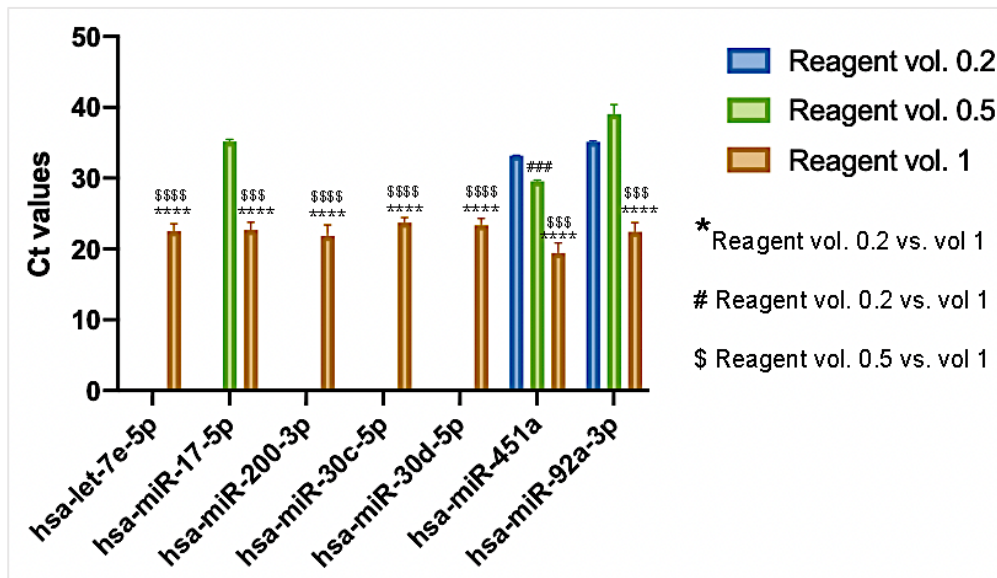
Figure 19. *Comparison of different amounts of Invitrogen Total Exosome Isolation Reagent.*

The graphs show the Ct values of the reference miRNAs evaluated via qPCR. The number of replicates for each condition was two and the data show the mean with SD. Each aliquot (400 µl) came from the setup pool cohort, and we ended up with n=2 for each condition. Statistical significance was determined using the paired Student's t-test analysis. *,$,# P < 0.05; **,$$,## P < 0.01; ***,$$$,### P < 0.001. * Reagent vol. 0.2 versus Reagent vol. 1. $ Reagent vol. 0.5 versus Reagent vol. 1. # Reagent vol. 0.2 versus Reagent vol. 0.5.

In the laboratory we were using Total Exosome Isolation Reagent from the cell culture media (#4478359) to isolate EVs from endometrial cell lines, so we decided to compare it with the Total Exosome Isolation Reagent from other body fluids (#4484453) in the EF, as #4478359 had a better cost-effectiveness ratio and we needed to use many mLs for subsequent experiments.

We used six samples (400 µL) from the setup pool cohort, three for each kit and we added 1 volume of reagent (1:1). RNA was extracted with the mirVana PARIS kit, and we analyzed the seven reference miRNAs by qPCR. The results did not show any significant difference between the two kits (**Figure 20**). Therefore, we decided to use the Total Exosome Isolation Reagent from the cell culture media in the subsequent experiments.
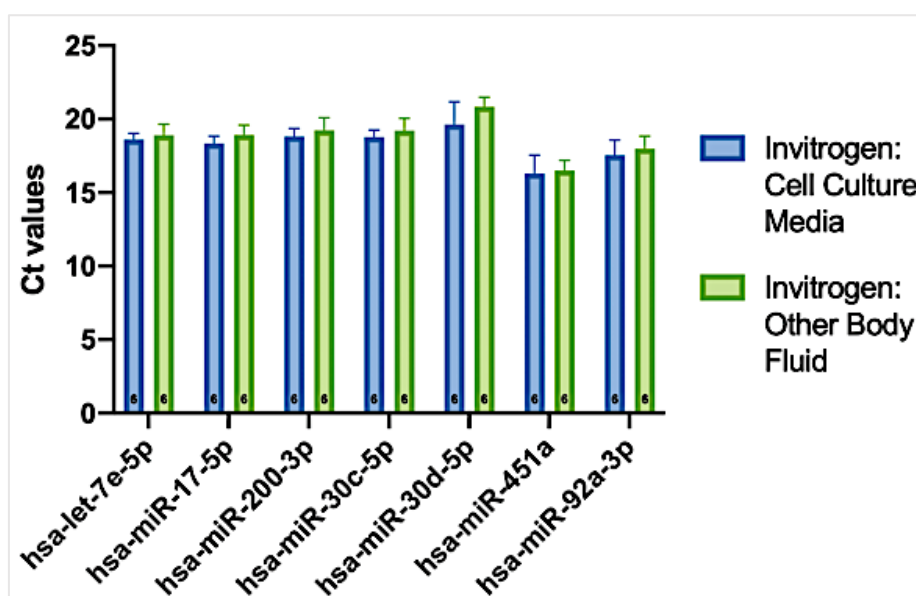
Figure 20. *Comparison of the Invitrogen Total Exosome Isolation Reagent kits.*

The graphs show the Ct values of the reference miRNAs evaluated via qPCR. The data show the mean with SD. Each aliquot (400 µl) came from the setup pool cohort, and we ended up with n=3 for each condition and the number of replicates per condition was six and is shown at the base of each column. Statistical analysis was performed using the paired Student's t-test, but there were no significant differences.

1.2. DTT treatment

The EF is a very viscous fluid and is very difficult to manipulate and work with. In clinical practice, the EF was collected with a catheter and the sample sticks to the wall, so, to avoid this, the sample was expelled from the catheter by passing 1.5 mL of DPBS. Then, the sample was centrifuged and the supernatant collected, leaving a non-dissolved mucus pellet at the bottom. To determine whether EVs were trapped in the pellet or released into the supernatant, EF samples were solubilized with a mucolytic agent called DTT. This was previously described by other authors that used DTT for sputum samples (275,276).

For this experiment, we prepared two pools with three replicates per group. We treated one pool with 1.4% DTT and left the other as a control. We found that DTT treatment was useful for degrading the mucus pellet formed after centrifugation as most of the mucus disappeared, as shown in (**Figure 21**).
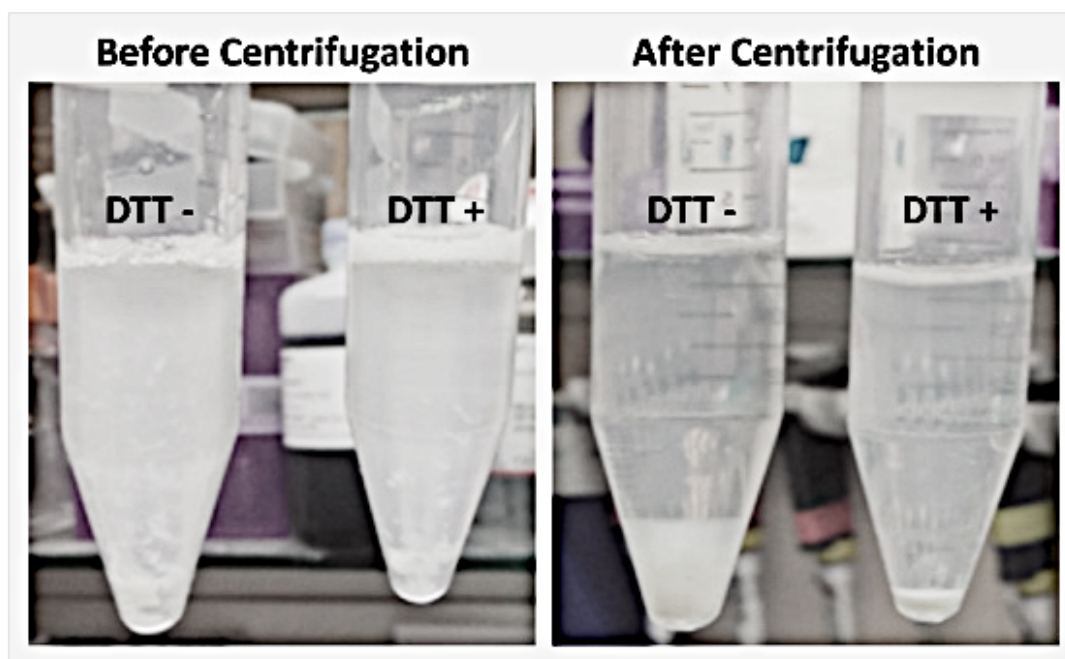
Figure 21. *Macroscopic view of the EF before and after DTT treatment.*

Two EF pools from the setup cohort were used to perform the experiment. One aliquot was treated with 1.4% dithiothreitol (DTT) solution at 1:1. The other was used as control and 1 x DPBS 1:1 was added instead.

Then, we enriched the supernatant from both conditions, DTT-treated and untreated, using the PBP method (1:1) and analyzed the EVs via different methodologies. We began the analyses with NTA (**Figure 22**) and cryo-EM (**Figure 23**). The results revealed heterogeneous EV populations with diameters between 100 and 800 nm under both conditions. In untreated samples, the average amount of particles detected was $1.9 \times 10^9 \pm 7.8 \times 10^7$ particles/mL, with a mean size of 291.5 ± 0.1 nm and mode 196.4 ± 3.2 nm. In DTT-treated samples, we detected more (mean $2.7 \times 10^9 \pm 5.9 \times 10^7$ particles/mL) and larger particles (mean 313.6 ± 2.5 nm and mode 248.5 ± 8.1 nm). These results suggested that sample pretreatment with DTT was able to release more vesicles from the mucus, including a subpopulation of larger size.
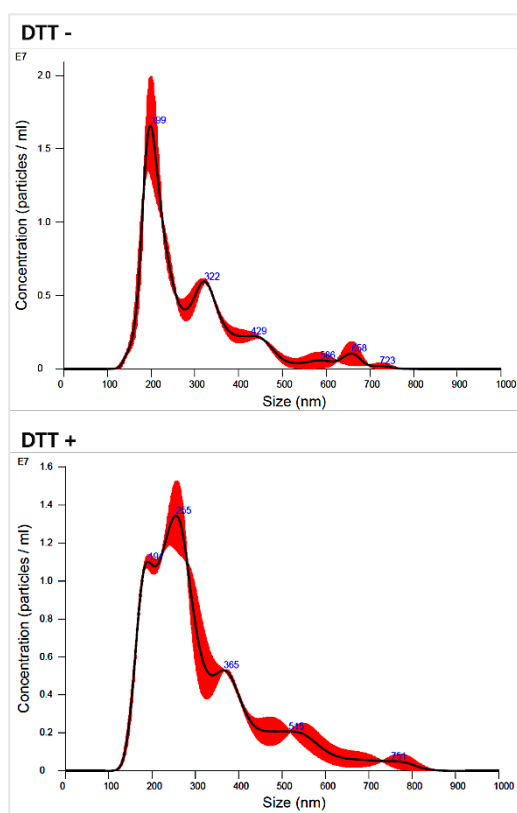
Figure 22. *NTA of purified EVs.*

Average of the concentration and size values from two different measurements. **DTT**: dithiothreitol. **NTA**: nanoparticle tracking analysis.
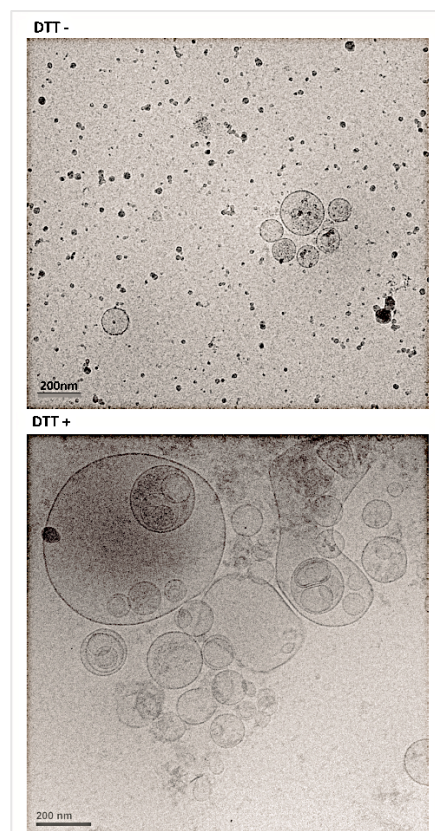
Figure 23. *Cryo-EM of purified EF-derived EVs.*

Scale bar 200n. **Cryo-EM:** cryo-electron microscopy. **DTT:** dithiothreitol.

WB presented a different pattern of vesicular markers under the two conditions (**Figure 24**). The intensity of marker RAB8 in treated samples was stronger than in untreated samples, in agreement with the number of particles detected via NTA. In contrast, EV marker intensities, including LIMP II, CD133 and CD63 proteins, were stronger in untreated samples.
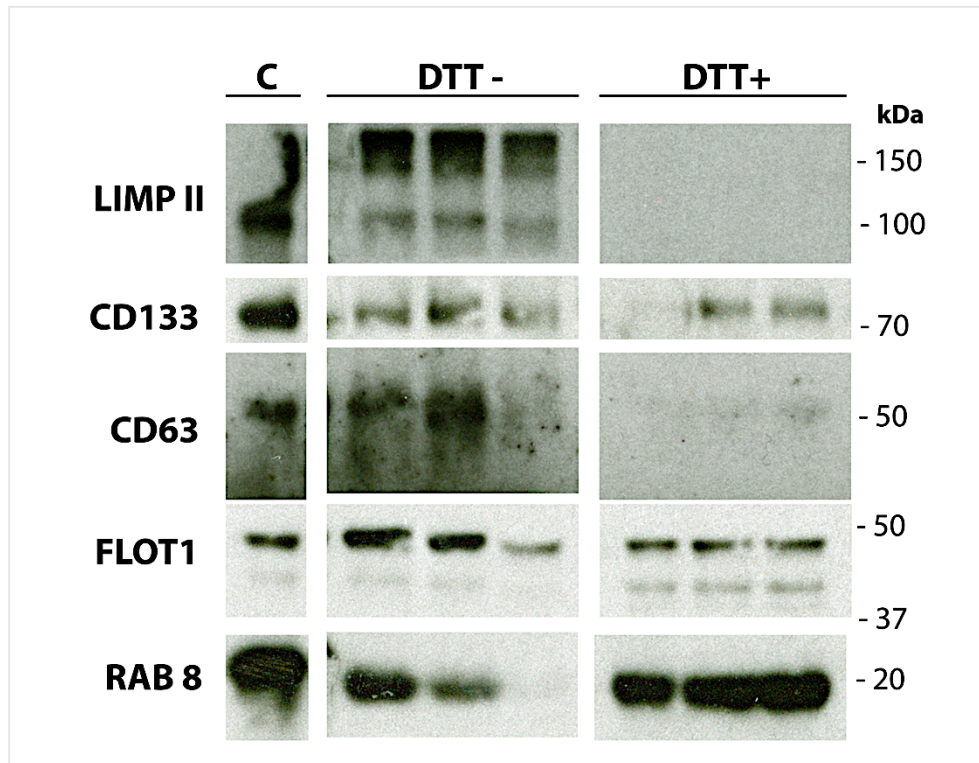
Figure 24. *WB of EV-associated proteins in DTT-treated and untreated samples.*

DTT: dithiothreitol. **DTT +:** DTT-treated. **DTT -:** Untreated. **EF:** endometrial fluid. **WB:** western blot analysis.

The RNA analysis revealed that it was possible to detect the seven reference miRNAs, all miRNAs were detected in all samples under both conditions. In the DTT-treated group, the levels of the following miRNAs were significantly reduced compared with the untreated group: hsa-let-7e-5p, hsa-miR-17-5p, hsa-miR-200c-3p, hsa-miR-30c-5p and hsa-miR-451a (**Figure 25**).
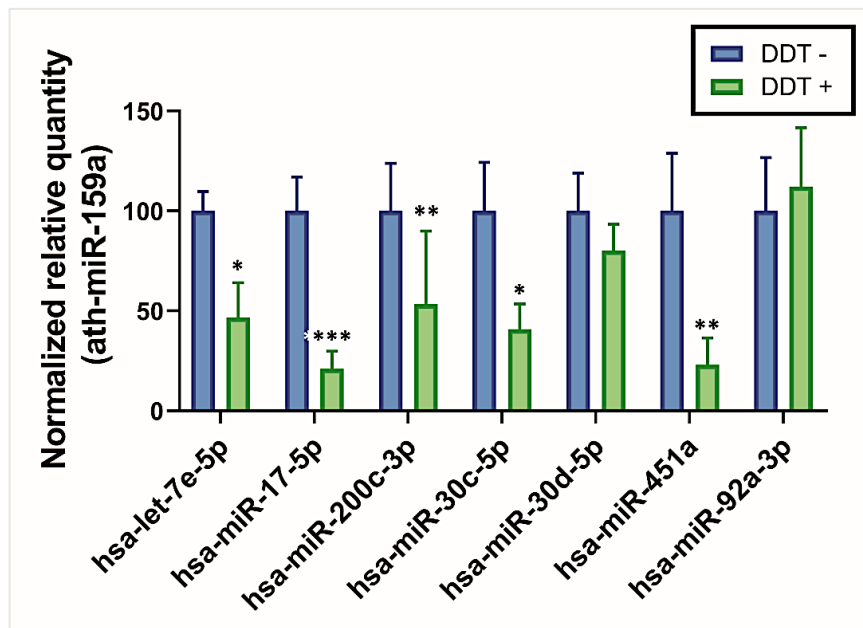
Figure 25. *qPCR analysis of DTT treated and untreated samples.*

Normalized relative quantification of the seven reference miRNAs analyzed is represented. miRNA expression is shown relative to untreated samples, for which the expression of each miRNA was set to 100%. The number of replicates per condition was three and data show the mean with SEM. Statistical significance was determined using the paired *t*-test analysis. * $p < 0.05$; **$p < 0.01$; ***$p < 0.001$. **DTT:** dithiothreitol. **DTT +:** DTT-treated. **DTT -:** untreated.

These results demonstrated that when samples were treated with DTT, a greater quantity of EVs were released into the supernatant. However, the relative quantification of reference miRNAs was worse in DTT-treated samples and some WB markers were not detected in DTT-treated samples. These results suggested that DTT treatment could be altering miRNA analyses, and as the main goal of this study is to detect miRNAs, we decided to collect and store EF samples without DTT, and all experiments were performed with untreated EF samples.

1.3. Characterization of EV and miRNA subpopulations in EF

We used SEC to characterize EVs and miRNAs in the EF samples and, to further explore the relationship between the miRNA content of EF and their association with EVs, we performed different RNase assays.

1.3.1. Size-exclusion chromatography

We performed SEC and analyzed the distribution of EVs, proteins and miRNAs along the different fractions (**Figure 29**). The SEC method separated the EF into 12 fractions, from F1 to F12.

WB analysis of the fractions demonstrated that it was possible to detect exosomal markers in a small volume of EF samples (**Figure 26**). The markers CD63 and CD81 were detected in F3 and to a lesser extent in fractions F4 and F5. RAB8 was also mainly detectable in F3–F5. Immunoglobulins were also found in fractions F6 to F11.
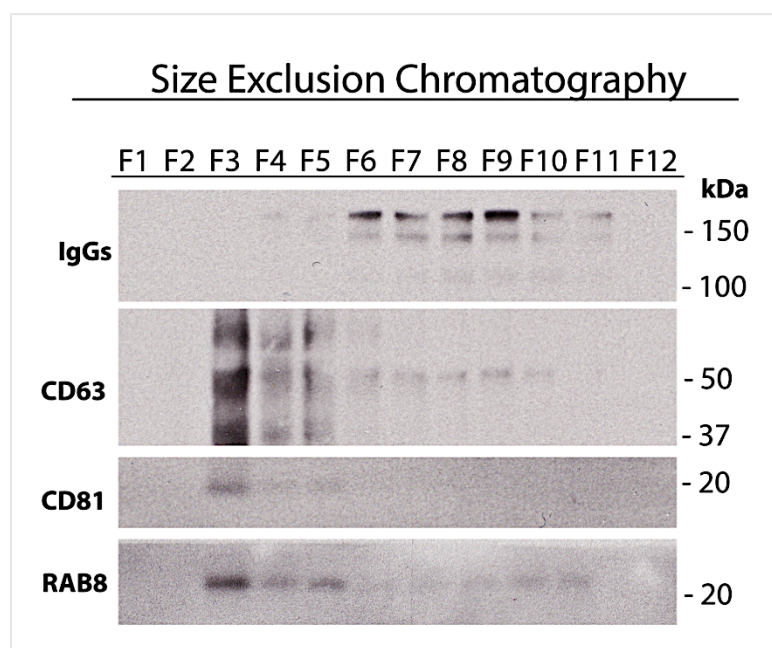
Figure 26. *WB characterization of the EF by SEC.*

Western blot shows different EV markers (CD63, CD81 and RAB8) and soluble proteins (IgGs) in the fractions of size-exclusion chromatography (SEC). The fractions obtained by SEC were numbered from F1 to F12. To perform the experiment, an aliquot of 400 µL from the setup pool cohort was added to the column. **EF:** endometrial fluid. **WB:** western blot analysis, **EVs**: extracellular vesicles.

Next, the study of the distribution of the seven reference miRNAs showed that the relative quantity of miRNAs increased in fractions F3 to F11 (**Figure 27**). In F3, which corresponds to the vesicular fraction, the most abundant miRNAs were hsa-miR-451a and hsa-miR-92a-3p, and the least abundant were hsa-miR-30d-5p and hsa-miR-200c-3p. This trend was maintained in the remaining fractions, except for F7, where hsa-miR-200c-3p was the second most abundant miRNA.
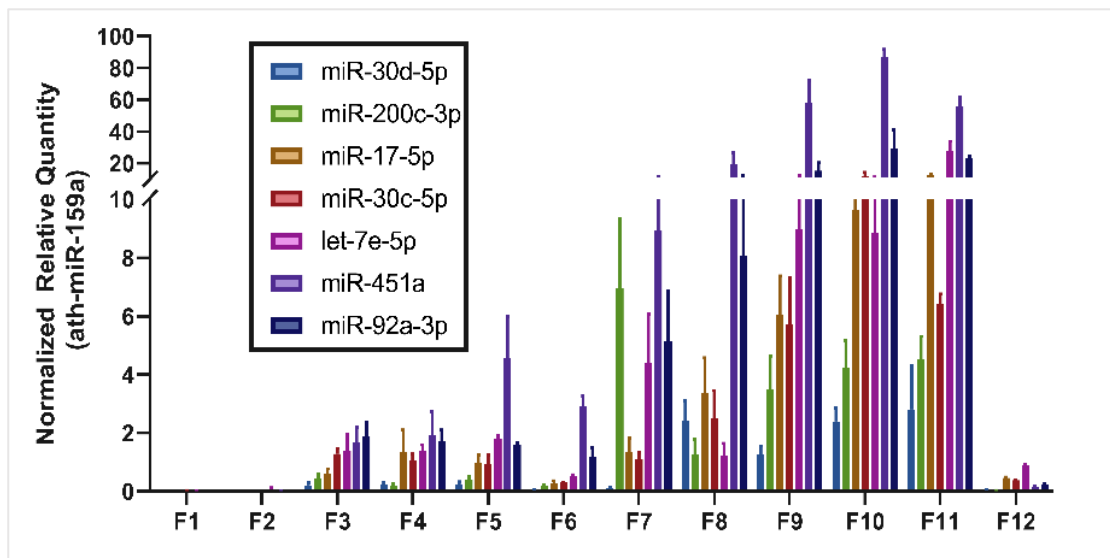
Figure 27. qPCR characterization of miRNAs in the EF by SEC.

Distribution of the seven reference miRNAs among the SEC fractions. Normalized relative quantification was used to determine the presence of miRNAs among fractions F1 to F12. To perform the experiment, an aliquot of 400 µL from the setup pool cohort was added to the column and we ended up with n=2 for each fraction. Different SEC fractions were numbered from F1 to F12. **EVs**: extracellular vesicles, **qPCR**: quantitative PCR, **miRNAs:** microRNAs.

1.3.2.   RNase protection assay

We performed the RNase protection assay to explore the relationship between the miRNA content of the EF and their association with EVs.

In the samples treated with RNase or Triton X-100 (TX-100) with RNase, only hsa-miR-30c-5p was significantly degraded compared with the control (**Figure 28**). In samples treated with proteinase K (PRT-K) and RNase, there was a significant decrease in the levels of all miRNAs analyzed (although all miRNAs were detectable in all replicates).

The miRNAs were further degraded when samples were treated with TX-100, PRT-K and RNase (TX+PRT). In this case, we could only detect hsa-miR-200c-3p and hsa-miR-92a-3p in all replicates. Under these conditions, hsa-miR-451a, hsa-miR-17-5p and hsa-miR-30d-5p were detected in four of six replicas, hsa-let-7-5p in two of six replicas and hsa-miR-30c-5p was undetectable. With TX+PRT treatment, the detection of all miRNAs was significantly reduced compared with previous combinations (**Figure 28**).

These results suggested that most miRNAs found in the EF were not only protein-associated but also protein-associated within the EVs, which protects them against degradation.
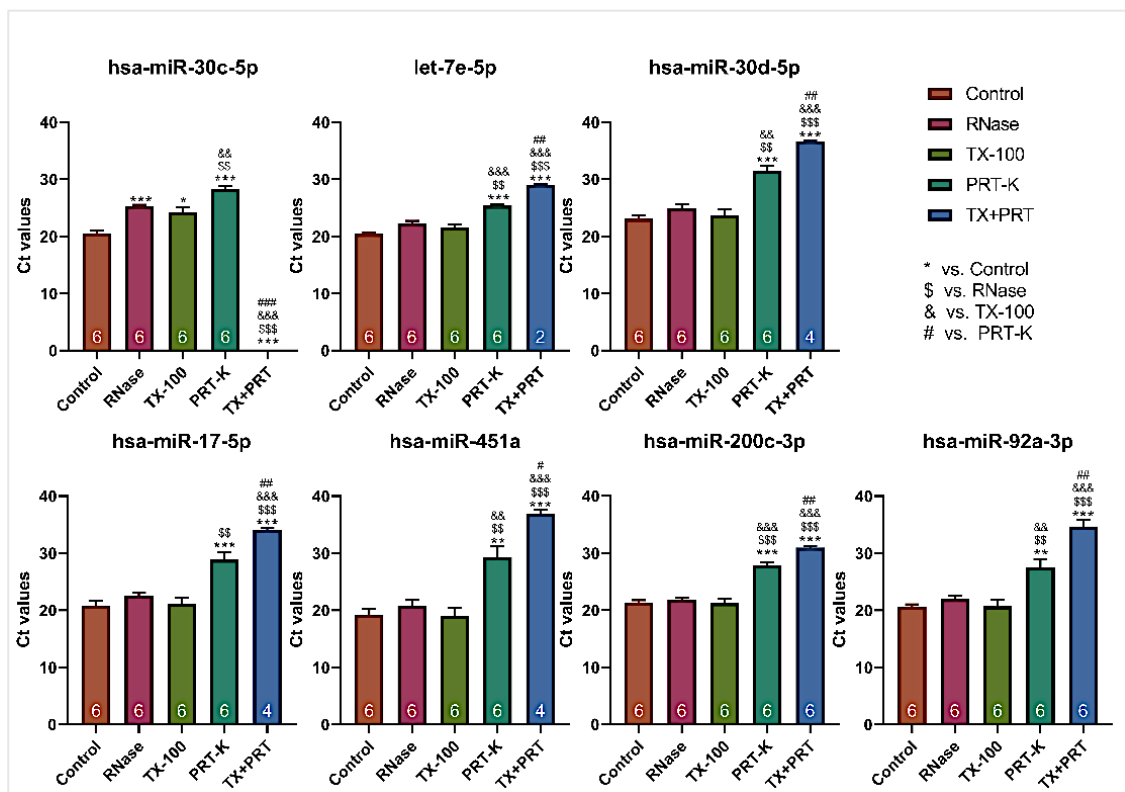
Figure 28. *RNase protection assay.*

Sample analysis to examine the association of miRNAs with proteins and EVs in the EF. The graphs show the Ct values of the reference miRNAs evaluated via qPCR. The number at the base of each column indicates the number of replicates in which that miRNA was detected. The number of replicates for each condition was six and the data show the mean with SEM. Each aliquot (400 µL) came from the setup pool cohort. Statistical significance was determined using the paired Student's t-test analysis. *, $, &, # $p<0.05$; **, $\$\$$, &&, ## $p<0.01$; ***, $\$\$\$$, &&& ,### $p<0.001$. **Control:** control sample without treatment: **RNase:** samples treated with RNase; **TX-100:** samples treated first with TX-100 followed by RNase treatment; **PRT-K:** samples treated first with proteinase K and then with RNase; **TX+PRT:** samples treated first with TX-100, then with proteinase K and finally with RNase. **EVs**: extracellular vesicles, **qPCR:** quantitative PCR, **miRNAs:** microRNAs, **EF:** endometrial fluid.

2. To establish a robust methodology for analyzing free and EV-associated miRNAs from EF in clinical settings

Once we established that we would analyze the samples without DTT, we compared various methodologies for EV enrichment and RNA extraction to define a simple and effective strategy for detecting vesicular and non-vesicular miRNAs from small volumes of EF. The results were first compared by qPCR and the most efficient were further analyzed using Small RNAseq. In addition, a technical reproducibility assay was performed to establish the most robust technique.

2.1. Comparison of different methodologies

Five different methodologies were compared to define a simple and effective strategy for detecting vesicular and non-vesicular miRNAs from small volumes of EF. Two consisted of direct extraction of RNA from EF with different RNA extraction kits: DCT-N (Norgen kit) and DCT-M (mirVana PARIS kit). The other three had EV enrichment prior to RNA extraction. In one of these, enrichment was performed via UC followed by RNA extraction with the mirVana PARIS kit (UC-M). In the other two, enrichment was performed with the PBP method followed by RNA extraction with either the Norgen (PBP-N) or mirVana PARIS kit (PBP-M) (**Figure 29**).

EF supernatant recovery volumes varied between samples due to many factors, such as the operator collecting the sample as well as the EF volume or viscosity, among others. In general, supernatants ranged from 400 μL to 1.3 mL. Therefore, we optimized the protocols to be used with the minimum volume available in all collected samples (400 μL). To determine the efficiency of each methodology, we analyzed the seven reference miRNAs via qPCR.
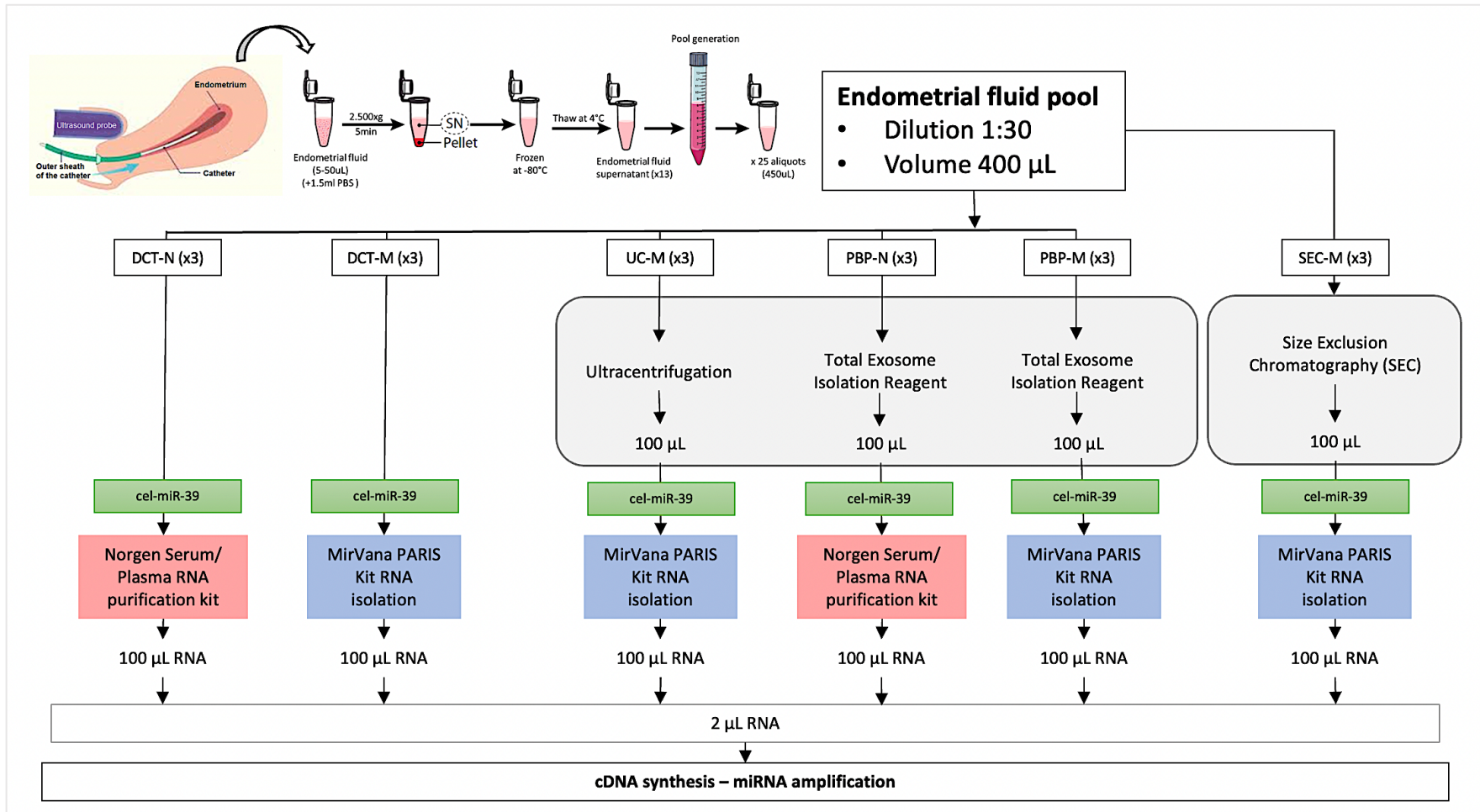
Figure 29. *Workflow of the different methods used to analyze microRNAs from the EF of patients from the setup cohort pool.*

We compared five different methods, two of which used direct RNA extraction A from the EF (DCT-N and DCT-M). The other three included EV enrichment (UC-M, PBP-N and PBP-M) before RNA extraction. In parallel, we carried out size-exclusion chromatography (SEC-M) to characterize proteins and miRNAs in the EF. The samples came from the setup pool cohort, and each experiment was performed in triplicate, using sample aliquots of 400 μl. **DCT-N:** direct RNA extraction with the Norgen Plasma/Serum RNA purification kit. **DCT-M:** direct RNA extraction with the mirVana PARIS kit. **UC-M:** EV enrichment by UC and RNA extraction using the mirVana PARIS kit. **PBP-N:** EV enrichment with a PBP method and RNA extraction with the Norgen Plasma/Serum RNA purification kit. **PBP-M:** EV enrichment using the PBP method and RNA extraction with the mirVana PARIS kit. **SEC-M:** EV enrichment with SEC and RNA extraction with the mirVana PARIS kit. **miRNAs:** microRNAs. **PBP**: polymer-based precipitation.

The PCR results showed that we were able to detect all reference miRNAs in all replicates of DCT-M, DCT-N, PBP-M, PBP-N and UC-M. However, we observed differences in the abundance of each miRNA. MiRNA analysis showed that methods with a prior EV enrichment step with polymer-based precipitation methods, PBP-N and PBP-M, performed better in comparison with the rest, PBP-N being the most efficient method. The methodologies with direct RNA extraction (DCT-N and DCT-M) and UC-M obtained a significantly lower quantity of our reference miRNAs in comparison with the PBP-N method (**Figure 30**).
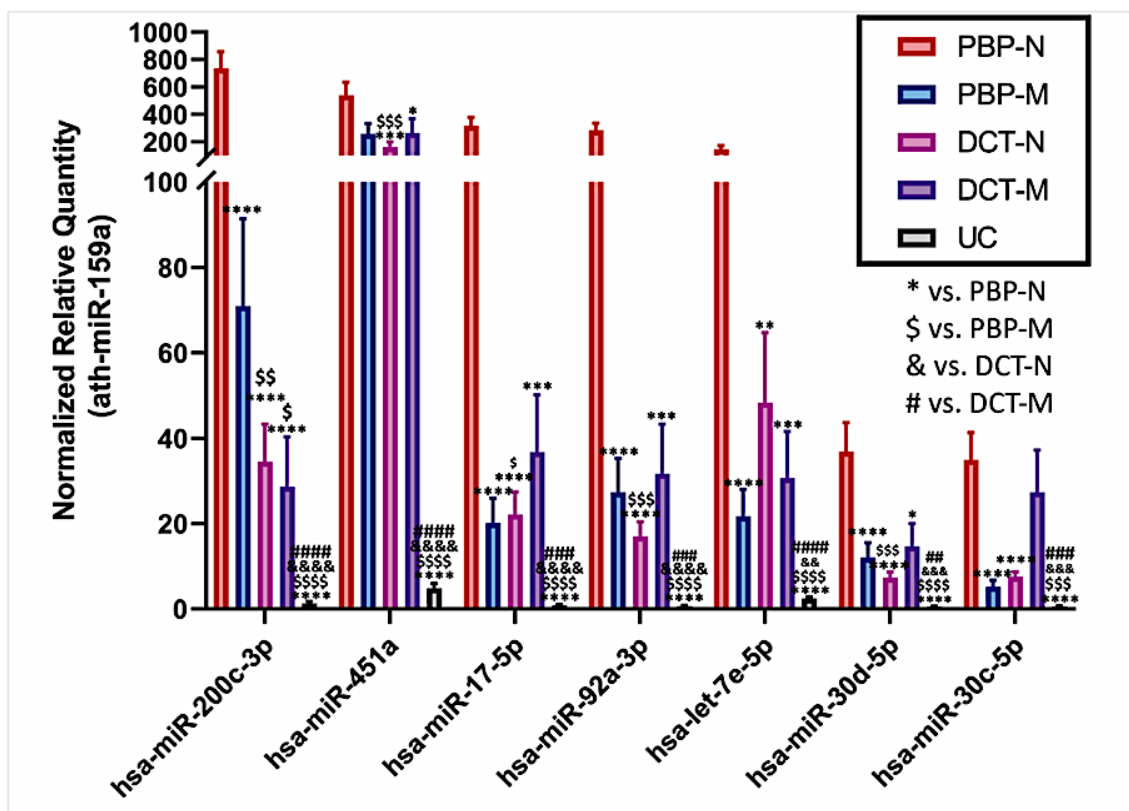
Figure 30. *Optimization of different methodologies for analyzing miRNAs from the EF of the setup pool cohort.*

Results for the seven reference miRNAs analyzed by quantitative PCR for each of the techniques compared. Normalized relative quantification revealed that the most efficient method was PBP-N, the UC-M method being the least efficient. Statistical significance was determined using paired t-test analysis. The number of replicates per case was 12 and data show the mean with SEM. * versus PBP-N; $ versus PBP-M; & versus DCT-N; # versus DCT-M. Statistical significance was determined using paired t-test analysis. * vs. PBP-N; $ vs. PBP-M; & vs. DCT-N; # vs. DCT-M. *, $, &, # $p<0.05$; **, $$, &&, ## $p<0.01$; ***, $$$, &&&, ### $p<0.001$; ****, $$$$, &&&& ,#### $p<0.0001$. **DCT-M:** direct RNA extraction with the mirVana PARIS kit; **DCT-N:** direct RNA extraction with the Norgen Plasma/Serum RNA purification kit; **PBP-M:** EV enrichment with a PBP method and RNA extraction with the mirVana PARIS kit; **PBP-N:** EV enrichment with a PBP method and RNA extraction with the Norgen Plasma/Serum RNA purification kit; **SEC-M:** EV enrichment with SEC and RNA extraction with the mirVana PARIS kit; **UC-M:** EV enrichment by ultracentrifugation before RNA extraction with the mirVana PARIS kit.

2.2. Small RNA-seq analysis

Using small RNA-seq, we further analyzed the RNA extracted via PBP-N and PBP-M, as they were the two most efficient methods (**Figure 30)**. In addition, by small RNA-seq, we also analyzed the RNA extracted in fractions F3 and F4 of the SEC, as they were positive for EVs markers in the WB (**Figure 26**).

On the one hand, the sequencing results detected 151 and 251 unique miRNAs in PBP-N and PBP-M, respectively; of these, 145 miRNAs were shared between both methodologies. On the other hand, the small RNA-seq analysis of fractions F3 and F4 detected 204 and 149 unique miRNAs, respectively. Furthermore, small RNA-seq from PBP methods and SEC fractions F3 and F4 shared a great number of miRNAs (**Figure 31**).

The results of the post-alignment quality assurance/quality control (QA/QC) analysis are shown in **Table 7.** The average percentage alignment with the human genome for each case was PBP-M: 74 ± 5.9 %, PBP-N: 68.4 ± 1.8 %, F3: 54 ± 6.8 % and F4: 67.7 ± 5.1 %.
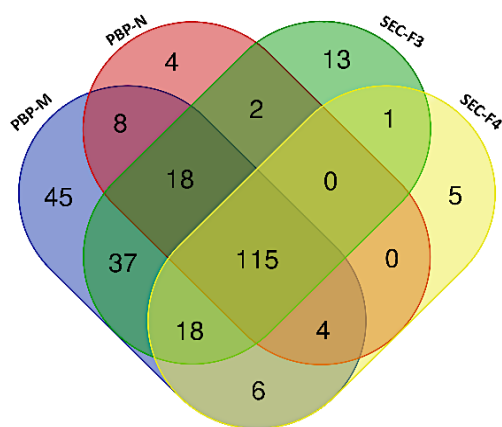
Figure 31. *Venn diagram showing the number of unique miRNAs detected by small RNA-seq for each method and the number of common miRNAs among them.*

The number of unique miRNAs detected by each technique was 251 for PBP-M, 151 for PBP-N, 204 for SEC F3 and 149 for SEC F4. The samples (400 µL) for small RNA-seq analysis came from the setup pool cohort, and each experiment was performed in triplicate. **PBP-M**: EV enrichment with a PBP method and RNA extraction with the mirVana PARIS kit; **PBP-N:** EV enrichment with a PBP method and RNA extraction with the Norgen Plasma/Serum RNA purification kit; **SEC-M:** EV enrichment with size exclusion chromatography and RNA extraction with the mirVana PARIS kit

Table 7. *Post-alignment quality assurance/quality control (QA/QC).*

Sample name	Total reads	Total alignments	**Aligned (%)**	Total unique	Unique	Coverage (%)	Avg. coverage depth	Avg. length	Avg. quality	%GC
SEF F3-1	15487948	7630986	**49.23**	7617259	49.18	0.03	294998	31.00	37.23	55.91
SEC F3-2	1.74E+07	8903708	**50.98**	8884995	50.92	0.03	279608	30.58	37.18	57.68
SEC F3-3	14871193	9193659	**61.76**	9174400	61.69	0.02	351794	29.00	37.12	57.30
SEC F4-1	13190600	8152206	**61.74**	8136734	61.69	0.02	349917	31.17	37.25	57.11
SEC F4-2	17391042	12372923	**71.04**	12337774	70.94	0.02	726286	31.28	37.26	56.91
SEC F4-3	15936514	11198425	**70.18**	11169232	70.09	0.02	526555	30.69	37.17	58.86
PBP-M 1	13591975	9273484	**68.15**	9253435	68.08	0.01	660741	28.25	37.23	52.63
PBP-M 2	13058148	9173020	**70.17**	9153482	70.10	0.01	641421	29.23	37.21	54.95
PBP-M 3	14575685	9738881	**66.74**	9716748	66.66	0.01	718495	29.47	37.21	55.14
PBP-N 1	16264576	12593333	**77.32**	12556764	77.20	0.01	812728	28.05	37.23	53.73
PBP-N 2	21826070	14696025	**67.22**	14645648	67.10	0.02	890627	28.30	37.22	54.96
PBP-N 3	16424952	12740376	**77.45**	12702510	77.34	0.01	893952	27.63	37.22	53.86
BLANK	15704810	692737	**4.41**	692607	4.41	0.01	37879	17.07	36.89	59.57

The table shows the data for each triplicate sample. Avg: average. %GC: percentage of guanine-cytosine content.

2.3. Technical reproducibility assay

Given the importance of selecting a robust methodology, two operators (JIP and MCG) carried out a technical reproducibility experiment. Each analyzed 20 samples from the same pool, 10 using PBP-N and 10 with PBP-M. In this case, qPCR was used to test reproducibility with the seven reference miRNAs and two other miRNAs obtained from the small RNA-seq results; hsa-miR-21-5p and hsa-miR-155-5p were among the most and least abundant, respectively. The technical reproducibility experiment showed that the nine miRNAs were detected with PBP-N regardless of the operator. However, neither operator was able to detect hsa-miR-155-5p and miR-21-5p with PBP-M in all replicates (**Table 8**). Unlike PBP-N, the coefficients of variation showed greater variability for PBP-M, both among the different aliquots and between operators performing the experiment. In addition, the normalized relative quantification of miRNAs showed significant differences between the techniques, PBP-N being able to detect a higher quantity of miRNAs in comparison with PBP-M (**Figure 32**).

Table 8. *Technical reproducibility assay to compare the performance of the PBP-M and PBP-N methods.*

miRNAs (Thermo Fisher)	Technical reproducibility assay							
	PBP-M-A		PBP-M-B		PBP-N-A		PBP-N-B	
	n	CV (%)	n	CV (%)	n	CV (%)	n	CV (%)
hsa-let-7-5p	10/10	2.8	10/10	3.4	10/10	0.5	10/10	2
hsa-miR-17-5p	10/10	5.6	10/10	10.7	10/10	3.9	10/10	3.5
hsa-miR-200c-3p	**10/10**	**3.2**	**10/10**	**3.1**	**10/10**	**2.4**	**10/10**	**2.7**
hsa-miR-30c-5p	10/10	9.4	10/10	3.4	10/10	1.9	10/10	2
hsa-miR-30d-5p	10/10	4.2	10/10	3.8	10/10	2.2	10/10	3.9
hsa-miR-451a	10/10	9.1	10/10	1.6	10/10	3.8	10/10	1.5
hsa-miR-92-5p	**10/10**	**4.8**	**10/10**	**3.8**	**10/10**	**2.7**	**10/10**	**2.2**
hsa-miR-21-5p	9/10	9.6	5/10	9.1	10/10	2.1	10/10	2.6
hsa-miR-155-5p	8/10	9.5	4/10	3.8	10/10	4.5	10/10	2.3

The samples (400 µL) came from the setup cohort. Twenty samples were analyzed by each operator (10 using PBP-M and 10 using PBP-N). The number of times that each miRNA was detected (n) and the coefficient of variation (CV, %) were considered. Letters A and B differentiate the results obtained between operators. **PBP-M:** EV enrichment using PBP and RNA extraction with the mirVana PARIS kit). **PBP-N:** EV enrichment using PBP and RNA extraction with the Norgen Plasma/serum RNA purification kit.
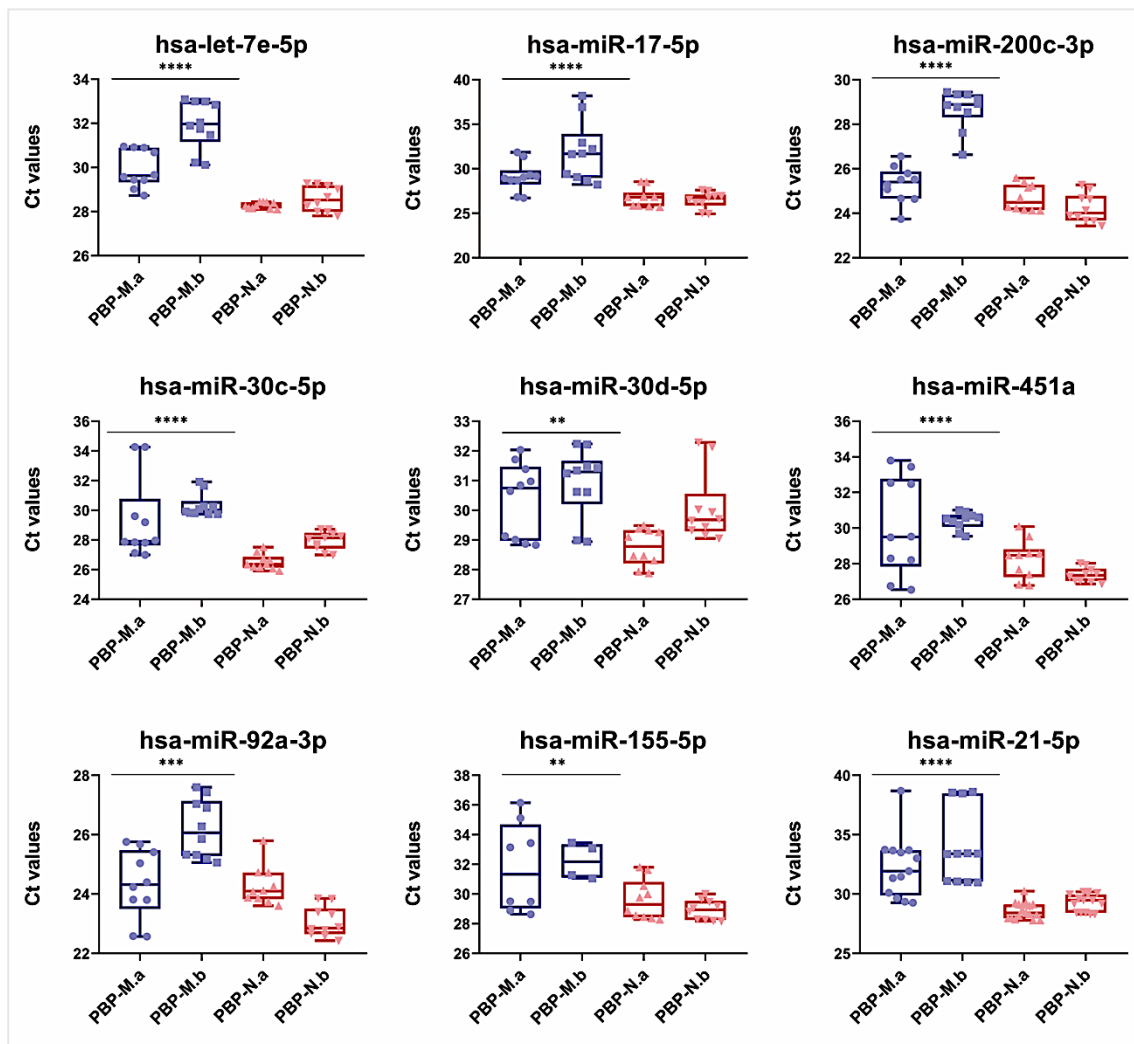
Figure 32. *Technical reproducibility experiment to compare the performance of PBP-M and PBP-N methods.*

The graphs show Ct values for each miRNA, each operator (a= JIP or b= MCG) and method (PBP-M or PBP-N). Box plots showing median, maximum and minimum values and all points. Aliquots (400 µL) came from the setup pool cohort and each operator analyzed 20 aliquots, 10 with PBP-M and 10 with PBP-N. Statistical significance was assessed with paired t-test analysis between the total results obtained with PBP-N and PBP-M. *p<0.05; **p<0.01; ***p<0.001; ****p<0.0001. **PBP-M:** EV enrichment with a PBP method and RNA extraction with the mirVana PARIS kit; **PBP-N:** EV enrichment with a PBP method and RNA extraction with the Norgen Plasma/Serum RNA purification kit.

2.4. Selected methodologies for their implementation in a sample set with different implantation outcomes.

Overall, PBP-M and PBP-N obtained the best results from this optimization procedure when starting with a limited amount of EF and were selected for implementation in the following analysis.

The PBP-M technique turned out to be more efficient since a greater number of miRNAs were detected by small RNA-seq. However, PBP-N proved to be more efficient in terms of qPCR detection as we were able to detect all analyzed miRNAs with lower coefficients of variation (**Table 9**).

Table 9. *Comparison of the selected methodologies for their implementation in a set of samples with different implantation outcomes.*

	PBP – M (mirVana)	PBP – N (NORGEN)
Advantages	EFFICIENCY - Greater number of miRNAs detected with small RNA-seq.	EFFICIENCY - Lower Ct values for the analyzed miRNAs. - More total RNA extracted. REPRODUCIBILITY - Lower coefficient of variation among the technical replicates. BACKGROUND - Less miRNAs detected in blank samples.
Disadvantages	EFFICIENCY - Higher Ct values for the analyzed miRNAs. - Less total RNA extracted. REPRODUCIBILITY - Higher coefficient of variation among the technical replicates. BACKGROUND - Higher miRNAs detected in blank samples.	EFFICIENCY - Lower number of miRNAs detected with small RNA-seq.
Protocol	- Requires carrying out the protocol in a fume hood (Organic extraction with acid phenol-chloroform).	- User-friendly protocol (No organic extraction).

3. To apply the selected methodology in a sample set (Discovery cohort) with different implantation outcomes to design a predictive model of implantative endometrium

To perform this specific objective, we used the samples from the discovery cohort, consisting of a sample set with different implantation outcomes. We collected the EF samples from women undergoing FET on day 5, just before transfer. Then, we divided the samples into two groups according to the outcome and we ended up with 30 samples, 15 from women in whom implantation was successful and 15 in whom it was not successful.

Before starting with the analyses, we characterized the EF samples from all the women. Then, we extracted the RNA with PBP-M and PBP-N and analyzed it via small RNA-seq. After that, we performed differential abundance analysis to discover miRNAs associated with implantation outcome and confirmed the results via qPCR in the same samples.

3.1. Characterization of EF samples

We started the characterization of the sample with CB and found high variability in the amount of protein in the samples (**Figure 33A**) (**Table 10**). The WB intensity measurement revealed that the expression of albumin and immunoglobulins was higher in those samples that also had a total protein higher concentration, with a correlation coefficient (r) of 0.65 (p-value= 0.0066) and 0.86 (p-value=0.0001), respectively (**Figure 33B**). Accordingly, vesicular markers like FLOTILLIN-1 (r= 0.76, p-value= 8.7×10^{-7}), RAB8 (r= 0.89, p-value= 1.4×10^{-12}) and HSP90 (r= 0.82, p-value=2.3×10^{-7}) were also detected in most samples and positively correlated with total protein content. However, exosomal tetraspanins CD63 and CD9 were detectable in some samples, but in a fashion that did not correlate with total protein quantity (**Figure 33C**).
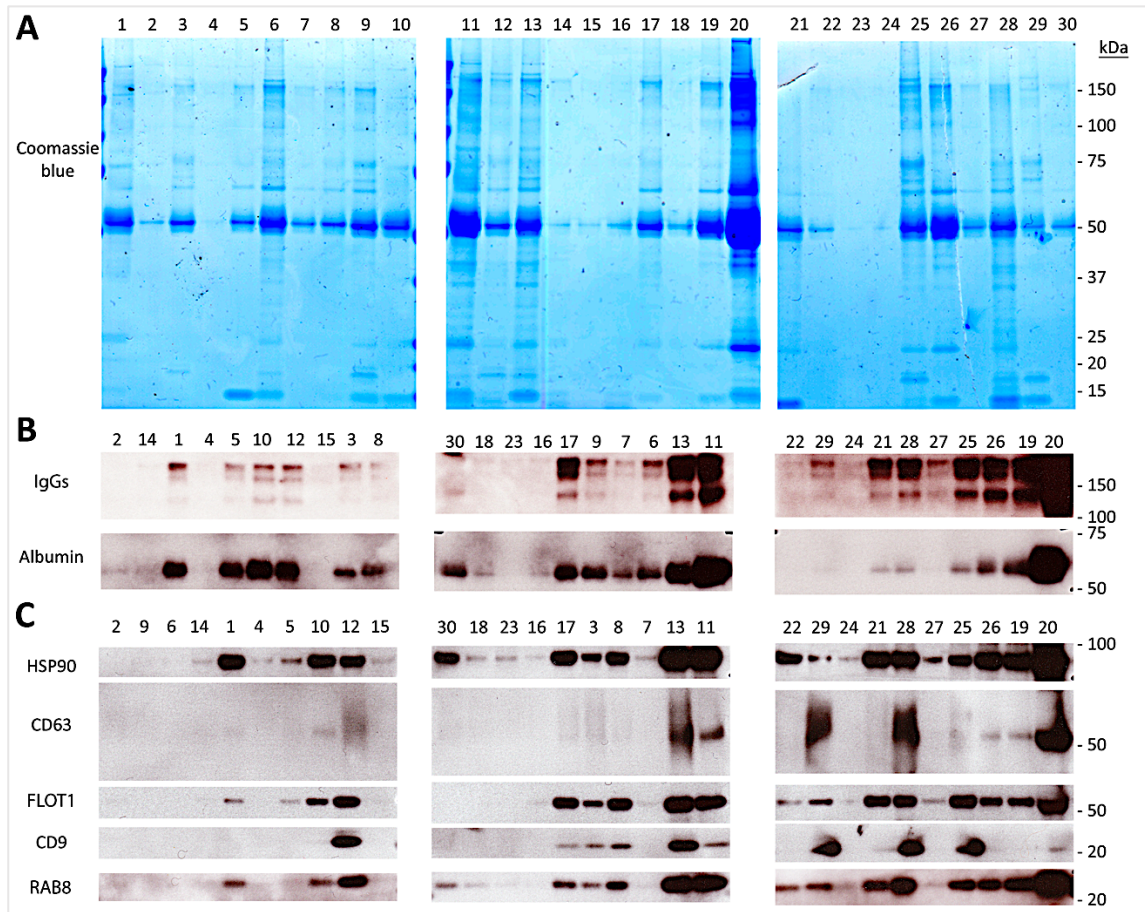
Figure 33. *Characterization of EF samples from the discovery cohort.*

(A) CB staining of precast gels. **(B)** WB of soluble proteins. **(C)** WB of EV-associated proteins. Statistical analysis was performed using the unpaired t-test with Welch's correction. We did not find differences between relative abundance levels of the proteins studied in implantative and non-implantative EF samples. The endometrium was considered implantative when pregnancy was confirmed by vaginal ultrasound showing a gestational sac four weeks after ET. The numbers above each lane correspond to the number assigned to each EF sample (1 = EF_1).

Table 10. *Features of the samples comprising the discovery cohort.*

Samples	Group	Total Volume (µL)	Protein content analysis					
			Coomassie Blue (RA)	Western blotting				
				ALBUMIN (RA)	IgGs (RA)	FLOTILIN-1 (RA)	RAB8 (RA)	HSP90 (RA)
EF_01	Imp.	1400	64634.6	31715	30240.5	5353.4	12030.5	23504.1
EF_02	Imp.	1200	49872.3	1848.7	47.8	-	-	-
EF_03	Imp.	1300	55001.9	17185.7	23513.2	13326.8	6429.7	9050.7
EF_04	Imp.	1300	49776.1	788.3	2355.7	-	-	5032.8
EF_05	Imp.	1250	56652.8	34604	18852.2	3167.8	6277	9050.6
EF_06	Imp.	825	71263.5	20022.4	14556.4	-	-	-
EF_07	Imp.	1300	55018.3	16827.3	7401.4	3901.8	3033.2	2630.5
EF_08	Imp.	1275	60176.5	25355.3	16043.34	27702.01	13817.1	16990.9
EF_09	Imp.	825	68197	21340.1	15962.2	-	-	-
EF_10	Imp.	1200	67450.3	40818	36659.6	13809.2	14499.3	24542.3
EF_11	Non-Imp.	1275	86916.4	64502.3	51219.5	37337.4	34037.7	40964.1
EF_12	Imp.	1350	58893.7	40232.7	34905.2	26713.6	30059.1	20165.4
EF_13	Imp.	1100	71498.6	33757.4	50343.4	42472.4	31891.6	38100.8
EF_14	Imp.	1100	46813.1	5739	314.7	-	-	3994.9
EF_15	Imp.	1350	46889.8	1091.7	7311.4	2295.9	-	6438
EF_16	Non-Imp.	1275	50968.9	6291.8	4042.6	-	-	1187.04
EF_17	Non-Imp.	1150	59538.5	24553.5	31661.9	26926.5	10406.9	19628.9
EF_18	Non-Imp.	1300	47443.4	6245.9	3299.6	-	2757.2	1960.8
EF_19	Non-Imp.	1260	59181.5	20477.7	46759.3	22778.7	22940.5	34522.7
EF_20	Non-Imp.	1350	125449.2	74924.2	80717.5	44320.1	53118.7	55859.7
EF_21	Non-Imp.	1200	71418.3	2440.9	27733.8	25146.6	17329.2	29292.7
EF_22	Non-Imp.	1350	61345.6	43.1	9203.1	5022.7	3203.4	20314.3
EF_23	Non-Imp.	1300	57171.3	871.2	2739.6	-	1455.1	1778.2
EF_24	Non-Imp.	1350	57982.8	61.9	10868.4	2085.7	5333.9	3173.6
EF_25	Non-Imp.	990	81140.4	7822.4	37895.7	31893.6	17376.23	21176.1
EF_26	Non-Imp.	1250	80462.9	14383.7	40474.2	19743.9	16926.8	34324.6
EF_27	Non-Imp.	1100	62586.8	1027.6	17401.4	7022.8	2589.2	8730
EF_28	Non-Imp.	1375	77260.7	4537.3	31760.1	24821.9	26951.1	30336.2
EF_29	Non-Imp.	1400	62988.5	1572.6	18609.2	9363.9	9686.3	6172.6
EF_30	Imp.	1300	62081.5	18729.2	9337.9	-	5842.8	18741

For protein analysis, both Coomassie blue and western blot were used and data were measured with Image J software. Results from both CB and WB were analyzed by densitometry of non-saturated films. Data represent the relative abundance of the band intensity. Statistical analysis was performed with unpaired t-tests with Welch's correction, we did not find differences in the relative abundance of proteins between implantative and non-implantative EF samples. **Imp.:** implantative endometrium group. **Non-Imp.:** non-implantative endometrium group. **(-):** not analyzed. **RA:** relative abundance with arbitrary units.

3.2. Small RNA-seq analysis of the RNA

PBP-M and PBP-N, the most efficient protocols tested, were chosen for their implementation in the discovery cohort and the total RNA extracted with each method was analyzed by small RNA-seq. We used 800 µL from each patient to perform the analyses, 400 µL for PBP-M and 400 µL for PBP-N, so we ended up with 60 samples for sequencing (**Figure 34**).
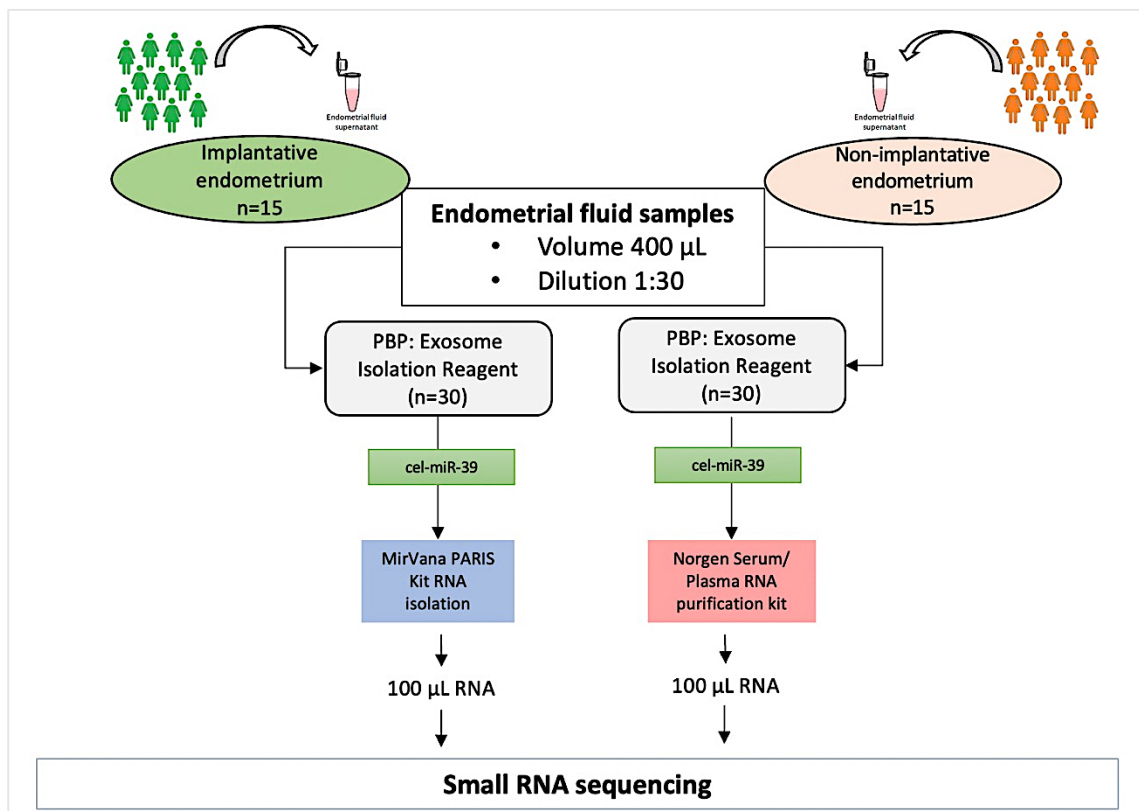
Figure 34. *Workflow of the two methods used to analyze microRNAs from the EF of patients from the discovery cohort.*

After sequencing, we performed post-alignment quality control (QA/QC) and found great variability not just between samples, but also between the results from each method for the same sample (**Table 11**).

Table 11. *Features of the samples from the discovery cohort selected for the regression study.*

Samples	Group	Small RNA-seq results (QA/QC)								Regression study
		PBP-M				PBP-N				
		Total Unique Aligned Reads (%)	Total reads	%GC	Detected miRNAs (miRBase)	Total Unique Aligned Reads (%)	Total reads	%GC	Detected miRNAs (miRBase)	
EF_01	Imp.	65.9	11523222	49	422	52.9	16970891	49.2	373	X
EF_02	Imp.	20.6	5428370	59.2	5	8.6	12782304	59	27	
EF_03	Imp.	22.1	5618614	65	109	36.3	15220592	54.3	348	X
EF_04	Imp.	13.9	6565685	54.7	51	8.8	10970380	58.6	47	
EF_05	Imp.	19.9	8531297	50.8	230	12.7	12665320	53.1	142	X
EF_06	Imp.	81.3	11024152	48.6	423	74.1	16058127	49.9	446	X
EF_07	Imp.	13.8	7948233	53	146	9.7	12099316	58.7	16	
EF_08	Imp.	49.5	8379125	51.9	327	40.3	14918455	49.3	344	X
EF_09	Imp.	57.8	10576549	51	424	47.5	15139029	50.7	398	X
EF_10	Imp.	48.3	15237405	49.2	394	40.5	8157371	46.7	313	X
EF_11	Non-Imp.	68.7	26570425	50.4	386	71.9	14883777	48.9	461	X
EF_12	Imp.	35.3	8273299	53.7	223	34.6	12162183	51.7	335	X
EF_13	Imp.	69.4	11454487	51.2	341	69.3	15422131	50.2	420	X
EF_14	Imp.	6.5	9586757	55.5	16	10.2	10978444	57.5	19	
EF_15	Imp.	5.9	8101447	53.5	17	8.1	14161997	57.7	18	
EF_16	Non-Imp.	4.2	7223708	53.2	14	9.1	14595741	59.4	38	
EF_17	Non-Imp.	52.6	11851513	50.8	262	58.9	15579659	49.3	411	X
EF_18	Non-Imp.	7.5	8866162	54.5	42	11.7	14343292	61.8	39	X
EF_19	Non-Imp.	40.2	8880607	47.5	295	61.8	16848708	46.5	472	X
EF_20	Non-Imp.	65.4	9540061	45.3	403	64.6	17112011	45.3	470	X
EF_21	Non-Imp.	47.5	10093215	47	298	54.4	15516426	45.2	412	X
EF_22	Non-Imp.	26.8	8528348	55.7	162	10.7	13333601	56.3	91	
EF_23	Non-Imp.	2.8	5274798	53.6	9	8.1	14705033	59.5	8	
EF_24	Non-Imp.	2.5	5362146	55.6	14	8.3	14372768	57.6	8	
EF_25	Non-Imp.	26.7	8869919	52.3	138	47.5	15185061	47.7	452	X
EF_26	Non-Imp.	79.4	9774751	52.5	338	72.1	15960924	52.2	419	X
EF_27	Non-Imp.	1.9	5627886	52.3	10	13.9	13421955	50.7	182	X
EF_28	Non-Imp.	77	12599904	52.8	373	61.6	17323428	49.2	502	X
EF_29	Non-Imp.	1.5	8758050	51	1	47.1	14686513	56.7	290	X
EF_30	Imp.	27.3	6168515	53.7	123	18.3	14896951	52.1	195	X

The small RNA-seq results show the results obtained for each sample in each technique used, PBP-M and PBP-N. The last column shows the samples used to design the predictive models (Marked "X"). Im**p.:** implantative endometrium group. **Non-Imp.:** non-implantative endometrium group. %GC corresponds to the percentage of cysteines and guanines of the sequences. **QA:** Quality assurance and **QC:** Quality control. **PBP-M:** EV enrichment with a PBP method + RNA extraction with the mirVana PARIS kit). **PBP-N:** EV enrichment with a PBP method + RNA extraction with the Norgen Plasma/serum RNA purification kit.

As shown in **Table 12**, the results for the PBP-M technique showed that the samples with the highest percentage alignment with the human genome were EF_06, (81.3 % and 423 miRNAs), EF_26 (79.4 % and 338) and EF_28 (77 % and 373), on the other hand, the three samples with the lowest percentage alignment were EF_29 (1.5 % and 1 miRNA), EF_27 (1.9 % and 10 miRNAs) and EF_24 (2.5 % and 14 miRNAs). However, sample EF_09, with an alignment percentage of 57.8 % was that in which more miRNAs were detected with miRbase, a total of 424.

For the PBP-N technique, the three samples with the highest percentage alignment were EF_06, (74.1 % and 446 miRNAs), EF_26 (72.1 % and 419) and EF_11 (71.9 % and 461), on the other hand, the three samples with the lowest percentage alignment were EF_23 (8.1 % and 8 miRNA), EF_15 (8.1 % and 10 miRNAs) and EF_24 (8.3 % and 8 miRNAs). In this case, the sample with the largest number of miRNAs detected was EF_28 with 502 miRNAs and an alignment percentage of 61.6 %.

When we compared the results obtained between the two techniques, we observed that the two samples with the highest percentage alignment coincided (EF_06 and EF_26). These samples obtained a higher percentage alignment with PBP-M, however, the number of miRNAs detected was different, being higher for the PBP-N method. Along this line, the samples with less alignment were also similar in both techniques. Remarkably, sample EF_29 in the case of PBP-M obtained very poor results (1.5 % and 1 miRNA), while with PBP-N the results were much better, 47.1 % alignment and 290 miRNAs. These results suggested that sample EF_29 was not properly extracted with the PBP-M technique. Something that had already been detected in previous experiments, since the PBP-M technique proved to be less reproducible as it is more complex to perform.

To visualize the results, we created two heatmaps (**Figure 35** and **36**) that show the abundance of each miRNA in the different samples.
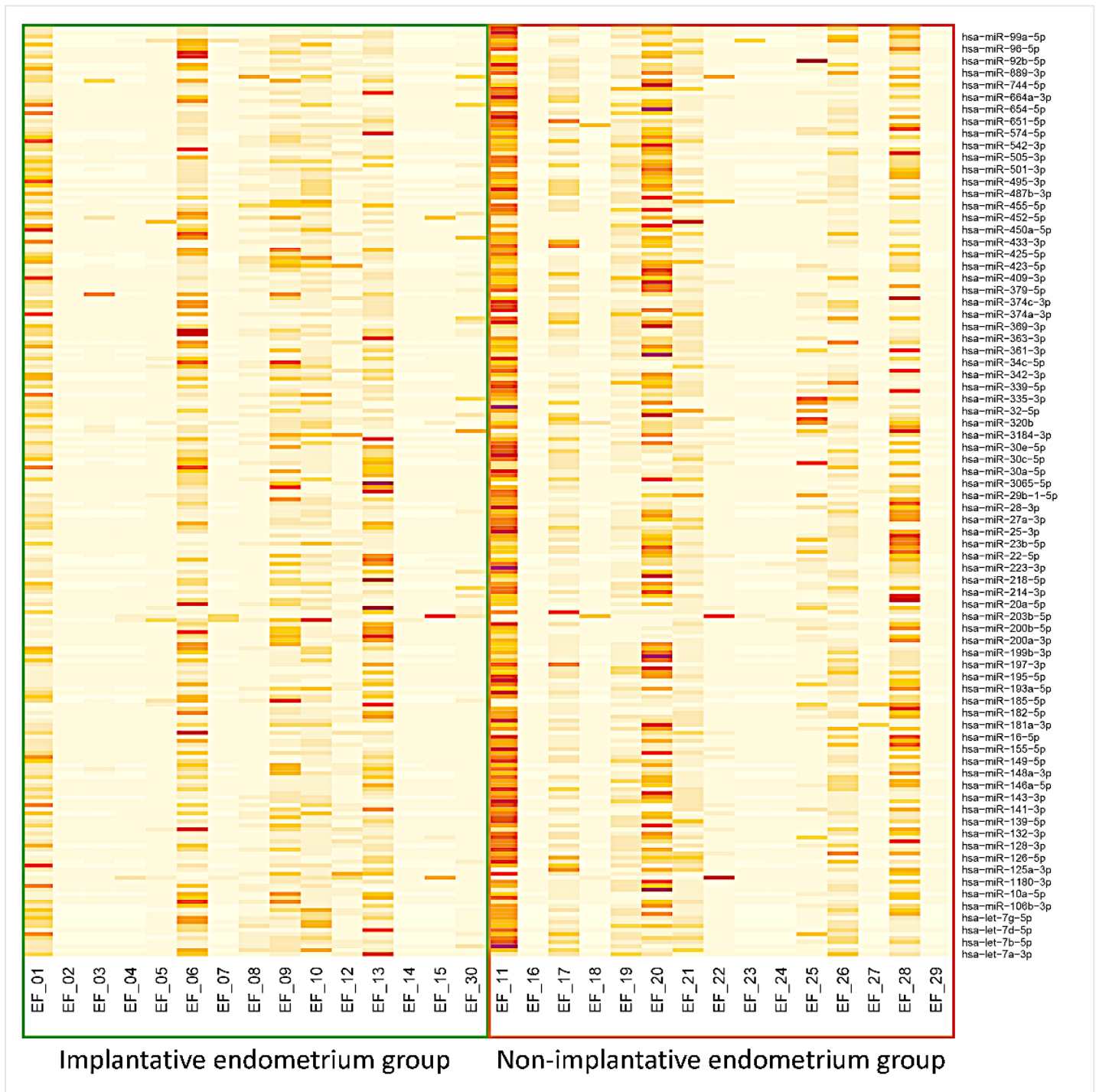
Figure 35. *Heatmap of small RNA-seq results obtained with the PBP-M method.*

Heatmap representing the abundance of each miRNA in each sample of the discovery group (n=30). 15 samples from women with successful implantation and 15 with implantation failure. **PBP-M:** EV enrichment with a PBP method + RNA extraction with the mirVana PARIS kit.
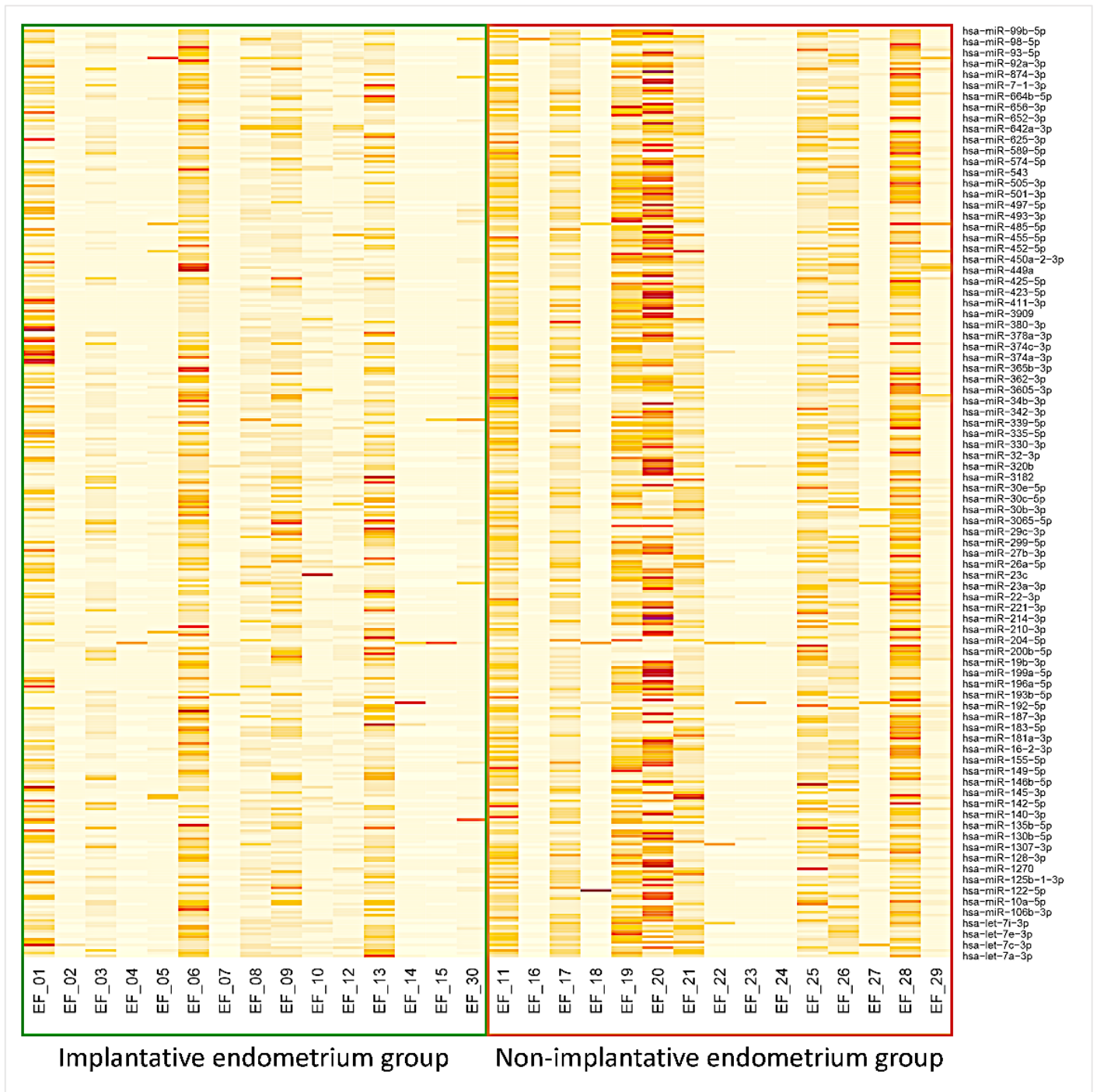
Figure 36. *Heatmap of small RNA-seq results obtained with the PBP-N method.*

Heatmap representing the abundance of each miRNA in each sample of the discovery group (n=30). 15 samples from women with successful implantation and 15 with implantation failure. **PBP-N:** EV enrichment with a PBP method + RNA extraction with the Norgen Plasma/serum RNA purification kit.

We also analyzed the correlation between EV-associated proteins and miRNAs in the EF. For that, we used the data obtained from WB, CB and small RNA-seq. We found that most miRNAs positively correlated with EV-associated proteins such as FLOTILIN-1, RAB8 and HSP90. These results were found with the data from both PBP-M (**Figure 37)** and PBP-N (**Figure 38**).
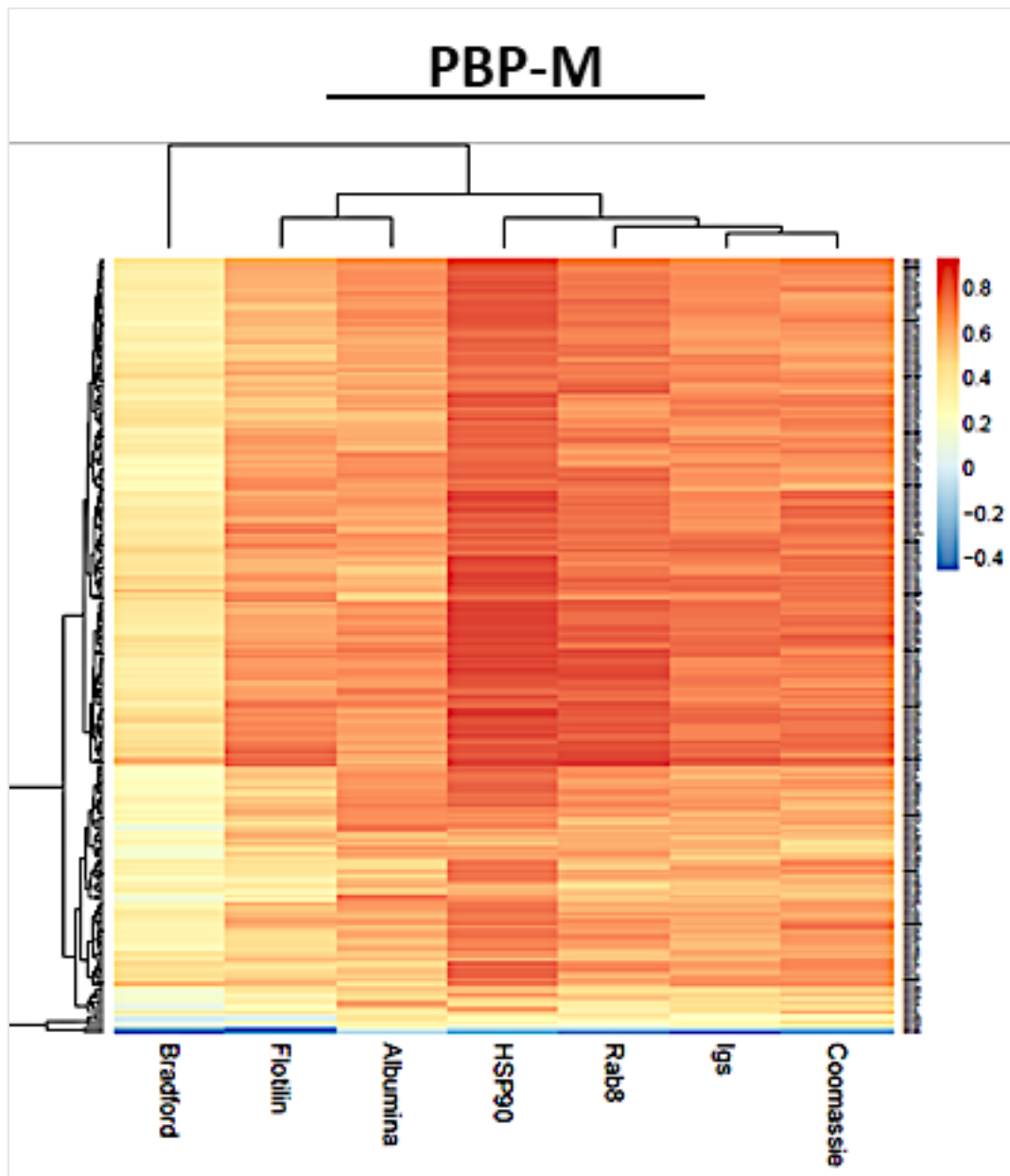
Figure 37. *Heatmap of the correlation between miRNAs and EV-associated proteins in PBP-M.*

Heatmap representing the correlation between miRNAs and EV-associated proteins in samples from the PBP-M technique. **PBP-M:** EV enrichment with a PBP method + RNA extraction with the mirVana PARIS kit.
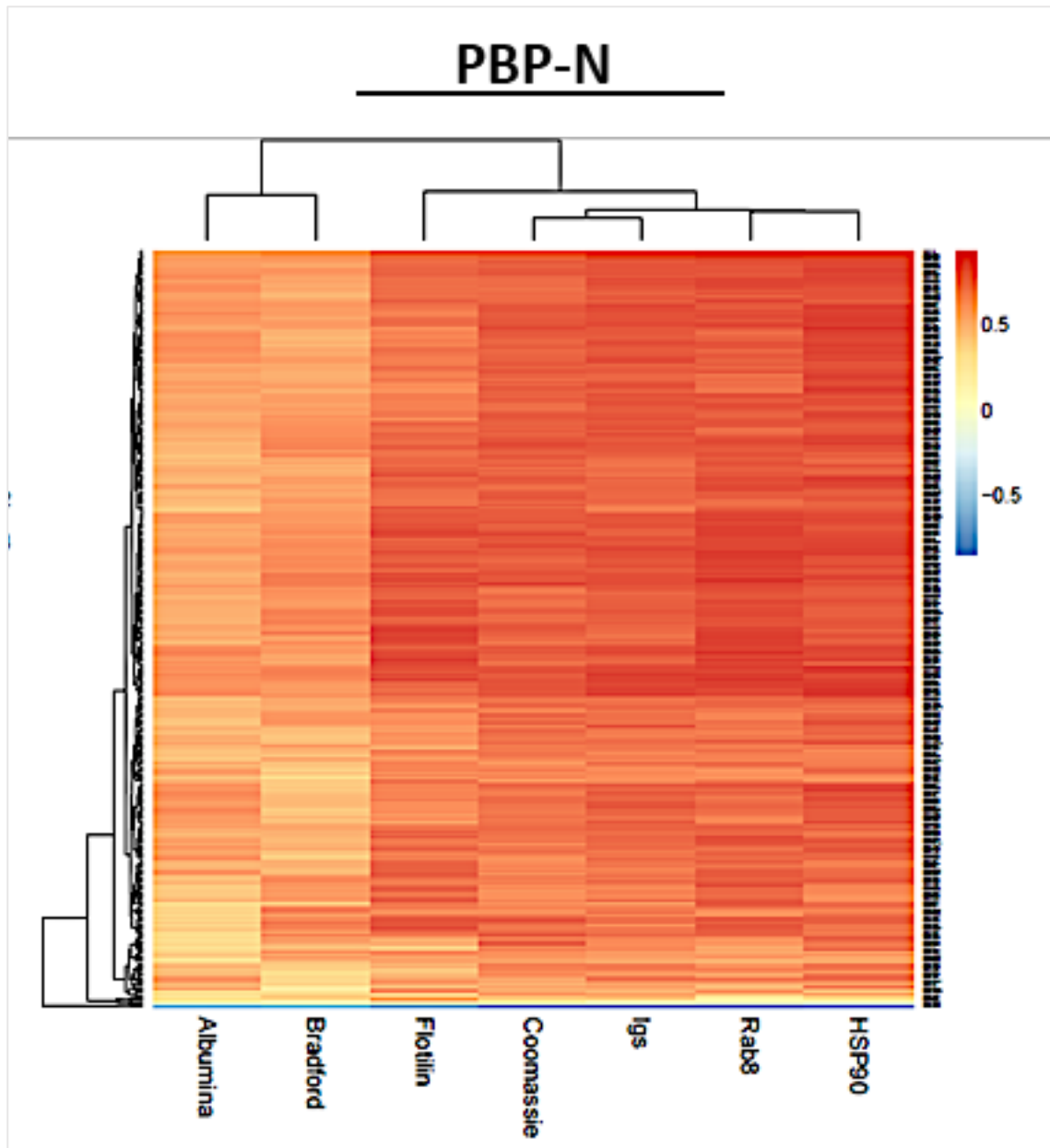
Figure 38. *Heatmap of the correlation between miRNAs and EV-associated proteins in PBP-N.*

Heatmap representing the correlation between miRNAs and EV-associated proteins in samples from the PBP-M technique. **PBP-N:** EV enrichment with a PBP method + RNA extraction with the Norgen kit.

Next, to discover differentially expressed miRNAs between implantative and non-implantative EF samples, we performed differential abundance analysis. As we found variances in the total amount of miRNA content in the EF samples and we wanted to avoid this variable as much as possible in the analysis, we applied TMM normalization before performing differential abundance analysis. In addition, as there were samples that had many miRNAs with zero or very low counts, and those miRNAs with very low counts in all samples provided little evidence for differential expression, we filtered out miRNAs with all zero counts or very low counts. We also kept any miRNA that was roughly expressed in at least one group (Filtering described in MM section 10.2). After the filtering analyses, we considered 231/845 and 341/910 unique miRNAs for differential abundance analysis for the PBP-M and PBP-N datasets respectively (**Figure 39**).
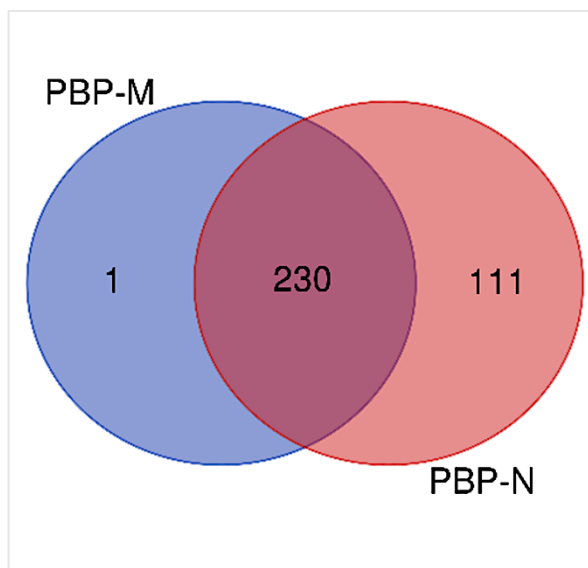
Figure 39. *Venn diagram showing the number of unique miRNAs for PBP-M and PBP-M detected by small RNA-Seq.*

These experiments were conducted using discovery cohort samples (n=30), 15 samples from women with successful implantation and 15 with implantation failure. The Venn diagram shows the number of common miRNAs detected by small RNA-seq (after TMM normalization) between PBP-M and PBP-M (n=230) and the number of miRNAs detected exclusively with each of the techniques PBP-M (n=1) and PBP-N (n=111). **PBP-N**: consisted of a prior step of EV enrichment with a PBP method and RNA extraction with the Norgen Plasma/Serum RNA purification kit. **PBP-M**: consisted of a prior step of EV enrichment with a PBP method and RNA extraction with the mirVana PARIS kit.

The differential abundance analysis applied to PBP-M data detected 34 /231 miRNAs with adjusted p-value <0.05. Of these, we selected the miRNAs that followed the same pattern between raw counts of the small RNA-seq data and the fold-change values of the differential abundance analysis. Thus, we ended up with 13 miRNAs suitable for further validation by qPCR in the same samples (**Table A1, Annex I**).

The differential abundance analysis applied to PBP-N data detected 11 /341 miRNAs with adjusted p-value <0.05. As explained above, we selected the miRNAs that followed the same trend in raw counts and fold-change values. Thus, we ended up with five miRNAs suitable for further validation by qPCR in the same samples (**Table A2, Annex II**).

However, we decided to validate all candidate miRNAs with both techniques, because these miRNAs were common to both methods and the results were derived from the same samples in all cases.

3.3. Design of a predictive model of implantative endometrium by qPCR

The 16 miRNAs detected by small RNA-seq were analyzed via qPCR in the RNA extracted via PBP-M and PBP-N; with the data, we performed differential abundance and regression analyses to design a predictive model of implantative endometrium. From these analyses, we defined two models; we called the model designed with PBP-M "Model 1", and that with PBP-N "Model 2".

However, to perform the differential abundance and regression analyses, we needed to normalize the samples since we observed great variability between biological samples, as we did for small RNA-seq data.

Our first approach was to select an adequate endogenous miRNA control for normalization, for that, we analyzed the seven reference miRNAs used in the previous experiments. We analyzed the variability of the seven reference miRNAs both in the implantation and non-implantation group.

We were looking for those normalizer miRNAs that were equally expressed in both groups (**Table 12**), had a positive correlation with the total amount of protein in the sample (PBP-N: hsa-miR-200c-3p r = 0.8; p-value 3.8×10^{-6}; and hsa-miR-92a-3p r = 0.8, p-value = 1.1×10^{-6} / PBP-M: hsa-miR-200c-3p r = 0.8; p-value 9.1×10^{-7}; and hsa-miR-92a-3p r = 0.7, p-value = 3.5×10^{-5}), had a positive correlation between small RNA-seq data and qPCR data (**Figure 40**), and that were abundantly detected by small RNA-seq (more than 100 raw counts and high *p*-value). Among the miRNAs fulfilling these criteria, the NormFinder algorithm identified hsa-miR-200c-3p (stability PBP-M=0.31 and PBP-N=0.24) and hsa-miR-92a-3p (stability PBP-M=0.27 and PBP-N=0.1) as the most suitable pair of normalizer miRNAs (**Table 12**).

Table 12. *Results of the NormFinder algorithm.*

miRNAs	NormFinder algorithm					
	PBP-M			PBP-N		
	Group difference	Group SD	Stability	Group difference	Group SD	Stability
hsa-let-7-5p	0.3	0.9	0.3	0.2	0.9	0.3
hsa-miR-17-5p	0.3	2.4	0.8	0.4	1.6	0.5
hsa-miR-200c-3p	**0.2**	**0.9**	**0.3**	**0.7**	**0.8**	**0.2**
hsa-miR-30c-5p	0.5	0.8	0.2	0.2	0.7	0.2
hsa-miR-30d-5p	0.5	0.6	0.2	0.1	0.6	0.2
hsa-miR-451a	0.1	1.9	0.6	0.3	1.8	0.6
hsa-miR-92-5p	**0.2**	**0.9**	**0.3**	**0.3**	**0.3**	**0.1**

The NormFinder algorithm was used to select the most appropriate endogenous miRNA control among the reference miRNAs analyzed. The stability score is a weighted measure of the intergroup and intragroup variation, and the most stable reference miRNA is that with the smallest stability value. The data from this experiment came from the analysis of each miRNA detected in the discovery cohort (n = 30; 15 implantative and 15 non-implantative endometrium). **PBP-M:** EV enrichment using a PBP method and RNA extraction with the mirVana PARIS kit. **PBP-N:** EV enrichment using PBP and RNA extraction with the Norgen Plasma/serum RNA purification kit.
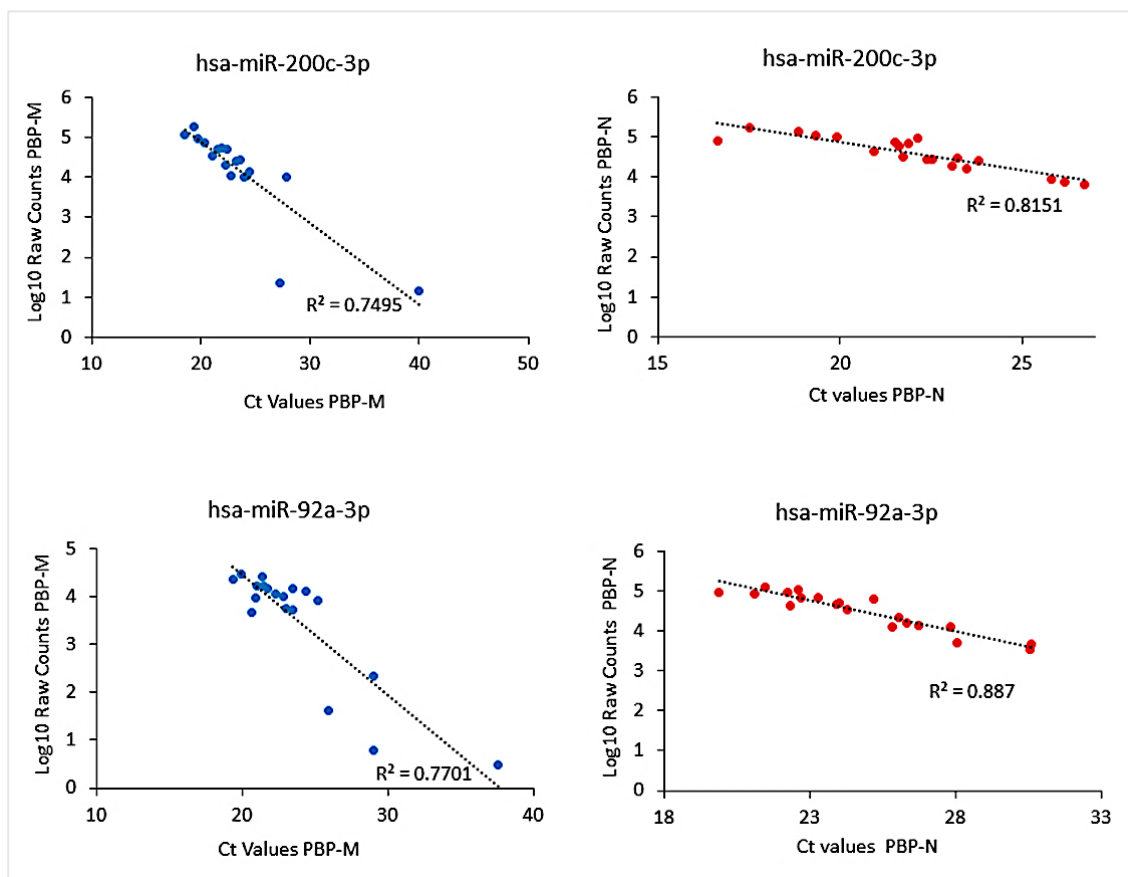
Figure 40. *Correlation analyses to determine the suitability of the selected internal controls.*

The graphs show the results obtained for each miRNA by small RNA-seq and qPCR. The miRNAs selected as internal normalizers were hsa-miR-200c-3p and hsa-miR-92a-3p. **PBP-N:** consisted of a prior EV enrichment step with a PBP method and RNA extraction with the Norgen Plasma/Serum RNA purification kit. **PBP-M:** consisted of a prior EV enrichment step with a PBP method and RNA extraction with the mirVana PARIS kit.

3.3.1.   Model 1 (PBP-M)

The results of the differential abundance analysis with the normalized dCt from PBP-M are summarized in **Table A1** (**Annex I**). We compared qPCR data with that from small RNA-seq and found that, out of 16 miRNAs, 10 followed the same trend as in the small RNA-seq data, of these, only two were significantly downregulated in the implantation group, hsa-miR-132-3p and hsa-miR-24-3p. There was another miRNA that was significantly downregulated in the implantation group (hsa-miR-185-5p); however, it was significantly upregulated in the implantation group according to small RNA-seq data. The normalized qPCR data were also used to determine predictive Model 1 via a regression study using bootstrapping correction.

To perform the regression study, we only considered those samples in which we were able to detect the internal controls with fewer than 30 Ct cycles by qPCR analysis (**Table 11**). The results for data obtained with PBP-M showed that Model 1, based on three miRNAs was robust against data that fitted within the given characteristics (**Figure 41**). The miRNAs selected in this case were: hsa-miR-24-3p, hsa-miR-200b-3p and hsa-miR-148b-3p. For model 1, we obtained the following results:

- Accuracy/efficiency: 0.86
- Area under the curve (AUC): 0.93
- p-value: 0.003259
- Sensitivity: 0.88
- Specificity: 0.83
- Positive predictive value: 0.84
- Negative predictive value: 0.88

3.3.2. Model 2 (PBP-N)

The results of the differential abundance analysis with the normalized dCt from PBP-N are summarized in **Table A2** (**Annex II**). We compared qPCR data with that from the small RNA-seq and found that, out of 16 miRNAs, eight followed the same trend as in the small RNA-seq data, of these, only two were significantly upregulated in the implantation group, hsa-miR-200b-3p and hsa-miR-99b-5p. There was another miRNA that was significantly downregulated in the implantation group (hsa-miR-24-3p); however, it was significantly upregulated in the implantation group according to small RNA-seq data.

To perform the regression study, we only considered those samples in which we were able to detect the internal controls with fewer than 30 Ct cycles by qPCR analysis (**Table 11**). The regression study using bootstrapping correction also showed a predictive model based on three miRNAs for the PBP-N method (**Figure 41**). Of the miRNAs selected for the predictive models, two were the same as in Model 1 (hsa-miR-24-3p, hsa-miR-200b-3p) while hsa-miR-99b-5p was unique to Model 2**.**

For Model 2, we obtained the following results:

- Accuracy/efficiency: 0.83
- Area under the curve (AUC): 0.92
- p-value: 0.00023
- Sensitivity: 0.80
- Specificity: 0.85
- Positive predictive value: 0.84
- Negative predictive value: 0.81

Both models were significantly predictive compared with a random chance hypothesis (AUC= 0.5).
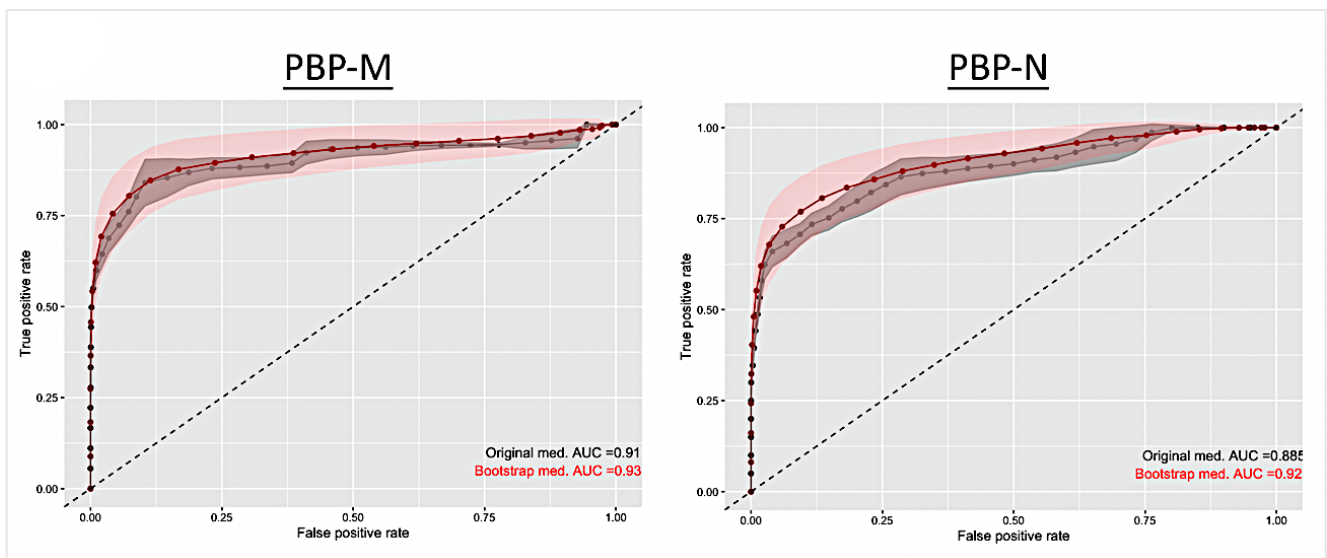
Figure 41. *ROC of the three miRNA-based predictive models tested by qPCR in the discovery cohort.*

The performance of the original model is shown in black, and mean performance of the bootstrap output is shown in red. The shading indicates the extent of the standard deviation. The AUC is shown in the respective colors in the lower right-hand corner of the graphs. **PBP-N:** extracellular vesicle enrichment using PBP and RNA extraction with the Norgen Plasma/Serum RNA purification kit. **PBP-M:** extracellular vesicle enrichment using a PBP method and RNA extraction with the mirVana PARIS kit, **miRNAs**: microRNAs, **PBP:** polymer-based precipitation, **qPCR**: quantitative PCR, **RNA-Seq**: RNA-sequencing, **TMM:** Trimmed Mean of M-values. **ROC:** Receiver Operating Characteristic curve.

4. To validate predictive models in a new independent cohort (Validation cohort) of women with different implantation outcomes

The performance of the two predictive models (Model 1 and Model 2) was validated in an independent cohort called the "validation cohort". As described before, EF samples were collected just before a day 5 FET; we analyzed 60 EF samples, 30 collected from women in whom implantation was successful and 30 in whom it was not **(Figure 42)**. In this experiment, the RNA extracted was used to validate the models by qPCR; before RNA extraction, the protein content of the EF samples was analyzed.
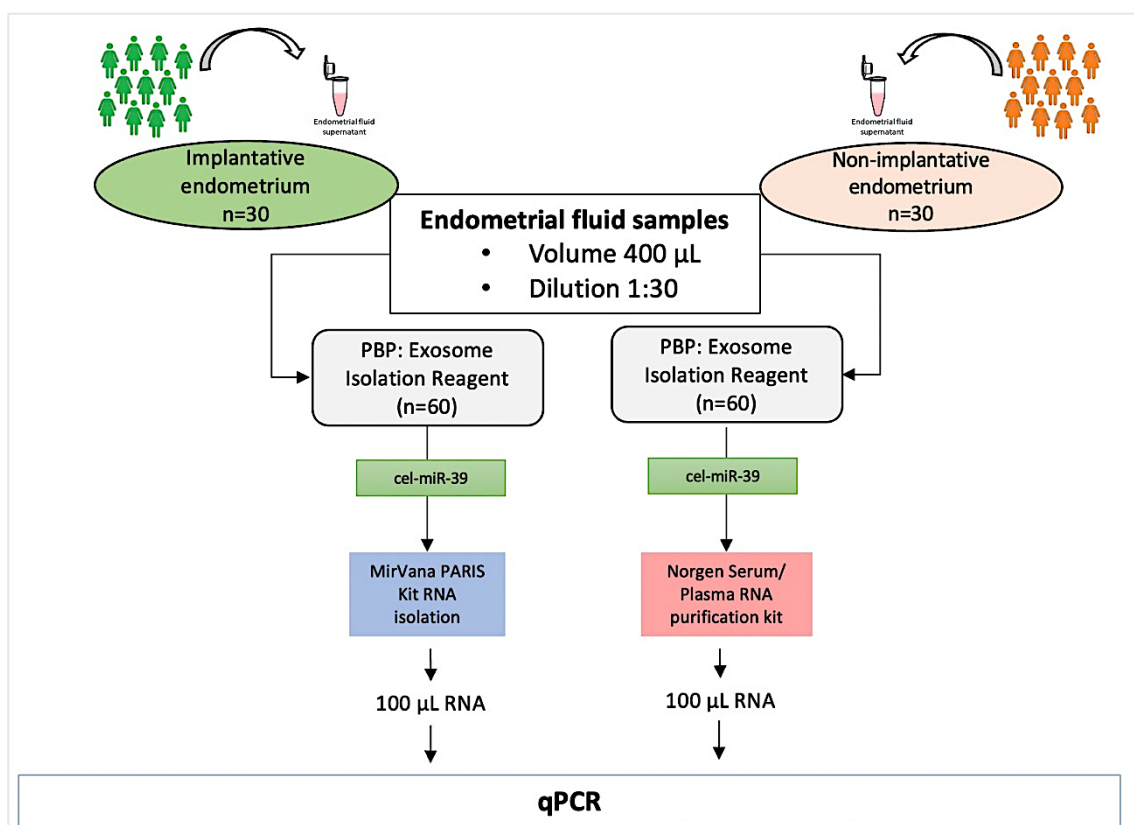
Figure 42. *Workflow of the two methods used to analyze microRNAs from the EF of patients from the discovery cohort.*

4.1. Characterization of EF samples

We carried out CB of the samples and, as expected, found considerable variability in the amount of protein in the samples (**Figure 44**). The WB results concorded with those obtained with CB, confirming that there was great biological variability among the samples; nevertheless, we were able to detect EV-associated proteins in all samples (**Figure 45**). We analyzed the total protein and miRNA content of the samples by spectrophotometry and found a very good correlation between total RNA and total protein amounts in the samples (**Figure 43**). All results are summarized in **Table 13**.
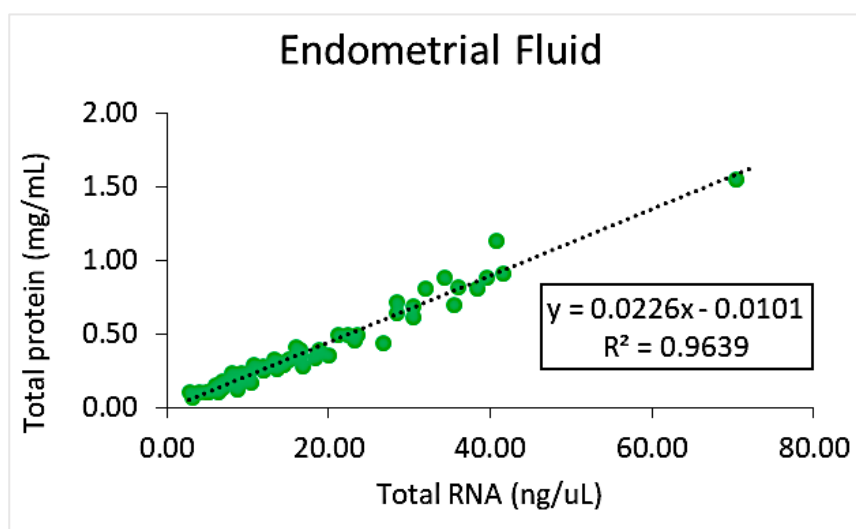
Figure 43. Correlation between the total protein and total RNA amount in the validation group.
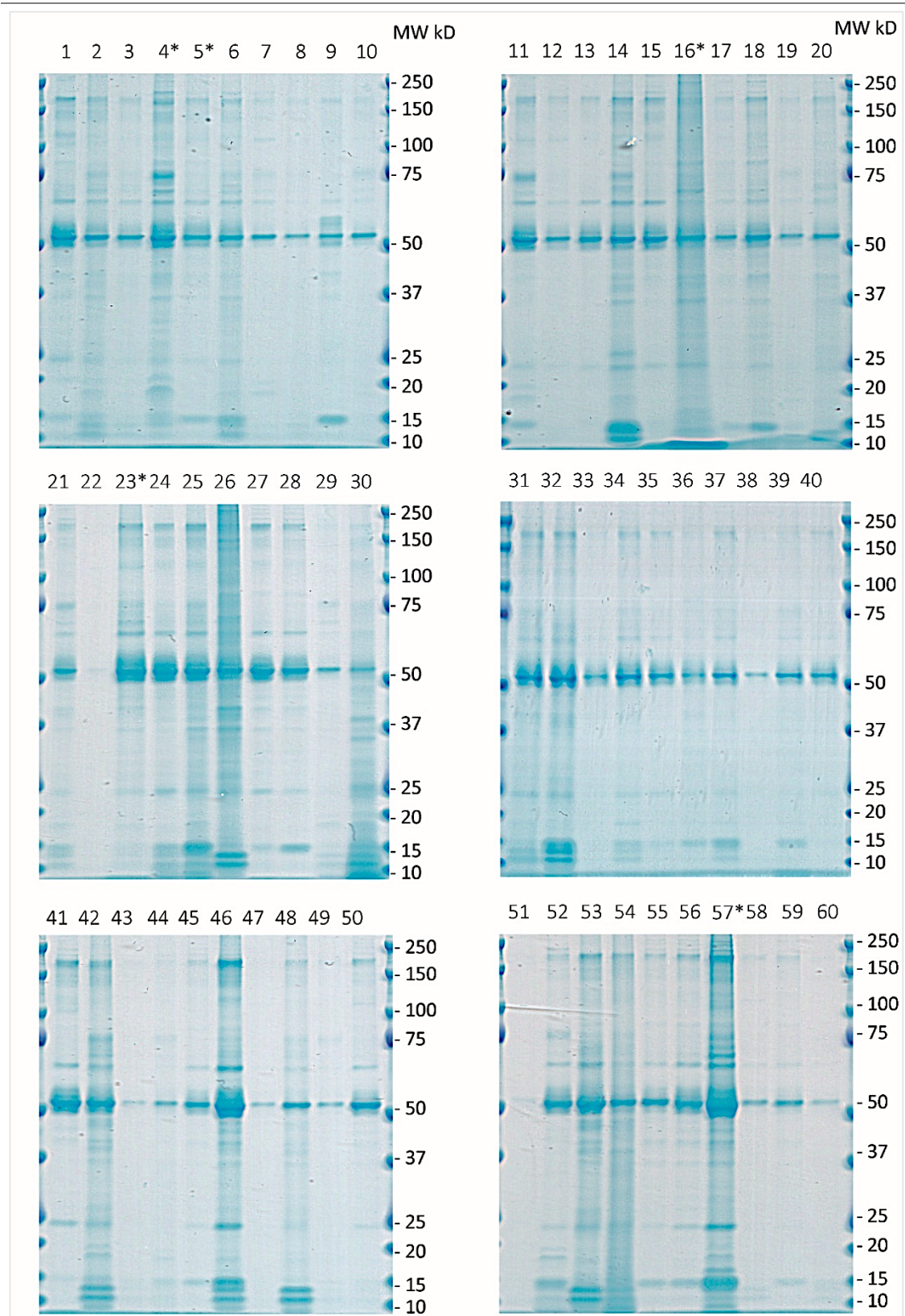
Figure 44. *CB of samples comprising the validation cohort.*

The numbers above each lane correspond to the number assigned to each EF (1 = EF_1). Statistical analysis was performed with the unpaired t-test with Welch's correction. We did not find any differences between relative abundance levels of the proteins studied in implantative and non-implantative EF samples. The endometrium was considered implantative when pregnancy was confirmed by vaginal ultrasound showing a gestational sac four weeks after ET. * Samples with less than 15 µL. **CB:** Coomassie blue staining.

113
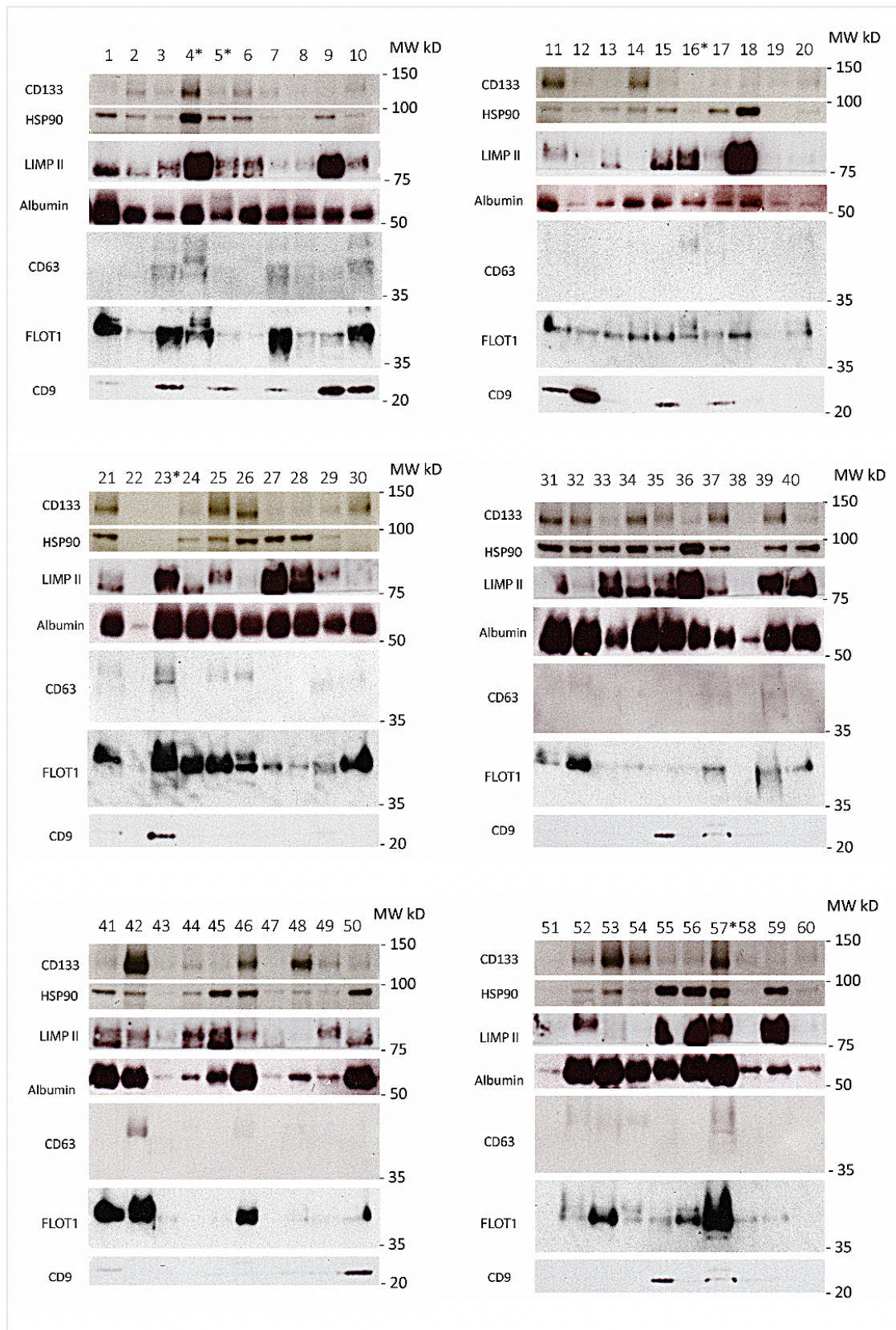
Figure 45. *WB of samples comprising the validation cohort.*

The numbers above each lane correspond to the number assigned to each EF (1 = EF_1). Statistical analysis was performed with the unpaired t-test with Welch's correction. We did not find any differences between the relative abundance levels of the proteins studied in implantative and non-implantative EF samples. The endometrium was considered implantative when pregnancy was confirmed by vaginal ultrasound showing a gestational sac four weeks after ET. * Samples with less than 15 µL. **WB**: Western blot analysis.

Table 13. *Characteristics of the samples comprising the validation cohort.*

Samples	Group	Characteristics				Samples selected to test the predictive models	
		Total Volume (µL)	Coomassie Blue (RA)	Total RNA (ug)	Total Protein (ug)	Model 1 (PBP-M)	Model 2 (PBP-N)
EF_01	Imp.	1180	87944.1	16.5	365.8	X	X
EF_02	Imp.	1070	103003.9	19.7	363.8	X	X
EF_03	Imp.	990	61359.4	8.7	217.8	X	X
EF_04	Imp.	830	112671.5	19.6	406.7	X	X
EF_05	Imp.	970	55133.3	11.6	242.5	X	X
EF_06	Imp.	1370	76484.9	25.8	520.6	X	X
EF_07	Imp.	1045	26464.9	4.2	104.5	X	X
EF_08	Imp.	1320	21958.8	11.6	158.4	X	X
EF_09	Imp.	1370	31332.9	8.2	205.5	X	X
EF_10	Imp.	1270	24739.0	8.6	228.6	X	X
EF_11	Imp.	910	50835.5	25.8	655.2	X	X
EF_12	Imp.	1345	27114.6	8.6	201.8	X	X
EF_13	Imp.	1045	28222.8	10.9	177.7	X	
EF_14	Imp.	920	101367.1	32.8	644.0	X	X
EF_15	Imp.	920	47532.1	15.1	322.0	X	X
EF_16	Imp.	670	143052.9	18.0	294.8	X	X
EF_17	Imp.	830	33289.7	12.6	273.9	X	X
EF_18	Imp.	1220	69852.9	24.4	427.0	X	X
EF_19	Imp.	1020	32609.6	9.4	183.6		
EF_20	Imp.	1120	58519.1	15.2	291.2	X	X
EF_21	Imp.	1320	49645.8	29.6	646.8	X	X
EF_22	Imp.	1020	23342.7	3.3	71.4		
EF_23	Imp.	771	74302.2	26.5	678.5	X	X
EF_24	Imp.	1120	57652.1	23.7	548.8	X	X
EF_25	Imp.	930	84436.6	28.3	641.7	X	X
EF_26	Imp.	1195	124808.6	45.9	968.0	X	X
EF_27	Imp.	1245	40717.8	17.4	373.5	X	X
EF_28	Imp.	1170	39135.3	14.0	327.6	X	X
EF_29	Imp.	1020	21330.7	10.2	224.4	X	X
EF_30	Imp.	871	75213.0	36.2	792.6	X	X
EF_31	Non-Imp.	1310	102319.9	37.2	838.4	X	X
EF_32	Non-Imp.	1200	117685.8	47.5	1056.0	X	X
EF_33	Non-Imp.	970	32518.0	9.7	223.1	X	X
EF_34	Non-Imp.	970	57543.0	15.5	397.7	X	X
EF_35	Non-Imp.	1045	40393.1	8.4	240.4	X	X
EF_36	Non-Imp.	1170	43271.1	15.4	339.3	X	X
EF_37	Non-Imp.	1120	56154.8	14.8	369.6	X	X
EF_38	Non-Imp.	1270	26142.3	3.6	127.0		
EF_39	Non-Imp.	1245	43957.1	17.9	361.1	X	X

Table 13. *Continued.*

Samples	Group	Characteristics				Samples selected to test the predictive models	
		Total Volume (µL)	Coomassie Blue (RA)	Total RNA (ug)	Total Protein (ug)	Model 1 (PBP-M)	Model 2 (PBP-N)
EF_40	Non-Imp.	1020	40699.1	9.4	234.6	X	X
EF_41	Non-Imp.	1070	66403.2	11.6	310.3	X	X
EF_42	Non-Imp.	1220	117420.5	43.9	1000.4	X	X
EF_43	Non-Imp.	1145	32186.8	6.9	160.3		
EF_44	Non-Imp.	1270	32667.5	21.3	355.6	X	
EF_45	Non-Imp.	980	36513.4	11.8	245.0	X	X
EF_46	Non-Imp.	990	129071.6	31.7	801.9	X	X
EF_47	Non-Imp.	980	15050.0	5.1	98.0		X
EF_48	Non-Imp.	970	57430.8	15.9	378.3	X	X
EF_49	Non-Imp.	1370	13618.1	9.3	178.1	X	X
EF_50	Non-Imp.	1045	34801.5	8.8	229.9	X	X
EF_51	Non-Imp.	1370	13300.8	8.8	137.0		
EF_52	Non-Imp.	1120	45350.2	26.0	515.2	X	X
EF_53	Non-Imp.	970	82659.8	68.3	1503.5	X	X
EF_54	Non-Imp.	1470	85854.6	44.7	896.7	X	X
EF_55	Non-Imp.	1220	33795.1	18.5	402.6	X	X
EF_56	Non-Imp.	1020	42170.2	19.2	397.8	X	X
EF_57	Non-Imp.	810	123228.1	33.0	915.3	X	X
EF_58	Non-Imp.	1220	20572.8	5.9	122.0		X
EF_59	Non-Imp.	1170	20133.8	10.8	210.6	X	X
EF_60	Non-Imp.	930	14511.1	7.8	158.1	X	

The table shows the biological features of the validation cohort. Statistical analysis was performed using unpaired t-tests with Welch's correction. We did not find any differences for relative abundance of proteins, total RNA or total protein content between the implantative and non-implantative EF samples. The last two columns represent the sample selected to validate the predictive models. Different samples were used to validate each method, depending on the qPCR result obtained in each case. Only samples in which the average Ct of the internal controls was less than 30 Ct were selected (marked with "X"). The endometrium was considered implantative when pregnancy was confirmed by vaginal ultrasound showing a gestational sac four weeks after ET. **Imp.:** implantative endometrium group. **Non-Imp.:** non-implantative endometrium group. **PBP-M:** EV enrichment with a PBP method + RNA extraction with the mirVana PARIS kit. **PBP-N:** EV enrichment with a PBP method + RNA extraction with the Norgen Plasma/serum RNA purification kit.

4.2. Validation of the predictive models in the validation cohort

The performance of the two predictive models (Model 1 and Model 2) was validated in the validation cohort. First, RNA was extracted via the PBP-M and PBP-N methods and analyzed by qPCR. The Ct values were normalized against the mean Ct values of the internal controls (hsa-miR-200c-3p and hsa-miR-92a-3p) due to the high biological variability between the samples. For method validation, we only considered those samples in which we were able to detect the internal controls with fewer than 30 Ct cycles by qPCR analysis.

4.2.1. Model 1 (PBP-M)

Model 1 (hsa-miR-200b-3p, hsa-miR-24-3p and hsa-miR-148b-3p) had an accuracy of 0.68 (95% CI = 0.54, 0.8) and an AUC of 0.69 (95% CI = 0.55, 0.86) (**Figure 46**). The test exhibited a statistically significant difference (p-value: 0.019) in AUC compared with a random chance hypothesis (AUC= 0.5). ROC analysis identified hsa-miR-148b-3p as the most likely variable to differentiate an implantative endometrium from a non-implantative endometrium, demonstrating significant differential expression between the groups at p-value <0.05; this miRNA was upregulated in the non-implantation group. We established the cut-off point as 2.34 dCt (dCt = Ct hsa-miR-148b-3p – Ct internal controls) based on Youden's J statistic with 0.56 sensitivity and 0.86 specificity. Values above the cut-off point would indicate an implantative endometrium (dCt >2.34) (negative predictive value=0.69) and values below would indicate a non-implantative endometrium (dCt <2.34) (positive predictive value = 0. 78).
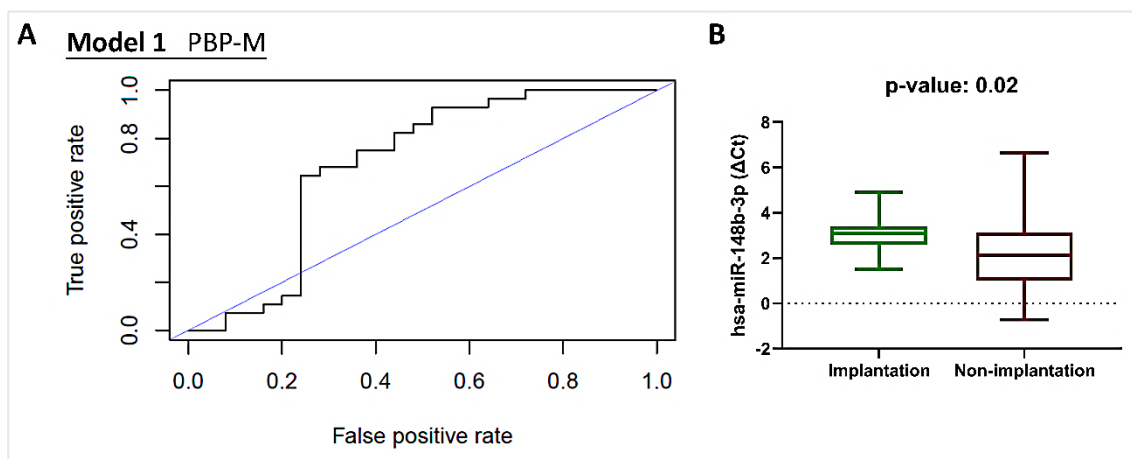
Figure 46. ROC of validated Model 1 and box plot of the most significant miRNA in the model.

The predictive models designed using the qPCR results for the PBP-M method applied to the discovery cohort were validated in a new group, the validation cohort (n = 60; 30 subjects in the implantative subgroup and 30 in the non-implantative subgroup). The endometrium was considered implantative when pregnancy was confirmed by vaginal ultrasound showing a gestational sac four weeks after ET. The analyses were performed in those samples that passed the quality control; amplification of the reference miRNAs (hsa-miR-200c-3p and hsa-miR-92a-3p) less than 30 Cts. For PBP-M, n = 28 in the implantative group and n = 25 in the non-implantative group. **(A)** Receiver operating characteristic (ROC) curve for qPCR data obtained for predictive Model 1 in the validation cohort. Model 1 PBP-M (hsa-miR-200b-3p, hsa-miR-24-3p and hsa-miR-148b-3p) had an AUC of 0.69 (95% CI, 0.55–0.86). **(B)** Box plot showing the most likely miRNA to differentiate between a non-implantative and implantative endometrium. miRNA level in the EF at the time of ET. The horizontal line in the middle of the box plot represents the median, while the horizontal limits of the boxes represent the first and third quartiles. The significance levels were assessed using unpaired t-tests with Welch's correction. ΔCt was inversely correlated with the amount of miRNA in the samples. **PBP-M:** EV enrichment with a PBP method and RNA extraction with the mirVana PARIS kit. **Ct:** cycle threshold. **ROC:** Receiver Operating Characteristic curve.

4.2.2.   Model 2 (PBP-N)

Model 2 (hsa-miR-200b-3p, hsa-miR-24-3p and hsa-miR-99b-5p) had an accuracy of 0.77 (95% CI = 0.63, 0.88) and an AUC of 0.78 (95% CI = 0.6, 0.89) (**Figure 47**). The test also exhibited a statistically significant difference (p-value: 0.0002) in AUC compared with a random chance hypothesis (AUC= 0.5). ROC analysis identified hsa-miR-99b-5p as the most likely variable to differentiate a non-implantative and implantative endometrium, demonstrating significant differential expression (≥ 1.5-fold) between the groups at p-value <0.05; this miRNA was upregulated in the implantation group. We established the cut-off point as 2.81 dCt (dCt = Ct hsa-miR-99b-5p – Ct internal controls) based on Youden's J statistic with 0.6 sensitivity and 0.93 specificity. Values above the cut-off point would indicate a non-implantative endometrium (dCt >2.81) (positive predictive value = 0.88) and values below would indicate an implantative endometrium (dCt <2.81) (negative predictive value = 0. 71).
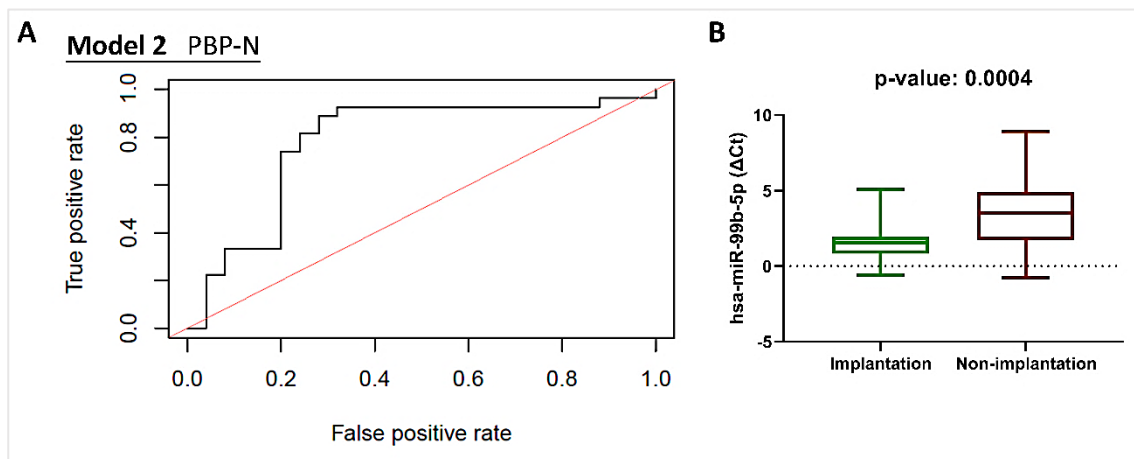
Figure 47. *ROC of validated Model 2 and box plot of the most significant miRNA in the model.*

The predictive models designed using the qPCR results for the PBP-M method applied to the discovery cohort were validated in a new group, the validation cohort (n = 60; 30 subjects in the implantative subgroup and 30 in the non-implantative subgroup). The endometrium was considered implantative when pregnancy was confirmed by vaginal ultrasound showing a gestational sac four weeks after ET. The analyses were performed in those samples that passed the quality control; amplification of the reference miRNAs (hsa-miR-200c-3p and hsa-miR-92a-3p) less than 30 Cts. For PBP-N, n = 27 in the implantative group and n = 25 in the non-implantative group. **(A)** Receiver operating characteristic (ROC) curve for qPCR data obtained for predictive Model 2 in the validation cohort. Model 2 PBP-N (hsa-miR-200b-3p, hsa-miR-24-3p and hsa-miR-99b-5p) had an AUC of 0.78 (95% CI, 0.6–0.89). **(B)** Box plot showing the most likely miRNA to differentiate between a non-implantative and implantative endometrium. The miRNA level in the EF at the time of ET. The horizontal line in the middle of the box plot represents the median, while the horizontal limits of the boxes represent the first and third quartiles. The significance levels were assessed using unpaired t-tests with Welch's correction. ΔCt was inversely correlated with the amount of miRNA in the samples. **PBP-N:** EV enrichment with a PBP method and RNA extraction with the Norgen kit. **Ct:** cycle threshold. **ROC:** Receiver Operating Characteristic curve.

5. To investigate the association of validated miRNAs with EVs and their biological function in the implantation process

To investigate the association of validated miRNAs with EVs and their biological function in the implantation process, we performed different experiments. First, we analyzed the distribution of these miRNAs by SEC and performed an RNase assay. In order to perform a functional analysis, we analyzed their predicted target genes.

5.1. Association of validated miRNAs in the EF

Using qPCR, we analyzed validated miRNAs (miRNAs hsa-miR-200b-3p, hsa-miR-24-3p, hsa-miR-148b-3p and hsa-miR-99b-5p) in the RNA extracted from SEC and RNase assays from the setup cohort. SEC analysis showed that the relative quantity of miRNAs decreased in most cases from F3 to F5/F6 (**Figure 48**), coinciding with fractions corresponding to EVs and then increased from F6/F7 to F10, which correspond to fractions associated with soluble proteins, as shown in **Figure 26**.
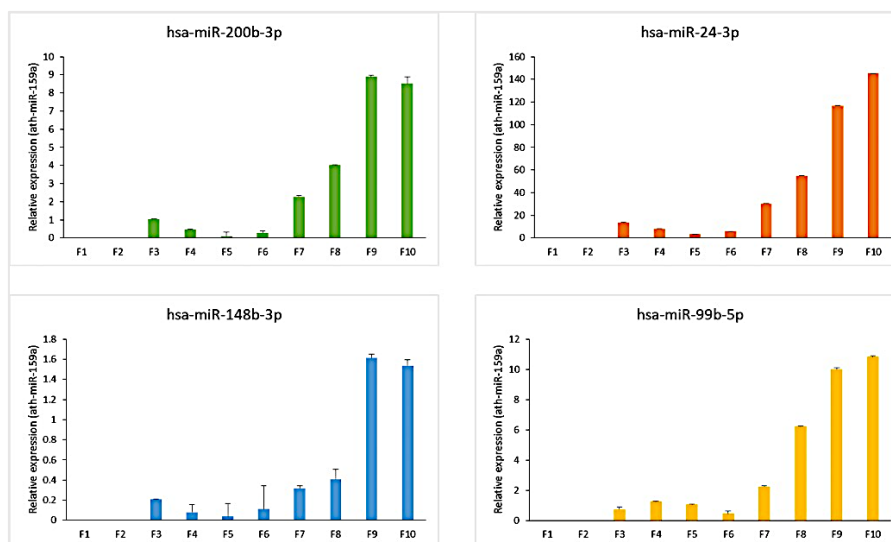
Figure 48. *qPCR characterization of validated miRNAs in the EF by SEC.*

Distribution of the four validated miRNAs among SEC fractions. Normalized relative quantification was used to demonstrate the presence of miRNAs among fractions F1 to F12. To perform the experiment, a 400 µL aliquot from the setup pool cohort was added to the column. Different SEC fractions were numbered from F1 to F12. **EVs**: extracellular vesicles, **qPCR:** quantitative PCR, **miRNAs:** microRNAs. **SEC**: size exclusion chromatography.

We performed the RNase protection assay to explore the relationship between the miRNA content of EF and their association with EVs. As can be seen in **Figure 49**, when EF samples were treated with RNase, Triton X-100 (TX-100) plus RNase or with proteinase-K (PRT-K) plus RNase, there was a significant decrease in all miRNAs analyzed, although it was possible to detect all miRNAs in all replicates. However, when samples were treated with TX-100 plus PRT-K plus RNase (TX+PRT), we were only able to detect hsa-miR-24-3p and hsa-miR-99b-5p in all replicates, whereas hsa-200b-3p and hsa-miR-148b-3p were undetectable, confirming the protective effect that EVs have on miRNAs.
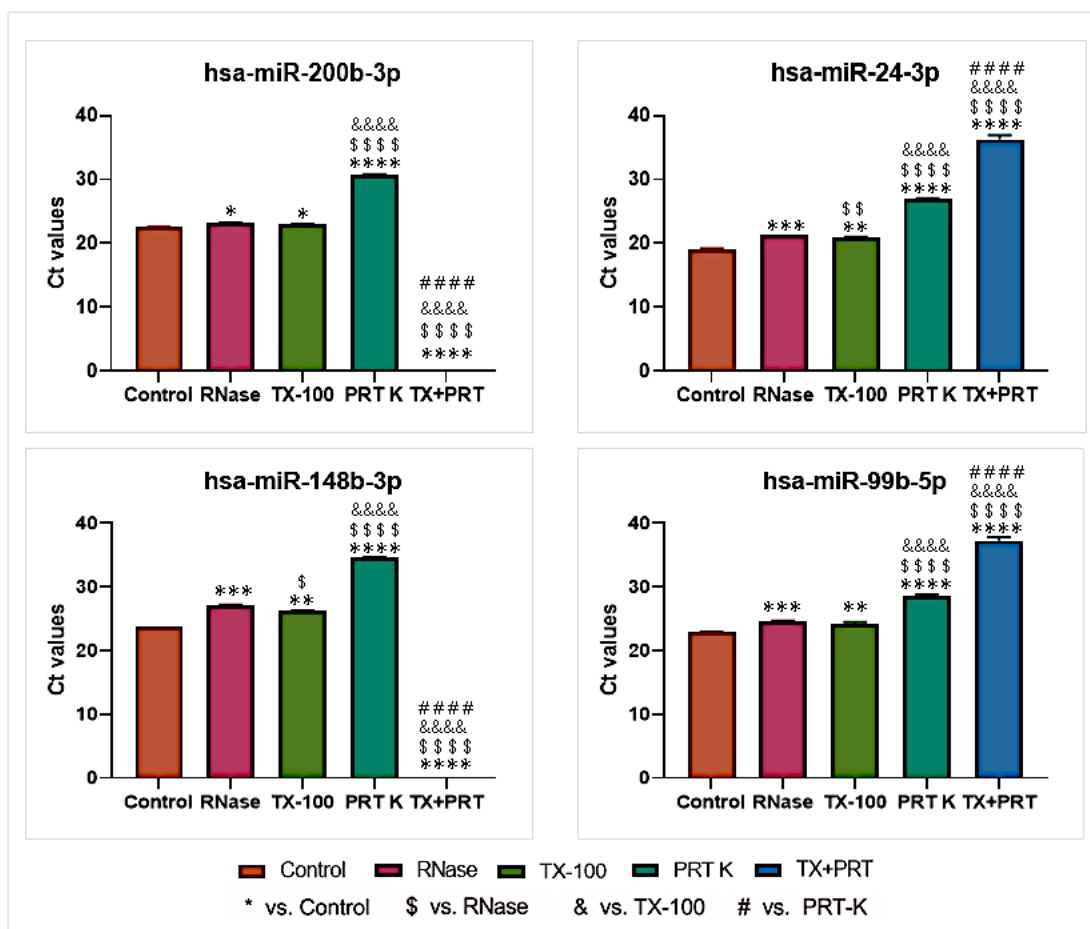
Figure 49. *RNase assay of validated miRNAs in the EF.*

EF sample analysis to examine the association of miRNAs with proteins and EVs in the EF. Graphs show the Ct values of the reference miRNAs evaluated using qPCR. The number of replicates per condition was six and data show the mean with SEM. Each aliquot (400 µL) came from the setup pool cohort. Statistical significance was determined using the paired Student's t-test analysis. *, \$, &, # $p<0.05$; **, \$\$, &&, ## $p<0.01$; ***, \$\$\$, &&& ,### $p<0.001$. **Control:** control sample without treatment: **RNase:** samples treated with RNase; **TX-100:** samples treated with TX-100 followed by RNase treatment; **PRT-K:** samples treated with proteinase K and then with RNase; **TX+PRT:** samples treated with TX-100, then with proteinase K and finally with RNase. **EVs**: extracellular vesicles, **qPCR:** quantitative PCR, **miRNAs:** microRNAs, **EF:** endometrial fluid.

5.2. Functional analysis of validated miRNAs

The regulatory functions of validated miRNAs (miRNAs hsa-miR-200b-3p, hsa-miR-24-3p, hsa-miR-148b-3p and hsa-miR-99b-5p) were broken down into biological process categories via analysis of their predicted target genes.

The KEGG pathways showed many different enriched pathways, including adherens junction proteins, TGF-beta signaling, fatty acid biosynthesis and fatty acid metabolism, all of which were significantly enriched (**Figure 50**).
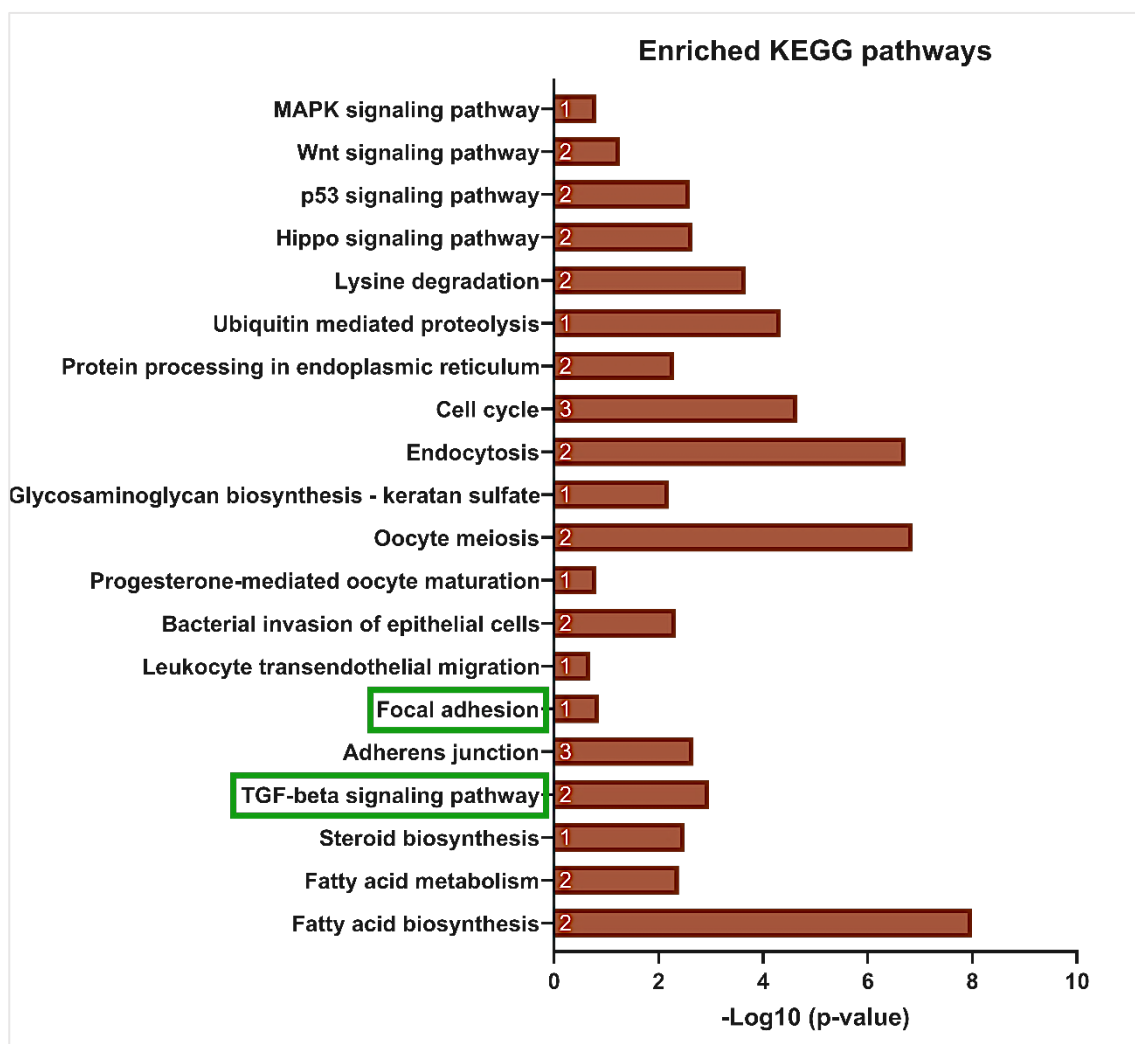
Figure 50. *Enriched KEGG pathways.*

Summary of the significantly enriched pathways related to the four miRNAs used in the predictive models (hsa-miR-200b-3p, hsa-miR-24-3p, hsa-miR-99b-5p and hsa-148b-3p). Overall, most pathways detected were closely associated with embryo implantation and endometrial decidualization. In green, pathways shared with GO. Number of miRNAs involved in each pathway is displayed inside the bar, in white. **KEGG:** Kyoto encyclopedia of genes and genomes; **MAPK:** mitogen-activated protein kinase; **TGF:** transforming growth factor. **GO:** gene ontology.

Along this line, Gene Ontology (GO) analysis also presented TGF-beta signaling pathway enrichment **(Figure 51**). In addition, in utero embryonic development, immune system processes and endosome and vesicle-mediated transport processes were found to be enriched, among others.
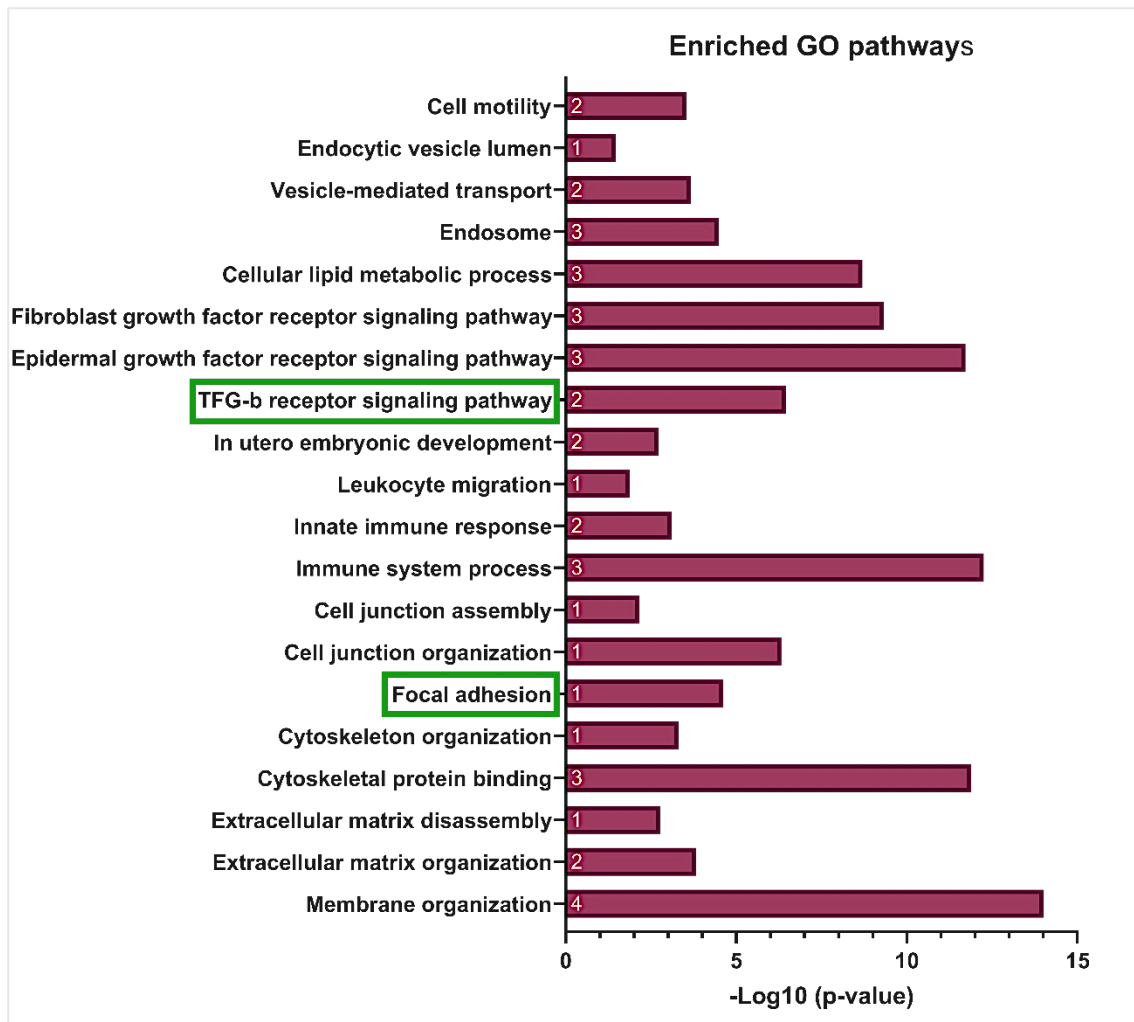
Figure 51. *Enriched GO pathways.*

Summary of the significantly enriched pathways related to the four miRNAs used in the predictive models (hsa-miR-200b-3p, hsa-miR-24-3p, hsa-miR-99b-5p, hsa-miR-148b-3p). Most of the pathways detected were closely associated with embryo implantation and endometrial decidualization. In green, pathways shared with KEGG. Number of miRNAs involved in each pathway is displayed inside the bar, in white. **GO:** gene ontology; **TGF-b:** transforming growth factor-beta. **KEGG:** Kyoto encyclopedia of genes and genomes.

DISCUSSION

VI.   <u>DISCUSSION</u>

The endometrium undergoes a series of changes during the ovarian cycle to reach the proper secretory phase, where endometrial glands achieve maximal secretory activity six days after ovulation (277). These glands are mainly responsible for producing EF, which is necessary to create an optimal uterine microenvironment for embryo implantation (277). It has always been thought that the embryo had the most important role in human implantation. However, it has been seen that maternal conditions can apparently be optimal and the transfer of a chromosomally normal embryo is carried out, however, in many cases, implantation does not occur (278). Thus, research into what is failing in that embryo-endometrium communication in the cycles without implantation is of paramount importance.

Consequently, this thesis is focused on EF as a non-invasive tool to determine the status of the endometrium to predict the implantation outcome (161–163). Our group first coined the term "implantative endometrium" as the endometrium in which implantation has occurred in the same cycle as EF aspiration, while non-implantative endometrium refers to one in which implantation does not occur after ET (162). We found that, in day-3 fresh ET, proteomic profiles (161,162) and lipidomic patterns (163) differ between implantative and non-implantative endometrium, which might indicate secretion alterations among the conditions. Variations in endometrial secretions could also be affecting the release of EVs, which are widely known to be mediators of intercellular communications (170,202).

There is growing evidence that the EVs present in the EF play an important role in the interaction between the pre-implantative embryo and the endometrium. Specifically, it was described that EF-derived EVs contain an miRNA cargo that can be internalized by the embryos and are able to modify their implantation capacity (97,130). Therefore, we thought that the evaluation of the miRNA composition of EF could be useful for determining the endometrial status.

Due to the low volume of EF collected after aspiration, few studies have attempted to study EVs in the EF; hence, before initiating the biomarker discovery and validation process, we optimized EF preparation methodology and characterized its composition. Sample preparation optimization suggested that pre-treatment of the sample with DTT enabled the release of more particles from the mucus, as described for sputum (275,276). We found that a greater quantity of EVs was released into the supernatant in DTT-treated samples, although the relative quantification of the reference miRNAs did not improve (**Figure 25**). This, along with the fact that DTT treatment could modify RNA-protein interactions (279), prompted us to collect and process the EF sample in the absence of DTT for subsequent experiments.

The results obtained from the characterization of miRNAs in the EF via SEC supported the good performance of SEC in separating the components present in biological fluids (265). Our data showed that, in the EF, there were both vesicular-associated miRNAs and non-vesicular miRNAs (**Figure 27**). In addition, the RNase experiment suggested that most miRNAs found in the EF were not only protein-associated but also protein-associated within the EVs, which protects them against degradation (**Figure 28**). Some authors have described the presence of circulating Ago2-miRNA complexes in human plasma, which suggests that Ago2 might have an important role in the stability of secreted miRNA (280,281). Additionally, Ago2 has been identified within EVs and has separately been shown to protect miRNA contained within EVs from RNase degradation (280,282). However, other authors did not find Ago2 in classic exosomes and they believe that no evidence could be uncovered that exosomes, or any other type of small EV, contain other major components of the miRNA biogenesis machinery (218). It is not clear which proteins are protecting these miRNAs from degradation. Nevertheless, our results suggest a strong association between miRNAs and proteins, and also miRNA-protein complexes within the EVs.

Once we had characterized the EF, we wanted to compare different methods for vesicle enrichment and RNA extraction. A few studies have compared various EV-enriching protocols for EF samples (168,234), but none compared different techniques for RNA extraction. A study published by Li *et al.,* (168) reported that, for EV isolation, UC was superior to PBP, contrasting with our results. One explanation of this difference could be the different protocols used; to isolate EVs from EF, Li *et al.,* (168) used a 1:2 PBP ratio with an overnight incubation at 4°C. In contrast, we optimized the PBP protocol as its use for EF had not been described, so we used a 1:1 PBP ratio and incubated the samples at room temperature for 30 minutes before centrifugation. In addition, UC methods are also different, Li *et al.,* (168) performed a two-step ultracentrifugation procedure and resuspended the EVs in 35 μL, while we only performed a single-step UC and resuspended EVs in 100 μL.

In our search for efficient methods for a comprehensive analysis of miRNAs from the EF, we compared five different methods (**Figure 29**). Two consisted of direct RNA extraction from the EF (DCT-M and DCT-N) and the other three included an EV enrichment step before RNA extraction (UC-M, PBP-M and PBP-N). Our results showed that PBP-based EV enrichment methods (PBP-M and PBP-N) increased the efficiency in detecting miRNAs present in EF samples (**Figure 30**). At the same time, we observed different populations of miRNAs via small RNA-seq depending on the RNA extraction method applied (**Figure 31**). This had also been reported by other authors who made similar comparisons, obtaining different results with the different RNA extraction kits used (283,284). Therefore, changing the RNA extraction protocols may lead to different results, complicating comparisons between studies. Given the importance of selecting a robust methodology, we also conducted a technical reproducibility experiment to compare the PBP-M and PBP-N methods. To do so, two operators (JIP and MCG) compared the two methods and the results showed better qPCR amplification data and lower coefficients of variation for PBP-N (**Figure 32**).

Overall, PBP-M and PBP-N obtained the best results from this optimization procedure when starting with the limited amount of EF obtained in a clinical setting. The PBP-M technique turned out to be more efficient since a greater number of miRNAs were detected by small RNA-seq. However, PBP-N proved to be more efficient in terms of qPCR detection as we were able to detect all analyzed miRNAs with lower coefficients of variation. Therefore, among the methodologies tested, PBP-M and PBP-N were chosen for their implementation in a set of individual samples for the discovery and validation of the predictive models.

First, the performance of PBP-M and PBP-N was tested in the discovery cohort (**Table 11**). The alignment rate of the sequenced data showed great variability among samples, with very variable alignment percentages. We believe that these differences were due to the low biological content of some samples and, also, EF composition, as it may also contain genetic material from the uterine microbiota (285). To overcome the problem of biological variability between samples, at the time of selecting differentially expressed miRNAs, we applied TMM normalization and retained miRNAs with (i) counts per million (CPM)>1, (ii) non-zero counts in at least 15 individuals and (iii) at most 10 zero counts in each of the two subgroups. In this way, we ended up with 231/ 845 unique miRNAs in PBP-M and 341/910 unique miRNAs in PBP-N suitable for differential abundance analysis (**Figure 39**). After the differential abundance analysis, we selected 16 miRNAs (**Table A1 and A2**) as suitable for further validation in the same samples via qPCR. To overcome the biological variability problem in the qPCR analyses, we selected two endogenous miRNA controls (hsa-miR-200c-3p and hsa-miR-92a-3p) with the help of the Normfinder algorithm. These miRNAs were selected because they were expressed equally in both groups, had a positive correlation with the amount of protein in the samples and were detected in high abundance in small RNA-seq and with low Ct values by qPCR.

Finally, we performed a regression study using bootstrapping correction with the qPCR (dCt) data of the differentially expressed miRNAs. We ended up with two predictive models, Model 1 with PBP-M (Discovery: AUC=0.93; p-value = 0.003): hsa-miR-200b-3p, hsa-miR-24-3p and hsa-miR-148b-3p, and Model 2 with PBP-N (Discovery: AUC=0.92; p-value = 0.0002): hsa-miR-200b-3p, hsa-miR-24-3p and hsa-miR-99b-5p.

Then, these predictive models were validated by qPCR in a new independent cohort (the validation cohort). As in the discovery cohort, we also observed high biological variability among the samples and, consequently, following the steps carried out in the discovery cohort, we used two endogenous miRNA controls (hsa-miR-200c-3p and hsa-miR-92a-3p) to normalize the data and validate predictive model 1 (PBP-M) and predictive model 2 (PBP-N) in the validation cohort.

The results obtained with Model 1 (PBP-M) were: AUC= 0.69 and p-value = 0.019. The expression pattern of the miRNAs analyzed varied depending on the technique employed and the group to which it was compared (**Table A1**). Specifically, hsa-miR-148-3p was significantly downregulated in the implantative endometrium group and was consistent with the data obtained by qPCR in the discovery group. However, these results did not accord with those obtained by small RNA-seq in the discovery cohort. In addition, hsa-miR-200b-3p did not follow the same trend among the discovery and validation cohorts. The only one that followed the same trend among the different analyses and cohorts was hsa-miR-24-3p, which was downregulated in the implantative endometrium groups.

The results obtained with Model 2 (PBP-N) in the validation cohort were: AUC= 0.78; p-value= 0.0002. In Model 2 (PBP-N), the results obtained for hsa-miR-24-3p were not consistent between different analyses; the qPCR results indicated that it was significantly downregulated in the implantative endometrium of the discovery cohort while, in contrast, it appeared upregulated in the small RNA-Seq analysis of that subgroup and the qPCR results for the validation cohort. However, the results for hsa-miR-200b-3p and hsa-miR-99b-5p were consistent, following the same trend in all the analyses, and these two miRNAs were upregulated in the implantative endometrium group (**Table A2**). To be precise, the ROC analysis identified hsa miR-99b-5p as the most likely variable to differentiate non-implantative and implantative endometrium and the results suggested that dCt values above the cut-off point indicate a non-implantative endometrium (dCt > 2.81).

Overall, the PBP-N method delivered the best results in this optimization procedure, starting with the limited amounts of EF obtained in a clinical setting. In addition, it proved to be the most efficient and reproducible, with a simplified protocol and its application in two independent cohorts presented consistent results. Currently, less than 60% of implantation attempts are successful (99) and, as our test in the validation cohort achieved high specificity (Model 2, 0.93), we believe that we may be able to improve the success rate by using our predictive model PBP-N. With the PBP-N method it would take 9h to obtain the results, so if the sample is collected in the morning, the results will be known in the afternoon. Thus, in cases with a diagnosis of "implantative endometrium" the transfer could be performed in the same afternoon.

One limitation of our approach was the inherent variability of the women involved in the trial and the embryos transferred. When pregnancy is achieved after ET, it can be said that the endometrium was implantative. However, when implantation fails, it cannot be assumed that the problem was only associated with the endometrium, because the fault might lie with the embryo, the endometrium or both. In our study, we tried to minimize the issue of individual variability as all transfers were performed during an artificial cycle under the same hormone supplement protocol.

Another limitation was the alignment rate of the sequenced data against the human genome, which showed great variability between samples, with highly variable alignment percentages (**Table 11**). We believe that these differences could be related to the different biological content of the samples because EF composition can vary as it may contain genetic material from uterine microbiomes (285). To overcome this problem of the biological variability effect on small RNA-Seq data, we used TMM normalization at the time of selecting the differentially expressed miRNAs. In the case of qPCR data, we selected two endogenous miRNA controls (hsa-miR-200c-3p and hsa-miR-92a-3p) with the help of the NormFinder algorithm. These miRNAs were chosen because they were equally expressed in both groups (implantative and non-implantative endometrium groups) and positively correlated with the amount of protein in the samples. Moreover, they were detected at high levels by small RNA-Seq and had low Ct values in the qPCR. However, normalization for analyzing small RNA-Seq data and selecting an endogenous miRNA suitable for normalizing qPCR data are critical points

that might generate great uncertainty. Since there is no standardized method for normalizing RNA-Seq data, each group selects the method that they consider most appropriate. This is also the case with internal controls, as the expression of such a control could also vary depending on the kit used for RNA extraction. The internal controls used should not be generalized and each should be adapted to the experiment performed.

The relatively low negative predictive value observed in our models (Model 1 = 0.69, Model = 0.71) is another limitation to be considered. We hypothesized that this was caused by the fact that we only evaluated the endometrium, signifying that the test will fail in cases where the implantation failure is caused by the embryo. We selected embryos based on their morphology, however, we did not use genetic and molecular data to improve the selection. Obtaining such data would certainly improve our test accuracy and the AUC.

Functional analysis of these miRNAs showed strong associations with key processes involved in implantation. Thus, some of the pathways targeted by differentially expressed miRNAs were related to adherens junctions, necessary for the initiation of implantation as they are required for cell attachment, adhesion and recognition (286). These miRNAs were also related to the TGF-beta signaling pathway, essential for the decidualization of the endometrial stromal cell (287). Furthermore, interactions with immune system processes (45), vesicle-mediated transport and *in utero* embryonic development (28), with key roles during implantation, were also found.

In addition, the data available about the role of hsa-miR-148b-3p suggest that its activity may be dependent on different tissue and cell types and its action mainly involved the regulation of cell progression (288). Some studies found that this miRNA inhibits malignant tumor progression (289,290), while others have related its overexpression with osteogenesis (291) and cancer cell progression (288). Furthermore, this miRNA had been selected as a reference gene in a study designed to identify candidate miRNA markers of endometriosis, as its mean Ct values did not differ significantly between women with endometriosis and the control group. Here, we observed that the expression of hsa-miR-148b-3p was upregulated in EF samples from

patients with implantation failure. This led us to believe that high concentrations of this miRNA could be inhibiting processes related to embryo implantation.

The role of hsa-miR-99b-5p in the EF could be related to its function as a pathway regulator, contributing to natural killer (NK) cell activation and effector function (292). NK cells have been described as the major leukocytes in the endometrium. They accumulate extensively around spiral arterioles in the mid-secretory-phase endometrium and early-pregnancy decidua in accordance with increasing levels of ovarian-derived E2 and P4 (293). These findings suggest that NK cells have a crucial role in implantation and decidualization. However, a meta-analysis of 22 studies examining uterine NK-cell percentages in infertile versus fertile women found no significant differences between groups (294). Taken together with our results, these studies could indicate that, in women with a low concentration of hsa-miR-99b-5p in the endometrium, the activation of uterine NK cells is suboptimal despite a normal cell count and, consequently, implantation does not occur.

In summary, this study introduces new protocols to analyze miRNAs in very small volumes (5-50 μL) of EF collected just before day-5 frozen ETs, which could be implemented in clinical practice. These new methods could be employed to assess endometrial competence using miRNA-based non-invasive tools. Hence, professionals in assisted reproduction centers could use hsa-miR-99b-5p (employing the PBP-N detection method) to predict endometrial status. This could potentially help improve implantation rates for women undergoing ART. It could be possible to change the ET strategy when results show an unfavorable implantative pattern and thus increase implantation rates. The application of this method may also reduce embryo loss, so common after ET to a potentially non-implantative endometrium.

CONCLUSIONS

VII. <u>**CONCLUSIONS**</u>

1. DTT is not required to analyze miRNAs and EVs present in the EF.

2. SEC is useful to separate EVs from soluble proteins in EF samples.

3. The miRNAs in the EF are both free and associated with EVs, which protect them against degradation.

4. The polymer-based precipitation method can be used with low volumes of EF to isolate EVs.

5. In comparison with direct RNA extraction, the most efficient methods for miRNA analysis in the EF are PBP methods followed by the RNA extraction methods (PBP-N and PBP-M).

6. The PBP-M method represented a robust model (AUC = 0.93; p-value 0.0032) to detect an implantative endometrium based on three microRNAs: hsa-miR-24-3p, hsa-miR-200b-3p and hsa-miR-148b-3p.

7. The PBP-N method represented a robust model (AUC = 0.92, p-value 0.00023) to detect an implantative endometrium based on three microRNAs: hsa-miR-24-3p, hsa-miR-200b-3p and hsa-miR-99b-3p.

8. PBP-M was validated with an accuracy of 0.68 (95% CI = 0.54, 0.8), an AUC of 0.69 (95% CI = 0.55, 0.86) and ROC analysis identified hsa-miR-148b-3p, upregulated in the non-implantation group, as the most likely variable to differentiate an implantative endometrium from a non-implantative endometrium.

9. The PBP-N was validated with an accuracy of 0.77 (95% CI = 0.63, 0.88), an AUC of 0.78 (95% CI = 0.6, 0.89) and ROC analysis identified hsa-miR-99b-5p, upregulated in the implantation group, as the most likely variable to differentiate an implantative endometrium from a non-implantative endometrium.

10. The validated miRNAs were involved in biological processes related to implantation.

11. Free or EV-associated miRNAs from the EF can be used as a non-invasive tool for the assessment of implantative endometrium, and we have defined two non-invasive methodologies to identify the implantative endometrium based on three miRNAs.

12. These protocols could be implemented in clinical practice to assess the status of the endometrium before attempting embryo transfer to avoid the loss of embryos transferred to a non-implantative endometrium.

BIBLIOGRAPHY

VIII. <u>BIBLIOGRAPHY</u>

1.   Zegers-Hochschild F, Adamson GD, de Mouzon J, Ishihara O, Mansour R, Nygren K, *et al*. International Committee for Monitoring Assisted Reproductive Technology (ICMART) and the World Health Organization (WHO) revised glossary of ART terminology, 2009*. Fertil Steril. 2009; 92(5):1520-4.

2.   Zegers-Hochschild F, Adamson GD, Dyer S, Racowsky C, De Mouzon J, Sokol R, *et al*. The international glossary on infertility and fertility care, 2017. Fertil Steril. 2017;108(3):393-406.

3.   vander Borght M, Wyns C. Fertility and infertility: Definition and epidemiology. Clin Biochem 2018;62(1):2–10.

4.   Inhorn MC, Patrizio P. Infertility around the globe: New thinking on gender, reproductive technologies and global movements in the 21st century. Hum Reprod Update. 2015;21(4):411-26.

5.   Mascarenhas MN, Flaxman SR, Boerma T, Vanderpoel S, Stevens GA. National, Regional, and Global Trends in Infertility Prevalence Since 1990: A Systematic Analysis of 277 Health Surveys. PLoS Med. 2012;9(12):e1001356.

6.   Ombelet W, Cooke I, Dyer S, Serour G, Devroey P. Infertility and the provision of infertility medical services in developing countries. Hum Reprod Update. 2008;14(6):605-21.

7.   Bergström S. Reproductive failure as a health priority in the Third World: a review. East Afr Med J. 1992;69(4):174-80.

8.   Vander BM, Wyns C. Fertility, and infertility: Definition and epidemiology. Clinical Biochemistry. 2018;62(1):2-10.

9.   Datta J, Palmer MJ, Tanton C, Gibson LJ, Jones KG, Macdowall W, *et al*. Prevalence of infertility and help seeking among 15 000 women and men. Human Reproduction. 2016;31(9):2108–18.

10.   Strauss J F, Barbieri RL. Yen & Jaffe's reproductive endocrinology: physiology, pathophysiology, and clinical management. Elsevier, 8th ed. Philadelphia, 2019.

11.   Sociedad Española de Fertilidad. Saber más sobre: fertilidad y reproducción asistida. SEF. Madrid, 2012. pp 1–82.

12. Allahbadia GN. Intrauterine Insemination: Fundamentals Revisited. J Obstet Gyneacol India. 2017;67(6):385–92.

13. Merviel P, Heraud MH, Grenier N, Lourdel E, Sanguinet P, Copin H. Predictive factors for pregnancy after intrauterine insemination (IUI): An analysis of 1038 cycles and a review of the literature. Fertil Steril. 2010;93(1):79-88.

14. World Health Organization. WHO laboratory manual for the examination and processing of human semen. WHO. 5th ed. 2010.

15. Martínez L, Romero B. Guías Clínicas SEF: Ciclos de FIV-ICSI: indicaciones, protocolos de estimulación ovárica. SEF. Madrid, 2021. pp.1-15.

16. Coroleu B. Guías Clínicas SEF: Ciclos de FIV ICSI: punción, transferencia embrionaria, técnica e indicaciones. SEF. Madrid, 2021. pp. 1-14.

17. Graham ME, Jelin A, Hoon Jr AH, Floet AMW, Levey E, Graham EM. Assisted reproductive technology: Short-and long-term outcomes. Dev Med Child Neurol. 2022;18:1–12.

18. Roque M, Haahr T, Geber S, Esteves SC, Humaidan P. Fresh versus elective frozen embryo transfer in IVF/ICSI cycles: a systematic review and meta-analysis of reproductive outcomes. Hum Reprod Update. 2019;25(1):2–14.

19. Matorras R, Pijoan JI, Perez-Ruiz I, Lainz L, Malaina I, Borjaba S. Meta-analysis of the embryo freezing transfer interval. Reprod Med Biol. 2021;20(2):144-158.

20. Kushnir VA, Barad DH, Albertini DF, Darmon SK, Gleicher N. Systematic review of worldwide trends in assisted reproductive technology 2004-2013. Reprod Biol Endocrinol. 2017;15(1):1-6.

21. Kontopoulos G, Simopoulou M, Zervomanolakis I, Prokopakis T, Dimitropoulos K, Dedoulis E, *et al*. Cleavage stage versus blastocyst stage embryo transfer in oocyte donation cycles. Medicina (Kaunas). 2019 20;55(6):293.

22. Roque M, Lattes K, Serra S, Solà I, Geber S, Carreras R, *et al*. Fresh embryo transfer versus frozen embryo transfer in in vitro fertilization cycles: A systematic review and meta-analysis. Fertil Steril. 2013;99(1):156-162.

23. Schoolcraft WB, Katz-Jaffe MG. Comprehensive chromosome screening of trophectoderm with vitrification facilitates elective single-embryo transfer for infertile women with advanced maternal age. Fertil Steril. 2013;100(3):615-9.

24. Gelbaya TA, Tsoumpou I, Nardo LG. The likelihood of live birth and multiple birth after single versus double embryo transfer at the cleavage stage: A systematic review and meta-analysis. Fertil Steril. 2010;94(3):936-45.

25. Huisman GJ, Fauser BCJM, Eijkemans MJC, Pieters MHEC. Implantation rates after in vitro fertilization and transfer of a maximum of two embryos that have undergone three to five days of culture. Fertil Steril. 2000;73(1):117-22.

26. Matorras R, Urquijo E, Mendoza R, Corcóstegui B, Expósito A, Rodríguez-Escudero FJ. Ultrasound-guided embryo transfer improves pregnancy rates and increases the frequency of easy transfers. Hum Reprod. 2002;17(7):1762-6.

27. Salamonsen LA, Evans J, Nguyen HPT, Edgell TA. The Microenvironment of Human Implantation: Determinant of Reproductive Success. Am J Reprod Immunol. 2016;75(3):218-25.

28. Kurian NK, Modi D. Extracellular vesicle mediated embryo-endometrial cross talk during implantation and in pregnancy. J Assist Reprod Genet. 2019;36(2):189-198.

29. Schünke M, Schulte E, Schumacher U, Voll M, Wesker K. Prometheus. Texto y atlas de anatomía humana. Editorial Médica Panamerica. Madrid, 2005.

30. Collage D. Douglas College human anatomy & physiology II. Douglas College, 1st ed. New Westminster, 2017.

31. Hur C, Rehmer J, Flyckt R, Falcone T. Uterine Factor Infertility: A Clinical Review. Clin Obstet Gynecol. 2019;62(2):257–70.

32. Graziottin A, Gambini D. Anatomy, and physiology of genital organs - women. Handb Clin Neurol. 2015;130(1):39-60.

33. Tresguerres J, Ariznavarreta C, Cachofeiro V, Cardinali D, Escrich E, Gil-Loyzaga P, *et al*. Fisiología del eje hipotálamo-hipófiso-ovárico. Fisiologia Humana. México, McGraw-Hill, 4ta edición, 2010.

34. Bajo JM, Laila JM, Xercavins J. Fundamentos de ginecología. Sociedad Española de Ginecología y Obstetricia (SEGO), Madrid, 2009.

35. Kong L, Tang M, Zhang T, Wang D, Hu K, Lu W, *et al*. Nickel nanoparticles exposure and reproductive toxicity in healthy adult rats. Int J Mol Sci. 2014;17(11):21253-69.

36. Simón C, Horcajadas JA, García-Velasco J, Pellicer A. *El* endometrio humano: desde la investigación a la clínica*. Editorial Médica Panamericana, 1ra ed. Buenos Aires, 2009. pp. 2–42.

37. Hall JE, Guyton AC. Guyton & Hall compendio de fisiología médica. Elsevier, 14 ed. Barcelona, 2021.

38. Clayton SG. Menstruation. Encyclopedia Britannica. 2019. https://www.britannica.com/science/menstruation

39. Clark GF, Schust DJ. Manifestations of immune tolerance in the human female reproductive tract. Front Immunol. 2013;4(26):1–14.

40. Lessey BA, Young SL. structure, function, and evaluation of the female reproductive tract. Yen & Jaffe's reproductive endocrinology: physiology, pathophysiology, and clinical management. Elsevier, 8th ed. Philadelphia, 2019.

41. Nguyen HPT, Sprung CN, Gargett CE. Differential expression of Wnt signaling molecules between pre- and postmenopausal endometrial epithelial cells suggests a population of putative epithelial stem/progenitor cells reside in the basalis layer. Endocrinology. 2012;153(6):2870–83.

42. Gargett CE, Nguyen HPT, Ye L. Endometrial regeneration, and endometrial stem/progenitor cells. Rev Endocr Metab Disord. 2012;13(4):235-51.

43. Cha J, Sun X, Dey SK. Mechanisms of implantation: strategies for successful pregnancy. Nat Med. 2012;18(12):1754-67.

44. Okada H, Tsuzuki T, Murata H. Decidualization of the human endometrium. Reprod Med Biol. 2018;17(3):220–7.

45. Lee JY, Lee M, Lee SK. Role of endometrial immune cells in implantation. Clin Exp Reprod Med. 2011;38(3):119–25.

46. Bischof P, Campana A. Trophoblast differentiation and invasion: its significance for human embryo implantation. Early Pregnancy. 1997;3(2):81-95.

47. Kim SM, Kim JS. A Review of Mechanisms of Implantation. Dev Reprod. 2017;21(4):351-359.

48.   James JL, Carter AM, Chamley LW. Human placentation from nidation to 5 weeks of gestation. Part I: What do we know about formative placental development following implantation? Placenta. 2012;33(5):327-34.

49.   Finn CA, Martin L. The control of implantation. Reproduction. 1974;39(1):195-206.

50.   Pope WF. Uterine Asynchrony: A Cause of Embryonic Loss. Biol Reprod. 1988;39(5):999-1003.

51.   Bergh PA, Navot D. The impact of embryonic development and endometrial maturity on the timing of implantation. Fertil Steril. 1992;58(3):537-42.

52.   Cha J, Sun X, Dey SK. Mechanisms of implantation: Strategies for successful pregnancy. Nat Med. 2012;18(12):1754-67.

53.   Diedrich K, Fauser BCJM, Devroey P, Griesinger G. The role of the endometrium and embryo in human implantation. Hum Reprod Update. 2007;13(4):365-77.

54.   Paria BC, Reese J, Das SK, Dey SK. Deciphering the cross-talk of implantation: Advances and challenges. Science. 2002;296(5576):2185-8.

55.   Psychoyos A. Hormonal control of ovoimplantation. Vitam Horm. 1973;31(1):201-56.

56.   Achache H, Revel A. Endometrial receptivity markers, the journey to successful embryo implantation. Hum Reprod Update. 2006;12(6):731-46.

57.   Matorras R, Valls R, Azkargorta M, Burgos J, Rabanal A, Elortza F, Mas JM, Sardon T. Proteomics based drug repositioning applied to improve in vitro fertilization implantation: an artificial intelligence model. Syst Biol Reprod Med. 2021;67(4):281-297.

58.   Navot D, Scott RT, Droesch K, Veeck LL, Liu HC, Rosenwaks Z. The window of embryo transfer and the efficiency of human conception in vitro. Fertil Steril. 1991;55(1):114-8.

59.   Miravet-Valenciano JA, Rincon-Bertolin A, Vilella F, Simon C. Understanding and improving endometrial receptivity. Curr Opin Obstet Gynecol. 2015;27(3):187-92.

60.   Wilcox AJ, Baird DD, Weinberg CR. Time of Implantation of the Conceptus and Loss of Pregnancy. Obstet Gynecol Surv. 1999;340(23):1796-9.

61.   Bui AH, Timmons DB, Young SL. Evaluation of endometrial receptivity and implantation failure. Curr Opin Obstet Gynecol. 2022;34(3):107–13.

62.   Makker A, Singh MM. Endometrial receptivity: Clinical assessment in relation to fertility, infertility, and antifertility. Med Res Rev. 2006;26(6):699–746.

63.   Bentin-Ley U. Relevance of endometrial pinopodes for human blastocyst implantation. Hum Reprod. 2000;15(6):67-73.

64.   Donaghay M, Lessey BA. Uterine receptivity: Alterations associated with benign gynecological disease. Semin Reprod Med. 2007;25(6):461-75.

65.   Lessey BA. Two pathways of progesterone action in the human endometrium: Implications for implantation and contraception. Steroids. 2003;68(10-13):809-15.

66.   Poncelet C, Leblanc M, Walker-Combrouze F, Soriano D, Feldmann G, Madelenat P, *et al*. Expression of cadherins and CD44 isoforms in human endometrium and peritoneal endometriosis. Acta Obstet Gynecol Scand. 2002;81(3):195-203.

67.   Behzad F, Seif MW, Campbell S, Aplin JD. Expression of Two Isoforms of CD44 in Human Endometrium1. Biol Reprod. 1994;51(4):739-47.

68.   Fukuda MN, Sato T, Nakayama J, Klier G, Mikami M, Aoki D, *et al*. Trophinin and tastin, a novel cell adhesion molecule complex with potential involvement in embryo implantation. Genes Dev. 1995;9(10):1199-210.

69.   Meseguer M, Aplin JD, Caballero-Campo P, O'Connor JE, Martín JC, Remohí J, *et al*. Human endometrial mucin MUC1 is up-regulated by progesterone and down-regulated in vitro by the human blastocyst. Biol Reprod. 2001;64(2):590-601.

70.   Seppala M, Suikkari AM, Julkunen SM. Human endometrial proteins. Reprod Nutr Dev. 1988;28(6B):1649-54.

71.   Bell SC, Patel SR, Kirwan PH, Drife JO. Protein synthesis and secretion by the human endometrium during the menstrual cycle and the effect of progesterone in vitro. J Reprod Fertil. 1986;77(1):221-31.

72.   Seppälä M, Koistinen R, Rutanen EM. Uterine endocrinology and paracrinology: Insulin-like growth factor binding protein-1 and placental protein 14 revisited. Hum Reprod. 1994;(9):917-925.

73. Seppälä M, Taylor RN, Koistinen H, Koistinen R, Milgrom E. Glycodelin: A major lipocalin protein of the reproductive axis with diverse actions in cell recognition and differentiation. Endocr Rev. 2002;23(4):401-30.

74. Klentzrics LD, Bulmer JN, Seppälä M, Li TC, Warren MA, Cooke ID. Placental protein 14 in cycles with normal and retarded endometrial differentiation. Hum Reprod. 1994;9(3):394-8.

75. Apparao KBC, Murray MJ, Fritz MA, Meyer WR, Chambers AF, Truong PR, *et al*. Osteopontin and its receptor αvβ3 integrin are coexpressed in the human endometrium during the menstrual cycle but regulated differentially. J Clin Endocrinol Metb. 2001;86(10):4991-5000.

76. Jain A, Karadag A, Fohr B, Fisher L, Fedarko N. Three SIBLINGs enhance factor H's cofactor activity enabling MCP-like cellular evasion of complement-mediated attack. J Biol Chem. 2002;277(16):13700-8.

77. King AE. Regulation of natural antibiotic expression by inflammatory mediators and mimics of infection in human endometrial epithelial cells. Mol Hum Reprod. 2002;4(4):341-9.

78. Quayle AJ, Porter E, Nussbaum AA, Wang YM, Brabec C, Yip KP, *et al*. Gene expression, immunolocalization, and secretion of human defensin-5 in human female reproductive tract. Am J Pathol. 1998; 152(5):1247-58.

79. Isaacson KB, Galman M, Coutifaris C, Lyttle CR. Endometrial synthesis and secretion of complement component-3 by patients with and without endometriosis. Fertil Steril. 1990;53(5):836-41.

80. Hasty LA, Lambris JD, Lessey BA, Pruksananonda K, Lyttle CR. Hormonal regulation of complement components and receptors throughout the menstrual cycle. Am J Obstet Gynecol. 1994;170(1):168-75.

81. Jensen TS, Bjorge L, Wollen A -L, Ulstein M. Identification of the Complement Regulatory Proteins CD46, CD55, and CD59 in Human Fallopian Tube, Endometrium, and Cervical Mucosa and Secretion. Am J Reprod Immunol. 1995;34(1):1-9.

82. Schatz F, Guzeloglu-Kayisli O, Arlier S, Kayisli UA, Lockwood CJ. The role of decidual cells in uterine hemostasis, menstruation, inflammation, adverse pregnancy outcomes and abnormal uterine bleeding. Hum Reprod Update. 2016;22(4):497-515.

83. Dimitriadis E, White CA, Jones RL, Salamonsen LA. Cytokines, chemokines and growth factors in endometrium related to implantation. Hum Reprod Update. 2005;11(6):613-30.

84. Dosiou C, Giudice LC. Natural killer cells in pregnancy and recurrent pregnancy loss: Endocrine and immunologic perspectives. Endocr Rev. 2005:26(1):44-62.

85. Hyde KJ, Schust DJ. Immunologic challenges of human reproduction: an evolving story. Fertil Steril. 2016;106(3):499-510.

86. Whitelaw PF, Croy BA. Granulated lymphocytes of pregnancy. Placenta. 1996;17(8):533-43.

87. Rodgers WH, Matrisian LM, Giudice LC, Dsupin B, Cannon P, Svitek C, *et al*. Patterns of matrix metalloproteinase expression in cycling endometrium imply differential functions and regulation by steroid hormones. J Clin Invest. 1994;94(3):946-53.

88. Henriet P, Cornet PB, Lemoine P, Galant C, Singer CF, Courtoy PJ, *et al*. Circulating ovarian steroids and endometrial matrix metalloproteinases (MMPs). Ann N Y Acad Sci. 2002;955:119-38.

89. Curry TE, Osteen KG. The matrix metalloproteinase system: Changes, regulation, and impact throughout the ovarian and uterine reproductive cycle. Endocr Rev. 2003;24(4):428-65.

90. Marbaix E, Kokorine I, Moulin P, Donnez J, Eeckhout Y, Courtoy PJ. Menstrual breakdown of human endometrium can be mimicked in vitro and is selectively and reversibly blocked by inhibitors of matrix metalloproteinases. Proc Natl Acad Sci U S A. 1996;93(17):9120-5.

91. Gargett CE, Rogers PA. Human endometrial angiogenesis. Reproduction. 2001;121(2):181-6.

92. Smith SK. Angiogenesis, vascular endothelial growth factor and the endometrium. Hum Reprod Update. 1998;4(5):509-19.

93. Gambino LS, Wreford NG, Bertram JF, Dockery P, Lederman F, Rogers PAW. Angiogenesis occurs by vessel elongation in proliferative phase human endometrium. Hum Reprod. 2002;17(5):1199-206.

94. Koga K, Osuga Y, Tsutsumi O, Yano T, Yoshino O, Takai Y, *et al*. Demonstration of angiogenin in human endometrium and its enhanced expression in endometrial tissues in the secretory phase and the decidua. J Clin Endocrinol Metab. 2001;86(11):5609-14.

95. Neufeld G, Cohen T, Gengrinovitch S, Poltorak Z. Vascular endothelial growth factor (VEGF) and its receptors. FASEB J. 1999:13(1):9-22.

96.   Moller B, Rasmussen C, Lindblom B, Olovsson M. Expression of the angiogenic growth factors VEGF, FGF-2, EGF and their receptors in normal human endometrium during the menstrual cycle. Mol Hum Reprod. 2001;7(1):65-72.

97.   Ng YH, Rome S, Jalabert A, Forterre A, Singh H, Hincks CL, *et al*. Endometrial exosomes/microvesicles in the uterine microenvironment: A new paradigm for embryo-endometrial cross talk at implantation. PLoS One. 2013;8(3)e58502.

98.   Greening DW, Nguyen HPT, Elgass K, Simpson RJ, Salamonsen LA. Human endometrial exosomes contain hormone-specific cargo modulating trophoblast adhesive capacity: insights into endometrial-embryo interactions. Biol Reprod. 2016;94(2):1–15.

99.   de Geyter C, Calhaz-Jorge C, Kupka MS, Wyns C, Mocanu E, Motrenko T, *et al*. ART in Europe, 2015: results generated from European registries by ESHRE†. Hum Reprod Open. 2020;2022(3):hoac022.

100.   Rafael ZB. Endometrial Receptivity Analysis (ERA) test: an unproven technology. Hum Reprod Open. 2021;2021(2):hoab010.

101.   Díaz-Gimeno P, Horcajadas JA, Martinez-Conejero JA, Esteban FJ, Alama P, Pellicer A, *et al*. A genomic diagnostic tool for human endometrial receptivity based on the transcriptomic signature. Fertil Steril. 2011;95(1):50-60.

102.   Maheshwari A, Pandey S, Raja EA, Shetty A, Hamilton M, Bhattacharya S. Is frozen embryo transfer better for mothers and babies? Can cumulative meta-analysis provide a definitive answer? Hum Reprod Update. 2018;24(1):35–58.

103.   Maheshwari A, Raja EA, Bhattacharya S. Obstetric and perinatal outcomes after either fresh or thawed frozen embryo transfer: an analysis of 112,432 singleton pregnancies recorded in the human fertilisation and embryology authority anonymized dataset. Fertil Steril. 2016;106(7):1703-1708.

104.   Scott L, Finn A, O'Leary T, McLellan S, Hill J. Morphologic parameters of early cleavage-stage embryos that correlate with fetal development and delivery: Prospective and applied data for increased pregnancy rates. Hum Reprod. 2007;22(1):230-40.

105.   Lemmen JG, Agerholm I, Ziebe S. Kinetic markers of human embryo quality using time-lapse recordings of IVF/ICSI-fertilized oocytes. Reprod Biomed Online. 2008;17(3):385-91.

106.   Gardner DK, Lane M, Stevens J, Schoolcraft WB. Noninvasive assessment of human embryo nutrient consumption as a measure of developmental potential. Fertil Steril. 2001;76(6):1175-80.

107. Leese HJ, Sturmey RG, Baumann CG, McEvoy TG. Embryo viability and metabolism: Obeying the quiet rules. Hum Reprod. 2007;22(12):3047-50.

108. Haggarty P, Wood M, Ferguson E, Hoad G, Srikantharajah A, Milne E, *et al*. Fatty acid metabolism in human preimplantation embryos. Hum Reprod. 2006;21(3):766-73.

109. Leese HJ. Quiet please, do not disturb: A hypothesis of embryo metabolism and viability. Bioessays. 2002;24(9):845-9.

110. Leese HJ. Metabolic control during preimplantation mammalian development. Hum Reprod Update. 1995;1(1):63-72.

111. Scott R, Upham K, Forman E, Hong K, Scott K, Taylor D, *et al*. Blastocyst biopsy with comprehensive chromosome screening and fresh embryo transfer significantly increases in vitro fertilization implantation and delivery rates: a randomized controlled trial. Fertil Steril. 2013;100(3):697–703.

112. Kirkegaard K, Agerholm IE, Ingerslev HJ. Time-lapse monitoring as a tool for clinical embryo assessment. Hum Reprod. 2012;27(5):1277-85.

113. Balaban B, Brison D, Calderón G, Catt J, Conaghan J, Cowan L, *et al*. Istanbul consensus workshop on embryo assessment: Proceedings of an expert meeting. Reprod Biomed Online. 2011;22(6):632–46.

114. ASEBIR. Cuadernos de embriologia clinica III. Criterios ASEBIR de valoración morfológica de oocitos, embriones tempranos y blastocistos humanos. Gobalo, 3a ed. Madrid, 2015.

115. Wong C, Chen AA, Behr B, Shen S. Time-lapse microscopy and image analysis in basic and clinical embryo development research. Reprod Biomed Online. 2013;26(2):120-9.

116. Milewski R, Ajduk A. Time-lapse imaging of cleavage divisions in embryo quality assessment. Reproduction. 2017;154(2):37–53.

117. Cruz M, Garrido N, Herrero J, Pérez-Cano I, Muñoz M, Meseguer M. Timing of cell division in human cleavage-stage embryos is linked with blastocyst formation and quality. Reprod Biomed Online. 2012;25(4):371–81.

118. Basile N, Vime P, Florensa M, Aparicio Ruiz B, García Velasco JA, Remohí J, *et al*. The use of morphokinetics as a predictor of implantation: A multicentric study to define and validate an algorithm for embryo selection. Hum Reprod. 2015;30(2):276–83.

119. Minasi MG, Greco P, Varricchio MT, Barillari P, Greco E. The clinical use of time-lapse in human-assisted reproduction. Ther Adv Reprod Health. 2020;14(1):1-15.

120. Louis CM, Erwin A, Handayani N, Polim AA, Boediono A, Sini I. Review of computer vision application in in vitro fertilization: the application of deep learning-based computer vision technology in the world of IVF. J Assist Reprod Genet. 2021;38(7):1627-39.

121. Bori L, Paya E, Alegre L, Viloria TA, Remohi JA, Naranjo V, *et al*. Novel and conventional embryo parameters as input data for artificial neural networks: an artificial intelligence model applied for prediction of the implantation potential. Fertil Steril. 2020;114(6):1232–41.

122. Fernandez EI, Ferreira AS, Cecílio MHM, Chéles DS, de Souza RCM, Nogueira MFG, *et al*. Artificial intelligence in the IVF laboratory: overview through the application of different types of algorithms for the classification of reproductive data. J Assist Reprod Genet. 2020;37(10):2359–76.

123. Armant DR. Blastocysts don't go it alone. Extrinsic signals fine-tune the intrinsic developmental program of trophoblast cells. Dev Biol. 2005;280(2):260-80.

124. Bhusane K, Bhutada S, Chaudhari U, Savardekar L, Katkam R, Sachdeva G. Secrets of endometrial receptivity: some are hidden in uterine secretome. Am J Reprod Immunol. 2016;75(3)226-36.

125. Beier HM. Oviducal and uterine fluids. J Reprod Fertil. 1974;37(1):221-37.

126. Andronico F, Battaglia R, Ragusa M, Barbagallo D, Purrello M, Di Pietro C. Extracellular vesicles in human oogenesis and implantation. Int J Mol Sci. 2019;20(9):1-11.

127. Homer H, Rice GE, Salomon C. Review: Embryo- and endometrium-derived exosomes and their potential role in assisted reproductive treatments–liquid biopsies for endometrial receptivity. Placenta. 2017,54(1):89-94.

128. Nguyen HP, Simpson RJ, Salamonsen LA, Greening DW. Extracellular Vesicles in the Intrauterine Environment: Challenges and Potential Functions. Biol Reprod. 2016;95(5):109–109.

129. Machtinger R, Laurent LC, Baccarelli AA. Extracellular vesicles: Roles in gamete maturation, fertilization and embryo implantation. Hum Reprod Update. 2016;22(2):182–93.

130.   Vilella F, Moreno-Moya JM, Balaguer N, Grasso A, Herrero M, Martínez S, *et al*. Hsa-miR-30d, secreted by the human endometrium, is taken up by the pre-implantation embryo and might modify its transcriptome. Development. 2015;142(18):3210-21.

131.   Giacomini E, Vago R, Sanchez AM, Podini P, Zarovni N, Murdica V, *et al*. Secretome of in vitro cultured human embryos contains extracellular vesicles that are uptaken by the maternal side. Sci Rep. 2017;7(1):1–13.

132.   Rai A, Poh QH, Fatmous M, Fang H, Gurung S, Vollenhoven B, *et al*. Proteomic profiling of human uterine extracellular vesicles reveal dynamic regulation of key players of embryo implantation and fertility during menstrual cycle. Proteomics. 2021;21(13-14):e2000211.

133.   Altmäe S, Koel M, Võsa U, Adler P, Suhorutšenko M, Laisk-Podar T, *et al*. Meta-signature of human endometrial receptivity: A meta-analysis and validation study of transcriptomic biomarkers. Sci Rep. 2017;7(1):1-15.

134.   Balaguer N, Moreno I, Herrero M, González M, Simón C, Vilella F. Heterogeneous nuclear ribonucleoprotein C1 may control miR-30d levels in endometrial exosomes affecting early embryo implantation. Mol Hum Reprod. 2018;24(8):411–25.

135.   Evans J, Rai A, Nguyen HPT, Poh QH, Elglass K, Simpson RJ, *et al*. Human endometrial extracellular vesicles functionally prepare human trophectoderm model for implantation: Understanding bidirectional maternal-embryo communication. Proteomics. 2019;19(23):e1800423.

136.   Craciunas L, Gallos I, Chu J, Bourne T, Quenby S, Brosens JJ, *et al*. Conventional and modern markers of endometrial receptivity: A systematic review and meta-analysis. Hum Reprod Update. 2019;25(2):202–23.

137.   Strowitzki T, Germeyer A, Popovici R, von Wolff M. The human endometrium as a fertility-determining factor. Hum Reprod Update. 2006;12(5):617-30.

138.   Noyes RW, Hertig AT, Rock J. Dating the endometrial biopsy. Am J Obstet Gynecol. 1975;122(2):262-3.

139.   Altmäe S, Esteban FJ, Stavreus-Evers A, Simón C, Giudice L, Lessey BA, *et al*. Guidelines for the design, analysis and interpretation of "omics" data: Focus on human endometrium. Hum Reprod Update. 2014;20(1):12–28.

140.   Riesewijk A, Martin J, van Os R, Horcajadas JA, Polman J, Pellicer A *et al*. Gene expression profiling of human endometrial receptivity on days LH+2 versus LH+7 by microarray technology. Mol Hum Reprod. 2003;9(5):253-64.

141. Horcajadas JA, Riesewijk A, Martín J, Cervero A, Mosselman S, Pellicer A, *et al*. Global gene expression profiling of human endometrial receptivity. J Reprod Immunol. 2004;63(1):41-9.

142. Talbi S, Hamilton AE, Vo KC, Tulac S, Overgaard MT, Dosiou C, *et al*. Molecular phenotyping of human endometrium distinguishes menstrual cycle phases and underlying biological processes in normo-ovulatory women. Endocrinology. 2006;147(3):1097-121.

143. Mirkin S, Arslan M, Churikov D, Corica A, Diaz JI, Williams S, *et al*. In search of candidate genes critically expressed in the human endometrium during the window of implantation. Hum Reprod. 2005;20(8):2104-17.

144. Gómez E, Ruíz-Alonso M, Miravet J, Simón C. Human endometrial transcriptomics: Implications for embryonic implantation. Cold Spring Harb Perspect Med. 2015;5(7):a022996.

145. Thomas K, Thomson A, Wood S, Kingsland C, Vince G, Lewis-Jones I. Endometrial integrin expression in women undergoing in vitro fertilization and the association with subsequent treatment outcome. Fertil Steril. 2003;80(3):502-7.

146. Chen G, Xin A, Liu Y, Shi C, Chen J, Tang X, *et al*. Integrins β1 and β3 are biomarkers of uterine condition for embryo transfer. J Transl Med. 2016;14(303):1-10.

147. Garrido-Gómez T, Quiñonero A, Antúnez O, Díaz-Gimeno P, Bellver J, Simón C, *et al*. Deciphering the proteomic signature of human endometrial receptivity. Hum Reprod. 2014;29(9):1957-67.

148. Kennedy TG, Gillio-Meina C, Phang SH. Prostaglandins and the initiation of blastocyst implantation and decidualization. Reproduction. 2007;134(5):635-43.

149. Cong J, Diao HL, Zhao YC, Ni H, Yan YQ, Yang ZM. Differential expression and regulation of cyclooxygenases, prostaglandin E synthases and prostacyclin synthase in rat uterus during the peri-implantation period. Reproduction. 2006;131(1):139-51.

150. van der Gaast MH, Beier-Hellwig K, Fauser BCJM, Beier HM, Macklon NS. Endometrial secretion aspiration prior to embryo transfer does not reduce implantation rates. Reprod Biomed Online. 2003;7(1):105-9.

151. Hannan NJ, Nie G, Rainzcuk A, Rombauts LJF, Salamonsen LA. Uterine lavage or aspirate: Which view of the intrauterine environment? Reprod Sci. 2012;19(10):1125-32.

152. Edgell TA. Protein biomarkers of endometrial receptivity. How to Prepare the Endometrium to Maximize Implantation Rates and IVF Success. Cambridge University Press. Cambridge, 2019. pp. 19–27.

153. Hou Z, He A, Zhang Q, Liu N, Liu D, Li Y, *et al*. Endometrial fluid aspiration immediately prior to embryo transfer does not affect IVF/vitrified-warmed embryo transfer outcomes - a prospective matched cohort study. Reprod Biomed Online. 2022;44(3):486–93.

154. Martinez-Garcia E, Lesur A, Devis L, Cabrera S, Matias-Guiu X, Hirschfeld M, *et al*. Targeted proteomics identifies proteomic signatures in liquid biopsies of the endometrium to diagnose endometrial cancer and assist in the prediction of the optimal surgical treatment. Clin Cancer Res. 2017;23(21):6458-67.

155. Ametzazurra A, Matorras R, García-Velasco JA, Prieto B, Simón L, Martínez A, *et al*. Endometrial fluid is a specific and non-invasive biological sample for protein biomarker identification in endometriosis. Hum Reprod. 2009;24(4):954-65.

156. Binder NK, Evans J, Salamonsen LA, Gardner DK, Kaitu'u-Lino TJ, Hannan NJ. Placental growth factor is secreted by the human endometrium and has potential important functions during embryo development and implantation. PLoS One. 2016;11(10):e0163096.

157. Scotchie JG, Fritz MA, Mocanu M, Lessey BA, Young SL. Proteomic Analysis of the Luteal Endometrial Secretome. Reprod Sci. 2009;16(9):883-93.

158. Hannan NJ, Paiva P, Meehan KL, Rombauts LJF, Gardner DK, Salamonsen LA. Analysis of fertility-related soluble mediators in human uterine fluid identifies VEGF as a key regulator of embryo implantation. Endocrinology. 2011;152(12):4948-56.

159. Van Der Gaast MH, Macklon NS, Beier-Hellwig K, Krusche CA, Fauser BCJM, Beier HM, *et al*. The feasibility of a less invasive method to assess endometrial maturation - Comparison of simultaneously obtained uterine secretion and tissue biopsy. BJOG. 2009;116(2):304-12.

160. Vilella F, Ramirez LB, Simón C. Lipidomics as an emerging tool to predict endometrial receptivity. Fertil Steril. 2012;99(4):1100-6.

161. Azkargorta M, Escobes I, Iloro I, Osinalde N, Corral B, Ibañez-Perez J, *et al*. Differential proteomic analysis of endometrial fluid suggests increased inflammation and impaired glucose metabolism in non-implantative IVF cycles and pinpoints PYGB as a putative implantation marker. Hum Reprod. 2018;33(10):1898–906.

162. Matorras R, Quevedo S, Corral B, Prieto B, Exposito A, Mendoza R, *et al*. Proteomic pattern of implantative human endometrial fluid in in vitro fertilization cycles. Arch Gynecol Obstet. 2018;297(6):1577–86.

163. Matorras R, Martinez-Arranz I, Arretxe E, Iruarrizaga-Lejarreta M, Corral B, Ibañez-Perez J, *et al*. The lipidome of endometrial fluid differs between implantative and non-implantative IVF cycles. J Assist Reprod Genet. 2020;37(2):385–94.

164. Boomsma CM, Kavelaars A, Eijkemans MJC, Lentjes EG, Fauser BCJM, Heijnen CJ, *et al*. Endometrial secretion analysis identifies a cytokine profile predictive of pregnancy in IVF. Hum Reprod. 2009;24(6):1427-35.

165. Parks JC, McReynolds S, McCallie BR, Strieby A, Schoolcraft WB, Katz-Jaffe MG. The molecular profile of uterine secretions is predictive of endometrial receptivity. Fertil Steril. 2013;100(3):S391.

166. Parks JC, McCallie BR, Strieby A, McReynolds S, Schoolcraft WB, Katz-Jaffe MG. Non-invasive omics analysis of endometrial secretions 24 hours prior to frozen embryo transfer is predictive of implantation outcome. Fertil Steril. 2014;102(3):134–5.

167. Braga DP de AF, Borges E, Godoy AT, Montani DA, Setti AS, Zanetti BF, *et al*. Lipidomic profile as a noninvasive tool to predict endometrial receptivity. Mol Reprod Dev. 2019;86(2):145-55.

168. Li T, Greenblatt EM, Shin MEJ, Brown TJ, Chan C. Cargo small non-coding RNAs of extracellular vesicles isolated from uterine fluid associate with endometrial receptivity and implantation success. Fertil Steril. 2021;115(5):1327-36.

169. Ibañez-Perez J, Díaz-Nuñez M, Clos-García M, Lainz L, Iglesias M, Díez-Zapirain M, Rabanal A, *et al*. microRNA-based signatures obtained from endometrial fluid identify implantative endometrium. Hum Reprod. 2022;37(10):2375-91.

170. Simons M, Raposo G. Exosomes - vesicular carriers for intercellular communication. Curr Opin Cell Biol. 2009;21(4):575-81.

171. Schneider A, Simons M. Exosomes: Vesicular carriers for intercellular communication in neurodegenerative disorders. Cell Tissue Res. 2013;352(1):33-47.

172. Raposo G, Stoorvogel W. Extracellular vesicles: Exosomes, microvesicles, and friends. J Cell Biol. 2013;200(4):373-83.

173. Ciardiello C, Cavallini L, Spinelli C, Yang J, Reis-Sobreiro M, Candia P, *et al*. Focus on extracellular vesicles: New frontiers of cell-to-cell communication in cancer. Int J Mol Sci. 2016;17(2):175-92.

174. Harding C, Heuser J, Stahl P. Receptor-mediated endocytosis of transferrin and recycling of the transferrin receptor in rat reticulocytes. J Cell Biol. 1983;97(2):329-39.

175. Pan BT, Johnstone RM. Fate of the transferrin receptor during maturation of sheep reticulocytes in vitro: Selective externalization of the receptor. Cell. 1983;33(3):967-78.

176. Raposo G, Nijman HW, Stoorvogel W, Leijendekker R, Harding C V., Melief CJM, *et al*. B lymphocytes secrete antigen-presenting vesicles. J Exp Med. 1996;183(3):1161-72.

177. Kim DK, Lee J, Simpson RJ, Lötvall J, Gho YS. EVpedia: A community web resource for prokaryotic and eukaryotic extracellular vesicles research. Semin Cell Dev Biol. 2015;40(1):4–7.

178. Ranghino A, Dimuccio V, Papadimitriou E, Bussolati B. Extracellular vesicles in the urine: Markers and mediators of tissue damage and regeneration. Clin Kidney J. 2015;8(1):23-30.

179. Pucci M, Taverna S, Reclusa P, Pinto JA, Durendez E, Lewintre EJ, *et al*. Exosomes in semen: Opportunities as a new tool in prostate cancer diagnosis. Transl Cancer Res. 2017;6(8):1331-8.

180. Lässer C, Seyed Alikhani V, Ekström K, Eldh M, Torregrosa PP, Bossios A, *et al*. Human saliva, plasma and breast milk exosomes contain RNA: Uptake by macrophages. J Transl Med. 2011;9(9):1-8.

181. Lasser C, Ekerljung L, O'Neil S, Ekstrom K, Sjostrand M, Lotvall J. RNA-containing exosomes in human nasal secretions. Detection and characterisation of exosomes in nasal lavage fluid. Am J Rhinol Allergy. 2011;25(2):89-93.

182. Gámez-Valero A, Lozano-Ramos SI, Bancu I, Lauzurica-Valdemoros R, Borràs FE. Urinary extracellular vesicles as source of biomarkers in kidney diseases. Front Immunol. 2015;6(6):1-10.

183. Aalberts M, Stout TAE, Stoorvogel W. Prostasomes: Extracellular vesicles from the prostate. Reproduction. 2013;147(1):1-14.

184. Verma M, Lam TK, Hebert E, Divi RL. Extracellular vesicles: Potential applications in cancer diagnosis, prognosis, and epidemiology. BMC Clin Pathol. 2015;15(6):1-9.

185. Rak J. Extracellular vesicles - biomarkers and effectors of the cellular interactome in cancer. Front Pharmacol. 2013;4(21):1-9.

186. Harp D, Driss A, Jefferson S, Baker J, Garcia-Barrio M, Sidell N, *et al*. Exosomes derived from endometriotic stromal cells have enhanced angiogenic effects in vitro. Cell Tissue Res. 2016;365(1):187-96.

187. Andreu Z, Otta Oshiro R, Redruello A, López-Martín S, Gutiérrez-Vázquez C, Morato E, *et al*. Extracellular vesicles as a source for non-invasive biomarkers in bladder cancer progression. Eur J Pharm Sci. 2017;98(1):70-9.

188. Théry C, Witwer KW, Aikawa E, Alcaraz MJ, Anderson JD, Andriantsitohaina R, *et al*. Minimal information for studies of extracellular vesicles 2018 (MISEV2018): a position statement of the International Society for Extracellular Vesicles and update of the MISEV2014 guidelines. J Extracell Vesicles. 2018;7(1):1-39.

189. Gould SJ, Raposo G. As we wait: Coping with an imperfect nomenclature for extracellular vesicles. J Extracell Vesicles. 2013;2(1):3–5.

190. Van Niel G, D'Angelo G, Raposo G. Shedding light on the cell biology of extracellular vesicles. Nat Rev Mol Cell Biol. 2018;19(4):213–28.

191. Caruso S, Poon IKH. Apoptotic cell-derived extracellular vesicles: More than just debris. Front Immunol. 2018;9(1):1-9.

192. György B, Szabó TG, Pásztói M, Pál Z, Misják P, Aradi B, *et al*. Membrane vesicles, current state-of-the-art: Emerging role of extracellular vesicles. Cell Mol Life Sci. 2011;68(16):2667-88.

193. Tricarico C, Clancy J, D'Souza-Schorey C. Biology and biogenesis of shed microvesicles. Small GTPases. 2017;8(4):220–32.

194. Sedgwick AE, D'Souza-Schorey C. The biology of extracellular microvesicles. Traffic. 2018;19(5):319–27.

195. Sims PJ, Faioni EM, Wiedmer T, Shattil SJ. Complement proteins C5b-9 cause release of membrane vesicles from the platelet surface that are enriched in the membrane receptor for coagulation factor Va and express prothrombinase activity. J Biol Chem. 1988;263(34):18205-12.

196. Satta N, Toti F, Feugeas O, Bohbot A, Dachary-Prigent J, Eschwège V, *et al*. Monocyte vesiculation is a possible mechanism for dissemination of membrane-associated procoagulant activities and adhesion molecules after stimulation by lipopolysaccharide. J Immunol. 1994;153(7):3245-55.

197.   Al-Nedawi K, Meehan B, Micallef J, Lhotak V, May L, Guha A, *et al*. Intercellular transfer of the oncogenic receptor EGFRvIII by microvesicles derived from tumour cells. Nat Cell Biol. 2008;10(5):619-24.

198.   van der Vlist EJ, Nolte-'t Hoen ENM, Stoorvogel W, Arkesteijn GJA, Wauben MHM. Fluorescent labeling of nano-sized vesicles released by cells and subsequent quantitative and qualitative analysis by high-resolution flow cytometry. Nat Protoc. 2012;7(7):1311-26.

199.   Klumperman J, Raposo G. The complex ultrastructure of the endolysosomal system. Cold Spring Harb Perspect Biol. 2014;6(10):1-22.

200.   Simon C, Greening DW, Bolumar D, Balaguer N, Salamonsen LA, Vilella F. Extracellular vesicles in human reproduction in health and disease. Endocr Rev. 2018;39(3):292–332.

201.   Akers JC, Gonda D, Kim R, Carter BS, Chen CC. Biogenesis of extracellular vesicles (EV): Exosomes, microvesicles, retrovirus-like vesicles, and apoptotic bodies. J Neurooncol. 2013;113(1):1-11.

202.   Théry C, Zitvogel L, Amigorena S. Exosomes: Composition, biogenesis and function. Nat. Rev Immunol. 2002;2(8):569-79.

203.   Baietti MF, Zhang Z, Mortier E, Melchior A, Degeest G, Geeraerts A, *et al*. Syndecan-syntenin-ALIX regulates the biogenesis of exosomes. Nat Cell Biol. 2012;14(7):677-85.

204.   Hurley JH. The ESCRT complexes. Crit Rev Biochem Mol Biol. 2010;45(6):463-87.

205.   Hurley JH, Odorizzi G. Get on the exosome bus with ALIX. Nat Cell Biol. 2012;14(7):654-5.

206.   Nabhan JF, Hu R, Oh RS, Cohen SN, Lu Q. Formation and release of arrestin domain-containing protein 1-mediated microvesicles (ARMMs) at plasma membrane by recruitment of TSG101 protein. Proc Natl Acad Sci U S A. 2012;109(11):4146-51.

207.   Pols MS, Klumperman J. Trafficking and function of the tetraspanin CD63. Exp Cell Res. 2009;315(9):1584-92.

208.   Raiborg C, Stenmark H. The ESCRT machinery in endosomal sorting of ubiquitylated membrane proteins. Nature. 2009;458(7):445-52.

209.   Stuffers S, Sem Wegner C, Stenmark H, Brech A. Multivesicular endosome biogenesis in the absence of ESCRTs. Traffic. 2009;10(7):925-37.

210. van Niel G, Charrin S, Simoes S, Romao M, Rochin L, Saftig P, *et al*. The tetraspanin CD63 regulates ESCRT-independent and -dependent endosomal sorting during melanogenesis. Dev Cell. 2011;21(4):708-21.

211. Matsuo H, Chevallier J, Mayran N, Le Blanc I, Ferguson C, Fauré J, *et al*. Role of LBPA and Alix in multivesicular liposome formation and endosome organization. Science. 2004;303(5):531-4.

212. De Gassart A, Géminard C, Février B, Raposo G, Vidal M. Lipid raft-associated protein sorting in exosomes. Blood. 2003;102(13):4336-44.

213. Edgar JR, Eden ER, Futter CE. Hrs- and CD63-dependent competing mechanisms make different sized endosomal intraluminal vesicles. Traffic. 2014;15(2):197-211.

214. Keerthikumar S, Chisanga D, Ariyaratne D, Al Saffar H, Anand S, Zhao K, *et al*. ExoCarta: A web-based compendium of exosomal cargo. J Mol Biol. 2016;428(4):688-92.

215. Kalra H, Simpson RJ, Ji H, Aikawa E, Altevogt P, Askenase P, *et al*. Vesiclepedia: A Compendium for Extracellular Vesicles with Continuous Community Annotation. PLoS Biol. 2012;10(12):1-5.

216. van Deun J, Mestdagh P, Agostinis P, Akay Ö, Anand S, Anckaert J, *et al*. EV-TRACK: transparent reporting and centralizing knowledge in extracellular vesicle research. Nat Methods. 2017;14(3):228–32.

217. Choi DS, Kim DK, Kim YK, Gho YS. Proteomics of extracellular vesicles: Exosomes and ectosomes. Mass Spectrom Rev. 2015;34(4):474-90.

218. Jeppesen DK, Fenix AM, Franklin JL, Higginbotham JN, Zhang Q, Zimmerman LJ, *et al*. Reassessment of exosome composition. Cell. 2019;177(2):428-45.

219. Pisitkun T, Shen RF, Knepper MA. Identification and proteomic profiling of exosomes in human urine. Proc Natl Acad Sci U S A. 2004;101(36):13368-73.

220. Lötvall J, Hill AF, Hochberg F, Buzás EI, Vizio D Di, Gardiner C, *et al*. Minimal experimental requirements for definition of extracellular vesicles and their functions: A position statement from the International Society for Extracellular Vesicles. J Extracell Vesicles. 2014;3(1):1-6.

221. Llorente A, Skotland T, Sylvänne T, Kauhanen D, Róg T, Orłowski A, *et al*. Molecular lipidomics of exosomes released by PC-3 prostate cancer cells. Biochim Biophys Acta. 2013;1831(7):1302-9.

222. Haraszti RA, Didiot MC, Sapp E, Leszyk J, Shaffer SA, Rockwell HE, *et al*. High-resolution proteomic and lipidomic analysis of exosomes and microvesicles from different cell sources. J Extracell Vesicles. 2016;5(1):1-14.

223. Laulagnier K, Motta C, Hamdi S, Roy S, Fauvelle F, Pageaux JF, *et al*. Mast cell- and dendritic cell-derived display a specific lipid composition and an unusual membrane organization. Biochem J. 2004;380(1):161-71.

224. Groot M, Lee H. Sorting Mechanisms for MicroRNAs into Extracellular Vesicles and Their Associated Diseases. Cells. 2020;9(4):1044-48.

225. Zhang J, Li S, Li L, Li M, Guo C, Yao J, Mi S. Exosome and exosomal microRNA: trafficking, sorting, and function. Genomics Proteomics Bioinformatics. 2015;13(1):17-24.

226. Colombo M, Raposo G, Théry C. Biogenesis, secretion, and intercellular interactions of exosomes and other extracellular vesicles. Annu Rev Cell Dev Biol. 2014;30(1):255-89.

227. Corrado C, Raimondo S, Chiesi A, Ciccia F, De Leo G, Alessandro R. Exosomes as intercellular signaling organelles involved in health and disease: Basic science and clinical applications. Int J Mol Sci. 2013;14(3):5338-66.

228. Qin J, Xu Q. Functions and applications of exosomes. Acta Pol Pharm. 2014;71(4):537-43.

229. Vlassov A V., Magdaleno S, Setterquist R, Conrad R. Exosomes: Current knowledge of their composition, biological functions, and diagnostic and therapeutic potentials. Biochim Biophys Acta. 2012;1820(7):940-8.

230. Mulcahy LA, Pink RC, Carter DRF. Routes and mechanisms of extracellular vesicle uptake. J Extracell Vesicles. 2014;3(1):1-14.

231. French KC, Antonyak MA, Cerione RA. Extracellular vesicle docking at the cellular port: Extracellular vesicle binding and uptake. Semin Cell Dev Biol. 2017;67(1):48-55.

232. Boukouris S, Mathivanan S. Exosomes in bodily fluids are a highly stable resource of disease biomarkers. Proteomics Clin Appl. 2015;9(3-4):358-67.

233. Lin J, Li J, Huang B, Liu J, Chen X, Chen XM, *et al*. Exosomes: Novel Biomarkers for Clinical Diagnosis. Scient World J. 2015;20(1):1-15.

234. Campoy I, Lanau L, Altadill T, Sequeiros T, Cabrera S, Cubo-Abert M, *et al*. Exosome-like vesicles in uterine aspirates: A comparison of ultracentrifugation-based isolation protocols. J Transl Med. 2016;14(1):180-92.

235.   Luddi A, Zarovni N, Maltinti E, Governini L, Leo V De, Cappelli V, *et al*. Clues to non-invasive implantation window monitoring: Isolation and characterisation of endometrial exosomes. Cells. 2019;8(8):1-15.

236.   Almeida MI, Reis RM, Calin GA. MicroRNA history: discovery, recent applications, and next frontiers. Mutat Res. 2011;717(1-2):1-8.

237.   Bhaskaran M, Mohan M. MicroRNAs: History, Biogenesis, and Their Evolving Role in Animal Development and Disease. Vet Pathol. 2014;51(4):759-74.

238.   Bohnsack MT, Czaplinski K, Görlich D. Exportin 5 is a RanGTP-dependent dsRNA-binding protein that mediates nuclear export of pre-miRNAs. RNA. 2004;10(2):185-91.

239.   Gregory RI, Chendrimada TP, Shiekhattar R. MicroRNA biogenesis: isolation and characterization of the microprocessor complex. Methods Mol Biol. 2006;342(1):33-47.

240.   Hutvágner G, McLachlan J, Pasquinelli AE, Bálint É, Tuschl T, Zamore PD. A cellular function for the RNA-interference enzyme dicer in the maturation of the let-7 small temporal RNA. Science. 2001;293(5531):834-8.

241.   Inada T, Makino S. Novel roles of the multi-functional CCR4-NOT complex in post-transcriptional regulation. Front Genet. 2014;5(1):1-15.

242.   Ketting RF, Fischer SEJ, Bernstein E, Sijen T, Hannon GJ, Plasterk RHA. Dicer functions in RNA interference and in synthesis of small RNA involved in developmental timing in C. elegans. Genes Dev. 2001;15(20):2654-9.

243.   Kim VN. MicroRNA precursors in motion: Exportin-5 mediates their nuclear export. Trends in Cell Biology. 2004;14(4):156-9.

244.   King VM, Borchert GM. MicroRNA expression: Protein participants in microRNA regulation. Methods Mol Biol. 2017;1617(1):27-37.

245.   Merritt WM, Bar-Eli M, Sood AK. The dicey role of dicer: Implications for RNAi therapy. Cancer Res. 2010;70(7):2571-4.

246.   Sana J, Faltejskova P, Svoboda M, Slaby O. Novel classes of non-coding RNAs and cancer. J Transl Med. 2012;10(103):1-21.

247.   Song JJ, Liu J, Tolia NH, Schneiderman J, Smith SK, Martienssen RA, *et al*. The crystal structure of the Argonaute2 PAZ domain reveals an RNA binding motif in RNAi effector complexes. Nat Struct Biol. 2003;10(12):1026-32.

248. Ha M, Kim VN. Regulation of microRNA biogenesis. Nat Rev Mol Cell Biol. 2014;15(8):509-24.

249. Graves P, Zeng Y. Biogenesis of mammalian microRNAs: A global view. Genomics, Proteomics and Bioinformatics. 2012;10(5):239-45.

250. Varol N, Konac E, Gurocak OS, Sozen S. The realm of microRNAs in cancers. Mol Biol Rep. 2011;38(2):1079-89.

251. Lewis BP, Burge CB, Bartel DP. Conserved seed pairing, often flanked by adenosines, indicates that thousands of human genes are microRNA targets. Cell. 2005;120(1):15-20.

252. Guo L, Zhao Y, Zhang H, Yang S, Chen F. Integrated evolutionary analysis of human miRNA gene clusters and families implicates evolutionary relationships. Gene. 2014;534(1):24-32.

253. Friedman RC, Farh KKH, Burge CB, Bartel DP. Most mammalian mRNAs are conserved targets of microRNAs. Genome Res. 2009;19(1):92-105.

254. Ambros V, Bartel B, Bartel DP, Burge CB, Carrington JC, Chen X, *et al*. A uniform system for microRNA annotation. RNA. 2003;9(3):277–9.

255.   Desvignes T, Batzel P, Berezikov E, Eilbeck K, Eppig JT, McAndrews MS, *et al*. microRNA nomenclature: A view incorporating genetic origins, biosynthetic pathways, and sequence variants. Trends Genet. 2015;31(11):613-26.

256. Griffiths-Jones S. miRBase: microRNA sequences, targets and gene nomenclature. Nucleic Acids Res. 2006;34(1):140–4.

257. Mitchell PS, Parkin RK, Kroh EM, Fritz BR, Wyman SK, Pogosova-Agadjanyan EL, *et al*. Circulating microRNAs as stable blood-based markers for cancer detection. Proc Natl Acad Sci U S A. 2008;105(30):10513-8.

258. Gilad S, Meiri E, Yogev Y, Benjamin S, Lebanony D, Yerushalmi N, *et al*. Serum microRNAs are promising novel biomarkers. PLoS One. 2008;3(9):1-7.

259. Kosaka N, Iguchi H, Ochiya T. Circulating microRNA in body fluid: A new potential biomarker for cancer diagnosis and prognosis. Cancer Sci. 2010;101(10):2087-92.

260. Mohammadi M, Goodarzi M, Jaafari MR, Mirzaei HR, Mirzaei H. Circulating microRNA: A new candidate for diagnostic biomarker in neuroblastoma. Cancer Gene Ther. 2016;23(11):371-2.

261. Elhefnawi M, Ibrahim S, Ibrahim D. Recent patents of microRNAs as biomarkers for breast, leukemia, prostate, and cervical cancers. Recent Pat Biomark. 2015;3(3):204-12.

262. McKenzie AJ, Hoshino D, Hong NH, Cha DJ, Franklin JL, Coffey RJ, *et al*. KRAS-MEK signaling controls Ago2 sorting into exosomes. Cell Rep. 2016;15(5):978-87.

263. Mittelbrunn M, Gutiérrez-Vázquez C, Villarroya-Beltri C, González S, Sánchez-Cabo F, González MÁ, *et al*. Unidirectional transfer of microRNA-loaded exosomes from T cells to antigen-presenting cells. Nat Commun. 2011;2(1):1-10.

264. Mori MA, Ludwig RG, Garcia-Martin R, Brandão BB, Kahn CR. Extracellular miRNAs: from biomarkers to mediators of physiology and disease. Cell Metab. 2019;30(4):656-73.

265. Prieto-Fernández E, Aransay AM, Royo F, González E, Lozano JJ, Santos-Zorrozua B, *et al*. A comprehensive study of vesicular and non-vesicular miRNAs from a volume of cerebrospinal fluid compatible with clinical practice. Theranostics. 2019;9(16):4567-79.

266. Dragovic RA, Gardiner C, Brooks AS, Tannetta DS, Ferguson DJP, Hole P, *et al*. Sizing and phenotyping of cellular vesicles using nanoparticle tracking analysis. Nanomedicine. 2011;7(6):780-8.

267. Rao X, Huang X, Zhou Z, Lin X. An improvement of the 2ˆ(-delta delta CT) method for quantitative real-time polymerase chain reaction data analysis. Biostat Bioinforma Biomath. 2013;3(3):71-85.

268. Andersen CL, Jensen JL, Ørntoft TF. Normalization of real-time quantitative reverse transcription-PCR data: A model-based variance estimation approach to identify genes suited for normalization, applied to bladder and colon cancer data sets. Cancer Res. 2004;64(15):5245-50.

269. Langmead B, Trapnell C, Pop M, Salzberg SL. Ultrafast and memory-efficient alignment of short DNA sequences to the human genome. Genome Biol. 2009;10(3):1-10.

270. Robinson MD, McCarthy DJ, Smyth GK. edgeR: A Bioconductor package for differential expression analysis of digital gene expression data. Bioinformatics. 2009;26(1):139–40.

271. Varet H, Brillet-Guéguen L, Coppée JY, Dillies MA. SARTools: A DESeq2- and edgeR-based R pipeline for comprehensive differential analysis of RNA-Seq data. PLoS One. 2016;11(6):1–8.

272. Sing T, Sander O, Beerenwinkel N, Lengauer T. ROCR: Visualizing classifier performance in R. Bioinformatics. 2005;21(20):3940–1.

273. Wei T, Simko V, Levy M, Xie Y, Jin Y, Zemla J. R package "corrplot": Visualization of a Correlation Matrix. Statistician. 2017;56(1):316–24.

274. Vlachos IS, Zagganas K, Paraskevopoulou MD, Georgakilas G, Karagkouni D, Vergoulis T, *et al*. DIANA-miRPath v3.0: Deciphering microRNA function with experimental support. Nucleic Acids Res. 2015;43(1):460-66.

275. Miller A, Bromhead C, Jones M, Tustin P. Mucus digestion improves the detection of chlamydia trachomatis and neisseria gonorrhoeae on the cobas 4800. Sex Transm Dis. 2012;39(9):733–4.

276. Wang QY, Zhang HR, Gao Y, Li RH, Shang XH. Sputasol (Dithiothreitol 0.54%) improves the detection of human papillomaviruses using the cobas 4800 system. Ann Lab Med. 2017;37(5):457–8.

277. Gellersen B, Brosens JJ. Cyclic decidualization of the human endometrium in reproductive health and failure. Endocr Rev. 2014;35(6):851–905.

278. Cozzolino M, Diaz-Gimeno P, Pellicer A, Garrido N. Evaluation of the endometrial receptivity assay and the preimplantation genetic test for aneuploidy in overcoming recurrent implantation failure. J Assist Reprod Genet. 2020;37(12):2989–97.

279. Zaman U, Richter FM, Hofele R, Kramer K, Sachsenberg T, Kohlbacher O, *et al*. Dithiothreitol (DTT) Acts as a Specific, UV-inducible Cross-linker in Elucidation of Protein–RNA Interactions. Mol Cell Proteomics. 2015;14(12):3196-210.

280. Groot M, Lee H. Sorting mechanisms for microRNAs into extracellular vesicles and their associated diseases. Cells. 2020;9(4):1044-60.

281. Arroyo JD, Chevillet JR, Kroh EM, Ruf IK, Pritchard CC, Gibson DF, *et al*. Argonaute2 complexes carry a population of circulating microRNAs independent of vesicles in human plasma. Proc Natl Acad Sci U S A. 2011;108(12):5003–8.

282. Li L, Zhu D, Huang L, Zhang J, Bian Z, Chen X, *et al*. Argonaute 2 Complexes Selectively Protect the Circulating MicroRNAs in Cell-Secreted Microvesicles. PLoS One. 2012;7(10):1-7.

283. El-Khoury V, Pierson S, Kaoma T, Bernardin F, Berchem G. Assessing cellular and circulating miRNA recovery: The impact of the RNA isolation method and the quantity of input material. Sci Rep. 2016;6(1):1-14.

284.   Wright K, de Silva K, Purdie AC, Plain KM. Comparison of methods for miRNA isolation and quantification from ovine plasma. Sci Rep. 2020;10(1):1-11.

285.   Agostinis C, Mangogna A, Bossi F, Ricci G, Kishore U, Bulla R. Uterine immunity and microbiota: A shifting paradigm. Front Immunol. 2019;10(1):1-11.

286.   Buck VU, Windoffer R, Leube RE, Classen-Linke I. Redistribution of adhering junctions in human endometrial epithelial cells during the implantation window of the menstrual cycle. Histochem Cell Biol. 2012;137(6):777-90.

287.   Jones RL, Stoikos C, Findlay JK, Salamonsen LA. TGF-β superfamily expression and actions in the endometrium and placenta. Reproduction. 2006;132(2):217-32.

288.   Dai W, He J, Zheng L, Bi M, Hu F, Chen M, *et al*. miR-148b-3p, miR-190b, and miR-429 regulate cell progression and act as potential biomarkers for breast cancer. J Breast Cancer. 2019;22(2):219–36.

289.   Wang G, Li Z, Tian N, Han L, Fu Y, Guo Z, *et al*. MiR-148b-3p inhibits malignant biological behaviors of human glioma cells induced by high HOTAIR expression. Oncol Lett. 2016;12(2):879–86.

290.   Li X, Jiang M, Chen D, Xu B, Wang R, Chu Y, *et al*. miR-148b-3p inhibits gastric cancer metastasis by inhibiting the Dock6/Rac1/Cdc42 axis. J Exp Clin Cancer Res. 2018;37(1):1–15.

291.   Mollazadeh S, Fazly Bazzaz BS, Neshati V, De Vries AAF, Naderi-Meshkin H, Mojarad M, *et al*. Overexpression of microRNA-148b-3p stimulates osteogenesis of human bone marrow-derived mesenchymal stem cells: The role of microRNA-148b-3p in osteogenesis. BMC Med Genet. 2019;20(1):1–10.

292.   Petty RD, McCarthy NE, Dieu R Le, Kerr JR. MicroRNAs hsa-miR-99b, hsa-miR-330, hsa-miR-126 and hsa-miR-30c: Potential diagnostic biomarkers in natural killer (NK) cells of patients with Chronic Fatigue Syndrome (CFS)/myalgic encephalomyelitis (ME). PLoS One. 2016;11(3):1–19.

293.   Quenby S, Farquharson R. Uterine natural killer cells, implantation failure and recurrent miscarriage. Reprod Biomed Online. 2006;13(1):24–8.

294.   Seshadri S, Sunkara SK. Natural killer cells in female infertility and recurrent miscarriage: A systematic review and meta-analysis. Hum Reprod Update. 2014;20(3):429–38.

ANNEXES

ANNEX I

Table A 1. *Data for microRNAs selected for validation, extracted using the PBP-M method.*

MiRNAs (Thermo Fisher)	PBP-M														
	Raw counts						Discovery cohort Small RNA-seq (edgeR)			Discovery cohort qPCR			Validation cohort qPCR		
	Non-Impl. (mean)	Non-Impl. (SD)	Impl. (mean)	Impl. (SD)	Diff SD (units)	CohenD	Exp.	FC	p-value (adj.)	Exp.	FC	p-value	Exp.	FC	p-value
hsa-miR-132-3p (477900_mir)	10657	39238	240	229	0.38	0.38	D	0.1	***	D	0.4	**	-	-	-
hsa-miR-136-3p (477902_mir)	176	209	135	151	0.23	0.22	D	0.8	ns	D	0.67	ns	-	-	-
hsa-miR-148b-3p (477824_mir)	**961**	643	**13167**	39322	**-0.44**	**-0.44**	**U**	**13.2**	***	**D**	**0.8**	**ns**	D	0.6	*
hsa-miR-185-5p (477939_mir)	41	54	557	1114	-0.63	-0.65	U	10.1	**	D	0.5	*	-	-	-
hsa-miR-196b-5p (478585_mir)	9640	19331	1449	1115	0.58	0.6	D	0.2	***	D	0.3	ns	-	-	-
hsa-miR-200b-3p (477963_mir)	**4942**	3458	**13771**	10217	**-1.01**	**-1.16**	**U**	**2.8**	*	**U**	**1.4**	**ns**	D	0.98	ns
hsa-miR-214-5p (478768_mir)	324	289	671	1501	-0.32	-0.32	U	1.9	ns	D	0.6	ns	-	-	-
hsa-miR-218-5p (477977_mir)	304	331	1442	2016	-0.74	-0.79	U	4.1	*	U	1.3	ns	-	-	-
hsa-miR-224-5p (483106_mir)	564	586	3008	8087	-0.42	-0.43	U	4.6	*	D	0.9	ns	-	-	-
hsa-miR-23a-3p (478532_mir)	58648	75396	18041	10384	0.72	0.75	D	0.3	*	D	0.7	ns	-	-	-
hsa-miR-24-3p (477992_mir)	**90375**	174102	**26261**	43808	**0.5**	**0.51**	**D**	**0.3**	*	**D**	**0.4**	****	D	0.8	ns
hsa-miR-34c-5p (478052_mir)	228	301	1266	1411	-0.92	-1.02	U	4.8	*	U	1.5	ns	-	-	-
hsa-miR-3529-3p (480652_mir)	75	97	3380	11502	-0.4	-0.41	U	33.1	***	U	1.7	ns	-	-	-
hsa-miR-378a-3p (478349_mir)	1310	3519	9564	25832	-0.44	-0.45	U	7.6	*	D	0.9	ns	-	-	-
hsa-miR-425-5p (478094_mir)	266	238	705	837	-0.68	-0.71	U	2.2	ns	U	1.1	ns	-	-	-
hsa-miR-99b-5p (478343_mir)	34422	67390	5028	2869	0.6	0.62	D	0.2	***	D	0.8	ns	-	-	-

miRNAs were selected employing small RNA-Seq analysis for the discovery cohort. These miRNAs were differentially expressed between the implantative and non-implantative groups, obtained using PBP-M. The results were confirmed by qPCR performed on the same samples from the discovery cohort and in a new independent group, the validation cohort. The results for each miRNA are summarized below. The mean and SD columns represent the average and standard deviation for each selected miRNA based on TMM-normalized counts obtained with edgeR. Diff SD and Cohen's D columns are the magnitudes of effect size corresponding to differences in S.D. units and Cohen's D for each comparison. "Expression" and "Fold Change" (FC) refer to the status of that miRNA in the implantative group. The endometrium was considered implantative when pregnancy was confirmed by vaginal ultrasound showing a gestational sac four weeks after ET. **Imp.:** implantative endometrium group; **Non-Imp.:** non-implantative endometrium group; **D**: down; **U**: up; Exp.: expression; **PBP-M:** EV enrichment with a PBP method + RNA extraction with the mirVana Paris kit. ns>0.05;*<0.05; **<0.01; ***<0.001; - not analyzed.

ANNEX II

Table A 2. Data for microRNAs selected for validation, extracted using the PBP-N method.

MiRNAs (Thermo Fisher)	PBP-N														
	Raw counts						Discovery cohort Small RNA-seq (edgeR)			Discovery cohort qPCR			Validation cohort qPCR		
	Non-Impl. (mean)	Non-Impl. (SD)	Impl. (mean)	Impl. (SD)	Diff SD (units)	CohenD	Exp.	FC	p-value (adj.)	Exp.	FC	p-value	Exp.	FC	p-value
hsa-miR-132-3p (477900_mir)	660	574	911	1570	-0.21	-0.21	U	1.3	ns	U	1.1	ns	-	-	-
hsa-miR-136-3p (477902_mir)	163	149	1405	4333	-0.4	-0.41	U	8.2	*	D	0.7	ns	-	-	-
hsa-miR-148b-3p (477824_mir)	932	480	968	746	-0.06	-0.06	U	1.1	ns	D	0.9	ns	-	-	-
hsa-miR-185-5p (477939_mir)	556	729	320	436	0.39	0.39	D	0.6	ns	U	1.4	ns	-	-	-
hsa-miR-196b-5p (478585_mir)	2042	1716	2267	2859	-0.1	-0.1	U	1.1	ns	D	0.6	ns	-	-	-
hsa-miR-200b-3p (477963_mir)	**21683**	20263	**30364**	29077	**-0.35**	**-0.35**	**U**	**1.4**	**ns**	**U**	**2.1**	*****	**U**	**1.1**	**ns**
hsa-miR-214-5p (478768_mir)	171	176	50	57	0.85	0.92	D	0.3	**	D	0.6	ns	-	-	-
hsa-miR-218-5p (477977_mir)	646	654	1528	1377	-0.77	-0.82	U	2.3	**	D	0.7	ns	-	-	-
hsa-miR-224-5p (483106_mir)	1982	1812	1810	1979	0.09	0.09	D	0.9	ns	U	1.2	ns	-	-	-
hsa-miR-23a-3p (478532_mir)	22524	11226	33048	34314	-0.41	-0.41	U	1.5	ns	U	1.2	ns	-	-	-
hsa-miR-24-3p (477992_mir)	**20392**	7674	**21042**	13322	**-0.06**	**-0.06**	**U**	**1.1**	**ns**	**D**	**0.6**	*****	**U**	**1.9**	**ns**
hsa-miR-34c-5p (478052_mir)	1318	2165	950	959	0.22	0.22	D	0.7	ns	U	1.4	ns	-	-	-
hsa-miR-3529-3p (480652_mir)	167	148	291	460	-0.36	-0.36	U	1.6	ns	U	2.7	ns	-	-	-
hsa-miR-378a-3p (478349_mir)	538	675	531	479	0.01	0.01	U	1.1	ns	U	1.2	ns	-	-	-
hsa-miR-425-5p (478094_mir)	5180	14036	869	531	0.43	0.43	D	0.2	*	D	0.9	ns	-	-	-
hsa-miR-99b-5p (478343_mir)	**12000**	5977	**13435**	5736	**-0.25**	**-0.24**	**U**	**1.1**	*****	**U**	**1.6**	*****	**U**	**2.7**	*****

miRNAs were selected employing small RNA-Seq analysis for the discovery cohort. These miRNAs were differentially expressed between the implantative and non-implantative groups, obtained using PBP-M. The results were confirmed by qPCR performed for the same samples from the discovery cohort and in a new independent group, the validation cohort. The results for each miRNA are summarized below. The mean and SD columns represent the average and standard deviation for each selected miRNA based on TMM-normalized counts obtained with edgeR. Diff SD and Cohen's D columns are the magnitudes of effect size corresponding to differences in S.D. units and Cohen's D for each comparison. "Expression" and "Fold Change" (FC) refer to the status of that miRNA in the implantative group. The endometrium was considered implantative when pregnancy was confirmed by vaginal ultrasound showing a gestational sac four weeks after ET. **Imp.:** implantative endometrium group; **Non-Imp.:** non-implantative endometrium group; **D**: down; **U**: up; Exp.: expression; **PBP-N:** EV enrichment with a PBP method + RNA extraction with Norgen. ns>0.05;*<0.05; **<0.01; ***<0.001; - not analyzed.

PUBLICATION

human reproduction

ORIGINAL ARTICLE *Infertility*

microRNA-based signatures obtained from endometrial fluid identify implantative endometrium

Jone Ibañez-Perez [iD] [1,2,3,4], María Díaz-Nuñez [iD] [1,2], Marc Clos-García[5], Lucía Lainz[1,2], María Iglesias[1,2], Miren Díez-Zapirain[1,2], Aintzane Rabanal[1,2], Laura Bárcena[6], Monika González[6], Juan J. Lozano[7], Urko M. Marigorta[8,9], Esperanza González[4], Félix Royo[4,10], Ana M. Aransay[6,10], Nerea Subiran [iD] [2,11], Roberto Matorras [iD] [1,2,3,12,*], and Juan Manuel Falcón-Pérez [iD] [4,9,10,13,*]

[1]Human Reproduction Unit, Cruces University Hospital, University of the Basque Country (UPV/EHU), Barakaldo, Spain [2]Innovation in Assisted Reproduction Group, Biocruces Bizkaia Health Research Institute, Cruces University Hospital, Barakaldo, Spain [3]Department of Obstetrics and Gynecology, University of the Basque Country (UPV/EHU), Leioa, Spain [4]Exosomes Laboratory, CIC bioGUNE-BRTA, Derio, Spain [5]Novo Nordisk Foundation Center for Basic Metabolic Research (CBMR), Faculty of Health and Medical Sciences, University of Copenhagen, Copenhagen, Denmark [6]Genome Analysis Platform, CIC bioGUNE-BRTA, Derio, Spain [7]Bioinformatics Platform, Centro de Investigación Biomédica en Red de Enfermedades Hepáticas y Digestivas (CIBERehd), Madrid, Spain [8]Integrative Genomics Lab, CIC bioGUNE-BRTA, Derio, Spain [9]IKERBASQUE, Basque Foundation for Science, Bilbao, Spain [10]Centro de Investigación Biomédica en Red en el Área temática de Enfermedades Hepáticas (CIBEReh), Madrid, Spain [11]Department of Physiology, Faculty of Medicine and Dentistry, University of the Basque Country (UPV/EHU), Leioa, Spain [12]Instituto Valenciano de Infertilidad (IVI) Bilbao/IVIRMA, Leioa, Spain [13]Metabolomics Platform, CIC bioGUNE-BRTA, Derio, Spain

*Correspondence address. Human Reproduction Unit, Cruces University Hospital, University of the Basque Country (UPV/EHU), Barakaldo, Spain; E-mail: joseroberto.matorrasweinig@osakidetza.eus (R.M.) [iD] https://orcid.org/0000-0002-4279-6823; Exosomes Laboratory, CIC bioGUNE-BRTA, Derio, Spain; E-mail: jfalcon@cicbiogune.es (J.M.F.-P.) [iD] https://orcid.org/0000-0003-3133-0670

STUDY QUESTION: Is it possible to use free and extracellular vesicle-associated microRNAs (miRNAs) from human endometrial fluid (EF) samples as non-invasive biomarkers for implantative endometrium?

SUMMARY ANSWER: The free and extracellular vesicle-associated miRNAs can be used to detect implantative endometrium in a non-invasive manner.

WHAT IS KNOWN ALREADY: miRNAs and extracellular vesicles (EVs) from EF have been described as mediators of the embryo–endometrium crosstalk. Therefore, the analysis of miRNA from this fluid could become a non-invasive technique for recognizing implantative endometrium. This analysis could potentially help improve the implantation rates in ART.

STUDY DESIGN, SIZE, DURATION: In this prospective study, we first optimized different protocols for EVs and miRNA analyses using the EF of a setup cohort ($n = 72$). Then, we examined differentially expressed miRNAs in the EF of women with successful embryo implantation (discovery cohort $n = 15$/validation cohort $n = 30$) in comparison with those for whom the implantation had failed (discovery cohort $n = 15$/validation cohort $n = 30$). Successful embryo implantation was considered when pregnancy was confirmed by vaginal ultrasound showing a gestational sac 4 weeks after embryo transfer (ET).

PARTICIPANTS/MATERIALS, SETTING, METHODS: The EF of the setup cohort was obtained before starting fertility treatment during the natural cycle, 16–21 days after the beginning of menstruation. For the discovery and validation cohorts, the EF was collected from women undergoing frozen ET on Day 5, and the samples were collected immediately before ET. In this study, we compared five different methods; two of them based on direct extraction of RNA and the other three with an EV enrichment step before the RNA extraction. Small RNA sequencing was performed to determine the most efficient method and find a predictive model differentiating between implantative and non-implantative endometrium. The models were confirmed using quantitative PCR in two sets of samples (discovery and validation cohorts) with different implantation outcomes.

MAIN RESULTS AND THE ROLE OF CHANCE: The protocols using EV enrichment detected more miRNAs than the methods based on direct RNA extraction. The two most efficient protocols (using polymer-based precipitation (PBP): PBP-M and PBP-N) were used to obtain two predictive models (based on three miRNAs) allowing us to distinguish between an implantative and non-implantative endometrium. The first Model 1 (PBP-M) (discovery: AUC = 0.93; *P*-value = 0.003; validation: AUC = 0.69; *P*-value = 0.019) used hsa-miR-200b-3p, hsa-miR-24-3p and hsa-miR-148b-3p. Model 2 (PBP-N) (discovery: AUC = 0.92; *P*-value = 0.0002; validation: AUC = 0.78; *P*-value = 0.0002) used hsa-miR-200b-3p, hsa-miR-24-3p and hsa-miR-99b-5p. Functional analysis of these miRNAs showed strong association with key implantation processes such as *in utero* embryonic development or transforming growth factor-beta signaling.

LARGE SCALE DATA: The FASTQ data are available in the GEO database (access number GSE178917).

LIMITATIONS, REASONS FOR CAUTION: One important factor to consider is the inherent variability among the women involved in the trial and among the transferred embryos. The embryos were pre-selected based on morphology, but neither genetic nor molecular studies were conducted, which would have improved the accuracy of our tests. In addition, a limitation in miRNA library construction is the low amount of input RNA.

WIDER IMPLICATIONS OF THE FINDINGS: We describe new non-invasive protocols to analyze miRNAs from small volumes of EF. These protocols could be implemented in clinical practice to assess the status of the endometrium before attempting ET. Such evaluation could help to avoid the loss of embryos transferred to a non-implantative endometrium.

STUDY FUNDING/COMPETING INTEREST(S): J.I.-P. was supported by a predoctoral grant from the Basque Government (PRE_2017_0204). This study was partially funded by the Grant for Fertility Innovation (GFI, 2011) from Merck (Darmstadt, Germany). It was also supported by the Spanish Ministry of Economy and Competitiveness MINECO within the National Plan RTI2018-094969-B-I00, the European Union's Horizon 2020 research and innovation program (860303), the Severo Ochoa Centre of Excellence Innovative Research Grant (SEV-2016-0644) and the Instituto de Salud Carlos III (PI20/01131). The funding entities did not play any role in the study design, collection, analysis and interpretation of data, writing of the report or the decision to submit the article for publication. The authors declare no competing interests.

Key words: embryo implantation / endometrial fluid / non-invasive biomarkers / extracellular vesicles / microRNAs / implantative endometrium / non-implantative endometrium / implantative IVF cycles / non-implantative IVF cycle / IVF

Introduction

Increasing embryo implantation rates is one of the greatest challenges in ART, as only 35% of embryo transfers (ETs) result in a clinical pregnancy (Matorras *et al.*, 2002; De Geyter *et al.*, 2020). Despite numerous studies focused on improving implantation rates, a reliable method of determining the competence of the endometrium, fundamental for successful implantation, is still lacking (Strowitzki *et al.*, 2006; Craciunas *et al.*, 2019). Currently, the endometrial biopsy is used to establish whether the endometrium is ready for ET (Casper, 2020). This is an invasive methodology, and the ET is not performed in the same cycle in which the sample is taken as it can have detrimental effects on implantation (van der Gaast *et al.*, 2009). If the biopsy shows that the endometrium is receptive, the results will be extrapolated to the next cycle. This assumption is not realistic, since the endometrial cycle is a dynamic process involving many factors affecting the receptivity of the endometrium. The analysis of endometrial fluid (EF) obtained in a non-invasive manner, without biopsy, is a promising alternative (van der Gaast *et al.*, 2003). It has been demonstrated that the aspiration of EF immediately before the ET does not affect the implantation. Moreover, the prompt analysis of EF composition might allow the ET in the same cycle (van der Gaast *et al.*, 2003; Azkargorta *et al.*, 2018; Matorras *et al.*, 2018, 2020). The EF can be obtained several times during the cycle and its analysis could reveal whether the endometrium is ready for implantation or therapeutic intervention is necessary for a successful procedure.

The EF is a complex biological fluid that can modulate endometrial homeostasis and receptivity, it can sustain the preimplantation embryo and initiate the implantation process and it plays an important role in the embryo–endometrium communication (Ng *et al.*, 2013; Vilella *et al.*, 2015; Bhusane *et al.*, 2016; Nguyen *et al.*, 2016). microRNAs (miRNAs) are small non-coding RNA sequences (18–22 nucleotides) that are important regulators of genes at the post-transcriptional level (Bhaskaran and Mohan, 2014). They are essential during early embryonic development since they regulate cell proliferation and differentiation (Bhaskaran and Mohan, 2014). Some of these miRNAs have been associated with the extracellular vesicles (EVs), also present in the fluid obtained from the uterine cavity (Vilella *et al.*, 2015). EVs are widely known mediators of intercellular communication, transmitting information from one cell to a multitude of other cells and locations (Han *et al.*, 2020). Moreover, analyses of miRNA content of endometrium-derived EVs show that they are taken up by the embryos, modifying their transcriptomic and adhesive phenotypes (Ng *et al.*, 2013; Vilella *et al.*, 2015; Greening *et al.*, 2016; Balaguer *et al.*, 2018; Marinaro *et al.*, 2019). For example, the EV-associated hsa-miR-30d is internalized by mouse trophoectoderm and increases the embryo adhesion via upregulation of adhesive molecules (Vilella *et al.*, 2015).

One of the main challenges in ART is finding non-invasive tools for detecting the best time to perform the ET. Here, we developed a reproducible, sensitive, low-invasive method to comprehensively examine the miRNA landscape of the EF. First, we optimized the EF sample collection technique. Then, we established a robust method for analyzing vesicular and non-vesicular miRNAs from EF obtained in clinical settings, where sample size is limited and no sophisticated equipment is available. Finally, we applied these methods to a set of EF samples from women with different implantation outcomes. Our aim was to define a miRNA signature to identify the competence of the endometrium. If we could determine the state of the endometrium, it would

then be possible to change the ET strategy when the results show an unfavorable implantative pattern. Thus, the implantation rates could potentially be improved and the loss of embryos minimized by avoiding their transfer to non-implantative endometrium.

Materials and methods

Ethical approval

Ethical approval for the study was obtained from the Cruces University Hospital Ethics Committee and Institutional Review Board (CEIC 11/45) and all the participants gave written consent for their participation.

Study population

The population under study consisted of a cohort of 162 women who attended the Human Reproduction Unit of Cruces University Hospital (Basque Country, Spain) from January 2018 to February 2021. For the setup and optimization of the techniques, the samples were collected before starting the fertility treatment. The samples were collected during the natural cycle, 16–21 days after the beginning of menstruation. To test the selected method, the samples were collected just before Day-5 frozen ETs, a practice which is performed increasingly often (Matorras et al., 2021). Out of 162 women (Supplementary Fig. S1), 72 participated in the setup, 30 in the discovery of the predicted models and 60 in the validation of the models. Forty-five women became pregnant and were included in the implantative endometrium group. The other 45, who did not achieve pregnancy, were included in the non-implantative endometrium group. The endometrium was considered implantative when pregnancy was confirmed by vaginal ultrasound showing a gestational sac 4 weeks after ET. Cases with a positive β-hCG test where a gestational sac was not seen on vaginal ultrasound (biochemical miscarriages) were not included in the study.

The inclusion criteria in the setup study were: age between 18 and 37 years; cycle duration between 27 and 29 days; absence of ovulatory disorders, myomas, endometriosis, polyps, uterine scars or hydrosalpinges; normal uterine and ovarian ultrasound; serum anti-Müllerian hormone > 0.4 ng/ml; and no history of gynecological infections, immune disorders or gynecological surgery. The inclusion criteria for the discovery and validation cohorts also included: frozen ET on Day 5 (good quality embryos; Types A and B of the Spanish Society for the Study of Reproductive Biology (ASEBIR) classification (ASEBIR, 2015) and transfer of 1–2 embryos derived from the oocytes of the same subject.

The management of endometrial preparation was always carried out using the same protocol. A vaginal ultrasound was performed on Day 1 or 2 to confirm ovarian quiescence (absence of follicles >10 mm). An artificial cycle was started on Day 2 by administering 6 mg of estradiol daily (Progynova, Bayer, Barcelona, Spain). The development of the endometrium was monitored using serial vaginal ultrasounds. When the endometrium became 7-mm thick, the transfer day was scheduled. Vaginal progesterone at a dose of 400 mg/12 hr (Utrogestan, SEID, Barcelona, Spain) was started the next morning, and the ET was performed on the 5th day of progesterone

administration. If pregnancy was achieved, the estradiol and progesterone treatment was maintained until the 12th week of gestation.

Embryo vitrification was performed on Day 4 or 5 using a Cryotop device (Kitazato BioPharma Co., Shizuoka, Japan). The embryos were cryopreserved and warmed using the Kitazato vitrification/warming kit (Kitazato BioPharma Co.), according to the manufacturer's instructions. Frozen Day-4 embryos were thawed and cultured for 24 hr before the ET and Day-5 blastocysts for 2 hr before the ET.

Sample collection and storage

The EF was aspirated with a catheter used for ET (Frydman, Instrumentos Médicos Estériles SA, Spain) connected to a 10-ml syringe under abdominal ultrasound guidance. Sample extraction was performed by gently applying a negative pressure with the syringe. The aspiration was interrupted at the internal cervical os to prevent contamination with cervical mucus. Special care was taken to avoid touching the uterine fundus or injuring the cervix and minimize sample contamination with blood and endometrial tissue. In cases with excessive vaginal secretions, the vagina was cleaned with saline solution before aspiration. Aspirate volumes ranged from 5 to 50 μl. After aspiration, the 10-ml syringe was replaced with a 2-ml syringe containing 1.5 ml of 1× Dulbecco's PBS (DPBS) (Gibco, Thermo Fisher Scientific, # 14190250, MA, USA) to expel the EF. The aspirates were mixed with the 1× DPBS and expelled into a cryogenic tube (5–50 μl of EF + 1500 μl of 1× DPBS). The mixed samples were centrifuged to remove contaminants at 2500g for 5 min at room temperature, and the supernatants were then kept frozen at −80°C until processed. The dilution of the supernatants was 1:30, with a final volume between 400 and 1300 μl.

EV enrichment methods

Size-exclusion chromatography

A Poly-Prep chromatography column (BioRad, # 731-1550, Hercules, USA) was filled with 2.5 ml of Sepharose CL-2B cross-linked resin (Sigma, # CL2B300-100ML) and left packing overnight at 4°C. The column was then washed twice with 2.5 ml of 1× DPBS. Three aliquots of 400 μl from the setup cohort sample pool were used. Each aliquot was applied to the column, and then 4 ml of 1× DPBS was added. The size-exclusion chromatography (SEC) separated the sample into 12 fractions (F1–F12); the EVs were eluted mainly in F3 but also in F4 and F5 fractions, as described by Prieto-Fernández et al. (2019). F1 to F10 had a final volume of 200 μl, and F11 and F12 of 1 ml. The 12 fractions of one aliquot were each used for RNA extraction with mirVana™ PARIS™ Kit (Thermo Fisher Scientific, # AM1556). The RNA obtained from fractions F3 and F4 was further analyzed by small RNA-sequencing (RNA-Seq). The 12 fractions of the other two aliquots were characterized using western blot (WB).

Polymer-based precipitation method

Since there was no published protocol for using the Invitrogen Total Exosome Isolation Reagent with the EF, we compared the Total Exosome Isolation Reagent for the cell culture media (Invitrogen by Thermo Fisher Scientific, # 4478359) with Total Exosome Isolation Reagent for other body fluids (Invitrogen by Thermo Fisher Scientific, # 4484453). Although both worked well with the EF, we used the # 4478359 because of its better cost-effectiveness ratio. The

optimized protocol was as follows: centrifuge the EF supernatants at 3000g for 30 min at 4°C; transfer the supernatants to a fresh tube and add an equal volume of the Total Exosome Isolation Reagent (1:1); stir the mixture by vortexing until there is a homogeneous solution and incubate the sample for 30 min at room temperature; after the incubation, centrifuge the samples at 10 000g for 1 hr at 4°C; aspirate the supernatant by pipetting and discard it; the EVs are contained in the pellet, which may not be visible at the bottom of the tube; and finally, add 100 µl of 1× DPBS to resuspend the pellet.

Ultracentrifugation

Ultracentrifugation (UC) was carried out in a single step (100 000g for 75 min at 4°C) using a Beckman-Coulter TLA 120.2 rotor. The EV pellets were resuspended in 100 µl of 1× DPBS.

RNA extraction methods

We used two RNA isolation methods; we followed the manufacturer's instructions for the mirVana™ PARIS™ Kit (Thermo Fisher Scientific, # AM1556) (DCT-M) and Norgen Plasma/Serum RNA Purification kit (DCT-N). Two different Norgen kits were used as needed; the midi kit (Norgen Biotek Corp., # 56100, Ontario, Canada) or the mini kit (Norgen Biotek Corp., # 55000). The RNA was eluted in nuclease-free water (Ambion, # AM9930 by Thermo Fisher Scientific).

cDNA synthesis and TaqMan miRNA assay

Following the manufacturer's recommendations, cDNA was synthesized from 2 µl of RNA using the TaqMan Advanced miRNA cDNA Synthesis kit (Applied Biosystems, # A28007, by Thermo Fisher Scientific). The TaqMan reactions used were the TaqMan Fast Advanced Master Mix (Thermo Fisher Scientific, # 4444557) and TaqMan Advance miRNA assays (Thermo Fisher Scientific, # A25576). The quantitative PCR was performed using a Viia7 or QS6 system, and the data were analyzed using the QuantStudio Real-Time PCR System version 1.3 (Applied Biosystems, by Thermo Fisher Scientific). The expression profiles of seven EV-associated miRNAs were used as reference (Thermo Fisher Scientific): hsa-let-7-5p (478579_mir), hsa-miR-17-5p (478447_mir), hsa-miR-200c-3p (478351_mir), hsa-miR-30c-5p (478008_mir), hsa-miR-30d-5p (478606_mir), hsa-miR-451a (478107_mir) and hsa-miR-92a-3p (477827_mir) (Supplementary Table SI). These miRNAs have been reported as secreted by endometrial epithelial cell lines (Ng *et al.*, 2013), found in the EF aspirates (Vilella *et al.*, 2015; Campoy *et al.*, 2016) and secreted in endometrial exosomes associated with early embryo implantation (Vilella *et al.*, 2015; Balaguer *et al.*, 2018). Two other miRNAs were selected after the small RNA-Seq analysis using the setup pool cohort sample. These were the hsa-miR-21-5p (477975_mir) and hsa-miR-155-5p (483064_mir) miRNAs, which were among the most and least abundant miRNAs in the pool, respectively (Supplementary Table SI). In addition, two exogenous miRNAs were used as internal controls. To examine the efficiency of the RNA extraction, 4 µl of cel-miR-39 (478293_mir, Thermo Fisher Scientific) of a 0.1 nM stock were added to the sample before each RNA extraction procedure. To test the differences between the cDNA synthesis reactions, 0.2 µl of ath-miR-159a (478411_mir, Thermo Fisher Scientific) of a 0.001 nM stock was added at the beginning of each cDNA synthesis reaction.

Comparing the miRNA extraction methods

Five different methods were compared to define a simple and effective strategy for detecting vesicular and non-vesicular miRNAs in small volumes of EF (Fig. 1). Two of these involved direct extraction using different RNA extraction kits, DCT-N (Norgen kit, # 56100) and DCT-M (mirVana PARIS kit, # AM1556). The other three required enrichment of EVs before RNA extraction. In one case, the enrichment was carried out by UC followed by RNA extraction with mirVana PARIS kit (UC-M). In the remaining two cases, the enrichment was carried out using the polymer-based precipitation (PBP) method and the RNA was extracted using the Norgen (# 55000) (PBP-N) or mirVana PARIS kit (PBP-M). In parallel, SEC was performed to characterize the protein and miRNA content of the EF (Fig. 1). The volumes of recovered EF samples varied depending on many factors, such as the operator collecting the sample and the EF volume or viscosity. In general, the volumes ranged from 400 µl to 1.3 ml. Therefore, we optimized the protocols to be used with the minimum volume available (400 µl) in all cases. All the tests were performed in triplicate.

Technical reproducibility experiment

A technical reproducibility experiment was conducted using the PBP-M and PBP-N protocols. Two operators (J.I.-P. and M.C.-G.) performed the tests independently. The samples used in these experiments came from the setup pool cohort, and each of the operators tested 10 aliquots using each method. Quantitative PCR (qPCR) was used to examine reproducibility; nine miRNAs were analyzed (seven reference miRNAs and two miRNAs obtained from the small RNA-Seq analysis) (Supplementary Table SI).

Dithiothreitol treatment assay

Two aliquots from the setup pool cohort were used to perform the experiment. One of the aliquots was treated with a 1.4% dithiothreitol (DTT) solution in a 1:1 ratio (Miller *et al.*, 2012; Wang *et al.*, 2017) and the other served as control; 1× DPBS (1:1) was added. The samples were mixed by vortexing and incubated at room temperature for 15 min. Then, 1× DPBS was added until the EF samples were diluted to the ratio of 1:8, and the samples were centrifuged at 3000g for 15 min at 4°C. The supernatants were recovered, and 400-µl aliquots were taken. The EV enrichment was conducted using 400-µl aliquots, following the PBP method, and the pellet was resuspended in 100 µl of 1× DPBS. From this volume, 15 µl was reserved for WB, 5 µl for cryo-electron microscopy, 5 µl for nanoparticle-tracking analysis (NTA), and the rest of the suspension was used for RNA analysis with Norgen (# 55000). The isolated RNA was eluted in 100 µl of nuclease-free water. Two microliters of the eluate was used for the subsequent cDNA synthesis, and the rest was stored at −80°C.

RNase protection assay

The samples used in this step came from the setup pool cohort, and each aliquot tested had a final volume of 400 µl. All the samples were first EV-enriched using the PBP method (described above) and the EVs were resuspended in 200 µl of DPBS. In the RNase protection assay, four different procedures were compared. Samples were treated according to following protocols: RNase A (Sigma-Aldrich, # 10109142001, MA, USA) (RNase); Proteinase K (Sigma-Aldrich,

Figure 1. Workflow summarizing the different methods used to analyze microRNAs from the endometrial fluid of patients undergoing ART. We compared five different methods, two of which used the direct extraction of RNA from the endometrial fluid (EF) (DCT-N and DCT-M). The other three included the extracellular vesicle (EV) enrichment (UC-M, PBP-N and PBP-M) before RNA extraction. In parallel, we carried out a size-exclusion chromatography (SEC-M) to characterize the proteins and miRNAs in the EF. The samples came from the setup pool cohort, and each experiment was performed in triplicate, using sample aliquots of 400 μl. DCT-N: direct RNA extraction with Norgen Plasma/Serum RNA purification kit. DCT-M: direct extraction of RNA with mirVana PARIS kit. UC-M: EV enrichment by ultracentrifugation and RNA extraction using mirVana PARIS kit. PBP-N: EV enrichment with a polymer-based precipitation method and RNA extraction with Norgen Plasma/Serum RNA purification kit. PBP-M: EV enrichment using the polymer-based precipitation method and RNA extraction with mirVana PARIS kit. SEC-M: EV enrichment with SEC and RNA extraction with mirVana PARIS kit. miRNAs, microRNAs; PBP, polymer-based precipitation.

03115879001) + RNase (PRT-K); Triton X-100 (Sigma-Aldrich, # T8787) + RNase (TX-100); and TX-100 + Proteinase K + RNase (TX + PRT). An untreated sample was used as a control. Samples were treated with TX-100 to a final concentration of 0.1%. Proteinase K (0.05 mg/ml concentration) was added and the mixture was incubated for 10 min at 37°C. The reaction was stopped by adding 5 mM of phenylmethylsulfonyl fluoride (Sigma-Aldrich, # 10837091001) and heating at 90°C for 5 min. The samples were finally treated with 0.1 mg/ml RNase A (RNase) for 20 min at 37°C. The control samples were kept at 4°C until RNA extraction. Before extraction, β-mercaptoethanol was used to inhibit RNases, as described by Norgen (# 55000). The RNA was eluted in 50 μl of nuclease-free water. Two microliters were used for the subsequent cDNA synthesis, and the rest was stored at −80°C. All the analyses were performed in triplicate with two technical duplicates, ending with six TaqMan qPCR replicates.

Analysis and quantification of the EF protein content

WB analysis

A sample of 15 μl was mixed with 5 μl of NuPAGE LDS Sample Buffer 4× (Invitrogen # NP0007, by Thermo Fisher Scientific). The fractions obtained by SEC were concentrated using 99.5% acetone (Panreac Applichem, # 161007, Darmstadt, Germany) and resuspended in 20 μl of 1× LDS sample buffer. They were heated for 5 min at 37°C, 10 min at 65°C and 15 min at 95°C and centrifuged for 10 min at 13 000g. Each protein preparation was loaded and separated under non-reducing conditions in 4–12% Bis–Tris precast gels (Invitrogen, # NP0336BOX, by Thermo Fisher Scientific) in MOPS SDS Running Buffer 1× (Invitrogen, # NP0001, by Thermo Fisher Scientific). Precision Plus Protein Dual Color Standard (BioRad, # 161-0374) was used as a marker for protein molecular weights. The proteins were transferred to an Immobilon-P Transfer membrane (Merck Millipore, # IPVH00010, MA, USA) in NuPAGE Transfer Buffer 1× (Invitrogen, # NP0006-1 by Thermo Fisher Scientific) for 1 hr at 100 V. The blocking was performed using 5% Blotting-Grade Blocker (BioRad, # 170-6404) and 0.2% Tween-20 (Sigma-Aldrich, # P2287, MA, USA) diluted in 1× DPBS, for 1 hr. Primary antibodies were incubated overnight and the membranes were washed three times for 10 min with 1× DPBS. Incubation with the secondary horse-radish peroxidase-conjugated antibody (1:6000) was performed at room temperature for 30 min. The chemiluminescence was detected using Pierce ECL Plus Western Blotting Substrate (Thermo Fisher Scientific, # 32132). The bands were visualized on high-performance films (GE Healthcare,

28906844, IL, USA) employing the AGFA Curix-60 automatic processor (Agfa, Cologne, Germany). The primary antibodies used in this study were mouse anti-CD63 (1:500; clone H5C6 from Developmental Studies Hybridoma Bank, IA, USA), mouse anti-CD9 (1:500; clone 209306, R&D Systems, Minneapolis, MN, USA), mouse anti-CD81 (1:500, Clone JS-81, 555675, BD, NJ, USA), mouse anti-CD133 (1:500 clone W6B3C1, Miltenyi Biotec, North Rhine-Westphalia, Germany), mouse anti-Rab8 (1:1000; Clone 4, 610844, BD, NJ, USA), mouse anti-Flotillin-1 (1:500; Clone 18 610820, BD, NJ, USA), mouse anti-HSP90 (1:500; 610418, BD, NJ, USA) and rabbit anti-Limp II (1:500; ab16522, Abcam, Cambridge, UK). The intensity of the bands was quantified by densitometry using ImageJ software v. 1.52a (ImageJ software, MD, USA).

Coomassie blue staining

SimplyBlue™ SafeStain from Invitrogen (Cat. # LC6060, Thermo Fisher Scientific) was used following the manufacturer's recommendations. The intensity of the bands was quantified by densitometry using ImageJ software (v. 1.52a).

Spectrophotometer

Spectrophotometric measurements were performed using a NanoDrop™ One Microvolume UV–Vis Spectrophotometer (Thermo Fisher Scientific) in the wavelength range of 230–576 nm. Concentrations of RNA and proteins were obtained after measuring the absorbance of 1 µl of the sample.

Nanoparticle-tracking analysis

The size distribution of the EV preparations was analyzed by measuring the rate of Brownian motion using a NanoSight LM10 system (NanoSight, Amesbury, UK), equipped with fast video capture and particle-tracking software. NTA acquisition settings were the same for all samples, and each video was analyzed to obtain the mean and mode of vesicle size and estimate the particle concentration (Dragovic *et al.*, 2011).

Cryo-electron microscopy

EV preparations were directly adsorbed onto glow-discharged holey carbon grids (Quantifoil, Großlöbichau, Germany). The grids were blotted at 95% humidity and rapidly plunged into liquid ethane with the aid of Vitrobot (Maastricht Instruments BV, Maastricht, The Netherlands). Vitrified samples were imaged at liquid-nitrogen temperature using a JEM-2200FS/CR transmission cryo-electron microscope (JEOL, Tokyio, Japan) equipped with a field emission gun and operated at an acceleration voltage of 200 kV.

Real-time qPCR assay

The relative expression levels of the miRNAs obtained for the setup pool cohort were normalized to ath-miR-159 expression and calculated using the $2^{-\Delta Ct \, (Ct \, miRNA - Ct \, ath-miR-159a)}$ method. The relative expression levels of the discovered and validated miRNAs were normalized to internal controls; the differences between the groups were calculated employing the $2^{-\Delta Ct \, (Ct \, miRNA - Ct \, mean \, internal \, controls)}$ equation. Subsequently, the fold changes were obtained using the $2^{-\Delta\Delta Ct}$ method (Rao *et al.*, 2013). Endogenous controls were selected from the reference miRNAs (Supplementary Table SI) using the

NormFinder software (MOMA, Aarhus, Denmark). The NormFinder is an algorithm using a model-based approach to calculate the stability of a reference transcript; the calculation is based on the intergroup and intragroup variations. The stability score is a weighted measure of these two parameters, and the most stable reference transcript is the one with the smallest stability value (Andersen *et al.*, 2004).

Only the samples for which we could find the internal controls with fewer than 30 Ct cycles (in qPCR) were used in the regression study of the discovery cohort (Supplementary Table SII) and to validate the models in the validation cohort (Supplementary Table SIII).

Correlation analysis

The *corrplot* package (Wei *et al.*, 2017) of the R 3.6.2 program was used to analyze the correlations between the proteins (2019-12-12, R Foundation for Statistical Computing, Vienna, Austria).

Statistical analysis

GraphPad Prism v.8.0 (GraphPad Software, California, USA) was employed to analyze the data. The statistical significance of the experiments carried out with the setup pool cohort was determined using paired Student's *t*-tests. For the results obtained for the discovery and validation cohorts, unpaired Student's *t*-tests with Welch's correction were employed. Statistical differences were considered significant at a *P*-value smaller than 0.05 (two-sided). Sample sizes and *P*-values are all shown in the figures and figure captions.

Small RNA-Seq

The quantity and quality of the RNA were evaluated using Agilent RNA 6000 Pico Chips (Agilent Technologies, Cat. # 5067-1513, CA, USA). Sequencing libraries were prepared following the protocol included with the NEXTflex™ Small RNA-Seq Kit v3 (©Bioo Scientific Corp., Cat. # 5132-06, protocol V19.01, Austin, TX, USA). Briefly, the total RNA from each sample was incubated for 2 min at 70°C. Then, a 3′ 4N adenylated adapter (adapter dilution 1/4) and ligase enzyme were added, and ligation was carried out by incubation overnight at 20°C. After removing the excessive 3′ adapter, 5' adapter was added with the ligase enzyme and the mixture was incubated at 20°C for 1 hr. The ligation product was used for reverse transcription with the M-MuLV reverse transcriptase in a thermocycler for 30 min at 42°C and 10 min at 90°C. Next, the enrichment of the cDNA was performed using PCR cycling: 2 min at 95°C; 20–27 cycles of 20 s at 95°C, 30 s at 60°C and 15 s at 72°C, with the final elongation of 2 min at 72°C and a pause at 4°C. The PCR products were resolved on 8% Novex TBE polyacrylamide gels (Cat. # EC6215BOX, Thermo Fisher Scientific), and a band between 150 and 400 bp was cut out. Small RNAs were extracted from the polyacrylamide gel using an adapted protocol in which the DNA from gel slices was dissolved in ddH$_2$O overnight at room temperature. Afterwards, the libraries were visualized employing an Agilent 2100 Bioanalyzer with an Agilent High Sensitivity DNA kit (Agilent Technologies, Cat. # 5067-4626) and quantified using a Qubit dsDNA HS DNA Kit (Thermo Fisher Scientific, Cat. # Q32854). The amount of cDNA in each library that was sent for sequencing was 10 nM. Sequencing was carried out in pools of isomolar libraries and all of them were sequenced in a

HiSeq2500 (Illumina Inc) to achieve at least 10 million 50-nt single-reads per sample.

Alignment

The FASTQs were trimmed for the adapters following the recommendations of the NEXTflex[TM] Small RNA-Seq Kit manufacturers. We used the Bowtie program (Langmead *et al.*, 2009) to align the reads against the human genome (GRCh38), with a mismatch of 0 to avoid false positives. We chose miRBase v22 to quantify the mature miRNAs, employing the Partek Flow application (version 7.0).

Small RNA-Seq data analysis

We performed differential abundance analyses to identify miRNAs associated with different implantation outcomes. To avoid rare molecules, following the Trimmed Mean of *M*-values (TMM) normalization, we retained miRNAs with counts per million > 1, non-zero counts in at least 15 individuals, and at most 10 zero counts in each of the two subgroups, i.e., the successful (n = 15) and unsuccessful implantations (n = 15). Differential expression was then assessed employing the edgeR (Robinson *et al.*, 2010) using the SARTools R package (Varet *et al.*, 2016). The program fits a log-linear model for each miRNA that uses a group (implantative versus non-implantative) as the factor of contrast. Applying the edgeR default parameters for normalization and shrinkage, this gives a fold change estimate that corresponds to the mean expression level in the implantative samples divided by the mean expression level in the non-implantative group. For further analysis, we selected the miRNAs with logFC > 1.5 or logFC < −1.5 and the adjusted *P*-value < 0.05. The Benjamini–Hochberg procedure was used to calculate the false discovery rate for each comparison and obtain the adjusted *P*-values (Supplementary Tables SIV and SV).

Regression study

A subset of miRNAs was used to generate two linear regression models with *k*-fold cross-validations, one for each miRNA extraction protocol assessed. Samples were randomly divided into training and testing datasets (80–20%). Three miRNAs were used per modeling process. The hsa-miR-24-3p, hsa-miR-200b-3p and hsa-miR-148b-3p were selected for PBP-M and hsa-miR-24-3p, hsa-miR-200b-3p and hsa-miR-99b-5p for PBP-N. The resulting model reproducibility was further tested by bootstrap correction with 500 replications. The analysis was performed using R v4.0.0 software (R Development Core Team; http://cran.r-project.org) with *ROCR* (Sing *et al.*, 2005) and *caTools* packages.

Functional analysis of the miRNAs

The target genes of the validated miRNAs were obtained from the TarBase database, v7.0. The biological processes in which these miRNAs are involved were analyzed using the Kyoto encyclopedia of genes and genomes (KEGG) and gene ontology (GO) in terms of biological process categories employing Diana-miRPath tools v3.0 (Vlachos *et al.*, 2015). The Fisher's exact test and false discovery rate correction were performed to select enriched KEGG pathways and GO processes. We selected only the pathways and processes with *P*-values < 0.05. The results for the KEGG were merged by 'pathway union' and the results for GO by 'category union'.

Results

## Optimization of EF sample preparation

The treatment of the samples with 1.4% DTT (Miller *et al.*, 2012; Wang *et al.*, 2017) was useful for degrading the mucus pellet formed after centrifugation; most mucus disappeared, as shown in Supplementary Fig. S2A. The NTA and cryo-electron microscopy analyses (Supplementary Fig. S2B and C) revealed heterogeneous EV populations with diameters between 100 and 800 nm under both experimental conditions (with and without DTT). In the untreated samples, the average concentration was $1.9 \times 10^9 \pm 7.8 \times 10^7$ particles/ml, with a mean size of 291.5 ± 0.1 nm and mode 196.4 ± 3.2 nm. In the DTT-treated samples, we detected more particles (mean $2.7 \times 10^9 \pm 5.9 \times 10^7$ particles/ml), with larger mean size (mean 313.6 ± 2.5 nm and mode 248.5 ± 8.1 nm). The WB showed different patterns of vesicular markers in the two conditions (Supplementary Fig. S2D). The intensity of the Rab8 marker in the DTT-treated samples was stronger than in the untreated samples, in agreement with the number of particles detected in the NTA. In contrast, the intensities of the Limp II, CD133 and CD63 markers were stronger in the untreated samples. The seven reference miRNAs (Supplementary Table SI) were detected in all the samples for both conditions. In the DTT-treated group, the levels of the following miRNAs were significantly reduced compared to the untreated group: hsa-let-7e-5p, hsa-miR-17-5p, hsa-miR-200c-3p, hsa-miR-30c-5p and hsa-miR-451a (Supplementary Fig. S2E).

Characterization of the miRNAs in EF

The SEC method separated the EF into several fractions. The results of WB analysis of the fractions demonstrate that it was possible to detect exosomal markers in small-volume EF samples (Fig. 2A). The CD63 and CD81 markers were detected in the F3 and to a lesser extent in F4 and F5 fractions. Rab8 was also mainly detectable in F3–F5 fractions. Immunoglobulins were also found in fractions F6 to F11. The study of the distribution of the seven reference miRNAs (Supplementary Table SI) showed that the relative quantity of miRNAs increased in fractions F3 to F11 (Fig. 2B). In F3, which corresponds to the vesicular fraction, the most abundant miRNAs were hsa-miR-451a and hsa-miR-92a-3p, and the least abundant were hsa-miR-30d-5p and hsa-miR-200c-3p. This trend was maintained in the rest of the fractions, except for F7, where hsa-miR-200c-3p was the second most abundant miRNA.

The protective effect of the EVs on the miRNAs was confirmed by the RNase assay. In the samples treated with RNase or Triton X-100 (TX-100) with RNase, only the hsa-miR-30c-5p was significantly degraded compared to the control (Fig. 2C). In the samples treated with proteinase K (PRT-K) and RNase, there was a significant decrease in the levels of all the analyzed miRNAs (although all the miRNAs were detectable in all the replicates). The miRNAs were further degraded when the samples were treated with TX-100, PRT-K and RNase (TX + PRT). In this case, we could only detect hsa-miR-200c-3p and hsa-miR-92a-3p in all the replicates. Under these conditions, hsa-miR-451a, hsa-miR-17-5p and hsa-miR-30d-5p were detected in four of six replicas, hsa-let-7-5p in two of six replicas and hsa-miR-30c-5p was undetectable. In the TX + PRT treatment, the detection of all miRNAs was significantly reduced compared to the previous combinations.
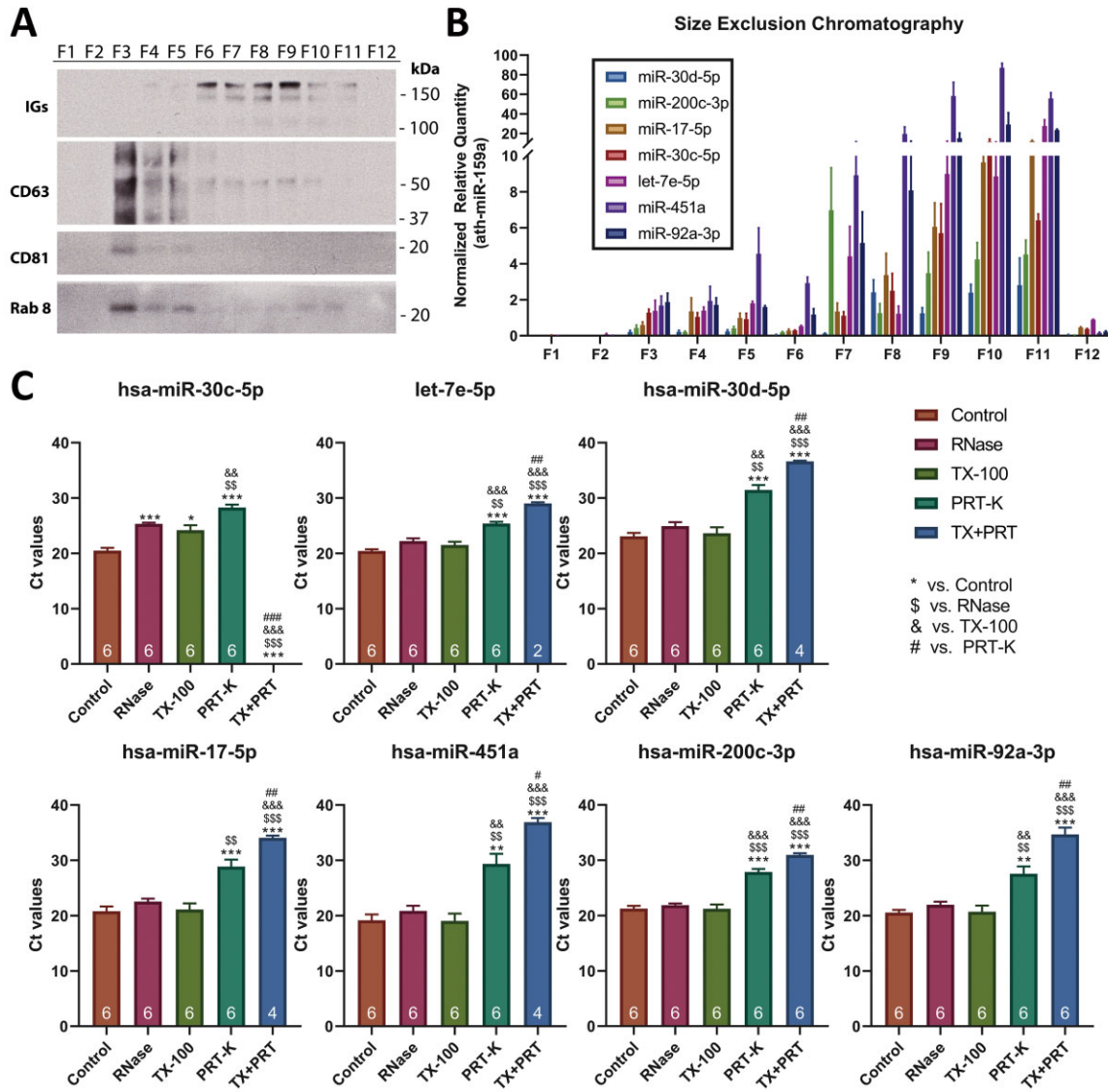
Figure 2. Characterization of the microRNAs (miRNAs) in the endometrial fluid of patients undergoing ART. (A) Western blot shows different EV markers (CD63, CD81 and RAB8) and soluble proteins (Igs) in the fractions of size-exclusion chromatography (SEC). The fractions obtained by SEC were numbered from F1 to F12. **(B)** Distribution of the seven reference miRNAs among the fractions of the SEC. Normalized relative quantification was used to detect the miRNAs in the fractions. To perform experiments A and B, a 400-µl sample aliquot from the setup pool cohort was added onto the column. The number of replicates for each fraction was six and the data show the mean with SEM. **(C)** RNase protection assay. Sample analysis to examine the association of miRNAs with proteins and EVs. The graphs show the Ct values of the reference miRNAs evaluated using the qPCR. The number of replicates for each condition was six and the data show the mean with SEM. The number of replicates in which each miRNA was detected is shown at the bottom of each column. Each aliquot (400 µl) came from the setup pool cohort. Statistical significance was determined using the paired Student's *t*-test analysis. $^{*,\$,\&,\#}P < 0.05$; $^{**,\$\$,\&\&,\#\#}P < 0.01$; $^{***,\$\$\$,\&\&\&,\#\#\#}P < 0.001$. * versus Control, $^{\$}$ versus RNase, $^{\&}$ versus TX-100, $^{\#}$ versus PRT-K. Control: control sample without treatment. RNase: samples treated with RNase. TX-100: samples treated first with Triton-X 100 (TX-100) followed by RNase treatment. PRT-K: samples treated first with proteinase K and then with RNase. TX-PRT: samples treated first with TX-100, then with proteinase K and finally with RNase. EVs, extracellular vesicles; qPCR, quantitative PCR.

Identification of an efficient method to perform a comprehensive analysis of miRNAs from EF

Although we detected all the reference miRNAs (Supplementary Table SI) in all the extraction replicates obtained using the DCT-M,

DCT-N, PBP-M, PBP-N and UC-M protocols, differences in the abundance of each miRNA were found among them (Fig. 3A). The miRNA analysis showed that the methods employing the EV enrichment step with PBP (PBP-N and PBP-M) performed better than the others, with PBP-N being the most efficient method. The protocols using direct
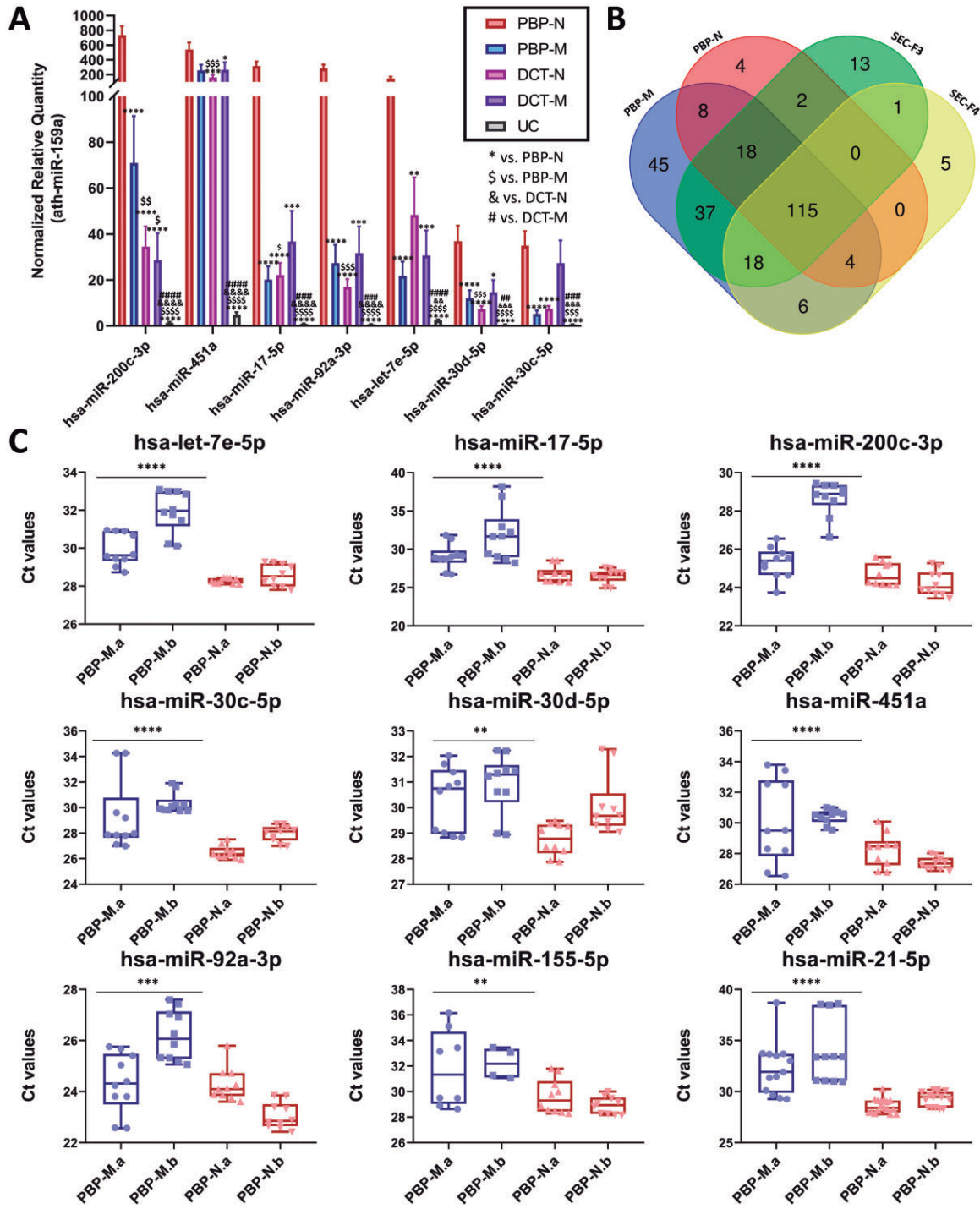
Figure 3. **Optimization of different methods for analyzing the miRNAs in endometrial fluid of patients undergoing ART. (A)** Results for the seven reference miRNAs analyzed by quantitative PCR for each of the compared techniques. Normalized relative quantification revealed that the most efficient method was the PBP-N, while the UC-M method was the least efficient. Statistical significance was determined using paired *t*-test analysis. The number of replicates for each case was 12 and the data show the mean with SEM. * versus PBP-N; $ versus PBP-M; & versus DCT-N; # versus DCT-M. **(B)** The Venn diagram shows the number of unique miRNAs detected using small RNA-Seq for each method and the number of miRNAs common among them. The number of unique miRNAs detected by each technique was 251 for PBP-M, 151 for PBP-N, 204 for SEC F3 and 149 for SEC F4. The samples (400 µl) for experiments A and B came from the setup pool cohort, and each experiment was performed in triplicate. **(C)** A technical reproducibility experiment was conducted to compare the performance of PBP-M and PBP-N methods. The graphs show Ct values for each miRNA, each operator (a, JIP; b, MCG) and method (PBP-M or PBP-N). Box plots show the median, maximum and minimum values and all the points. The 400-µl samples came from the setup pool cohort. Each operator analyzed 20 aliquots, 10 by employing the PBP-M and 10

(continued)

extraction (DCT-N and DCT-M) and the UC-M method obtained significantly smaller signals of our reference miRNAs than the PBP-N procedure (Fig. 3A). Small RNA-Seq analysis of the RNA obtained using PBP-N and PBP-M detected 151 and 251 unique miRNAs, respectively. Of these, 145 miRNAs were shared between the two methods (Fig. 3B). Moreover, the small RNA-Seq analysis of fractions F3 and F4 detected 204 and 149 unique miRNAs, respectively. The samples obtained using PBP methods and SEC fractions F3 and F4 shared a large number of miRNAs (Fig. 3B). The percentage of alignments with the human genome for PBP-M, PBP-N, F3 and F4 were $74 \pm 5.9\%$, $68.4 \pm 1.8\%$, $54 \pm 6.8\%$ and $67.7 \pm 5.1\%$, respectively.

The technical reproducibility experiment showed that using the PBP-N method, the nine miRNAs were detected by both operators (Supplementary Table SI). However, using the PBP-M protocol, no operator could detect hsa-miR-155-5p and hsa-miR-21-5p in all the replicates (Supplementary Table SI). PBP-M showed bigger differences between coefficients of variation than PBP-N, both for the different aliquots and the operators performing the experiment (Supplementary Table SI). In addition, the normalized relative quantification of the miRNAs showed significant differences between the techniques, with the PBP-N method being the most efficient, as judged by the detection of all the miRNAs with lower Ct values (Fig. 3C).

Performance of the selected methods in a set of samples with different implantation outcomes

PBP-M and PBP-N, the most efficient of the tested protocols, were chosen for implementation in the discovery cohort. There were no significant differences between the clinical characteristics of the women for whom the implantation was successful and those for whom the procedure failed (Table I). We observed large variability in the total amounts of protein in the samples (Supplementary Fig. S3A and Supplementary Table SII). The WB analysis revealed that the expression of albumin and Igs was higher in the samples with higher total protein concentration, with correlation coefficients (r) of 0.65 (P-value $= 0.0066$) and 0.86 (P-value $= 0.0001$), respectively (Supplementary Fig. S3B). The vesicular markers, such as flotillin-1 ($r = 0.76$, P-value $= 8.7 \times 10^{-7}$), Rab8 ($r = 0.89$, P-value $= 1.4 \times 10^{-12}$) and HSP90 ($r = 0.82$, P-value $= 2.3 \times 10^{-7}$), were also detected in most of the samples and positively correlated with total protein content. However, the exosomal tetraspanins CD63 and CD9 were detectable in some samples but not correlated with the total protein quantity (Supplementary Fig. S3C). Both the Coomassie blue and WB results were analyzed by densitometry of non-saturated films (data summarized in Supplementary Table SII).

The post-alignment quality assurance/quality control of the small RNA-Seq analysis showed great variability among the samples (Supplementary Figs S4 and S5 and Supplementary Table SII). After the TMM normalization of the small RNA-Seq results, we considered the 341/910 and 231/845 unique miRNAs for further differential abundance analysis for the PBP-N and PBP-M datasets, respectively (Fig. 4A). Statistical analysis applied to the PBP-M data detected 13 miRNAs suitable for further validation by qPCR in the same samples. In the case of PBP-N, five miRNAs were deemed suitable for validation (fold changes and P-values are shown in Supplementary Tables SIV and SV). The NormFinder algorithm identified the hsa-miR-200c-3p (stability for PBP-M, 0.31 and for PBP-N, 0.24) and hsa-miR-92a-3p (stability for PBP-M, 0.27 and for PBP-N, 0.1) as the most suitable pair of normalizer miRNAs (Fig. 4B) (Supplementary Table SI).

The predictive model was chosen by conducting a regression study using bootstrapping correction of the normalized qPCR data (dCt) for the differentially expressed miRNAs in the discovery group. For the PBP-M method, Model 1 (AUC $= 0.93$; P-value $= 3.3 \times 10^{-3}$), based on three miRNAs (hsa-miR-24-3p, hsa-miR-200b-3p and hsa-miR-148b-3p), was robust against the data that fitted the given characteristics. The results for PBP-N also highlighted a predictive model based on three miRNAs, Model 2 (hsa-miR-24-3p, hsa-miR-200b-3p and hsa-miR-99b-5p) (AUC $= 0.92$; P-value $= 2.3 \times 10^{-4}$) (Fig. 4C). Both models were significantly predictive compared to random chance results (AUC $= 0.5$).

The regulatory functions of these miRNAs were broken down into biological process categories by analyzing their predicted target genes. The KEGG pathways showed many different enriched pathways, including adherens junction proteins, transforming growth factor (TGF)-beta signaling, fatty acid biosynthesis and fatty acid metabolism, all of which turned out to be significantly enriched (Supplementary Fig. S6). The GO analysis also showed TGF-beta signaling pathway enrichment (Supplementary Fig. S7). The *in utero* embryonic development, immune system processes, endosome and vesicle-mediated transport processes were also enriched. Overall, most detected pathways were closely related to embryo implantation and endometrial decidualization.

Validation of the models in an independent cohort of samples with different implantation outcomes

The performance of the two predictive models (Model 1 and Model 2) was validated in an independent cohort. There were no significant differences between the clinical characteristics of the women in the validation cohort (implantative versus non-implantative) or validation

Figure 3. Continued
by PBP-N. Statistical significance was assessed using the paired *t*-test analysis of the total results obtained with PBP-N and PBP-M. *,$,&,#$P < 0.05$; **,$$,&&,##$P < 0.01$; ***,$$$,&&&,###$P < 0.001$; ****,,&&&&,####$P < 0.0001$. DCT-M: direct extraction of RNA with mirVana PARIS kit. DCT-N: direct RNA extraction with Norgen Plasma/Serum RNA purification kit. PBP-M: extracellular vesicle enrichment using the polymer-based precipitation method and RNA extraction with mirVana PARIS kit. PBP-N: extracellular vesicle enrichment with a polymer-based precipitation method and RNA extraction with Norgen Plasma/Serum RNA purification kit. SEC-M: extracellular vesicle enrichment with size-exclusion chromatography and RNA extraction with mirVana PARIS kit. UC-M: extracellular vesicle enrichment by ultracentrifugation before RNA extraction with mirVana PARIS kit. miRNAs, microRNAs; PBP, polymer-based precipitation; RNA-Seq, RNA-sequencing.

Table I Main characteristics of the study population of women undergoing ART.

| | Discovery cohort | | Validation cohort | |
| | Implantative endometrium | Non-implantative endometrium | Implantative endometrium | Non-implantative endometrium |
	(n = 15)	(n = 15)	(n = 30)	(n = 30)
Woman's age at transfer (years)	36.7 ± 2.6	36.3 ± 1.8	36.6 ± 2.3	36 ± 3.4
Woman's age at cryopreservation (years)	35.5 ± 2.4	35.1 ± 1.7	35.8 ± 2.5	35.1 ± 3.4
BMI (kg/m^2)	26.2 ± 4.4	25.3 ± 1.9	24 ± 5.2	23.9 ± 4.7
Smokers (%)	26.7	25	25	14.3
Primary infertility (%)	78.6	73.3	53.6	64.3
Previous insemination failure (%)	40	41.6	17.3	25
Male factor (%)	37.5	26.7	14.8	39.3
Tubal factor (%)	6.7	0	28.6	17.9
Estradiol on the day of hCG (pg/ml)	3580.1 ± 1820.2	4101.4 ± 1154.6	3807.9 ± 2560.3	3937.1 ± 1445.5
Oocytes obtained	13.5 ± 5.2	15.6 ± 7.5	14.1 ± 6.9	13.3 ± 6.7
Metaphase II oocytes	11.73 ± 5.1	13.2 ± 5.7	12.3 ± 5.9	11.2 ± 6.1
Fertilized oocytes	7.2 ± 2.4	7.9 ± 3.8	8 ± 4.8	7.5 ± 4.5
Frozen embryos	3 ± 1.7	3.9 ± 3.9	4 ± 3	3.6 ± 2.5
Embryos transferred	1.3 ± 0.5	1.3 ± 0.5	1.4 ± 0.5	1.1 ± 0.4
Twins (%)	6.7	NA	0	NA

Statistical significance was assessed using the unpaired Student's *t*-test. There were no significant differences between the clinical characteristics of the women in the discovery and validation cohort (implantative versus non-implantative) or discovery versus validation cohort. Data are expressed as mean ± SD unless specified otherwise. NA, not applicable. The endometrium was considered implantative when pregnancy was confirmed by vaginal ultrasound showing a gestational sac 4 weeks after embryo transfer.

versus discovery cohort (Table I) or between the total RNA and protein amounts in the different groups (Supplementary Table SIII). The results showed that our two models based on miRNA signature remained predictive of the implantation status, especially Model 2.

Model 1 (hsa-miR-200b-3p, hsa-miR-24-3p and hsa-miR-148b-3p) has an accuracy of 0.68 (95% CI (0.54, 0.8)) and an AUC of 0.69 (95% CI (0.55, 0.86)) (Fig. 5). The test showed a statistically significant difference (*P*-value: 0.019) in AUC compared to random chance (AUC = 0.5). The receiver operating characteristic (ROC) curve analysis identified hsa-miR-148b-3p as the mostly likely variable to differentiate between implantative and non-implantative endometrium. A significant differential expression of this miRNA was seen in group comparisons (*P*-value 0.02); it was upregulated in the non-implantative group.

We established the cutoff point as 2.34 dCt (dCt = Ct$^{hsa-miR-148b-3p}$ − Ct$^{internal\ controls}$) based on Youden's *J* statistic with sensitivity of 0.56 and specificity of 0.86. Values above the cutoff point would indicate an implantative endometrium (dCt > 2.34) (negative predictive value = 0.69) and values below, a non-implantative endometrium (dCt < 2.34) (positive predictive value = 0. 78).

Model 2 (hsa-miR-200b-3p, hsa-miR-24-3p and hsa-miR-99b-5p) had an accuracy of 0.77 (95% CI (0.63, 0.88)) and an AUC of 0.78 (95% CI (0.6, 0.89)) (Fig. 5). The test also showed a statistically significant difference (*P*-value: 0.0002) in AUC compared to random chance results (AUC = 0.5). The ROC analysis identified hsa-miR-99b-5p as the most able variable to distinguish the non-implantative from implantative endometrium. A significant difference in the expression of this

miRNA (≥1.5-fold) was found between the groups at *P*-value 0.0004 (the miRNA upregulated in the implantative group). We established the cutoff point as 2.81 dCt (dCt = Ct$^{hsa-miR-99b-5p}$ − Ct$^{internal\ controls}$) based on Youden's *J* statistic with 0.6 sensitivity and 0.93 specificity. Values above the cutoff point would indicate a non-implantative endometrium (dCt > 2.81) (positive predictive value = 0.88) and values below, implantative endometrium (dCt < 2.81) (negative predictive value = 0. 71) (Fig. 5).

Discussion

The endometrium undergoes a series of changes during the ovarian cycle until the endometrial glands achieve maximal secretory activity 6 days after ovulation, which is necessary to create an optimal uterine microenvironment for embryo implantation (Gellersen and Brosens, 2014). It has been widely believed that the embryo has the most important role in human implantation. However, in many cases, even when the maternal conditions are apparently optimal and the transferred embryo is chromosomally normal, implantation does not occur (Cozzolino *et al.*, 2020). The term 'implantative endometrium' was coined to signify the endometrium in which implantation succeeds in the same cycle as the EF aspiration (Matorras *et al.*, 2018). Thus, the aim of this study was to investigate predictive markers of the implantation failure. We have found differences in the miRNA patterns between implantative and non-implantative cycles, and these results have led us to define two predictive models of implantative endometrium.
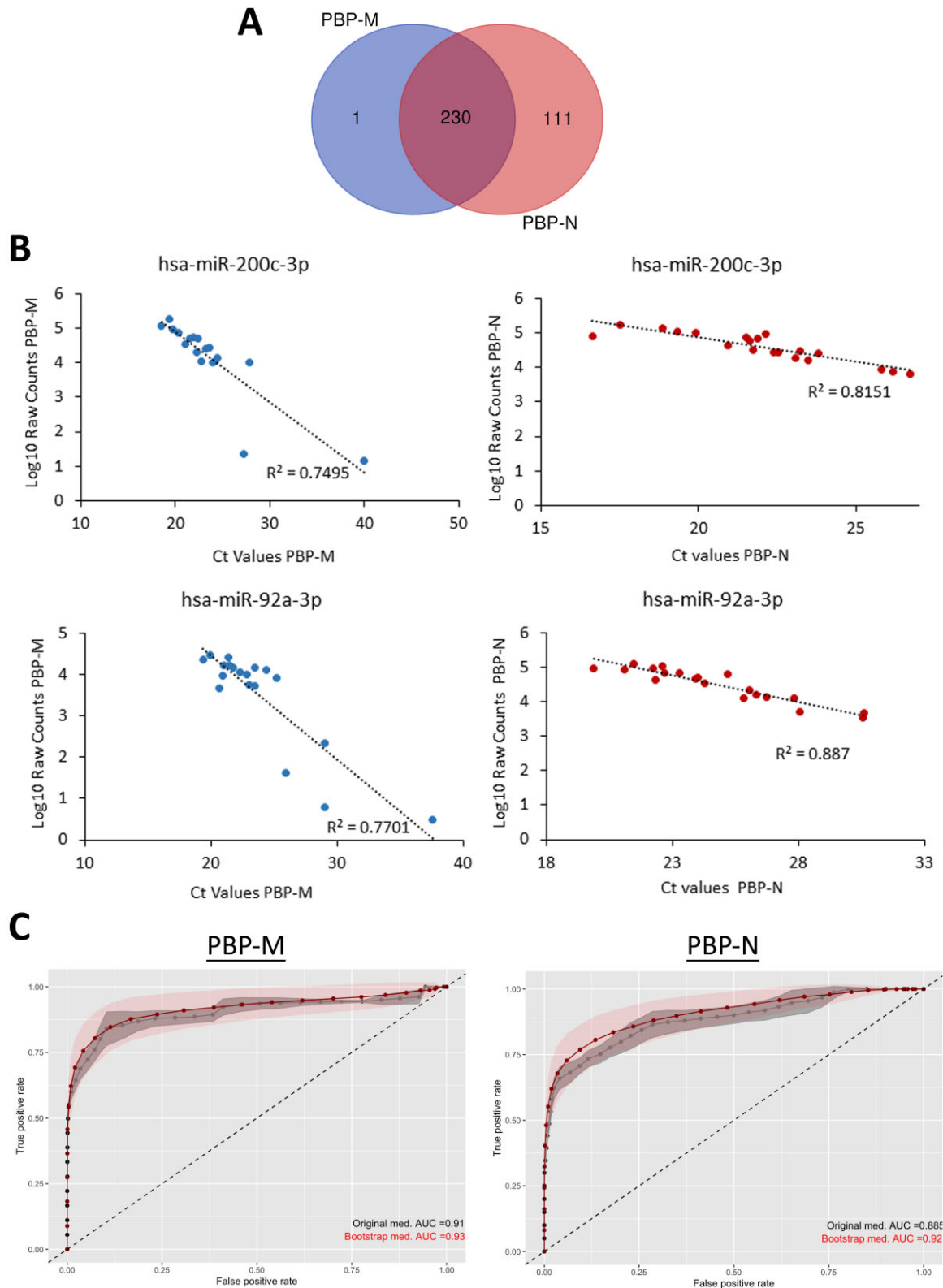
Figure 4. Performance of the selected methods (PBP-M and PBP-N) in the discovery cohort. These experiments were conducted using the discovery cohort samples (n = 30): 15 samples from women with successful implantation and 15 from women with implantation failure. The endometrium was considered implantative when pregnancy was confirmed by vaginal ultrasound showing a gestational sac 4 weeks after embryo transfer. **(A)** The Venn diagram shows the number of miRNAs common for the PBP-M and PBP-M (n = 230) detected by small RNA-Seq (after

In this study, we optimized the EF preparation starting from a small volume of sample. As described previously for sputum (Miller et al., 2012; Wang et al., 2017), pre-treatment of the samples with DTT increased the number of particles released from the mucus. However, it did not improve the relative quantification of the reference miRNAs in such samples (Supplementary Fig. S2). This finding and the report that DTT treatment might modify RNA–protein interactions (Zaman et al., 2015) prompted us to collect and process the EF samples without DTT. The RNase experiment suggested that most of the miRNAs found in the EF were not only protein-associated but also protein-associated within the EVs, which protects them from degradation. Some authors have described the circulating Ago2-miRNA complexes in human plasma, which suggests that Ago2 protein might play an important role in the stability of secreted miRNA (Arroyo et al., 2011; Groot and Lee, 2020). This protein has been identified within exosomes and has also been shown to protect the miRNAs within EVs from RNase degradation (Li et al., 2012; Groot and Lee, 2020). However, other authors have not found the Ago2 in classical exosomes and they believe that there is no evidence that exosomes, or any other type of small EV, contain other major components of the miRNA biogenesis machinery (Jeppesen et al., 2019). It is not clear which proteins are protecting these miRNAs from degradation; nevertheless, our results suggest a strong association between miRNAs and proteins and indicate the existence of miRNA-protein complexes within the EVs.

Once we had characterized the EF, we compared different vesicle enrichment and RNA extraction methods. A few studies have compared various EV-enriching protocols for EF samples (Campoy et al., 2016; Li et al., 2021), but none has evaluated different techniques for RNA extraction. A study published by Li et al. (2021) reports that, for EV isolation, UC is superior to PBP. However, our findings do not agree with their results, and the differences could be due to the fact that different protocols are used. To isolate EVs from EF they (Li et al., 2021) have used a 1:2 ratio of PBP and an overnight incubation at 4°C, while we used 1:1 ratio of PBP and incubation at room temperature for 30 min. The UC methods were also different; they (Li et al., 2021) used a two-step UC procedure and resuspended the EVs in 35 μl, while we only performed a single step UC and resuspended the EVs in 100 μl.

In our search for efficient methods for a comprehensive analysis of miRNAs from EF, we found that the PBP-based EV enrichment techniques (PBP-M and PBP-N) increased the efficiency of miRNAs detection in EF samples (Fig. 3A). Moreover, our small RNA-Seq analysis revealed that different populations of miRNAs could be obtained depending on the RNA extraction method (Fig. 3B). Similar findings have been reported by other authors who have made such comparisons, showing different results with different RNA extraction kits

(El-Khoury et al., 2016; Wright et al., 2020). Therefore, changing the RNA extraction protocols may lead to different results, complicating the comparisons between studies. Given the importance of selecting a robust methodology, we conducted a technical reproducibility experiment to compare the PBP-M and PBP-N methods. The results demonstrated that the PBP-N improves the qPCR amplification results and lowers the coefficients of variation (Fig. 3C).

Finally, we ended up with two predictive models, Model 1 using the PBP-M method and Model 2 based on PBP-N. The results obtained with Model 1 (PBP-M) showed differences between the discovery and validation cohorts. Specifically, the qPCR showed that hsa-miR-148-3p was significantly downregulated in the validation implantative endometrium group. This was consistent with the data obtained by the qPCR for the discovery group. However, these results did not agree with the data obtained by small RNA-Seq for the discovery cohort. In addition, hsa-miR-200b-3p did not follow the same trend in the discovery and validation cohorts. The only miRNA that followed the same trend in the different analyses and cohorts was hsa-miR-24-3p (downregulated in the implantative endometrium groups). In Model 2 (PBP-N), the results obtained for hsa-miR-24-3p were not consistent between different analyses; the qPCR results indicated that it was significantly downregulated in the implantative endometrium of the discovery cohort while, in contrast, it appeared upregulated in the small RNA-Seq analysis of that subgroup and in the qPCR results for the validation cohort. However, the results for the hsa-miR-200b-3p and hsa-miR-99b-5p were consistent, following the same trend in all the analyses, and these two miRNAs were upregulated in the implantative endometrium group (Supplementary Table SV). To be precise, the ROC analysis identified hsa-miR-99b-5p as the most likely variable to differentiate the non-implantative and implantative endometrium, and the results suggest that the dCt values above the cutoff point indicate a non-implantative endometrium (dCt > 2.81).

Overall, the PBP-N method delivered the best results in this optimization procedure, starting with the limited amounts of EF obtained in a clinical setting. In addition, it proved to be the most efficient and reproducible, with a simplified protocol and its application in two independent cohorts has shown consistent results. Currently, only 35% of the implantation attempts are successful (De Geyter et al., 2020) and, as our test in the validation cohort achieved high specificity (Model 2, 0.93), we believe that we may be able to improve the success rate by using our predictive model PBP-N.

One limitation of our approach is the inherent variability of the women involved in the trial and the embryos transferred. When the pregnancy is achieved after ET, it can be said that the endometrium was implantative. However, when the implantation fails, it cannot be assumed that the problem was associated with the endometrium only, because the fault might lie with the embryo, the endometrium or

Figure 4. **Continued**

TMM normalization) and the number of miRNAs unique for each of the techniques (PBP-M, 1 and PBP-N, 111). **(B)** Correlation analyses were carried out to determine the suitability of the selected internal controls. The graphs show the results for each miRNA in each sample (n = 30), obtained using the small RNA-Seq and qPCR. The miRNAs selected as internal normalizers were hsa-miR-200c-3p and hsa-miR-92a-3p. **(C)** Receiver operating characteristic curves for the three miRNA-based predictive models tested by qPCR in the discovery cohort. The performance of the original model is shown in black, and the mean performance of the bootstrap output is shown in red. The shading indicates the extent of the standard deviation. The AUC is shown in the respective colors in the lower right-hand corner of the curves. PBP-N: extracellular vesicle enrichment using polymer-based precipitation and RNA extraction with Norgen Plasma/Serum RNA purification kit. PBP-M: extracellular vesicle enrichment using polymer-based precipitation method and RNA extraction with mirVana PARIS kit. miRNAs, microRNAs; PBP, polymer-based precipitation; qPCR, quantitative PCR; RNA-Seq, RNA-sequencing; TMM, Trimmed Mean of M-values.
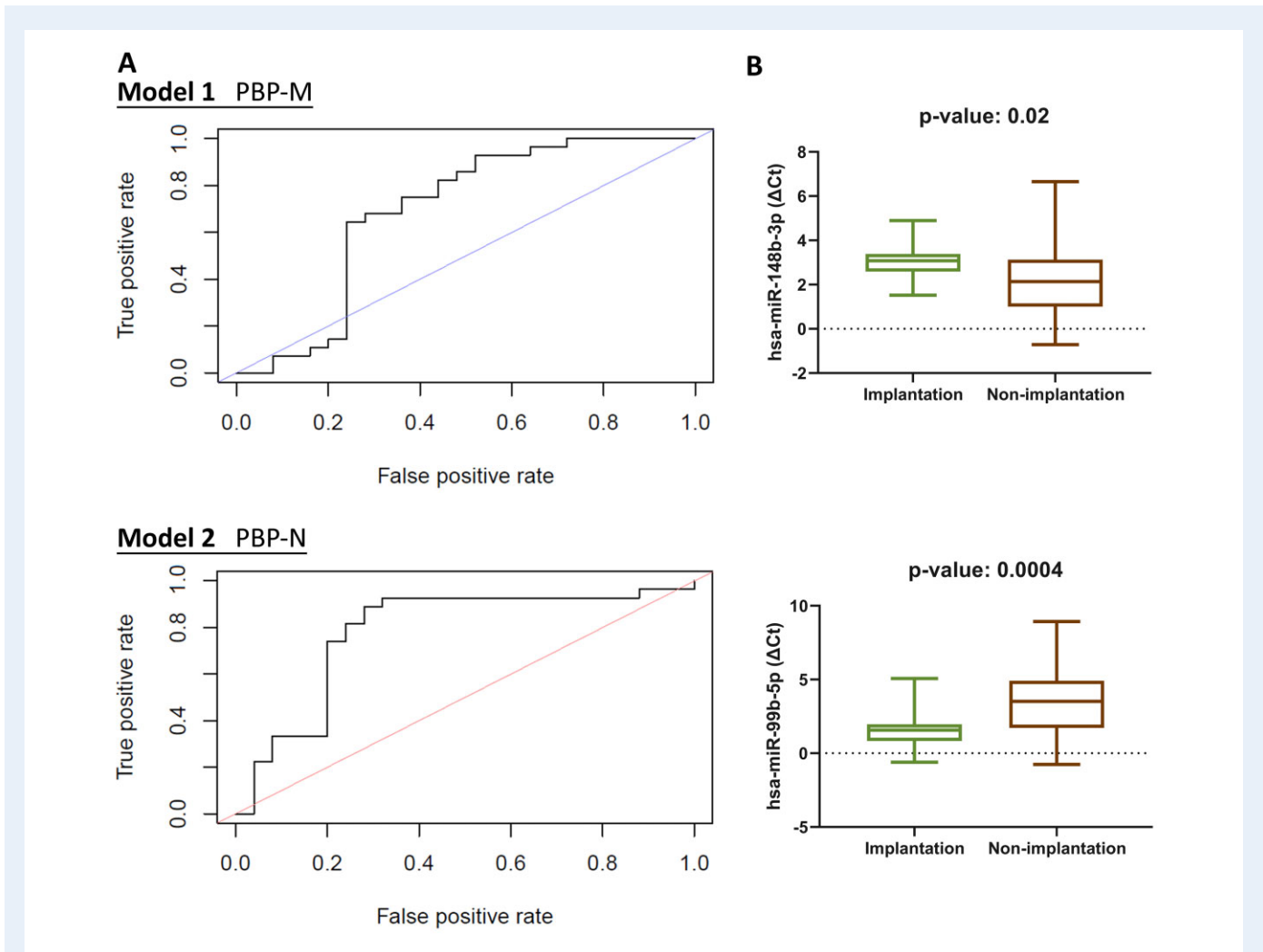
Figure 5. Receiver operating characteristic curves of the validated models and box plots for the most significant miRNAs in each model. The predictive models designed using the qPCR results for the PBP-M and PBP-N methods applied to the discovery cohort were validated in a new group, the validation cohort (n = 60; 30 subjects in the implantative subgroup and 30 in the non-implantative subgroup). The endometrium was considered implantative when pregnancy was confirmed by vaginal ultrasound showing a gestational sac 4 weeks after ET. The analyses were carried out with those samples that pass the quality control; amplification of the reference miRNAs (hsa-miR-200c-3p and hsa-miR-92a-3p) less than 30 Cts. For PBP-M were: n = 28 in the implantative group and n = 25 in the non-implantative group. For PBP-N were: n = 27 in the implantative group and n = 25 in the non-implantative group. **(A)** Receiver operating characteristic curves for the qPCR data obtained for the two predictive models in the validation cohort. Model 1 PBP-M (hsa-miR-200b-3p, hsa-miR-24-3p and hsa-miR-148b-3p) had an AUC of 0.69 (95% CI, 0.55–0.86) and Model 2 PBP-N (hsa-miR-200b-3p, hsa-miR-24-3p and hsa-miR-99b-5p) had an AUC of 0.78 (95% CI, 0.6–0.89). **(B)** Box plots showing the most likely miRNAs to differentiate between the non-implantative and implantative endometrium. The microRNA levels in the EF at the time of embryo transfer. The horizontal line in the middle of the box plot represents the median, while the horizontal limits of the boxes represent the first and third quartiles. The levels of significance were assessed using unpaired *t*-tests with Welch's correction. ΔCt is inversely correlated with the amount of miRNA in the samples. PBP-N: enrichment with polymer-based precipitation method and RNA extraction with Norgen Plasma/Serum RNA purification kit. PBP-M: extracellular vesicle enrichment with a polymer-based precipitation method and RNA extraction with mirVana PARIS kit. Ct, cycle threshold; ET, embryo transfer; miRNAs, microRNAs; PBP, polymer-based precipitation; qPCR, quantitative PCR.

both. In our study, we tried to minimize the issue of individual variability as all transfers were performed during an artificial cycle under the same hormone supplement protocol. Another limitation was the alignment rate of the sequenced data against the human genome, which showed great variability between the samples, with highly variable alignment percentages (Supplementary Table SII). We believe that these differences could be related to the different biological content of the samples, because the EF composition can vary as it may contain genetic material from the uterine microbiomes (Agostinis *et al.*, 2019). To overcome the problem of the biological variability effect on small RNA-Seq data, we used the TMM normalization at the time of selecting the differentially expressed miRNAs. In the case of qPCR data, we selected two endogenous miRNA controls (hsa-miR-200c-3p and hsa-miR-92a-3p) with the help of the NormFinder algorithm (Fig. 4B).

These miRNAs were chosen because they were equally expressed in both groups (implantative and non-implantative endometrium groups) and positively correlated with the amount of protein in the samples. Moreover, they were detected at high levels by small RNA-Seq and had low Ct values in the qPCR. However, the normalization for analyzing the small RNA-Seq data and selecting an endogenous miRNA suitable for normalizing the qPCR data are critical points that might generate great uncertainty. Since there is no standardized method to normalize the RNA-Seq data, each group selects the method that they consider most appropriate. This is also the case with internal controls as the expression of such a control could also vary depending on the kit used for RNA extraction. The internal controls used should not be generalized, and each should be adapted to the experiment performed. The relatively low negative predictive value observed here in the models (Model 1 = 0.69, Model 2 = 0.71) is another limitation to be taken into account. We hypothesize that this was caused by the fact that we have only evaluated the endometrium, and this means that the test will fail in cases where the implantation failure is caused by the embryo. We selected the embryos on the basis of their morphology; however, we did not use genetic and molecular data to improve the selection. Obtaining such data would certainly improve our test accuracy and the AUC.

Functional analysis of the validated miRNAs showed strong associations with key processes involved in implantations. Thus, some of the pathways targeted by the differentially expressed miRNAs were related to adherens junctions, necessary for the initiation of implantation as they are required for cell attachment, adhesion and recognition (Buck et al., 2012). These miRNAs were also associated with the TGF-beta signaling pathway, essential for decidualization of the endometrial stromal cells (Jones et al., 2006). Furthermore, interactions with immune system processes (Lee et al., 2011), vesicle-mediated transport and in utero embryonic development (Kurian and Modi, 2019), with key roles during implantation, were also found. In addition, the available hsa-miR-148b-3p data suggest that its activity may depend on tissue and cell types and is mainly involved in the regulation of cell progression (Dai et al., 2019). Some studies have found that this miRNA inhibits malignant tumor progression (Wang et al., 2016; Li et al., 2018). Its overexpression has also been associated with osteogenesis (Mollazadeh et al., 2019) and cancer cell progression (Dai et al., 2019). Furthermore, this miRNA has been selected as a reference in a study designed to identify candidate miRNA markers of endometriosis, as its mean Ct values did not differ significantly between the women with endometriosis and the control group. Here, we observed that the expression of hsa-miR-148b-3p was upregulated in the EF samples of patients with implantation failure. This leads us to believe that high concentrations of this miRNA could be inhibiting processes related to embryo implantation. The role of hsa-miR-99b-5p in the EF could be related to its function as a pathway regulator, contributing to natural killer (NK) cell activation and effector function (Petty et al., 2016). The NK cells have been described as the major leukocytes in the endometrium. They accumulate extensively around spiral arterioles in the mid-secretory-phase endometrium and early-pregnancy decidua in accordance with increasing levels of ovarian-derived estrogen and progesterone (Quenby and Farquharson, 2006). These findings suggest that the NK cells have a crucial role in implantation and decidualization. However, a meta-analysis using 22 studies examining the uterine NK-cell percentages in infertile versus fertile women showed no significant differences between the groups (Seshadri and Sunkara, 2014). Taken together with our results, these studies could indicate that in women with a low concentration of hsa-miR-99b-5p in the endometrium, the activation of uterine NK cells is suboptimal despite a normal cell count and, as a consequence, implantation does not occur.

In summary, this study introduces new protocols to analyze the miRNAs in very small volumes (5–50 µl) of EF collected just before Day-5 frozen ETs, which could be implemented in clinical practice. These new methods could be employed to assess endometrial competence using miRNA-based non-invasive tools. Hence, the professionals in assisted reproduction centers could use hsa-miR-99b-5p (employing the PBP-N detection method) to predict the endometrial status. This could potentially help to improve the implantation rates for women undergoing ART. It could be possible to change the ET strategy when the results showed an unfavorable implantative pattern and thus increase the implantation rates. Using this method may also reduce the loss of embryos, so common after ET to a potentially non-implantative endometrium.

Supplementary data

Supplementary data are available at *Human Reproduction* online.

Data availability

FASTQ data are available in GEO with the access number GSE178917 (https://www.ncbi.nlm.nih.gov/geo/query/acc.cgi?acc=GSE178917).

Acknowledgements

We are grateful to the Cruces University Hospital for allowing us to carry out this investigation and to all the couples who participated in the study.

Authors' roles

Conceptualization and design: R.M., J.M.F.-P., N.S. and J.I.-P. Sample collection: M.I., M.D.-Z., A.R. and J.I.-P. Technical reproducibility assay: M.C.-G. and J.I.-P. Databases: M.D.-N., L.L. and J.I.-P. Small RNA-Seq: A.M.A., L.B., M.-C.G. and N.S. Data analysis: J.J.L., U.M.M. and M.C.-G. Interpretation of the results: J.I.-P., F.R., E.G., R.M. and J.M.F.-P. Writing of the original draft: J.I.-P. All authors have read, critically reviewed and approved the final manuscript.

Funding

Instituto de Salud Carlos III (PI20/01131). The funding entities did not have any role in study design, sample collection, analysis and interpretation of data, report writing or decision to submit the article for publication.

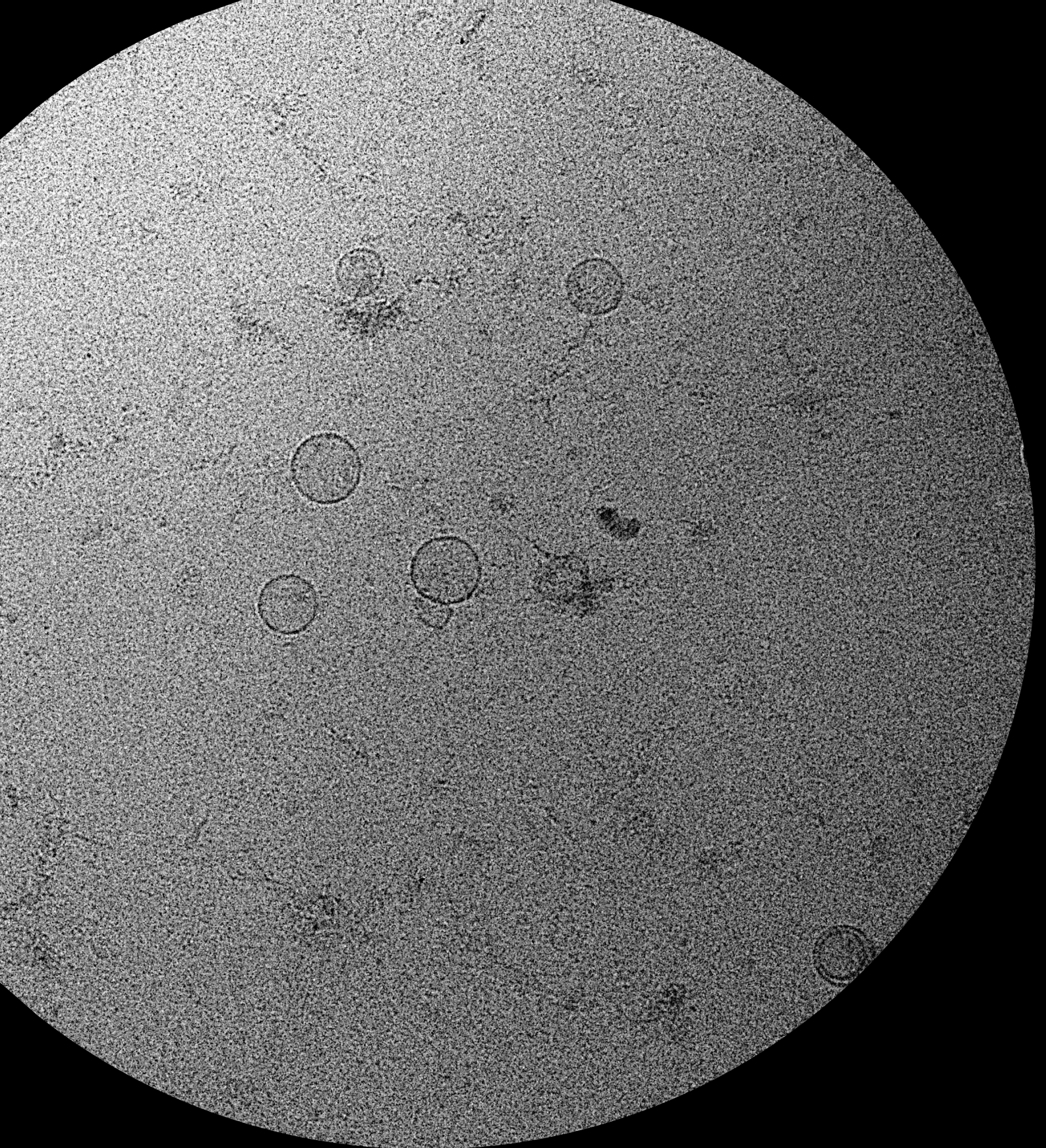# Conflict of interest

The authors declare no competing interests.

References

Agostinis C, Mangogna A, Bossi F, Ricci G, Kishore U, Bulla R. Uterine immunity and microbiota: a shifting paradigm. *Front Immunol* 2019;**17**:10–2387.

Andersen CL, Jensen JL, Ørntoft TF. Normalization of real-time quantitative reverse transcription-PCR data: a model-based variance estimation approach to identify genes suited for normalization, applied to bladder and colon cancer data sets. *Cancer Res* 2004;**64**:5245–5250.

Arroyo JD, Chevillet JR, Kroh EM, Ruf IK, Pritchard CC, Gibson DF, Mitchell PS, Bennett CF, Pogosova-Agadjanyan EL, Stirewalt DL et al Argonaute2 complexes carry a population of circulating microRNAs independent of vesicles in human plasma. *Proc Natl Acad Sci U S A* 2011;**108**:5003–5008.

ASEBIR. *Cuadernos de embriología clínica III*. Criterios ASEBIR de valoración morfológica de oocitos, embriones tempranos y blastocistos humanos. 3ª ed. Madrid: Gobalo, 2015.

Azkargorta M, Escobes I, Iloro I, Osinalde N, Corral B, Ibañez-Perez J, Exposito A, Prieto B, Elortza F, Matorras R. Differential proteomic analysis of endometrial fluid suggests increased inflammation and impaired glucose metabolism in non-implantative IVF cycles and pinpoints PYGB as a putative implantation marker. *Hum Reprod* 2018;**33**:1898–1906.

Balaguer N, Moreno I, Herrero M, González M, Simón C, Vilella F. Heterogeneous nuclear ribonucleoprotein C1 may control miR-30d levels in endometrial exosomes affecting early embryo implantation. *Mol Hum Reprod* 2018;**24**:411–425.

Bhaskaran M, Mohan M. MicroRNAs: history, biogenesis, and their evolving role in animal development and disease. *Vet Pathol* 2014;**51**:759–774.

Bhusane K, Bhutada S, Chaudhari U, Savardekar L, Katkam R, Sachdeva G. Secrets of endometrial receptivity: some are hidden in uterine secretome. *Am J Reprod Immunol* 2016;**75**:226–236.

Buck VU, Windoffer R, Leube RE, Classen-Linke I. Redistribution of adhering junctions in human endometrial epithelial cells during the implantation window of the menstrual cycle. *Histochem Cell Biol* 2012;**137**:777–790.

Campoy I, Lanau L, Altadill T, Sequeiros T, Cabrera S, Cubo-Abert M, Pérez-Benavente A, Garcia A, Borrós S, Santamaria A et al. Exosome-like vesicles in uterine aspirates: a comparison of ultracentrifugation-based isolation protocols. *J Transl Med* 2016;**14**:1–12.

Casper RF. Frozen embryo transfer: evidence-based markers for successful endometrial preparation. *Fertil Steril* 2020;**113**:248–251.

Cozzolino M, Diaz-Gimeno P, Pellicer A, Garrido N. Evaluation of the endometrial receptivity assay and the preimplantation genetic test for aneuploidy in overcoming recurrent implantation failure. *J Assist Reprod Genet* 2020;**37**:2989–2997.

Craciunas L, Gallos I, Chu J, Bourne T, Quenby S, Brosens JJ, Coomarasamy A. Conventional and modern markers of endometrial receptivity: a systematic review and meta-analysis. *Hum Reprod Update* 2019;**25**:202–223.

Dai W, He J, Zheng L, Bi M, Hu F, Chen M, Niu H, Yang J, Luo Y, Tang W et al. miR-148b-3p, miR-190b, and miR-429 regulate cell progression and act as potential biomarkers for breast cancer. *J Breast Cancer* 2019;**22**:219–236.

De Geyter C, Calhaz-Jorge C, Kupka MS, Wyns C, Mocanu E, Motrenko T, Scaravelli G, Smeenk J, Vidakovic S, Goossens V. ART in Europe, 2015: results generated from European registries by ESHRE. *Hum Reprod Open* 2020;**2020**:1–17.

Dragovic RA, Gardiner C, Brooks AS, Tannetta DS, Ferguson DJP, Hole P, Carr B, Redman CWG, Harris AL, Dobson PJ et al. Sizing and phenotyping of cellular vesicles using nanoparticle tracking analysis. *Nanomed Nanotechnol Biol Med* 2011;**7**:780–788.

El-Khoury V, Pierson S, Kaoma T, Bernardin F, Berchem G. Assessing cellular and circulating miRNA recovery: the impact of the RNA isolation method and the quantity of input material. *Sci Rep* 2016;**6**:19529.

Gellersen B, Brosens JJ. Cyclic decidualization of the human endometrium in reproductive health and failure. *Endocr Rev* 2014;**35**:851–905.

Greening DW, Nguyen HPT, Elgass K, Simpson RJ, Salamonsen LA. Human endometrial exosomes contain hormone-specific cargo modulating trophoblast adhesive capacity: insights into endometrial-embryo interactions. *Biol Reprod* 2016;**94**:1–15.

Groot M, Lee H. Sorting mechanisms for microRNAs into extracellular vesicles and their associated diseases. *Cells* 2020;**9**:1044.

Han TT, Li W, Li GP. Progress in understanding the functional roles of extracellular vesicles in reproduction. *Biomed Environ Sci* 2020;**33**:518–527.

Jeppesen DK, Fenix AM, Franklin JL, Higginbotham JN, Zhang Q, Zimmerman LJ, Liebler DC, Ping J, Liu Q, Evans R et al. Reassessment of exosome composition. *Cell* 2019;**177**:428–428.

Jones RL, Stoikos C, Findlay JK, Salamonsen LA. TGF-β superfamily expression and actions in the endometrium and placenta. *Reproduction* 2006;**132**:217–232.

Kurian NK, Modi D. Extracellular vesicle mediated embryo-endometrial cross talk during implantation and in pregnancy. *J Assist Reprod Genet* 2019;**36**:189–198.

Langmead B, Trapnell C, Pop M, Salzberg SL. Ultrafast and memory-efficient alignment of short DNA sequences to the human genome. *Genome Biol* 2009;**10**:R25.

Lee JY, Lee M, Lee SK. Role of endometrial immune cells in implantation. *Clin Exp Reprod Med* 2011;**38**:119–125.

Li L, Zhu D, Huang L, Zhang J, Bian Z, Chen X, Liu Y, Zhang CY, Zen K. Argonaute 2 complexes selectively protect the circulating microRNAs in cell-secreted microvesicles. *PLoS One* 2012;**7**:e46957.

Li T, Greenblatt EM, Shin MEJ, Brown TJ, Chan C. Cargo small non-coding RNAs of extracellular vesicles isolated from uterine fluid associate with endometrial receptivity and implantation success. *Fertil Steril* 2021;**115**:1327–1336.

Li X, Jiang M, Chen D, Xu B, Wang R, Chu Y, Wang W, Zhou L, Lei Z, Nie Y et al. MiR-148b-3p inhibits gastric cancer metastasis by inhibiting the Dock6/Rac1/Cdc42 axis. *J Exp Clin Cancer Res* 2018; **37**:15.

Marinaro F, Macías-García B, Sánchez-Margallo FM, Blázquez R, Álvarez V, Matilla E, Hernández N, Gómez-Serrano M, Jorge I, Vázquez J et al. Extracellular vesicles derived from endometrial human mesenchymal stem cells enhance embryo yield and quality in an aged murine model. *Biol Reprod* 2019;**100**:1180–1192.

Matorras R, Martinez-Arranz I, Arretxe E, Iruarrizaga-Lejarreta M, Corral B, Ibañez-Perez J, Exposito A, Prieto B, Elortza F, Alonso C. The lipidome of endometrial fluid differs between implantative and non-implantative IVF cycles. *J Assist Reprod Genet* 2020;**37**: 385–394.

Matorras R, Pijoan JI, Perez-Ruiz I, Lainz L, Malaina I, Borjaba S. Meta-analysis of the embryo freezing transfer interval. *Reprod Med Biol* 2021;**20**:144–115.

Matorras R, Quevedo S, Corral B, Prieto B, Exposito A, Mendoza R, Rabanal A, Diaz-Nuñez M, Ferrando M, Elortza F et al. Proteomic pattern of implantative human endometrial fluid in in vitro fertilization cycles. *Arch Gynecol Obstet* 2018;**297**:1577–1586.

Matorras R, Urquijo E, Mendoza R, Corcóstegui B, Expósito A, Rodríguez-Escudero FJ. Ultrasound-guided embryo transfer improves pregnancy rates and increases the frequency of easy transfers. *Hum Reprod* 2002;**17**:1762–1766.

Miller A, Bromhead C, Jones M, Tustin P. Mucus digestion improves the detection of *Chlamydia trachomatis* and *Neisseria gonorrhoeae* on the cobas 4800. *Sex Transm Dis* 2012;**39**:733–734.

Mollazadeh S, Fazly Bazzaz BS, Neshati V, De Vries AAF, Naderi-Meshkin H, Mojarad M, Mirahmadi M, Neshati Z, Kerachian MA. Overexpression of MicroRNA-148b-3p stimulates osteogenesis of human bone marrow-derived mesenchymal stem cells: the role of MicroRNA-148b-3p in osteogenesis. *BMC Med Genet* 2019;**20**: 1–10.

Ng YH, Rome S, Jalabert A, Forterre A, Singh H, Hincks CL, Salamonsen LA. Endometrial exosomes/microvesicles in the uterine microenvironment: a new paradigm for embryo-endometrial cross talk at implantation. *PLoS One* 2013;**8**:e58502.

Nguyen HPT, Simpson RJ, Salamonsen LA, Greening DW. Extracellular vesicles in the intrauterine environment: challenges and potential functions. *Biol Reprod* 2016;**95**:109.

Petty RD, McCarthy NE, Le Dieu R, Kerr JR. MicroRNAs hsa-miR-99b, hsa-miR-330, hsa-miR-126 and hsa-miR-30c: potential diagnostic biomarkers in natural killer (NK) cells of patients with Chronic Fatigue Syndrome (CFS)/myalgic encephalomyelitis (ME). *PLoS One* 2016;**11**:e0150904.

Prieto-Fernández E, Aransay AM, Royo F, González E, Lozano JJ, Santos-Zorrozua B, Macias-Camara N, González M, Garay RP, Benito J et al. A comprehensive study of vesicular and non-vesicular miRNAs from a volume of cerebrospinal fluid compatible with clinical practice. *Theranostics* 2019;**9**:4567–4579.

Quenby S, Farquharson R. Uterine natural killer cells, implantation failure and recurrent miscarriage. *Reprod Biomed Online* 2006;**13**:24–28.

Rao X, Huang X, Zhou Z, Lin X. An improvement of the 2^(-delta delta CT) method for quantitative real-time polymerase chain reaction data analysis. *Biostat Bioinforma Biomath* 2013;**26**:139–140.

Robinson MD, McCarthy DJ, Smyth GK. edgeR: a bioconductor package for differential expression analysis of digital gene expression data. *Bioinformatics* 2010;**26**:139–140.

Seshadri S, Sunkara SK. Natural killer cells in female infertility and recurrent miscarriage: a systematic review and meta-analysis. *Hum Reprod Update* 2014;**20**:429–438.

Sing T, Sander O, Beerenwinkel N, Lengauer T. ROCR: visualizing classifier performance in R. *Bioinformatics* 2005;**21**:3940–3941.

Strowitzki T, Germeyer A, Popovici R, von Wolff M. The human endometrium as a fertility-determining factor. *Hum Reprod Update* 2006;**12**:617–630.

van der Gaast MH, Beier-Hellwig K, Fauser BCJM, Beier HM, Macklon NS. Endometrial secretion aspiration prior to embryo transfer does not reduce implantation rates. *Reprod Biomed Online* 2003;**7**:105–109.

van der Gaast MH, Macklon NS, Beier-Hellwig K, Krusche CA, Fauser BCJM, Beier HM, Classen-Linke I. The feasibility of a less invasive method to assess endometrial maturation—comparison of simultaneously obtained uterine secretion and tissue biopsy. *BJOG* 2009;**116**:304–312.

Varet H, Brillet-Guéguen L, Coppée JY, Dillies MA. SARTools: a DESeq2- and edgeR-based R pipeline for comprehensive differential analysis of RNA-Seq data. *PLoS One* 2016;**11**:e0157022.

Vilella F, Moreno-Moya JM, Balaguer N, Grasso A, Herrero M, Martínez S, Marcilla A, Simón C. Hsa-miR-30d, secreted by the human endometrium, is taken up by the pre-implantation embryo and might modify its transcriptome. *Development* 2015;**142**:3210–3221.

Vlachos IS, Zagganas K, Paraskevopoulou MD, Georgakilas G, Karagkouni D, Vergoulis T, Dalamagas T, Hatzigeorgiou AG. DIANA-miRPath v3.0: deciphering microRNA function with experimental support. *Nucleic Acids Res* 2015;**43**:W460–466.

Wang G, Li Z, Tian N, Han L, Fu Y, Guo Z, Tian Y. MiR-148b-3p inhibits malignant biological behaviors of human glioma cells induced by high HOTAIR expression. *Oncol Lett* 2016;**12**:879–886.

Wang QY, Zhang HR, Gao Y, Li RH, Shang XH. Sputasol (dithiothreitol 0.54%) improves the detection of human papillomaviruses using the cobas 4800 system. *Ann Lab Med* 2017;**37**:457–458.

Wei T, Simko V, Levy M, Xie Y, Jin Y, Zemla J. R package "corrplot": visualization of a correlation matrix. *Statistician* 2017;**56**:316–324.

Wright K, K de S, Purdie AC, Plain KM. Comparison of methods for miRNA isolation and quantification from ovine plasma. *Sci Rep* 2020;**10**:825.

Zaman U, Richter FM, Hofele R, Kramer K, Sachsenberg T, Kohlbacher O, Lenz C, Urlaub H. Dithiothreitol (DTT) acts as a specific, UV-inducible cross-linker in elucidation of protein–RNA interactions. *Mol Cell Proteomics* 2015;**14**:3196–3210.